Ionad Taighde Hiodráilice agus Mara,
Rionn na hInnealtóireachta Sibhialta agus Timpleallachta,
Coláiste na hOllscoile Corcaigh,
Éire.

ucc

Coláiste na hOllscoile Corcaigh, Éire
University College Cork, Ireland

Characteristics of the Wave Energy Resource at the Atlantic Marine Energy Test Site

Brendan Cahill

A thesis submitted for the Degree of Doctor of Philosophy

In the School of Engineering
Department of Civil and Environmental Engineering
National University of Ireland, Cork

Supervisor: Prof. Tony Lewis,
Hydraulics & Maritime Research Centre,
Dept. Civil & Environmental Engineering,
University College Cork,
Ireland.

Head of Department: Prof. Alastair Borthwick

ABSTRACT

The wave energy industry is progressing towards an advanced stage of development, with consideration being given to the selection of suitable sites for the first commercial installations. An informed, and accurate, characterisation of the wave energy resource is an essential aspect of this process. Ireland is exposed to an energetic wave climate, however many features of this resource are not well understood. This thesis assesses and characterises the wave energy resource that has been measured and modelled at the Atlantic Marine Energy Test Site, a facility for conducting sea trials of floating wave energy converters that is being developed near Belmullet, on the west coast of Ireland. This characterisation process is undertaken through the analysis of metocean datasets that have previously been unavailable for exposed Irish sites. A number of commonly made assumptions in the calculation of wave power are contested, and the uncertainties resulting from their application are demonstrated. The relationship between commonly used wave period parameters is studied, and its importance in the calculation of wave power quantified, while it is also shown that a disconnect exists between the sea states which occur most frequently at the site and those that contribute most to the incident wave energy. Additionally, observations of the extreme wave conditions that have occurred at the site and estimates of future storms that devices will need to withstand are presented. The implications of these results for the design and operation of wave energy converters are discussed. The foremost contribution of this thesis is the development of an enhanced understanding of the fundamental nature of the wave energy resource at the Atlantic Marine Energy Test Site. The results presented here also have a wider relevance, and can be considered typical of other, similarly exposed, locations on Ireland's west coast.

ACKNOWLEDGEMENTS

I would not have been able to complete this PhD thesis without the support of many people. I would like to thank my supervisor, Prof. Tony Lewis, for initially encouraging me to undertake this research and for his enthusiasm and guidance over the past few years.

I have been lucky to have been part of a fantastic team at the Hydraulics and Maritime Research Centre. Thanks to my colleagues, past and present, for your camaraderie and inspiring me with your work. I am also grateful to have met many other researchers in the marine renewable energy industry, particularly through the International Network on Offshore Renewable Energy (INORE). It has been a privilege to share some great experiences with you and I look forward to working together again in the future.

I wish to acknowledge the financial support of the Irish Research Council for Science Engineering and Technology (IRCSET) and the Science Foundation Ireland Charles Parsons Research Award which funded this PhD. I would also like the Marine Institute and the Sustainable Energy Authority of Ireland (SEAI) for providing the ocean wave data required for this research.

Thanks to my teachers at Tiernaboul National School, St. Brendan's College and University College Cork. Without your input I could not have made it this far.

Thanks to my friends and family for making sure that I never forgot that there is more to life than wave energy! In particular, I am grateful to Niamh and Stephen for giving up their time to proof read this thesis

Finally, I would like to thank my parents, Willie and Noreen, for their unwavering support and Claire, for her patience and love, and for keeping me going through the difficult times.

Contents

LIST OF FIGURES

Nomenclature

γ	Peak shape parameter for JONSWAP Spectrum	[-]
ε_1	Bandwidth parameter	[-]
ε_2	Narrowness parameter	[-]
μ_w	Weighted mean of instantaneous peak frequency	[Hz]
σ_w	Weighted standard deviation of instantaneous peak frequency	[Hz]
θ_p	Wave direction at peak frequency	[°]
λ	Wavelength	[m]
λ_0	Deepwater wavelength	[m]
σ	Spectral width parameter for JONSWAP Spectrum	[-]
AEP	Annual energy production	[GWh]
AI	Abnormality Index	[-]
C	Wave celerity	[ms^{-1}]
C_g	Group velocity	[ms^{-1}]
d	Water depth	[m]
F_m	Plotting function in POT analysis	
f	Wave frequency	[Hz]
f_{peak}	Frequency of the largest spectral ordinate	[Hz]
g(t)	Mother wavelet function	
H	Height of a regular wave	[m]
H_0	Deepwater height of a regular wave	[m]
H_o	Height threshold for POT analysis	[m]
H_{Max}	Height of the largest wave in a record	[m]
H_{m0}	Significant wave height (spectral)	[m]
H_s	Significant wave height (zero-crossing)	[m]
K	Refraction factor	[-]
k	Shape parameter in Weibull distribution	[-]
MAE	Mean Absolute Error	
m_n	n^{th} spectral moment	
N_T	Number of peaks returned in POT analysis	[-]

P	Wave power per metre crest width	[kW/m]
P_0	Deepwater wave power per metre crest width	[kW/m]
P_{exp}	Exploitable wave power	[kW/m]
R	Correlation Coefficient	[-]
RMSE	Root Mean Square error	
S(f)	Spectral Density	[m^2/Hz]
SI	Scatter Index	[-]
S_S	Significant steepness of a sea state	
T	Period of a regular wave	[s]
T_{01}	Mean Period	[s]
T_{02}	Spectral equivalent to T_z	[s]
T_E	Energy Period	[s]
T_P	Peak Wave Period	[s]
T_Z	Zero-Crossing Period	[s]
x_R	Maximum expected H_{m0} for return period R	[m]

Acronyms

ADCP	Acoustic Doppler Current Profiler
AMETS	Atlantic Marine Energy Test Site
AWS	Archimedes' Wave Swing
CDIP	Coastal Data Information Program
CORES	Components for Ocean Renewable Energy Systems (EU FP7 project)
EERA	European Energy Research Alliance
EMEC	European Marine Energy Centre
ESBI	ESB International
EVA	Extreme Value Analysis
FT-I	Fisher-Tippett Type I distribution
FFT	Fast Fourier Transform
GPD	Generalised Pareto Distribution
HMRC	Hydraulics and Maritime Research Centre
IMERC	Irish Marine and Energy Resource Cluster
IQR	Inter-quartile range
JONSWAP	Joint North Sea Wave Project
MOC	Maximum Operating Condition
NDBC	National Data Buoy Centre
NNMREC	Northwest National Marine Renewable Energy centre
NOAA	National Oceanic and Atmospheric Administration
NOMAD	Navy Oceanographic Meteorological Automatic Device (wave buoy)
ODAS	Ocean Data Acquisition System (wave buoy)
POT	Peaks Over Threshold
PRH	Pitch-roll-heave
PTO	Power Take Off
QC	Quality Control
ROC	Rated Operating Condition
SBWR	Shipborne Wave Recorder
SEAI	Sustainable Energy Authority of Ireland
SOWFIA	Streamlining of Ocean Wave Farms Impact Assessment EU FP7 project

SWAN	Simulating Waves Nearshore
TOC	Threshold Operating Condition
TRL	Technology Readiness level
WEC	Wave Energy Converter
WPR	Wave period ratio

CHAPTER 1 Introduction

1.1 Wave Energy: Historical Context and Future Potential

Whether the observer is at the shore or aboard a seagoing vessel, demonstrations of the energy contained in ocean waves are stirring, imposing and often frightening. For this reason waves have long been the subject of stories and works of art. In recent years the exploits of big-wave surfers, and their accompanying camera crews, have seen breaks such as ‘Mavericks’ in California, ‘Dungeons’ near Cape Town and ‘Prowlers’ off Co. Sligo enter popular culture as illustrations of the power inherent in the seas off our coastlines. The unconstrained potential for the various ocean energy technologies currently being developed, including wave energy as well as systems that exploit tidal range, tidal currents, ocean currents, ocean thermal energy and salinity gradients, has been estimated at 7,400 EJ/yr (Lewis et al. 2011) ─ a figure well in excess of the current global primary energy use of 470 EJ (Sims et al. 2007) and of any possible scenario of human requirements. While such absolute utilisation of these resources is implausible, the possibility of harnessing ocean waves to supplant the fossil fuels that currently supply our energy needs is an enticing prospect.

Figure 1.1: 'The Great Wave off Kanagawa' by Katsushika Hokusai (Image from Wikipedia.com)

The history of the efforts to extract useful energy from ocean waves is fraught with examples of innovative ideas and boundless enthusiasm tempered by false starts and costly failures. Patents for devices capable of harnessing this energy, henceforth referred to as Wave Energy Converters (WECS), appeared as early as 1799 with the raft and pulley mechanism developed by the Girards from France. Lacking readily available cheap fuel and hydroelectric resources, California saw a surge of interest in the potential of harnessing the power of the Pacific Ocean at the turn of the 20th century to drive the expansion of its growing cities. Shares in complex creations such as Duffy's Wave Motor were sold without the devices ever being constructed, while one of the few projects to be physically realised, the Starr Wave Motor at Redondo Pier near Los Angeles, "sunk like a lump of sugar when dropped into water" (Madrigal 2011). Efforts were renewed in the 1970s, spurred by Europe's greatly reduced access to Middle Eastern oil. This period saw the development of promising new devices, the foremost being Salter's Duck. This advancement, however, was halted by the vagaries of politics ─ UK Department of Energy funding for the project was discontinued when the associated cost of energy was overstated in a report by the Advisory Council on Research and Development (Salter 2008).

While wave energy still remains a nascent industry, with total installed capacity worldwide reported to be approximately 2MW in 2010 (Implementing Agreement on Ocean Energy Systems (OES-IA) 2010), a move towards commercialisation is evident. Detailed reviews of the state of the art in wave energy conversion and outlines of the leading technologies have been compiled by various sources (Falnes 2007; Waveplam 2009; Falcão 2010; Bahaj 2011) and will not be repeated in this work. The sector resembles a pyramid, with a base consisting of a large number of developers still operating in the early phases of the suggested staged development plans (Holmes 2003). Meanwhile, a select group of the most advanced companies form the apex of the industry and are deploying their concepts in real sea conditions and beginning to move towards multi-device farms. New installations with capacities totalling approximately 2.4MW were added globally in 2011 with a further 9.2MW predicted to be in place by the end of

2012 (Kennedy 2012). The majority of projects comprise of single device demonstrations but by 2015 these should be superseded by larger arrays of devices across Europe such as the 10MW Aegir Wave Power Ltd. project off the southwest coast of Shetland (Aegir Wave Power 2012); the NER300 funded Ocean SWELL 5MW project near the town of Peniche in Portugal (AW-Energy 2012); and a project that has been proposed for the Island of Lewis by Aquamarine Power through a subsidiary company, Lewis Wave Power Ltd, that could potentially become a 50 device (40MW) wave farm (Aquamarine Power 2012). In the United States, Ocean Power Technologies plans to deploy up to 200 of the company's 500kW rated PowerBuoys at the proposed Reedsport OPT Wave Park near Coos Bay, Oregon (Ocean Power Technologies 2012a).

While these proposals appear impressive it is likely that many of these ambitious projects will be reduced in scale or even discontinued given the high attrition rate that is seemingly inherent to the wave energy industry. A lack of funding for continued development is one of the major threats to the future growth of the sector. The large financial outlay associated with progressing commercial sites is beyond the reach of device developers. The Carbon Trust (2006) has identified that the financial support mechanisms available at this stage of development are inadequate; the so-called 'valley of death'. Funding from venture capital sources has also been steadily reduced, due as much to the apparent lack of return on investment as to the global financial crisis. It has been estimated (McCrone 2012) that the 12 leading wave and tidal energy companies have cumulatively spent approximately $600 million of investor capital without achieving profitability. This shortfall has been mitigated however by the introduction of large energy utilities and industrial players such as ABB, Vattenfall and Alstom to the market (reNews 2012).

1.2 Wave Energy in Ireland

Ireland benefits from a particularly abundant wave energy resource, as illustrated in Fig. 1.2. This is unsurprising given the island's geographical location. Sitting at the western edge of Europe, Ireland is exposed to fetches of over 1,800km towards Greenland to the

Northeast, 2,800km towards Newfoundland to the West and 6,000km to the Caribbean islands to the Southwest. In combination with the prevailing south-westerly winds, this vast expanse of ocean acts as an immense transmission line transporting wind-generated wave energy to the Irish west coast. Previous attempts have been made to quantify this resource and calculate the potential contribution wave power could make to the country's energy mix. One of the earliest studies employed a UK Met Office wind-wave hindcasting model and demonstrated that average power levels varied from 57-77 kW/m along the west coast and estimated that approximately one quarter of Ireland's electricity demand could be provided for by a 10km string of the most advanced WECs in development at that time (Mollison 1982). A more recent report calculated a theoretical annual energy resource of up to 460 TWh, with an average annual accessible energy resource of approximately 20.76 TWh (ESB International 2005). To put these figures in context Ireland's consumer side electrical energy demand for 2010 was 25.2 TWh (Sustainable Energy Authority of Ireland 2011b). European (WERATLAS 2001; Serri et al. 2012) and global (Cornett 2008; Mørk et al. 2010; Reguero et al. 2011) atlases of wave energy resource also allow the average power levels the off the Irish coast to be inferred.

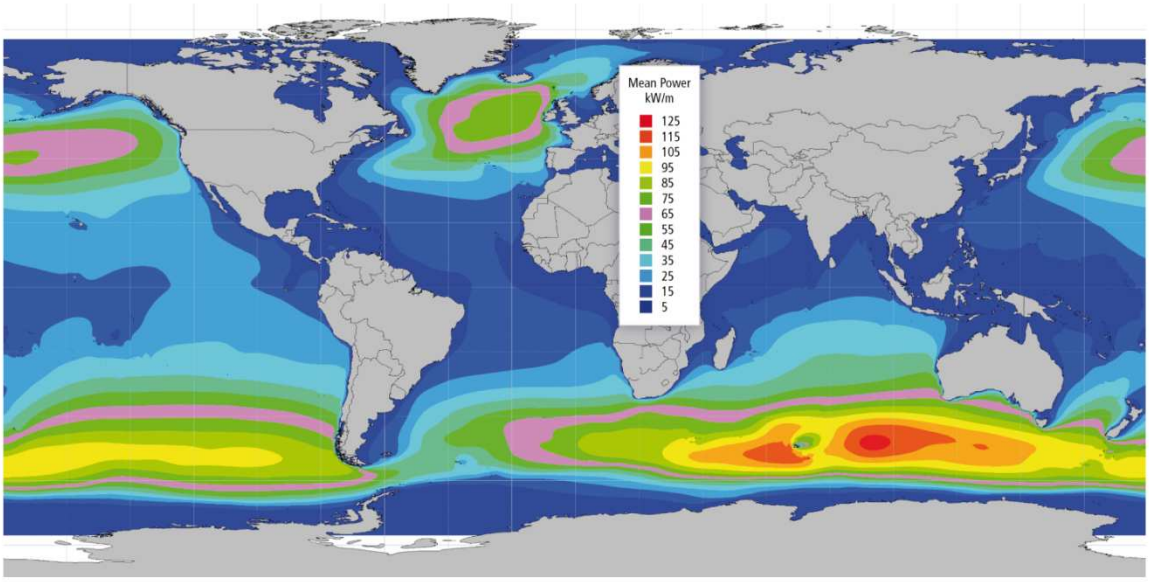

Figure 1.2: Global annual mean wave power [kW/m] (Cornett 2008)

The economic promise of this profuse wave energy resource has been recognised at the highest political levels. *An Taoiseach* (Irish Prime Minister) Enda Kenny has expressed the belief that the ocean energy industry has the potential to create up to 70,000 jobs with a cumulative economic benefit approaching €120 billion by 2050 (Mayo Today 2012), while the former Energy Minister Eamon Ryan envisaged Ireland becoming "the Saudi Arabia of ocean and wind energy" (Department of Communications Marine and Natural Resources 2007b). The Ocean Energy Roadmap to 2050 (Sustainable Energy Authority of Ireland 2010) outlines the possible development possibilities for an ocean energy industry in Ireland. Following a baseline growth scenario an annual output from ocean energy sources (mostly from wave with some contribution from tidal) of close to 25 TWh is expected by 2050 while this increases to almost 120 TWh — significantly higher than the ESB International estimate from 2005 — for the most optimistic projection, which also anticipates that energy that will be surplus to domestic requirements will be exported to Britain and mainland Europe through large scale grid interconnection.

In order to realise these goals firm actions such as the creation of supportive funding structures and the provision of suitable incubation facilities are required in order to stimulate the expansion of indigenous start-ups that possess promising device concepts and to incentivise the most advanced companies to deploy and operate wave farms in Irish waters. Device developers have been assisted by SEAI's Prototype Development Fund and this fundamental research will be furthered by the improved tank testing facilities at the Hydraulics and Maritime Research Centre which are being enhanced with the construction of the new Beaufort Laboratory as part of the IMERC Campus (University College Cork 2012). The quarter scale Galway Bay Test Site has seen three separate device deployments by Ocean Energy Ltd., Wavebob and as part of the FP7-funded CORES Project (Thiebaut et al. 2011). The final piece of infrastructure planned for the ocean energy sector is the Atlantic Marine Energy Test Site, AMETS (Ascoop and Frielding 2010), a grid connected test area which will allow developers to prove the survivability of their devices at full scale in an energetic wave climate that is equivalent to the conditions that can be expected at potential commercial sites off the Irish west coast (Fig. 1.3). While it is unlikely that the original government target of having

500MW of ocean energy installed by 2020 (Department of Communications Marine and Natural Resources 2007a) will be met, progress is being made towards bringing early commercial developments to fruition. What will likely become Ireland's first full scale WEC array, the 5MW WestWave Project, is being developed by ESB and is intended to be operational by 2015 (Sharkey 2012). In addition, Carnegie Wave Energy has lodged an application for a foreshore license with the Department of the Environment in the first stage of its plan to deploy a 5MW installation near Spanish Point, Co. Clare (Carnegie Wave Energy 2012).

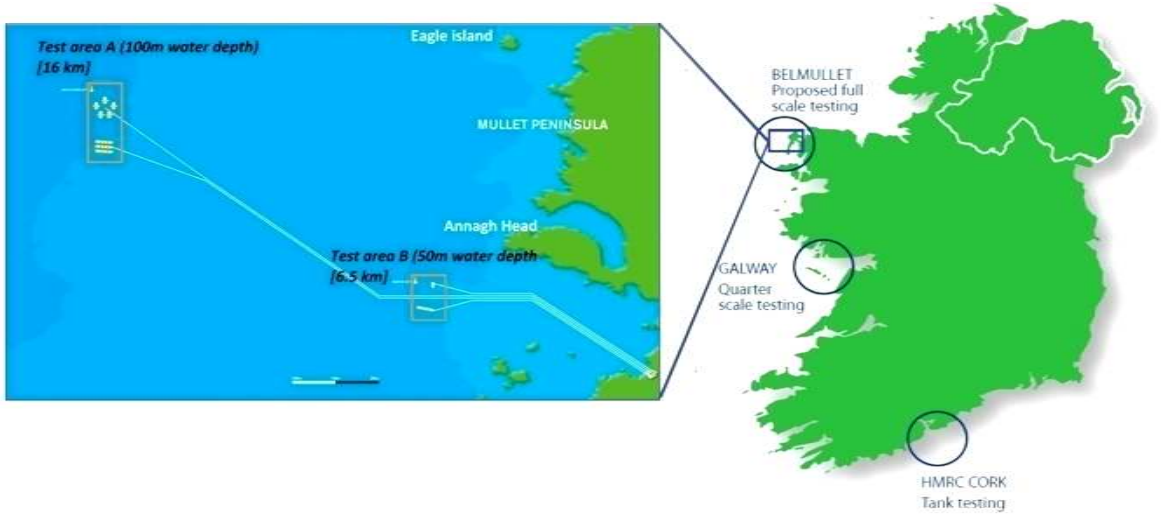

Figure 1.3: Layout of AMETS and locations of Ireland's wave energy test centres (image courtesy of SEAI).

While the scale of the wave resource off the west coast has been recognized, a historical lack of sources of high quality metocean data in Irish waters to allow for more comprehensive and localised studies represents a potential impediment in Ireland's path to developing a viable wave energy industry. The Marine Institute operates a network of six buoys located around the Irish Coast, however these provide only a limited number of summary statistics such as significant wave height (H_s) and the average zero-crossing period (T_z) —the detailed spectral information required for wave energy resource assessments is not provided. Ad hoc deployments of more suitable sensors have been supported (O'Sullivan 1985; Holmes and Barret 2007), but the databases of measurements tend to be of short duration due to the limited nature of these projects. In

contrast to the paucity of sensors in Irish waters, the National Data Buoy Centre in the United States maintains 110 moored buoys which provide full spectral data and which often retain archives of measurements dating back over 20 years. The NDBC also hosts the measurements from academic research groups such as the Scripps Institute of Oceanography at the University of California San Diego, which itself operates approximately 50 Datawell Waverider buoys.

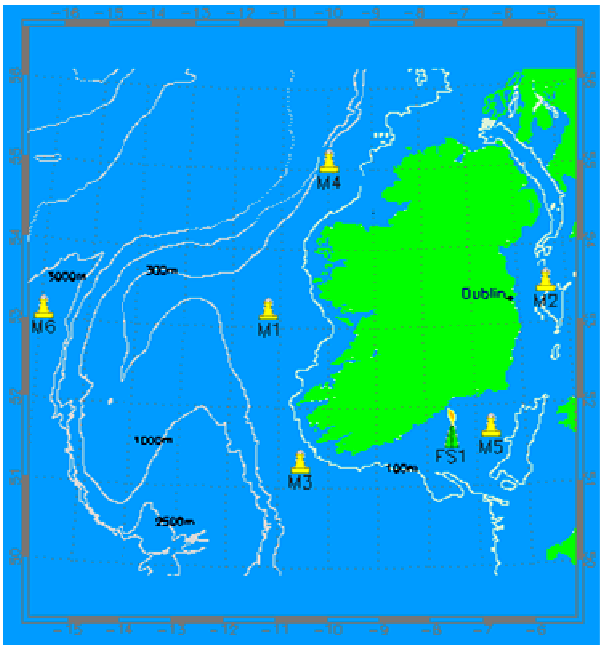

Figure 1.4: Marine Institute M-Buoy Network (Marine Institute 2012)

The recent developments of the test sites in Galway Bay and near Belmullet have had the additional benefit of significantly augmenting the wave measurement network off the Irish west coast. Individual Waverider buoys have been deployed on an almost continuous basis since 2005 to monitor the wave conditions at the benign, quarter scale wave energy test site and motivated a previous study conducted at HMRC of the wave climate in Galway Bay (Barrett 2010). The proposed development of AMETS has also seen the initialisation of a metocean measurement campaign with buoys deployed at depths of 50m and 100m, while a detailed sixteen year numerical climatology was also commissioned for the site by SEAI (Curé 2011a) and made available for analysis. More

detailed descriptions of the range of measurements being attained at these sites and the types of instruments being used will be provided later in this work.

1.3 Research Outline

The recent availability of these data sources presents a unique opportunity for the study of the wave climate in Irish waters. The characterisation of the sea-states in which future wave farms will operate in forms the basis for this project. This research does not aspire to supersede earlier studies to produce a revised assessment of the Irish wave energy resource at a national scale. Nor will it endeavour to select the most promising locations for the deployment of WECs. Instead, the measured data were collated, analysed and interpreted expressly to further the following research objectives:

- Characterise the wave energy resource at AMETS and assess the appropriateness of the site, and by extension other similarly exposed locations along Ireland's Atlantic coast, for the deployment of WEC projects.
- Utilise the high quality spectral measurements that are currently being collected to further the understanding of prevailing wave conditions in Irish waters and enhance the results gained from preceding studies which relied on more limited datasets.
- Identify extreme wave events, and their frequency of occurrence, for the purpose of establishing the conditions wave energy devices will be required to withstand if they are intended for deployment at AMETS or similar sites.

Through pursuing these actions a more detailed understanding of the nature of the wave energy resource off the Irish west coast could be formed to supplement the existing knowledge of the nature of the resource. The full body of the research is outlined in this thesis which adheres to the following structure:

Chapter 2 outlines the importance of resource assessment in developing wave energy projects and presents a review of the current literature in this area. The various stages involved in generating the required metocean datasets to inform these assessments are

described, including the theory of wave measurement using in-situ buoy instruments, the operating principles of some of the most widely used sensors and methods of processing and analysing the data. Numerical wave models and their role in resource assessment are also discussed.

Chapter 3 introduces Ireland's real sea wave energy test sites in Galway Bay and near Belmullet, Co. Mayo and details the wave measurement campaigns that have been conducted there, which have provided the necessary data for this research project. Other similar test areas in Europe and the United States, a number of which encompass unique examples of infrastructure, are also summarised. In addition, the importance of these facilities within the context of staged development pathways for wave energy conversion concepts is also discussed.

Chapter 4 is a detailed study on the variability of measured spectral shapes and how they differ from the standard formulations prescribed by theory. In particular dissonance between the ratio of the energy period (T_E) to the average zero-crossing period (T_{02}) was investigated at a range of open ocean locations. This relationship is important in the context of resource assessment as many previous works, lacking in detailed spectral data, have often assumed an incorrect ratio which in turn has influenced the accuracy of the resulting estimates of wave energy. Ongoing collaborative work to advance this understanding, undertaken as part of the European Energy Research Alliance (EERA) Joint Programme on Ocean Energy, is also described.

Chapter 5 presents analysis techniques and methods of data interpretation for characterising the wave energy at a site of interest. Spectral shapes at a range of sites from different geographical regions are evaluated, with reference to their influence on WEC power production, in order to assess the respective locations' suitability for device deployments.

Chapter 6 builds on the work in the previous section to present a detailed characterisation of the wave energy resource at AMETS. Outputs from the SWAN model commissioned

for the site are compared to in-situ measurements to assess how accurately they replicate the overall wave climate and are utilised to identify the suitability of the site for commercial scale WEC deployments. The variability of the resource, both with respect to water depth as well as fluctuations on a seasonal and interannual basis, and how this will impact WEC operation is illustrated and discussed. Measurements from AMETS and Galway Bay are also directly compared to assess the degree of scalability that exists between Ireland's real sea test facilities.

Chapter 7 departs from addressing the potential for energy extraction from the incident wave climate and instead focuses on the extreme conditions WECs are likely to face during open ocean deployments. The long-term model of the wave conditions surrounding AMETS allows for the prediction of the most severe storm conditions that should be expected for return values relevant to the lifetime of potential commercial deployments. Extreme individual waves are also considered and measurements of these events recorded at AMETS are studied. An awareness of these conditions will be fundamental for the design of WEC components and moorings.

Chapter 8 explores the short term variability of wave energy and how this may impact on WEC operation. Wavelet analysis is applied as a further tool to investigate short term variability and an analysis of the brief dataset from concurrently deployed measurement buoys is undertaken to assess the fluctuations of wave conditions along temporal and spatial scales.

Chapter 9 contains a final discussion of the results presented previously and the conclusions that can be drawn from the project.

1.4 Publications

The research outlined in this thesis has contributed a number of publications and papers, outlined below. Additionally, the research outlined in Chapter 4 is being prepared as a

standalone journal paper, and will also be included in a collaborative paper being written as part of the EERA project.

- Cahill, B. G. (2012). *Resource Characterisation of the Galway Bay 1/4 Scale Wave Energy Test Site*, Commercial report prepared on behalf of the Sustainable Energy Authority of Ireland.
- Cahill, B. G. and A. W. Lewis (2012). *Long Term Wave Energy Resource Characterisation at the Atlantic Marine Energy Test Site*. World Renewable Energy Forum (WREF), Denver, USA.
- Cahill, B. G. and A. W. Lewis (2011). *Wave Energy Resource Characterization and the Evaluation of Potential Wave Farm Sites.* MTS/IEEE OCEANS'11 Conference. Kona, Hawaii, U.S.A.
- Cahill, B. and A. W. Lewis (2011). *Wave Energy Resource Characterization of the Atlantic Marine Energy Test Site.* 9th European Wave and Tidal Energy Conference. Southampton, United Kingdom.
- Cahill, B. G. (2011). *Characterizing Ireland's wave energy resource*. The Boolean **2**(00): 13-17.
- Cahill, B. G. and A. W. Lewis (2010). *Wavelet analysis applied to the wave energy resource at an Irish west coast site.* MTS/IEEE OCEANS' 10 Conference, Seattle, U.S.A
- Cahill, B. G. (2010). *Wave farm modelling: harnessing Ireland's greatest energy resource*. The Boolean **1**(00): 22-25.

Chapter 2 Wave Measurement, Data Analysis and Wave Energy Resource Assessment

Development of an understanding of the magnitude and characteristics of the resource at the site of a potential wave energy installation requires the measurement, analysis and interpretation of the incident wave climate. This process is the focus of this chapter. The most commonly utilised wave measurement instruments are described in Section 2.1. Particular reference is given to wave buoys, from which the observations used in this research were obtained. The methods for processing and analysing this data are also detailed in this chapter, including the application of quality control checks for ensuring the validity of the measurements. A review of published literature has been undertaken to determine the accepted methods of defining and characterising wave energy resource, and these are summarised in Section 2.3. Previous studies relating to the Irish wave energy resource are discussed, and the specific knowledge gaps that exist are identified in order to place the contribution of this research in context.

2.1 Wave Measurement

Accurate measurements of ocean waves are essential for the direct assessment and characterisation of wave energy resource, and as a means to validate numerical models. Historically, wave data were derived from visual observations taken aboard ships. Even though the errors associated with visual observations have been shown to be within acceptable limits when compared to instrument records (Guedes Soares 1986), this method is unsuitable for studying the wave energy resource as the data are transient in time and space, are clustered along shipping lanes, and other unsuitable areas for developing WEC installations, and are inherently biased as ships will generally avoid the most severe conditions if it is possible to do so. Tucker and Pitt (2001) described the development of early, scientific sensors from the 1940s onwards by wave research groups in the UK . Many of the first instruments were variants of fixed wave staffs, which measure the change of certain properties of parallel wires that are partially submerged in

the wave field, such as resistance or capacitance, which allows the time series of surface elevation to be determined. These sensors were particularly suitable for providing information about the wave climate for the design of coastal infrastructure and offshore structures for the oil and gas industries as they could be mounted on existing installations. It would be impractical and expensive, however, to construct the bespoke structures that would be required to apply these instruments to a wider coastal observation network, particularly in deep water areas. The first wave buoys were developed in the 1960s as a response to the need for accurate and portable systems that could be deployed at a wide range of sites and operate autonomously. Wave buoy data are analysed extensively throughout this thesis, and two of the most frequently utilised types of buoys — the pitch-roll-heave (PRH) type and particle-following buoys — are described in detail in the following section. Some of the other established instruments that are commonly utilised as alternatives, or complements, to buoys are also discussed, as well a number of novel measurement systems that are currently undergoing development and have the to potential to be of practical use to the wave energy industry.

2.1.1 Particle Following Buoys

Surface following buoys have seen widespread application as measurement instruments in ocean engineering studies. The small size of these buoys means that they can be easily deployed and recovered by hand from a small craft, removing the need for specialist, and expensive, vessels. Datawell Directional Waverider buoys (Datawell BV 2010) are one of the most commonly utilised buoys of this type, and have been deployed at the AMETS and Galway Bay wave energy test sites, as detailed in Chapter 3. Other commercial particle following buoys include the Seawatch Mini II manufactured by Fugro-Oceanor, the model used in the Wave Hub measurement array (Ashton 2011), and the Triaxys directional buoy (AXYS Technologies Inc. 2012).

Figure 2.1: Datawell Waverider at the quarter scale test site in Galway Bay. Image courtesy of the Marine Institute.

Measurement Principle

Wave measurement from particle following buoys is predicated on the assumption that the buoy, which is small in comparison to the incident wavelengths, replicates the profile of passing waves. This is referred to as Lagrangian motion, as opposed to the Eulerian motion associated with surface profiles measured from fixed sensors. The buoy's low-frequency threshold for accurate response is dictated by its natural period. The Datawell Waverider has a diameter of 0.9 m; as a result it can accurately measure waves with periods in the range 1.6 – 30 s (Datawell BV 2010). The surface elevation is measured using an accelerometer that is housed within a stabilised platform. The observed vertical acceleration signal is double integrated to produce the heave motion of the buoy. Directional information is determined through analysis of the vertical and horizontal acceleration.

The accuracy of the directional Waverider, and its non-directional predecessor, has been validated in a number of studies against other sensors (Allender et al. 1989; Barstow and Kollstad 1991; O'Reilly et al. 1996). In particular, O'Reilly et al. showed that the estimates of directional parameters from the Datawell Waverider are a significant improvement on those produced by the NDBC 3 m Discus buoy that will be introduced in

subsequent sections. The latest Waverider models have dispensed with the traditional accelerometer and have incorporated a new sensor that operates using a differential Global Positioning System (GPS). This GPS sensor has been shown to replicate accurately the results provided by the accelerometer (Krogstad et al. 1999; de Vries et al. 2003), and has the additional advantages of having a low weight and no complex moving parts, which allows for trouble free transport and handling of the buoy.

Mooring

Mooring systems are an important component in wave buoy installations as they are required to keep the instrument on station without excessively affecting the motion of the buoy and the resulting measurements. The mooring requirements at different sites will depend on the water depth, as well as other processes such as the tidal wave, currents and the severity of the expected wave climate. Mooring layouts suggested by Datawell (Datawell BV 2010) for the water depths encountered at the Galway Bay and AMETS sites are shown in Fig. (2.2). The mooring line itself is composed of sections of polypropylene rope and rubber cord, with floats added to keep the line clear of the sea bed.

Poorly designed mooring arrangements have been shown to induce artificial buoy responses, which correspondingly add uncertainty to the derived wave parameters (James 1986; Allender et al. 1989; Niclasen and Simonsen 2007). Analytical analysis by James (1986) showed that for an idealised case a tethered buoy is unable to follow the surface particle motion. Allender et al (1989) conducted an extensive series of sea trials with several types of buoy and demonstrated that Waveriders display a tendency to underestimate highest waves in the most severe sea states as they traverse around the crest or get dragged below the surface to the wave. This issue is of concern to the research detailed in Chapter 7 of this thesis, which includes the analysis of extreme individual waves, and adds a degree of uncertainty to observations of large and steep waves. Niclasen and Simonsen (2007) observed variations in the measured wave height that were correlated with tidal conditions in buoy data collected at a number of locations around the Faroe Islands. It was postulated that increased drag forces, due to insufficient

mooring flexibility when current velocities were strongest, prevented the buoys from following the true profile of the highest wave. The influence of tidal currents on the measurements of wave height at AMETS is likely to be minimal as previous measurement campaigns have indicated that the velocity rarely exceeds 0.4 m/s (Murphy 2011).

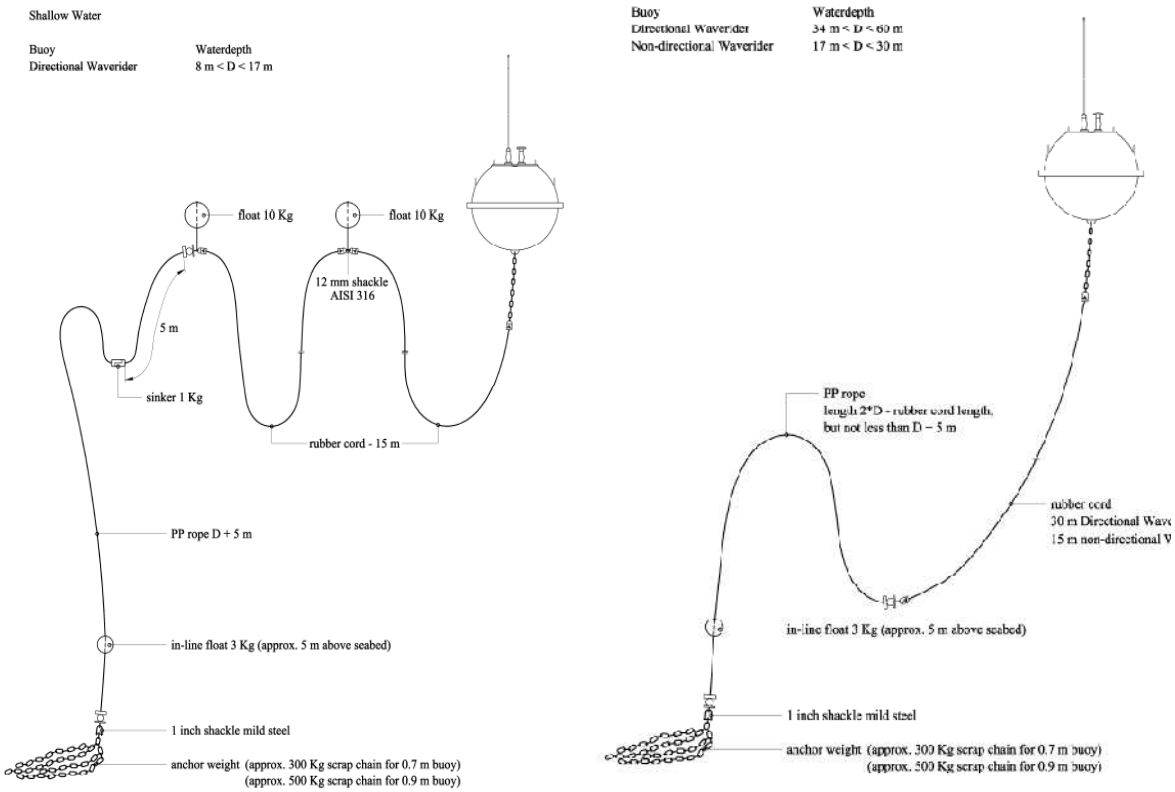

Figure 2.2: Mooring arrangements for Datawell Waveriders in shallow (< 17 m) water (left) and water depths up to 60 m (right). Images from Datawell (Datawell BV 2010)

2.1.2 Pitch-Roll-Heave Buoys

Pitch-roll-heave buoys (PRH) are disc-shaped buoys that follow the slope of the sea surface, as opposed to tracking the orbital motion like the particle following buoys discussed previously. As the name suggests, the pitch and roll inclinations are measured, along with the vertical heave, using a sensor such as the Datawell Hippy (Mettlach 2010) or the OCEANOR Wavesense (Fugro OCEANOR 1999). The combination of these measurements allow the directional properties of waves to be determined; these were the

earliest buoys that had this capability (Tucker and Pitt 2001). The large size of these buoys also makes them suitable platforms for housing other metocean sensors for the measurement of wind speed, barometric pressure and air temperature. Data from PRH buoys have been used in this research to complement the measurements collected by the Waverider buoys at AMETS and in Galway Bay. A Fugro Wavescan buoy was positioned at the 100 m depth berth at AMETS over the course of two deployments, with a cumulative duration of almost 12 months. Records from the NDBC network, described in Section 3.4. have also been of use. The NDBC primarily operated the 3 m Discus buoy, though 6 m and 12 m diameter variants are also used in areas where survivability is a concern. These buoy types are shown in Fig. 2.3.

Figure 2.3: PRH Buoys; Fugro Wavscan deployed at AMETS and NDBC 3 m Discus Buoy. Images courtesy of SEAI and NDBC.

2.1.3 Alternative Wave Measurement Systems

Acoustic Doppler Current Profilers

Acoustic Doppler Current Profilers (ADCP) have been widely used in the assessment of the tidal energy resource, however information about wave conditions can be obtained by

adapting the existing system. Directional wave spectra are computed from the orbital velocities of passing wave, which are measured using high frequency pulses which are reflected from the moving water particles. The water surface elevation is measured by either a pressure sensor or an additional vertical beam. Comparisons between the measurements of co-located ADCPs and wave buoys have been shown to display good agreement, particularly for wave height parameters (Jeans et al. 2002; Hoitink and Schroevers 2004; Strong et al. 2012).

These instruments are generally positioned on the ocean floor. The seabed location has the advantage of reducing the risk of the instrument being lost to extreme environmental conditions or damaged by passing vessels, however it also increases the complexity of deploying and recovering the ADCP and requires the measured data to be stored internally, rather than being transmitted back to shore. This eliminates the opportunity to conduct real time monitoring of the wave conditions — an important consideration for WEC deployments — unless the instrument is serviced by a costly cable. Additionally, the deployment depths of ADCPs are limited by the angles of the side beams. Deployment durations are determined by operating life of the battery system, and unlike large buoys there is no option to augment the power budget with photovoltaic cells.

HF Radar Systems

Wave measurement using high frequency (3 – 30 MHz) radar systems is based on the scattering of electromagnetic waves from the rough ocean surface. It is possible to derive wave spectra from the application of processing techniques to the backscattered Doppler spectra, as described by Essen et al. (1999). Pairs of radar stations can measure wave data from a wide area; for example the WERA system has an operational limit of 110 km, with a spatial resolution as fine as 150 m over shorter ranges, depending on its range of operational frequencies (Helzel Messtechnik 2009). This gives the system the potential to quantify the spatial variability of the wave field, which will be an important consideration once WEC arrays are developed. Comparisons of data collected from a Pisces HF system with buoy measurements from the Celtic Sea and showed that there was a good degree of correlation between the concurrent values of H_{m0}, thought the results for period and

directional parameters were not as promising (Wyatt 2009). Radar systems can also be used to measure surface currents, though they are unable to produce depth profiles of the current speed, and as they are remote sensing instruments and they have the advantage of being easy to access and maintain.

Figure 2.4: WERA system overlooking Dingle Bay with the antenna array visible in the foreground. Image courtesy of James Kelly, HMRC.

Satellite Measurements

Satellite measurements, using either altimeter or synthetic aperture radar (SAR) systems allow wave data to be collected at a global scale, and have been used as input for a number of assessments of the worldwide wave energy resource (Mørk et al. 2010; Arinaga and Cheung 2012). Altimeters compute wave statistics from the backscatter detected in high frequency pulses that the sensor directs at the ocean surface, whereas SAR systems produce a directional spectrum from analysis of high resolution representations it captures of the wave fields beneath its path (Holthuijsen 2007). Other authors have provided validations of altimetery and SAR measurements against in situ buoy data (Durrant and Greenslade 2007; Collard et al. 2009). Long duration datasets of these measurements are also available (GlobWave Project 2012), and have been utilised as a complement to hindcast models in studies of the interannual variability of wave

energy resource, and its influence on WEC output (Mackay et al. 2010). Unfortunately the data collected by these methods are not continuous, as gaps of several days exist between satellite passes over the same point, and altimeter systems perform poorly when operating close to land, where most WEC farms will be installed.

Pressure Sensors

Pressure sensors are measurement instruments which incorporate strain gauges to monitor the fluctuations in pressure – which attenuates with increasing depth – as waves pass overhead. As with ADCPs the accuracy of pressure sensors is limited by the deployment depth as high frequency waves penetrate the water column less than long period swell. For example the Valeport MIDAS recorder is only able to measure was with periods greater than 7 seconds at a depth of 20m (Valeport Ltd. 2004). This limits the use of these instruments to nearshore studies. Additionally, pressure sensors share many of the access issues faced by ADCPs due to their positioning on the seabed, though they have been observed to operate satisfactorily even when covered by a layer of sand and mud (Tucker and Pitt 2001).

Wave Gliders

Wave gliders, such as the model operated by Liquid Robotics, are mobile measurement platforms that can operate autonomously or be manually controlled by a technician onshore. The glider is propelled by a group of sub-surface foils which convert wave action into forward motion, while onboard solar panels power the data measurement and communication systems. Wave measurement is carried out using a Datawell GPS sensor, with a filter applied to account for the hydrodynamic response of the glider (Liquid Robotics 2012). The instrumentation that the glider carries can also measure physical oceanographic parameters, such as salinity and CO_2 concentration, as well as detecting the presence of marine mammals (Hine et al. 2012). In 2011 Liquid Robotics initiated the Pac-X project, involving four Wave Gliders deployed in Monterey Bay, California, crossing the Pacific; two to Australia and two to Japan (Liquid Robotics 2012). The progress of the buoys can be followed on the project website referenced earlier and the

measured data have been made freely available to access. Potential applications for wave gliders in the context of wave energy could include a series of short term deployments to provide validation data for numerical wave models at a large number of locations of interest at a prospective commercial site or the collection of a range of distances in the lee of an array of devices to help understand wake effects.

Seismic Observation

Another novel method for measuring wave conditions through the analysis of measurements from terrestrial seismic stations is being developed by researchers at University College Dublin. Ocean waves induce pressure changes on the sea bed, which in turn generate 'microseisms' that can be detected within the background seismic noise. Preliminary results that have been presented indicate that values of significant wave height computed from the recorded seismic data are reasonably well matched to the conditions observed offshore by measurement buoys (Moni et al. 2012). It is not possible to generate time series of surface elevation, or wave spectra, using this method so it would be unsuitable as a standalone system for the purpose of wave energy resource characterisation. It could be useful, however, as a complement to point measurements and as a means to validate numerical wave models. An extensive network of observation stations already exists in Ireland and maintenance of the equipment is relatively cheap and uncomplicated; unlike other wave measurement instruments it is positioned onshore and can be easily accessed, similar to the radar systems mentioned previously.

2.2 Wave Data Processing and Analysis

Analysis tools are applied to measured wave data in order to extract useful parameters which describe sea states and information about the composition of the wave spectra, important factors for characterising the wave energy resource and predicting the performance of WECs. The research detailed in this thesis utilises the data output files produced by measurement buoys — primarily Datawell Waveriders — that have been operating at the Irish wave energy test sites introduced in Chapter 3. Three file-types were processed and analysed for the research work presented in this thesis:

- Time series of the measured surface elevation, with a duration of 30 minutes, measured at a sampling frequency of 1.28 Hz for directional waveriders (.raw files)
- Spectral density, including directional parameters, for 64 frequency components ranging from 0.025 Hz to 0.58 Hz (.spt files). These are the average eight spectra produced from the Fourier analysis of 200 s of surface elevation time series.
- Processed results of wave-by-wave analysis performed using the zero-upcross method (.wvs files).

Further details about these, and several other, files generated by the buoys can be found in the Datawell documentation (Datawell BV 2012a). The collected wave data are initially processed and stored by the Marine Institute and can be accessed through a secure FTP website (Marine Institute Data Requests 2012). The analysis methods applied to these data files to produce sea state descriptors are described in the following sections.

2.2.1 Spectral Analysis

The irregular profiles of surface elevation that are observed in real sea states, such as the measured time series illustrated in Fig. 2.4, initially appear complex. They can be simplified and understood, however through the application of a variety of techniques. Time series analysis using a wave-by-wave approach, such as the downcrossing method outlined by Tucker and Pitt (2001), can produce parameters such as the significant wave height, H_s, the maximum wave height, H_{Max}, and the average period, T_z. Longuet-Higgins (1952) demonstrated that the wave heights in a record follow a Rayleigh distribution, which allows the variance of the sea state to be computed.

Frequency domain analysis is perhaps the most powerful tool for the analysis of wave data. Sea surface elevations can be decomposed into combinations of a number of harmonic components of varying amplitudes, spread over a range of frequencies. Applying spectral analysis to the discrete measured data, most commonly through the use of the fast Fourier Transform (FFT) algorithm (Cooley and Tukey 1965) allows the spectral variance density function, S(f), — generally referred to as the wave spectrum — to be calculated. S(f) indicates the contribution that discrete bands of frequency make to the total variance, and corresponding energy, of an irregular sea surface. The process

followed to determine S(f) is already well understood and it was not necessary to modify or enhance existing techniques to carry out the research described in this thesis. Complete descriptions of the theory of spectral analysis and its application to wave data are provided by Barrett (2010) and a number of ocean engineering textbooks (Dean and Dalrymple 1991; Tucker and Pitt 2001).

Dean and Dalrymple (1991) also describes methods of smoothing the resultant spectra through the use of segmenting and the application of moving averages to curtail any errors or noise associated with spectral analysis. Segmenting involves splitting the time series into a number of portions (N), applying spectral analysis to each individual section and averaging the resulting spectra. The resulting spectral estimate is then considered to have a chi-squared probability distribution with 2N degrees of freedom. Examples of the results of this process are presented in Fig. 2.5. Spectra for a 30 minute time series (part of which is illustrated in Fig. 2.4) are computed while varying the number of segments (N = 1, 3, 6, 9) and applying a fixed moving average. Increasing N is shown to reduce noise and result in a smoother spectral profile; however adding degrees of freedom also reduces the spectral resolution, so this must be balanced by ensuring that important spectral details are not lost in the smoothing process.

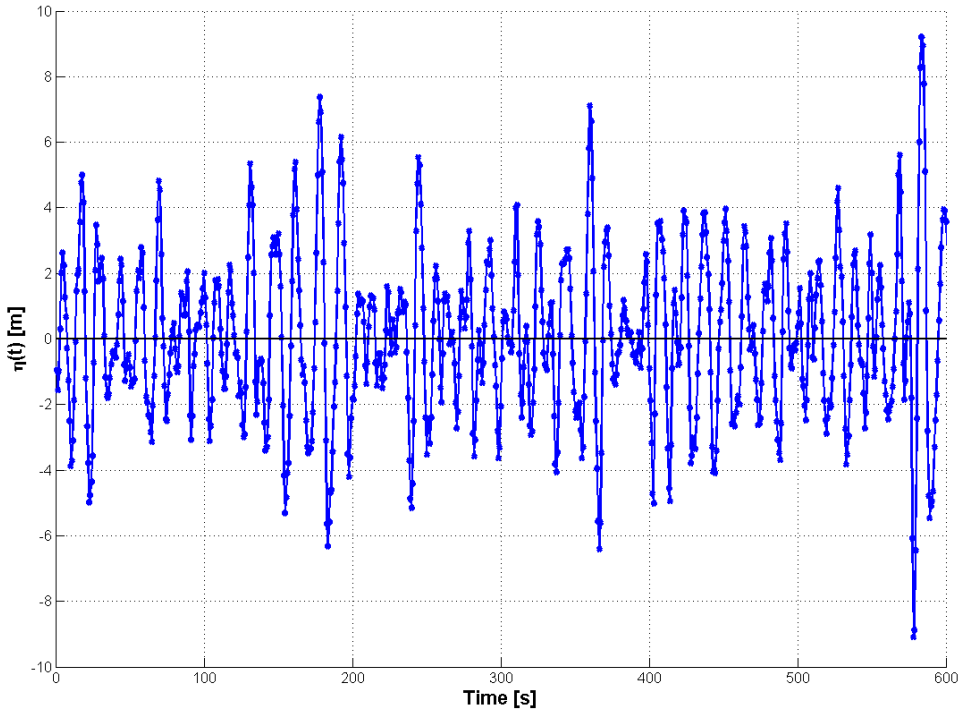

Figure 2.5: Measured time series of sea surface elevation from the Atlantic Marine Energy Test Centre.

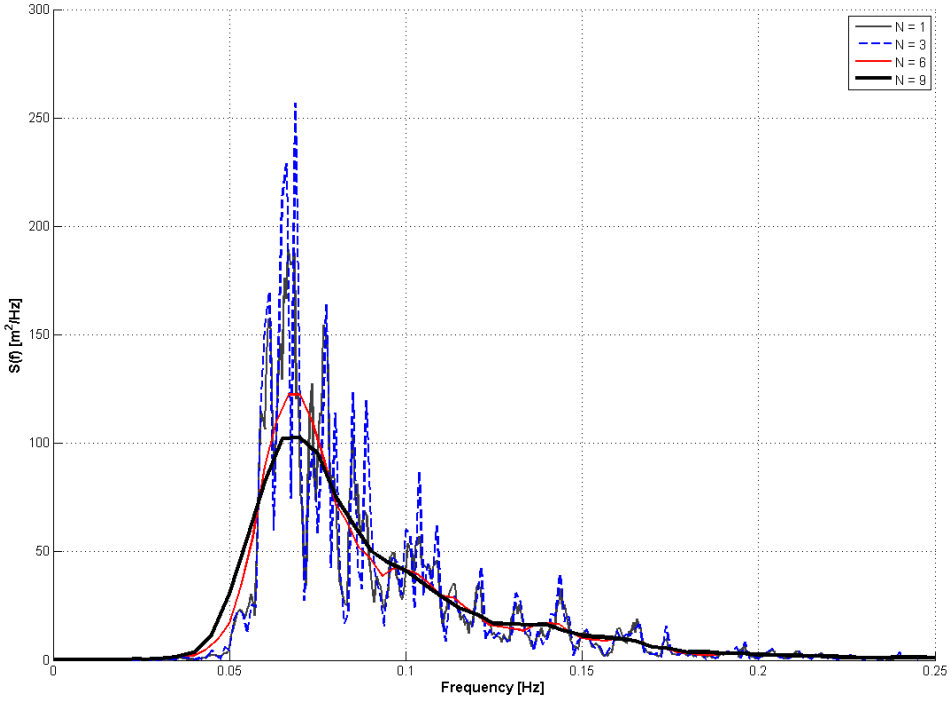

Figure 2.6: Wave spectra produced by N segments

The resulting variations in the derived parameters from measurements collected over the course of one day from the Waverider buoy deployed at the Atlantic Marine Energy Test Site (AMETS) are plotted together in Fig. 2.6. It is noticeable that different methods of spectral estimation do not have a significant effect on the calculation of the significant wave height, H_{m0}, and the energy period, T_E, whose magnitude depend on the overall spectral shape. Parameters derived from higher order spectral moments, or those such as T_p which is the inverse of the peak frequency, are seen to be more sensitive to spectral smoothing. These parameters are described in more detail in Section 2.2.4. Increased variability is observed in parameters which depend on a small number of spectral points, in this case the peak period, T_P. This is consistent with results presented by Rodriguez et al. (1999), who assessed a range of different segmenting and alternatives to Fourier analysis such as the maximum entropy method.

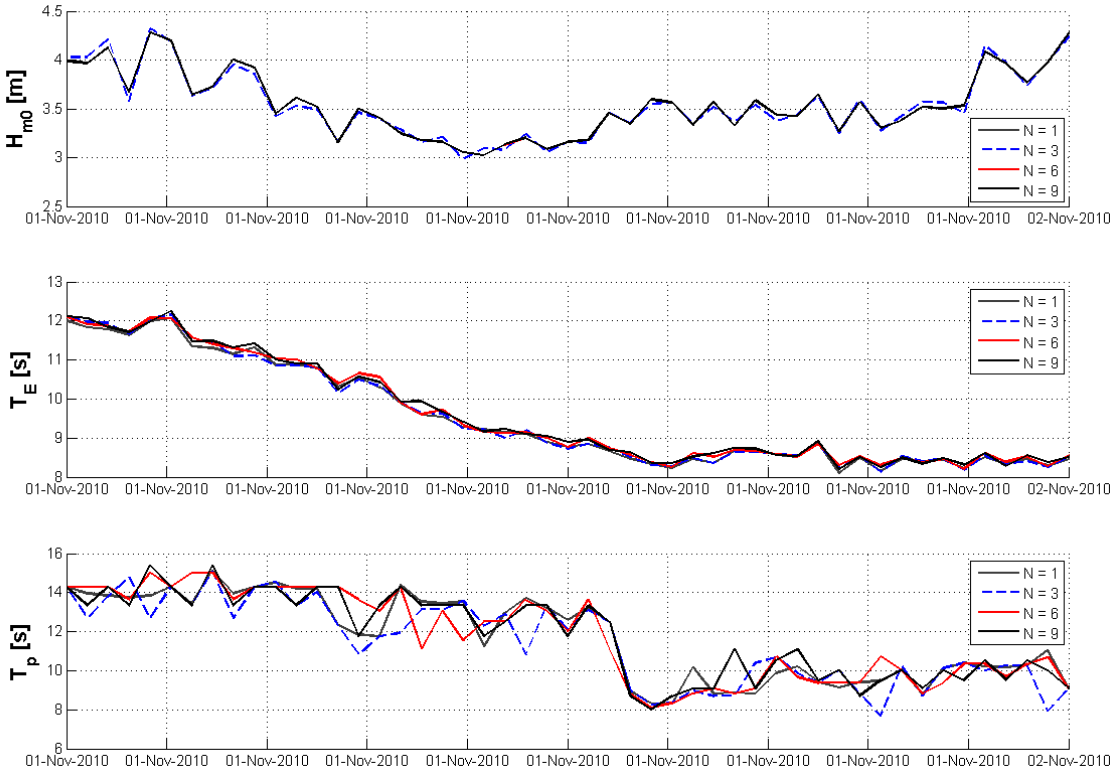

Figure: 2.7: Parameters derived from wave spectra produced by N segments

2.2.2 Analysis of Wave Spectra

Computing the moments of the wave spectrum provides a means to calculate summary statistics which describe the nature of a sea state and also allows the time-averaged incident power to be estimated. The n^{th} spectral moment is given by Equation (2.1) and the formulae for determining some of the most commonly utilised parameters are detailed in Table 2.1. H_{m0} is an approximation of H_s, the significant wave height derived from time series analysis; similarly T_{02} is equivalent to the zero-crossing period T_z. T_E, the energy period, is defined as being equivalent to the period of monochromatic wave whose height is equal to H_{m0}, and which has the same energy as the irregular sea state in question. The peak period, T_P, is not calculated using spectral moments. It is instead given by $1/f_p$, where f_p is the frequency component with the highest value of S(f).

$$m_n = \int_0^\infty f^n S(f) df \tag{2.1}$$

Parameter	Symbol	Moment Definition
Significant Wave Height (m)	H_{m0}	$4\sqrt{m_0}$
Energy Period (s)	T_E	m_{-1}/m_0
Zero-crossing period (s)	T_{02}	$\sqrt{m_0/m_2}$
Mean Period (s)	T_{01}	m_0/m_1

Table 2.1: Wave parameters derived from Spectral Moments

The power per unit width, P, of a regular wave was given by Falnes (2002) in terms height, H, and period, T, in Equation (2.2). A derivation of P for the more practical case of an irregular sea state, described by the spectrum S(f), is provided by Tucker and Pitt (Tucker and Pitt, 2001), and is presented here as Equation (2.3).

$$P = \frac{\rho g^2}{32\pi} T H^2 \quad [W/m] \tag{2.2}$$

$$P = \rho g \int C_g(f) S(f) df \quad [W/m] \tag{2.3}$$

ρ is the density of sea water, usually taken as 1025 kg/m^3, and g is acceleration due to gravity. C_g refers to the group velocity of the frequency components of the wave

spectrum and is a depth-dependant term. Equation (2.3) can be simplified and written in terms of the m_{-1} spectral moment — Equation (2.4) — if deep water conditions are assumed, though the validity of applying this assumption is questioned in Chapter 5 of this thesis.

$$P_0 = \frac{\rho g^2}{4\pi} m_{-1} \quad [W/m] \tag{2.4}$$

In practice, Equation (2.4) is usually rewritten in terms of H_{m0}, significant wave height, and T_E, the energy period.

$$P_0 = 0.49 H_{m0}^2 T_E \quad [kW/m] \tag{2.5}$$

Spectral bandwidth is increasingly becoming considered as an important parameter for the representation of sea-states, and is particularly useful in the study of spectral shape. Saulnier et al. (2011) illustrated the sensitivity of the performance of certain types of WECs to the spectral bandwidth and proposed that bandwidth be included with H_{m0} and T_E as one of the standard sea state descriptors for characterising the energy resource . Saulnier et al. also compiled a comprehensive review of bandwidth parameters that have been proposed in literature and outline the strengths and weaknesses of the various formulations. Two bandwidth parameters, ε_1 and ε_2, which are defined below, are particularly useful as they exhibit less sensitivity to high frequency, low energy components of sea-states when compared to their alternatives that are derived using higher order spectral moments. The parameter ε_1 was first computed with studies of wave energy in mind (Smith et al. 2006) and is defined in Equation 2.6 as:

$$\varepsilon_1 = \sqrt{\frac{m_1 m_{-1}}{m_0^2} - 1} \tag{2.6}$$

The commonly utilised Narrowness Parameter, ε_2, is expressed in Equation 2.7 as

$$\varepsilon_2 = \upsilon = \sqrt{\frac{m_0 m_2}{m_1^2} - 1} \tag{2.7}$$

The values of these bandwidth parameters range from 0 to 1, with narrow banded spectra having the lowest values. For the theoretical Bretschneider Spectrum, introduced in Section 2.2.3, it can be shown that ε_1=.33 and ε_2=0.42.

2.2.3 Standard Spectral Shapes

Several standard spectral shapes have been derived empirically. These are useful instruments as they allow idealised spectra to be produced when only summary statistics are available at a location and can also be used as references to compare measured spectra to. One of the most frequently utilised of the standard spectral shapes is the Generalised Pierson-Moskowitz Spectrum, also known as the Bretschneider Spectrum (Pierson and Moskowitz 1964). This formula describes the case of fully developed conditions that exist in deep water where the sea-state and the local winds are in equilibrium and is generally considered to be representative of conditions off the Irish west coast (Holmes and Barret 2007). While the original Pierson-Moskowitz spectrum requires only the wind speed at a height of 19.5m above water level ($U_{19.5}$) as its sole input parameter, the spectral density function for the Bretschneider spectrum is specified by input values of H_{m0} and T_{02} and takes the form

$$S(f) = Af^{-5}e^{-Bf^{-4}} \tag{2.8}$$

A and B are independent parameters. As Tucker and Pitt (2001) show, these can be found from the relationships

$$T_{02} = 0.751B^{-0.25} \tag{2.9}$$

$$H_{m0} = 2\sqrt{\frac{A}{B}} \tag{2.10}$$

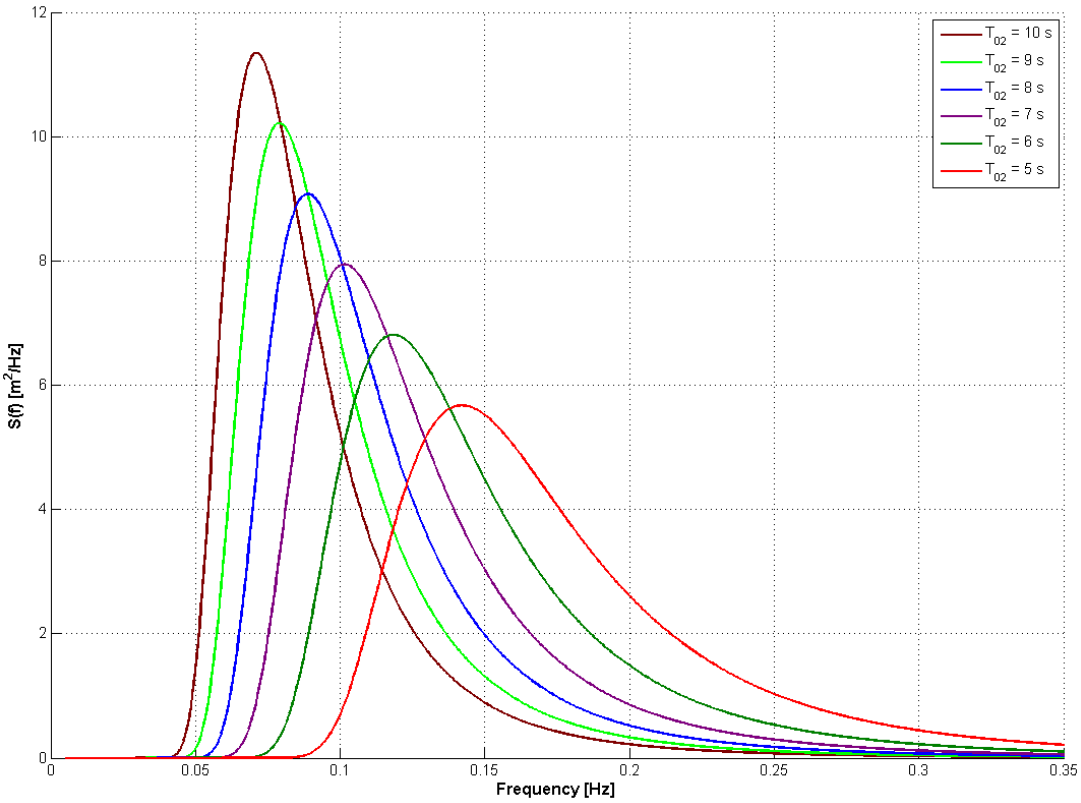

Figure: 2.8: Bretschneider Spectrum with constant Hm0 (3 m) and T02 = 5 – 10 s.

Equation (2.1) can also be given the general form

$$m_n = \frac{1}{4} A B^{\left(\frac{n}{4}\right)-1} \Gamma\left[1 - \left(\frac{n}{4}\right)\right] \tag{2.11}$$

where Γ is the Gamma Function mathematical operator and n<4. The application of Equation (2.11) allows the moments of the Bretschneider Spectrum to be rewritten in Table 2.2 in terms of the constants A and B.

Spectral Moment	Bretschneider Form
m_{-1}	$0.226 \frac{A}{B^{5/4}}$
m_0	$\frac{A}{4B}$
m_1	$0.306 \frac{A}{B^{3/4}}$
m_2	$0.443 \frac{A}{\sqrt{B}}$

Table 2.2: Moments of the Bretschneider Spectrum

The JONSWAP Spectrum is employed to idealise fetch-limited wave conditions as well as to represent sea-states generated by storm events (Holthuijsen 2007). This formulation was developed through the Joint North Sea Wave Project and originally derived from measurements collected from thirteen wave measurement stations over a period of ten weeks in 1968 and 1969 (Hasselmann et al. 1973). The JONSWAP spectrum, $S_J(f)$, is commonly presented as a modification of the peak of the Pierson Moskowitz spectrum, referred to as $S_{PM}(f)$ in Equation (2.12).

$$S_J(f) = S_{PM}(f)\gamma^{exp\,(-0.5(\frac{f-f_p}{\sigma f_p})^2)} \tag{2.12}$$

In this case γ is the non-dimensional peak shape parameter and σ is a spectral width parameter. In the original data the average γ value was 3.3 and according to Equation (2.12) the JONSWAP spectrum follows the Pierson-Moskowitz shape when γ=1. The JONSWAP spectra for a fixed value of H_{m0} and T_{02} are plotted for a range of γ values in Fig. 2.8

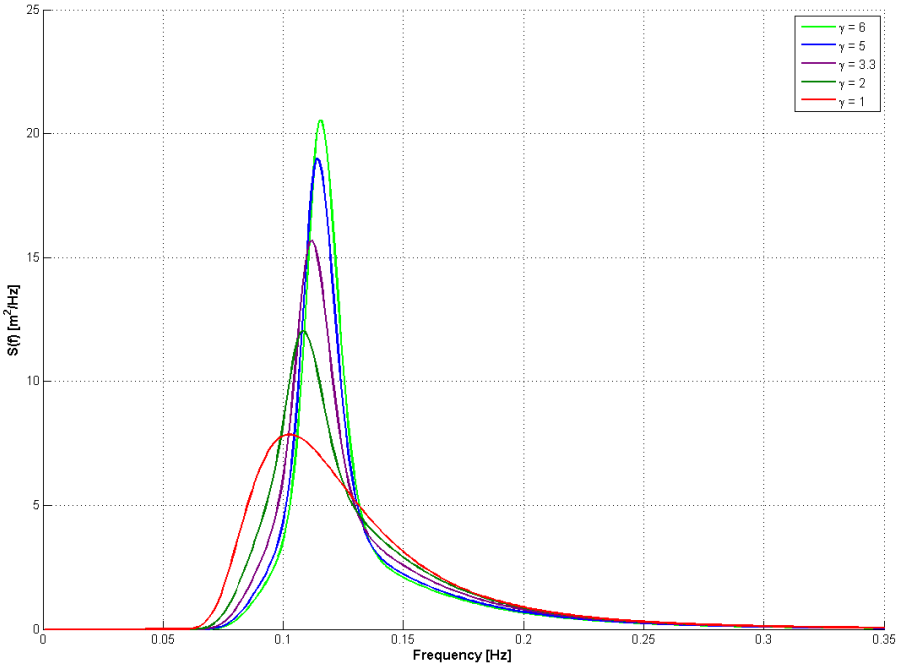

Figure: 2.9: JONSWAP Spectrum with constant H_{m0} (3 m) and T_{02} (7 s) for γ=1, γ=2, γ=3.3, γ=5 and γ=6.

Approximate spectral moments for the JONSWAP Spectrum have been derived previously (Det Norske Veritas 2010) and are presented in terms of H_{m0} and f_p in Table 2.3.

Spectral Moment	JONSWAP Form
m_{-1}	$\frac{1}{32\pi} H_{m0}^2 f_p^{-1} \frac{4.2+\gamma}{5+\gamma}$
m_0	$\frac{1}{16} H_{m0}^2$
m_1	$\frac{1\pi}{8} H_{m0}^2 f_p \frac{6.8+\gamma}{5+\gamma}$
m_2	$\frac{\pi^2}{4} H_{m0}^2 \omega_p^2 \frac{11+\gamma}{5+\gamma}$

Table 2.3: Moments of the JONSWAP Spectrum

2.2.4 Wavelet Analysis

One of the weaknesses of the spectral analysis method outlined in the previous section is that the signal being analysed is assumed to be stationary and ergodic, and that the frequency components do not change in time. As a result it has a limited capacity to monitor the short term temporal variability of wave records due to the presence of wave groups or the influence of fast moving meteorological fronts. This variability may impact on the power captured by WECs, many of which can only achieve optimal performance over a narrow frequency bandwidth. Many devices will also incorporate control systems whose design could be better informed by knowledge of the level of variability that can be expected over short time scales (Fusco 2012). The problems associated with using a frequency spectrum derived from Fourier analysis to describe wind waves are discussed thoroughly by Liu (2000), who remarked that the because the wave spectrum suppresses information about the temporal variability in the time series of wave elevation, the nature of potentially important local processes, which may occur in short time scales, is concealed .

A practical example of some of the weaknesses related to analyzing time series record using the Fourier transform is given by Massel (2001). Two distinct signals are compared. Signal A, illustrated in Fig. 2.9(a), is a superposition of three sinusoidal components with periods of 2 s, 5 s and 20 s respectively. Signal B is a 'chirp' type signal where the same three sinusoids in A exist at three different time intervals, Fig. 2.9(b). The frequency spectra for both these signals are calculated and plotted in Fig. 2.9 (c) and (d) respectively. Despite the intrinsic differences between A and B their resulting spectra display a great similarity in shape, though not in variance, with three distinct peaks corresponding to the frequencies of their component sinusoids. While the spectra highlight which frequency components exist in the analyzed signals they are unable to provide any information into when these components appear in time. This demonstrates the unsuitability of the wave spectrum for indicating the temporal variability in non-stationary signals.

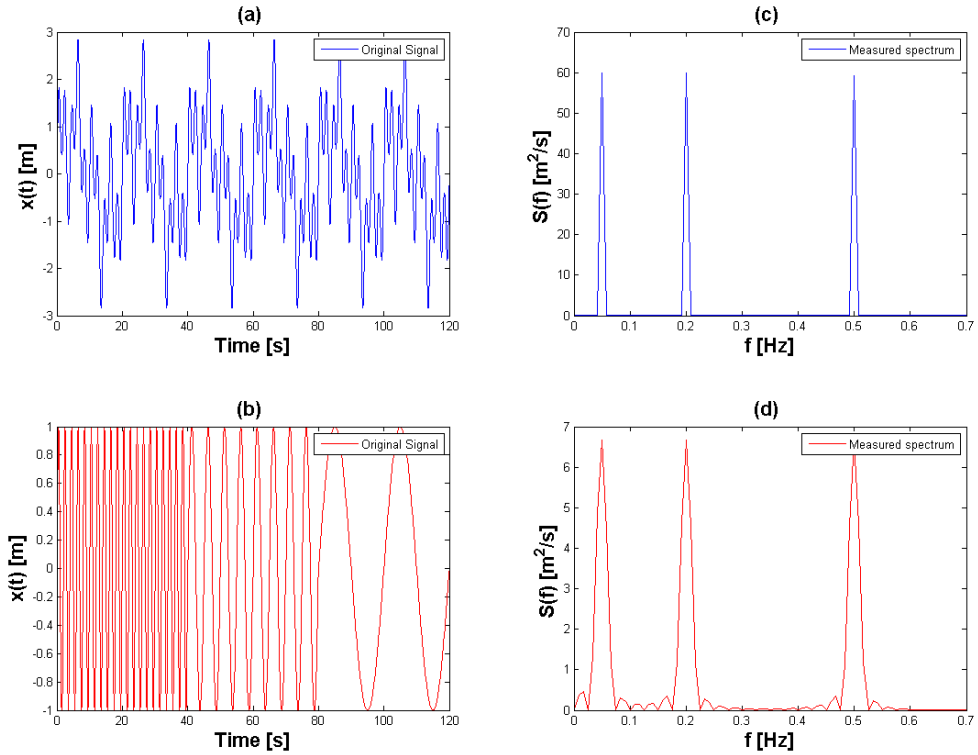

Figure: 2.10: (a) Three component sinusoidal signal (Signal A), (b) 'Chirp' type signal (Signal B), (c) Wave spectrum of Signal A, (d) Wave spectrum of Signal B.

The short-time Fourier transform based spectrogram has also been proposed as a tool to study the time-frequency variation of ocean waves (Guedes Soares and Cherneva 2005). This approach has an inherent disadvantage when compared to wavelet analysis as there is a lack of precision in the information it provides about temporal frequency development. This is due to the difficulty in selecting an appropriate section size into which the signal is divided. Long sections, while providing a good level of frequency resolution, offer a poor time resolution. Correspondingly, short sections perform well in terms of resolution in time but lack precision in frequency.

The wavelet transform is performed by decomposing the signal being analyzed into a set of localized basis functions which are formed by scaling the mother wavelet and shifting it in time. In contrast, in the Fourier transform the basis functions take the form of sines, cosines or complex exponential functions of infinite length. More detailed descriptions of the wavelet transform and mother wavelets can be found in a number of comprehensive references (Daubechies 1992; Torrence and Compo 1998). In summary, the wavelet transform, WT, of a signal x(t) represents the level of correlation between the wavelet and a localized portion of the signal and is defined by

$$WT(\tau, b) = \int_{-\infty}^{\infty} x(t) g_{\tau b}^{*}(t; \tau, b) dt \tag{2.13}$$

From Equation (2.14) the family of continuously translated and dilated wavelets is constructed by shifting a mother wavelet, g(t), the position, τ in time, and dilation with scale, b,

$$g_{\tau b}(t; \tau, b) = \frac{1}{\sqrt{b}} g\left(\frac{t-\tau}{b}\right). \tag{2.14}$$

The Morlet wavelet has been selected as the mother wavelet for the study described in this thesis as it has been employed extensively in ocean engineering applications (Massel 2001; Nolan et al. 2007). The Morlet wavelet, illustrated in Fig. 2.10, is given by

$$g(t) = e^{\frac{-t^2}{2}} . e^{ict} \tag{2.15}$$

where c is the frequency of the mother wavelet. For this study the routines contained in the MATLAB Wavelet Toolbox (Misiti et al. 2010) are utilized throughout.

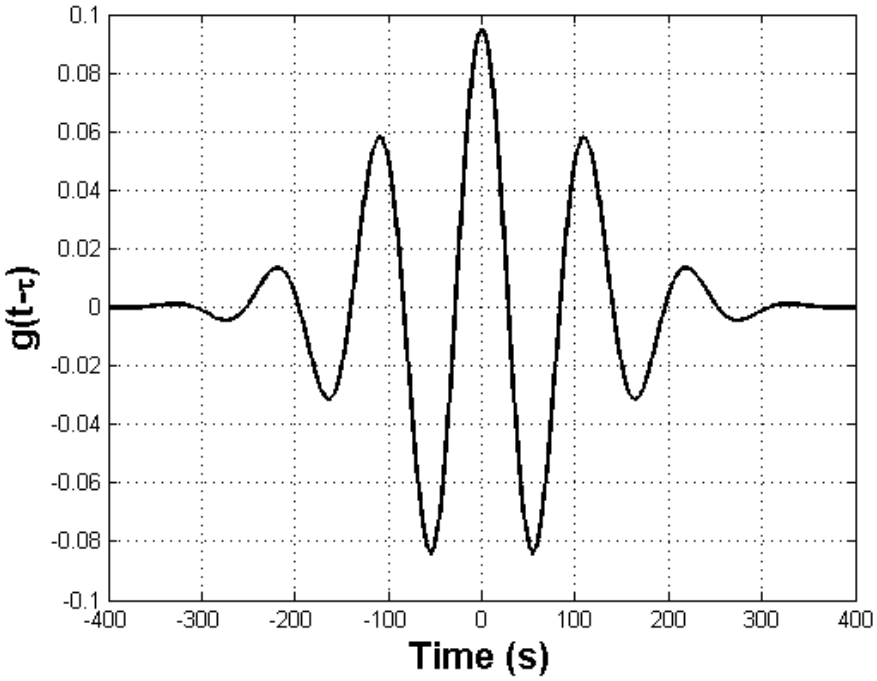

Figure: 2.11: Morlet wavelet

The benefit of using the wavelet transform over the Fourier transform is that it allows for precise localization in the both the time and frequency domains. This is evident when the wavelet transform is applied to the case of the simple signals introduced previously in Fig. 2.9. The absolute value of the wavelet transform of Signal A is illustrated in the contour plot in Fig. 2.11 with the corresponding values for Signal B shown in Fig. 2.12. In Fig. 2.11 it is possible to detect the presence of each of the three superimposed sine waves appearing throughout the time series whereas in Fig. 2.12 a noticeable shift through low to high scale — equivalent to wave period — components is evident.

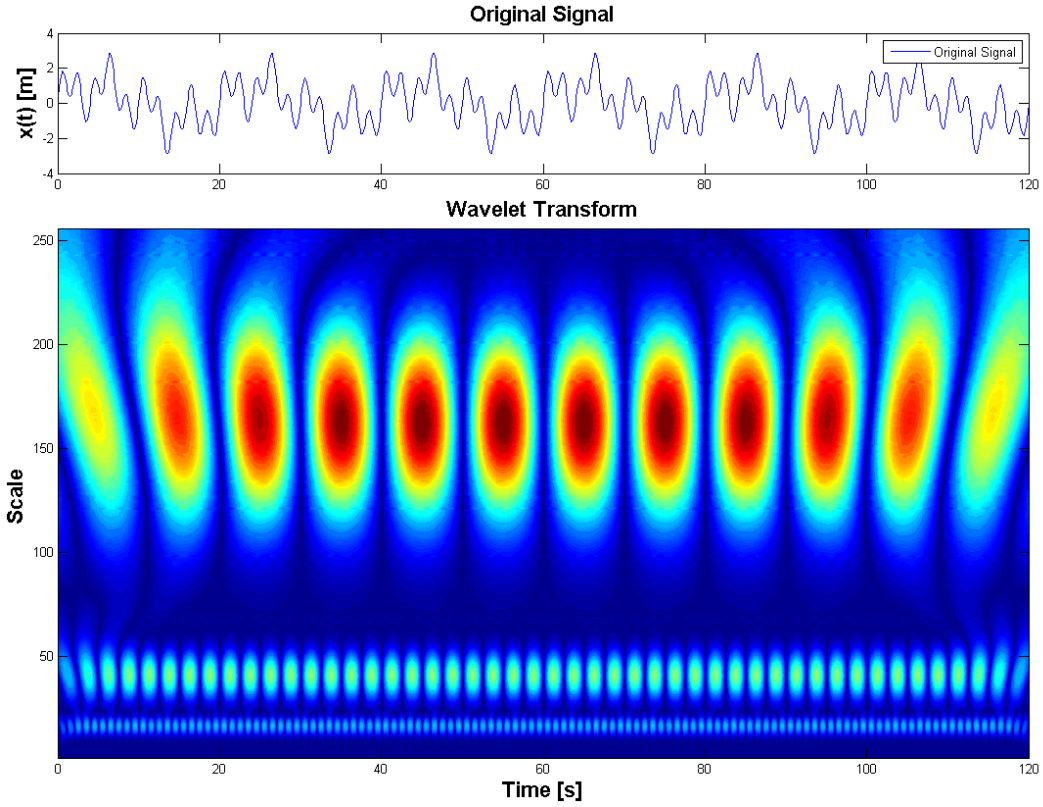

Figure: 2.12: Wavelet transform of the three component sinusoidal signal (Signal A)

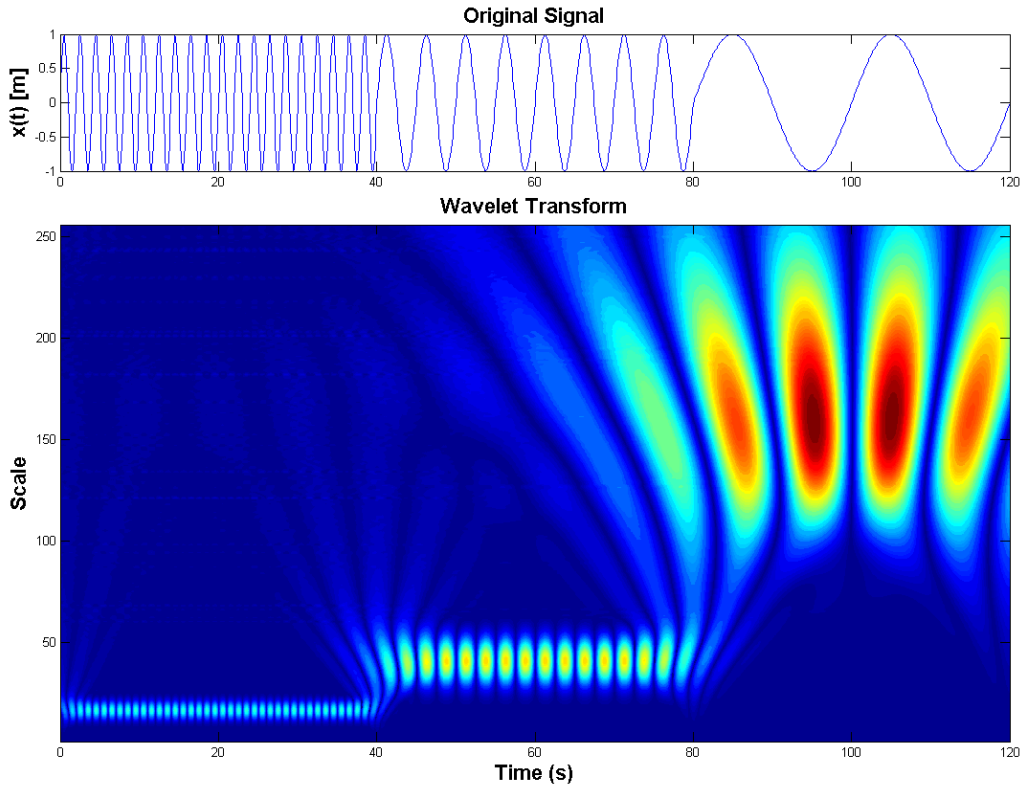

Figure: 2.13: Wavelet transform of the 'chirp' type signal (Signal B)

The wavelet transform has previously been proposed as an appropriate tool for quantifying the level of short term variability in wave energy (Nolan et al. 2007). This technique has also been applied to a wide range of ocean engineering research questions, such as the prediction of snap loads in tethered floating bodies (Lueck et al. 2000), the analysis of freak waves (Mori et al. 2002) and in a non-intrusive method of wave profiles in a laboratory flume (Lee and Kwon 2003). Wavelet analysis techniques are applied to measured wave data from the Galway Bay quarter scale test site in Chapter 8 of this thesis, where potential applications of this tool for characterising wave energy resource are discussed. Inspection of data from a concurrent deployment of two buoys also allows the deviation in short term resource variability over a 200m spacing to be examined.

2.2.5 Quality Control

Quality control (QC) of the data provided from measurement buoys is required to prevent erroneous or corrupted data from influencing the processing of spectra and the calculation of sea state parameters. The spectral files from the Datawell Waverider buoys in Galway Bay and AMETS are repaired during processing, but a QC procedure had to be implemented to ensure the validity of the surface elevation time series files. Many excellent references have been produced which outline QC methods, particularly the reports produced by the Quality Assurance of Real-Time Ocean Data (QARTOD) Working Group (Cruz et al. 2007; European Marine Energy Centre (EMEC) 2009; QARTOD 2009; van Os et al. 2011). An important point to note is that the purpose of these quality checks is to alert whoever is analysing the data to the presence of possible errors. It is recommended that no data should be automatically discarded. Instead, a series of flags should be created with the final decision on the suitability of the identified datasets resting with the user

The QC procedures implemented for this study are outlined below and draw from the references cited previously, as well as the methods applied by Barrett during analysis of the wave energy resource in Galway Bay (Barrett 2010). During the processing of time series files during this research QC flags were returned if any of the following criteria were met:

- Flag if the data transmission status is assigned a value greater than 1.
- Spike Test: Flag if a crest or trough height is exceeds $5\sqrt{m_0}$. The spectral value of m_0 will not have been calculated at this stage of the analysis process. Therefore an initial estimate is instead determined by following the approach of Cruz et al. (2007). It is assumed that the surface elevation follows a normal distribution, which allows m_0 to be calculated from the inter-quartile range (IQR) of the surface elevation. This estimate of m_0 is compared to the spectrally derived value for one month of measurements from AMETS in Fig. 2.13, and good agreement can be seen between the two parameters.
- Mean Test: Flag if surface elevation readings don't oscillate around zero, with a tolerance of ±1cm. Repair or delete dataset depending on visual inspection.
- Mean shift test: Flag if the mean of consecutive sections of the time series varies by more than ±10cm. The time series is divided into sections of 256 points for this test.
- Flat episodes test: Flag if there are five or more sections in the series with unchanging, or very slowly changing (±1cm), values.

Additionally, the H_{m0} vs. T_E occurrence scatter diagram is visually inspected once the parameters are computed to check for possible outliers such as unusually high or steep sea states and the directional wave rose plot is checked to ensure that significant contributions of energy are not indicated as arriving from unusual directions, such as from the shoreline.

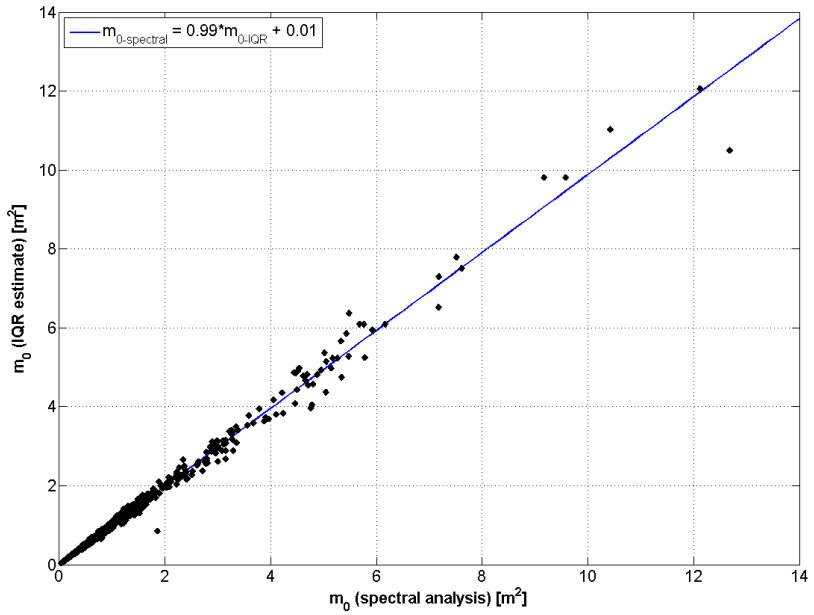

Figure: 2.14: m_0 values produced by spectral analysis and from the inter-quartile range.

Flagged time series would be visually inspected and an attempt to repair if the error count was not excessive (< 5% of points). Spurious points or spikes would be replaced by mean value of the surface elevation and any mean trends removed so that the time series oscillates around zero.

2.3 Review of Existing Resource Assessment and Characterisation Studies

A detailed understanding of the metocean environment and the wave energy resource is imperative for the design of WEC concepts and the planning and deployment of arrays of devices. Standards and guidelines being proposed in this area have identified the development of this understanding as being a multi-stage process (EquiMar Group 2010a; Folley et al. 2012). In this work the initial estimation the wave energy available for capture by WECS at a point of interest will be referred to as resource assessment. Resource characterisation will be considered an extension of the site assessment phase and explore the fundamental qualities of the resource that will influence the performance of a device undergoing testing or a commercial scale installation. These characteristics

include the relative occurrence and energy contribution of particular sea states, seasonal and interannual variability of the resource, extreme events and short term temporal and spatial variability.

2.3.1 Defining the wave energy resource

Bi-variate scatter plots of important summary statistics, typically pairs of H_{m0} and T_E, provide a useful method of ascertaining an overall understanding of the wave climate and the energy resource at an area of interest. The Equimar Protocols attempt to standardise the production of scatter plots (EquiMar Group 2010a), as does a similar EMEC publication (EMEC 2009). A number of the suggested conventions include:

- Each bin should display the cumulative occurrences of the H_{m0}-T_E pair. For normalised scatter diagrams, for example the contribution to energy of particular sea states, the total number of data points must be included.
- H_{m0} bins should be defined in intervals of 0.5 m over the range 0.5 m - 15 m
- T_E bins should be defined in intervals of 0.5 s over the range 0.5 s – 25 s

The format presented here was originally developed by Barrett (2010), though some adaptations have been made. A typical scatter plot is illustrated in Fig 2.14 for the measurements returned by the Waverider buoy at AMETS for October 2010. The standards mentioned previously were used as guidelines, but were not rigidly followed. In particular, the proposed range and sizes for the period bins is unwieldy as it results in too many small, and difficult to read, cells. These are also spread over a greater range than is necessary as T_E values exceeding 20 s are unlikely for the sites that are studied in this research. Lines of limiting sea state steepness, S_S, — determined using H_{m0} and T_Z in Equation (5.3) — are also included, following the DNV guidelines (Det Norske Veritas 2010). DNV recommend that the limiting sea state steepness for severe conditions — $T_Z \geq 12$ s — is represented by the 1/13 line. The slope of 1/10 is appropriate for shorter period sea states ($T_Z \leq 6$ s). The slope of a fully developed sea, following the Pierson-Moskowitz shape, is 1/20. As these limits were initially defined in terms of T_Z it was necessary to convert them to their equivalent T_E values using an appropriate wave period ratio, as discussed in Chapter 4.

$$S_s = \frac{2\pi H_{m0}}{gT_Z^2} \tag{2.16}$$

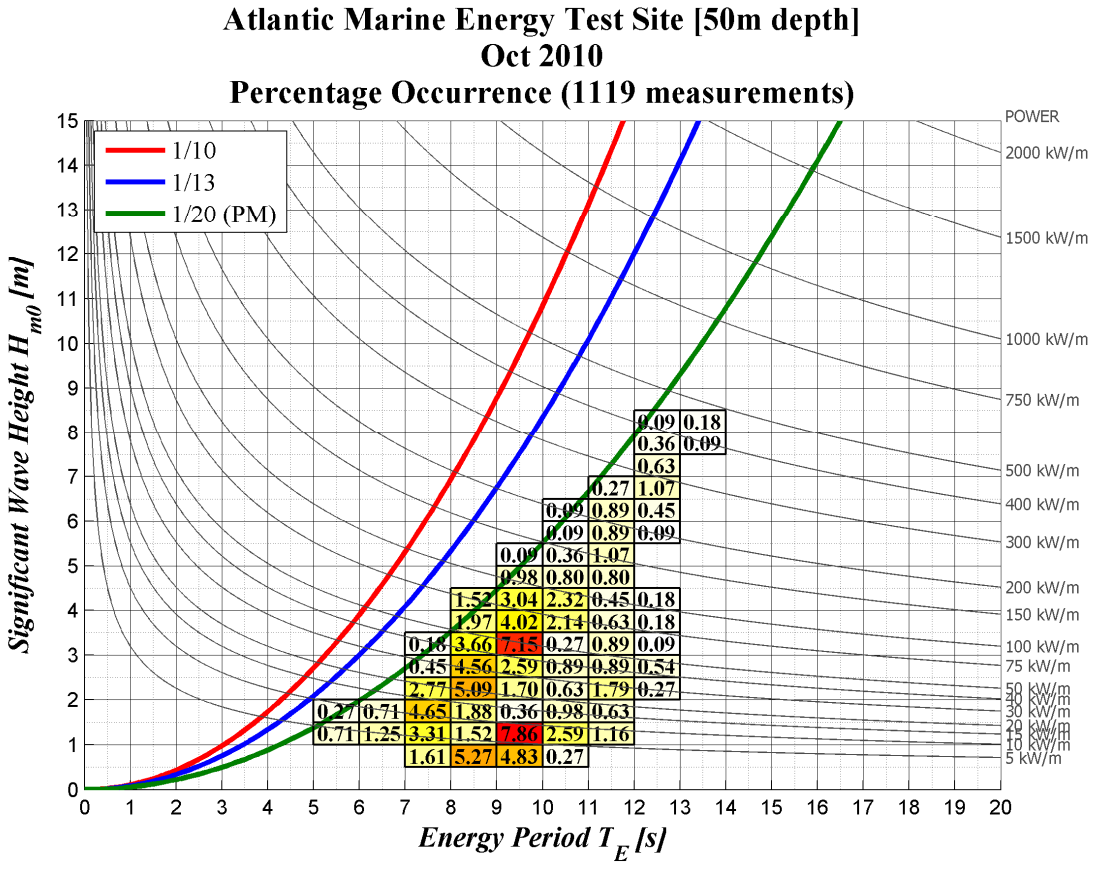

Figure: 2.15: H_{m0} – T_E scatter plot of percentage occurrence for October 2010 data from 50 m depth at AMETS.

The standard parameter for defining the magnitude of the theoretically available wave energy at a location of interest is the mean omni-directional wave power derived from Equation (2.3), often referred to as the wave power density (EMEC 2009; EquiMar Group 2010a; Folley et al. 2012; IEC Technical Committee 114 2012). In many cases the simplified formulae presented in Equations (2.4 – 2.5), which assume deep water conditions, are used in place of Equation 2.3 (Gunn and Stock-Williams 2012). If values of T_E are unavailable for the measured or modelled data, T_{02} (or its equivalent T_z that is derived from time series analysis) is usually provided in its place. This was true of the standard Irish wave energy resource atlas (ESB International 2005). The conversion of T_{02} to T_E is discussed in detail in Chapter 4, where it is shown that incorrect assumptions

about the relationship between these period parameters have led to inaccurate estimates of wave power.

Chapter 5 of this work will demonstrate that the highest sea states experienced at a typical site on the Irish west coast disproportionately contribute to the total incident wave energy. These sea states occur infrequently and are the products of severe storms. WECs are unlikely generate power in these conditions as they will be designed to enter survival mode to protect components from the extreme forces present. This problem was identified in an early paper by Salter, who suggested that installations should be capable of submerging to avoid the worst conditions (Salter 1974). As a result the average theoretical power will not accurately reflect the magnitude of the resource that can be safely captured by devices. The concept of exploitable power, P_{exp}, was introduced by Folley and Whittaker to account for this discrepancy (Folley and Whittaker 2009). P_{exp} is defined in Equation (2.17) as four times the mean of the average incident wave power, where P_i refers to the individual values of theoretical power calculated from Equation (2.3). For highly energetic sea states any power above the P_{exp} is deemed to be superfluous and is discounted. Though the value of P_{exp} given by Equation (2.17) is somewhat arbitrary, it nonetheless provides a useful tool for ascertaining more realistic estimates of the accessible wave energy resource and of what sea states should be deemed to be most important for the capture of wave power by a WEC.

$$P_{exp} = 4\frac{\sum_{i=1}^{N} P_i}{N} \tag{2.17}$$

This approach is extended and refined in the most recent study of the national wave energy resource of the United States (Electric Power Research Institute 2011). The technically available wave energy is computed to three operating conditions: the threshold operating condition (TOC), the rated operating condition (ROC); and the maximum operating condition (MOC). The TOC is the equivalent to the cut-in speed of a wind turbine; it is assumed that a WEC could not generate efficiently below this value. The ROC represents the maximum amount of energy that can be extracted from a unit width of the wave field. Several different ROC values were used in the US resource assessment to account increased device performance efficiencies and packing densities. No energy is captured if the incident wave power exceeds the MOC as devices are

assumed to enter survival mode. The TOC and MOC values were adjusted to reflect the wave climate and to ensure a sensible operating range by maintaining a 1:100 ratio between the TOC and MOC. Thus for the west coast of the US TOC and MOC values of 3 kW/m and 300 kW/m were applied, whereas TOC = 1 kW/m and MOC = 100 kW/m for the less energetic Gulf of Mexico. This approach has a similar weakness to the exploitable power metric as it relies on relatively subjective thresholds and does not fully simulate the performances of real WEC types. Real data from full scale device testing would allow for more appropriate thresholds, tailored to individual device designs, to be determined, however this information is seldom made available due to commercial considerations.

2.3.2 Sea State Influence on WEC Output

The expected power output from a WEC is commonly presented as a function of two variables — usually the significant wave height, H_{m0}, and a period parameter such as T_E or T_P — and referred to as a power matrix. Power matrices are similar to the performance curves produced for wind turbines, and allow estimates of device energy capture to be determined from the available wave data at a site. Power matrices are usually derived from numerical models or the performance data gathered from scaled versions of the device at test sites or from model tests carried out in wave basins or similar facilities. Examples of power matrices are illustrated in Figs 2.15-17 and represent the expected output for three types of WEC with differing operation principles: Pelamis, an attenuator rated at 750 kW; the 7 MW Wave Dragon, an overtopping device; and the original design of the Archimedes Wave Swing (AWS) which was a point absorber (Carbon Trust 2005).

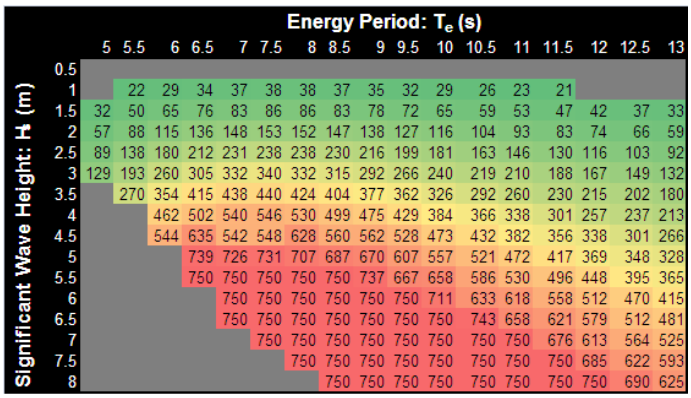

Figure: 2.16: Power matrix for the 750 kW Pelamis device.

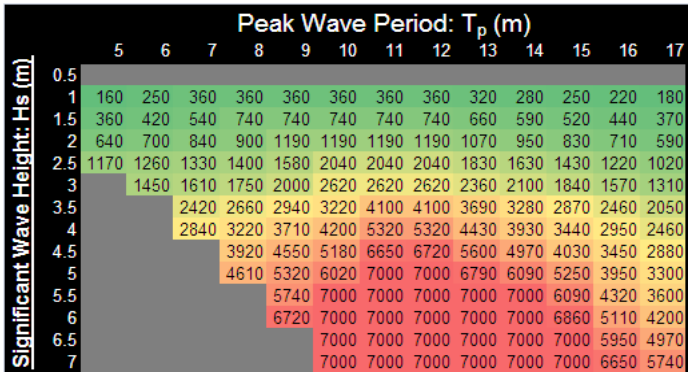

Figure: 2.17: Power matrix for the 7 MW Wave Dragon device.

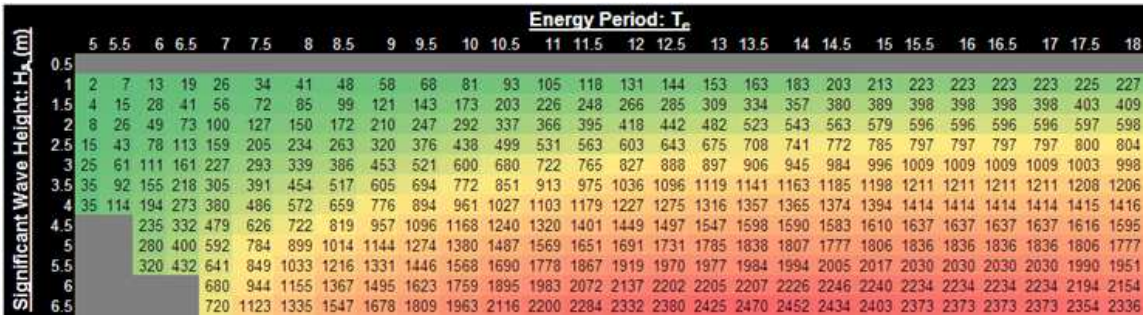

Figure: 2.18: Power matrix for the 2.5 MW AWS Point Absorber.

While the accuracy of these particular power matrices may be questioned they can be considered generally representative of typical device performance, and they have been extensively employed in many previous studies. They are frequently used in high level resource assessments to calculate the technically accessible energy (Carbon Trust 2005; ESB International 2005), and to calculate the interannual variability of the resource

(Mackay et al. 2010). Power production estimates are also important inputs from economic models which aim to select the most profitable site for a particular device (Dunnett and Wallace 2009) or the most appropriate type of WEC for a specific site (Dalton and Lewis 2011). The Pelamis power matrix has also been used to determine the contribution that wave energy devices could make to the combined output from farms of co-located WECs and offshore wind turbines (Fusco et al. 2010; Stoutenburg et al. 2010; Cradden et al. 2011).

There are limitations associated with the use of WEC power matrices and it is inadvisable to define the expected device output from summary statistics alone. For example, there is a danger that slightly different observations of H_{m0}, and T_E will fall into different power matrix cells, leading to a larger variation in output power than what would be expected in reality, which suggests that there is a need to interpolate between adjacent cells to ensure accuracy. It is also notable that some developers produce power output values for sea states which are too steep to exist in practice, which calls the veracity of their predicted performances into question. Additionally, WEC performance is also influenced by the frequency composition of the incident wave spectrum, and information about the variability of the spectral shape is not provided by these power matrices. A previous study by Barrett et al. (2009) showed that many sea states with similar values of wave height and period display distinctly different spectral shapes and that this variability is significant in the context of the performance of WECs. Barrett et al. (2008) also established that different power levels can be produced by a WEC for the same summary statistics due to this spectral variability from the analysis of concurrent wave and device output data collected during sea trials of the OE Buoy device in Galway Bay. Sea states with spectra that were well matched to the device response characteristics were found to perform as predicted but in cases when the resonant frequency of the device was observed to fall within the valley of a double peaked spectrum the resulting power production was observed to diminish to as low as 5% of its expected value. Saulnier et al. (2011) also demonstrated the importance of spectral shape. For a fixed T_E of 7 s improvements in the capture width of a numerically modelled buoy was shown to be strongly correlated with the bandwidth of the incident spectra. In contrast, physical

modelling of the Oyster WEC by Clabby et al. (2012) indicated that the device is less sensitive to spectral shape. This is attributed to the nature of flap type devices, whose responses are less influenced by resonance than floating bodies. Physical tests of the WEPTOS device also found that altering the incident JONSWAP spectrum had a limited impact on device performance, suggesting that various WEC concepts will display different levels of sensitivity to changes in the spectral shape (Pecher et al. 2012).

Many authors suggest that H_{m0} and T_E alone are insufficient to fully predict device output and propose that other parameters, such as spectral bandwidth, mean direction at peak frequency and the directional spreading, also be included in power matrices (Kerbiriou M.A et al. 2007; Saulnier et al. 2011). Nevertheless, power matrices are a useful tool for gaining an understanding of the scale of energy output that could be expected of a real device and are utilized in sections of this work to demonstrate which sea states at particular locations are significant with regards to the performance of typical WECs. A number of groups have proposed standardised guidelines for building and interpreting power matrices, which should assist in reducing any uncertainties associated with their use (Equimar Group 2010b; IEC TC 114 2012).

2.3.3 High Level Resource Assessment

Several studies of the global wave energy resource have been completed (Cornett 2008; Mørk et al. 2010; Reguero et al. 2011; Arinaga and Cheung 2012; Gunn and Stock-Williams 2012). These calculate wave power using outputs from large scale, low resolution models such as NOAA's WaveWatch III (Tolman 2002) or the WAM model run by the European Centre for Medium Range Weather Forecasts (Persson and Grazzini 2005). In general these papers present similar conclusions. The most energetic areas are identified in the Southern Ocean, see Fig 1.2, and according to Barstow et al. (2008) the location with the highest annual average wave power — in excess of 140 kW/m — is approximately 1,000 km east of Kerguelen Island in the southern Indian Ocean. These regions are situated too far from major population centres to be of commercial interest, so with this consideration in mind the western seaboards of Europe and the United States are the most promising locations for the large scale development of industrial scale wave

farms. The average wave power returned in these studies for the west coast of Ireland is generally in the range 60 – 80 kW/m.

Resource assessments have also been commissioned at national and regional levels in many areas where it is envisaged that wave energy has to potential to contribute to the energy mix (WERATLAS 2001; ESB International 2005; ABP Marine Environmental Research 2008; Electric Power Research Institute 2011). These reports follow global assessments as they attempt to identify the most suitable areas for developing WEC installations. These studies also attempt to relate the available theoretical energy to that which could feasibly be extracted and so utilise tools introduced previously, such as exploitable power metrics and power matrices, to determine the technical resource.

2.3.4 Detailed Site Studies and Resource Characterisation

An enhanced understanding of the wave energy resource must be developed once appropriate locations for the deployment of WEC installations are determined. The relevant guidelines suggest that this process should be conducted with a combination of measured and modelled data (EquiMar Group 2010a; Folley et al. 2012). These data sources have complementary roles. Wave data from instruments are essential for validating the accuracy of numerical models, for ascertaining precise details about the composition of spectra and when time series of surface elevation are required. Model outputs allow for the spatial variability of the resource to be determined. Iglesias and Carballo utilised SWAN models to map the distribution of wave energy at a number of sites along the Spanish coast (Iglesias and Carballo 2009; Iglesias and Carballo 2010a; Iglesias and Carballo 2010b). The model outputs allow for the precise localisation of the areas where the wave energy is greatest. Hindcast models derived from meteorological records also allow long duration (> 10 years) estimates of the resource to be determined. These are necessary to determine the interannual variability of the resource, and are rarely available from in situ observations. An exception to this statement is provided by Lenee-Bluhm et al. (2011) who characterised the temporal trends exhibited by the wave energy resource of the US Pacific Northwest using measurements from NDBC buoys with data archives of up to 21 years. These buoys were part of an existing network

however, and are not specific to a proposed site for potential WEC deployments. Numerical models have also been adapted to yield an understanding of the likely interactions between arrays of WECs and the incident wave climate, such as the impact of energy extraction to the wave field in the lee of the devices (Venugopal and Smith 2007; Stratigaki et al. 2011) and on the climate closer to the shoreline (Smith et al. 2012). The ability of models to propagate wave conditions to the nearshore area is an additional attribute of wave models, and allows the variability in the resource as water depth decreases to be observed (Folley and Whittaker 2009; Forrest 2010; van Nieuwkoop-McCall et al. 2012). A significant conclusion of Folley and Whittaker's work is the hypothesis that while the magnitude of the theoretical resource offshore is far greater that that at nearshore locations, the potential for WEC production at the respective sites will be relatively similar if metrics such as P_{exp} are used. This is due to the fact that the influence of storm sea states, which occur more frequently in deeper water, is discarded.

2.3.5 Characterisation of the Irish Wave Energy Resource and Existing Knowledge Gaps

There have been relatively few examples of research projects undertaken to assess the wave climate and energy resource in Irish coastal waters. Mollison (1982) provided an initial estimate of the average power levels at five sites off the Irish coast using a model run by the UK Met Office. The highest average power value returned from the model data was 77 kW/m, at a point located far offshore near the Porcupine Bank. The model used was not compared to buoy measurements in Irish waters however, so it is difficult to assess whether it accurately represents the wave climate. The model station 50 km offshore of Belmullet is shown to have an average power of 70 kW/m, while the resource is reduced at the locations further to the North and the Southwest along the west coast. An updated reference — the Accessible Wave Energy Atlas — was developed from a WAM model validated against the Marine Institute's M-buoy network (ESB International 2005). This computed both the theoretical energy resource and the annual accessible electrical energy potential by accounting for device output — using the Pelamis power matrix — and considering the feasible installed capacity that could be derived from wave farms.

The resource assessments made by Mollison and ESBI were derived from limited datasets. Wave power was calculated using summary statistics and without reference to measured spectral shape and water depth. Consequently there is a degree of uncertainty associated their outputs. It was possible to address this knowledge deficit in this thesis owing to the increased level of data — particularly in situ measurements — that has recently become available for the Irish west coast.

More detailed research has been carried out in recent years by Barrett who assessed the variability of spectral shapes (Barrett et al. 2009), and the nature of the wave energy resource at Ireland's quarter scale test site and its influence on the power output from an OWC device undergoing sea trials (Barrett 2010). These projects were initiated by the deployment of Datawell Waverider buoys near Loop Head, Co. Clare, and in Galway Bay and have proven to be a useful basis for guiding aspects of the work undertaken during this research.

Chapter 3 Wave Energy Test Sites and Measured Wave Data

3.1 Introduction

The staged development protocol has gained widespread acceptance as the most appropriate process for advancing WEC technologies from an initial concept to a commercial installation. Several alternative pathways have been proposed, such as the Danish three step approach (IEC TC114 2012), the five stage Development Protocols (Fig. 3.1), originally outlined by Holmes (2003) and formalised as a set of standards by the International Energy Agency (Holmes and Nielsen 2010), and a nine stage Technology Readiness Level (TRL) framework based on NASA procedures (U.S. Department of Energy 2011; Fitzgerald and Bolund 2012). While these guidelines may vary in the details they are all predicated on the same underlying philosophy; design development should follow a prescribed sequence of steps, which entail increasing technical complexity and investment requirements, in order to gain the required understanding of the device characteristics while minimising the project's risk of failure.

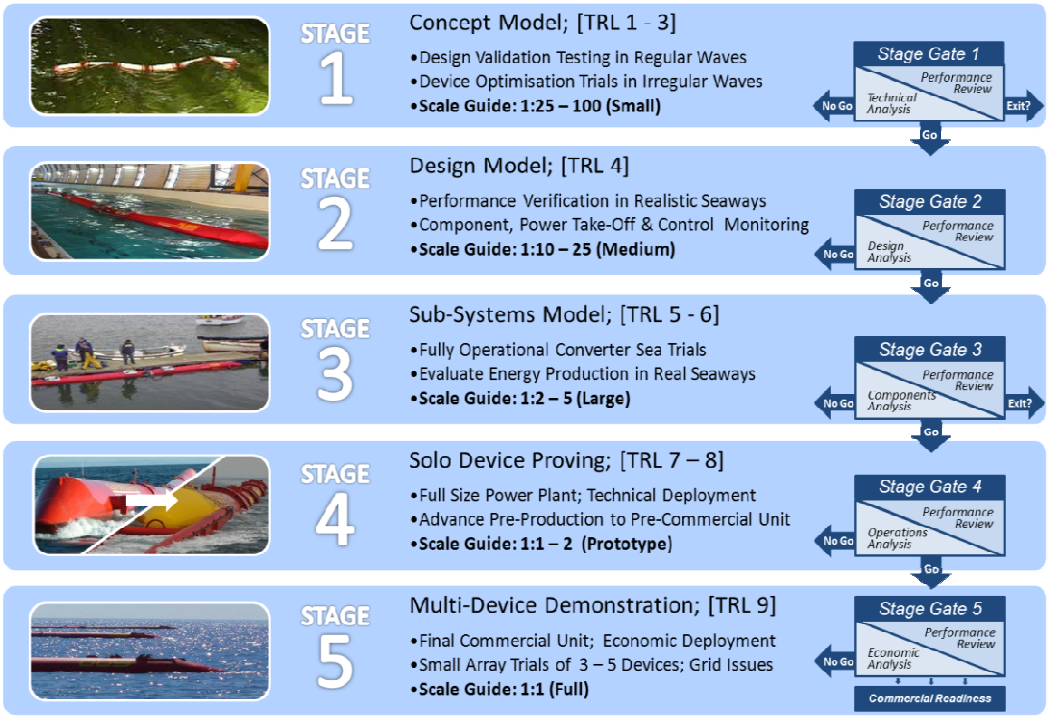

Figure: 3.1: Five stage development schedule. Image courtesy of Brian Homes, HMRC.

Real sea test sites are vital pieces of infrastructure for bridging the gap between refining the performance of small scale physical models in controlled laboratory settings and the

open sea trials suggested for the later stages (3 – 4 in Fig. 3.1) of the development protocols. The United Kingdom has been the pioneer within Europe in terms of providing these facilities to the wave energy industry. To date, the most frequently utilised test site in the world has been the European Marine Energy Centre (EMEC) on the island of Orkney, which has hosted deployments by developers such as Pelamis, Aquamarine Power, AW Energy, Seatricity and Wello Oy (EMEC 2012). The EMEC facilities for testing WECs are extensive: five grid connected berths (50 m – 75 m water depth); a nearshore site serviced by a pipeline for conveying pressurised fluid; and a nursery site for sub-prototype scale devices. EMEC also operates a similarly impressive suite of test berths for assessing tidal energy devices. Wave Hub, located off the coast of Cornwall, is another exposed, grid connected test area. Wave Hub is notable due to the thorough measurement campaign being conducted at the site, including an array of four SeaWatchMini II buoys arranged in a 500 m x 500 m square grid layout which allows the spatial variability of the wave energy resource to be quantified (Ashton 2011). Several more test sites exist, or are being developed, across the western seaboard of Europe and are described in a comprehensive catalogues that have been compiled as part of the EU-funded Waveplam and SOWFIA projects (Waveplam 2009; Mora-Figueroa et al. 2011).

In the United States open water testing of WEC has occurred sporadically, including sea trials by Ocean Power Technologies in Hawaii (Ocean Power Technologies 2012b), Neptune Wave Power off the coast of New Hampshire (Neptune Wave Power 2012) and Columbia Power Technologies in Puget Sound, Washington (Bassett et al. 2011). This process will be formalised with the designation of the test sites operated off the coast of Oregon by the Northwest National Marine Renewable Energy Centre (NNMREC) as the Pacific Marine Energy Centre (PMEC). This facility will include up to five grid connected berths, well as a floating load bank and data acquisition system, referred to as the Ocean Sentinel Buoy illustrated in Fig. 3.2, for monitoring the performance of sub-prototype scale devices (Casson 2012)

Figure: 3.2: NNMREC Ocean Sentinel monitoring buoy (left) connected to the WET NZ wave energy device (right). (Photo by Pat Knight/Oregon Sea Grant)

Test facilities exist in Ireland in the form of the existing quarter scale site in Galway Bay and the Atlantic Marine Energy Test Centre (AMETS), currently being developed by the Sustainable Energy Authority of Ireland. The aim of the research outlined in this thesis is to develop an increased knowledge about the wave climate off the Irish coast. Therefore, the in-situ measurements collected at these sites are essential resources and are utilised in the analysis presented throughout this work. Galway Bay and AMETS are described in detail in Section 3.2 and Section 3.3 respectively, with particular reference to the metocean data available from the sites. Supplementary wave measurements were also required during this project and were sourced from the US National Data Buoy Centre (NDBC) and the Coastal Data Information Program (CDIP), introduced in Section 3.4.

3.2 Galway Bay Quarter Scale Test Site

3.2.1 Introduction

The benign, quarter scale, wave energy test site in Galway Bay on the west coast of Ireland provides an ideal location for WEC developers to deploy and monitor sub-prototype scale devices in relatively sheltered conditions, as suggested in Phase 3 of the standard development protocol (Fig. 3.1). This site was established by the Marine

Institute in partnership with the Sustainable Energy Authority of Ireland, as a bridge between testing small scale, inexpensive, models in a controlled setting such as an indoor wave basin and operating pre-commercial prototypes in the high risk environment of the open ocean. The site has an area of 37 hectares, with a water depth of between 21m-24m and a tidal range of 4m. Due to the semi enclosed nature of Galway Bay, illustrated in Fig. 3.3 the site experiences swell waves from the west and south west as well as the local, fetch limited, wind seas. Results presented later in this thesis, along with previous work by Barrett et al (2007), indicate that these wind seas are a good representation at quarter scale of combinations of height and period for exposed Atlantic Ocean conditions.

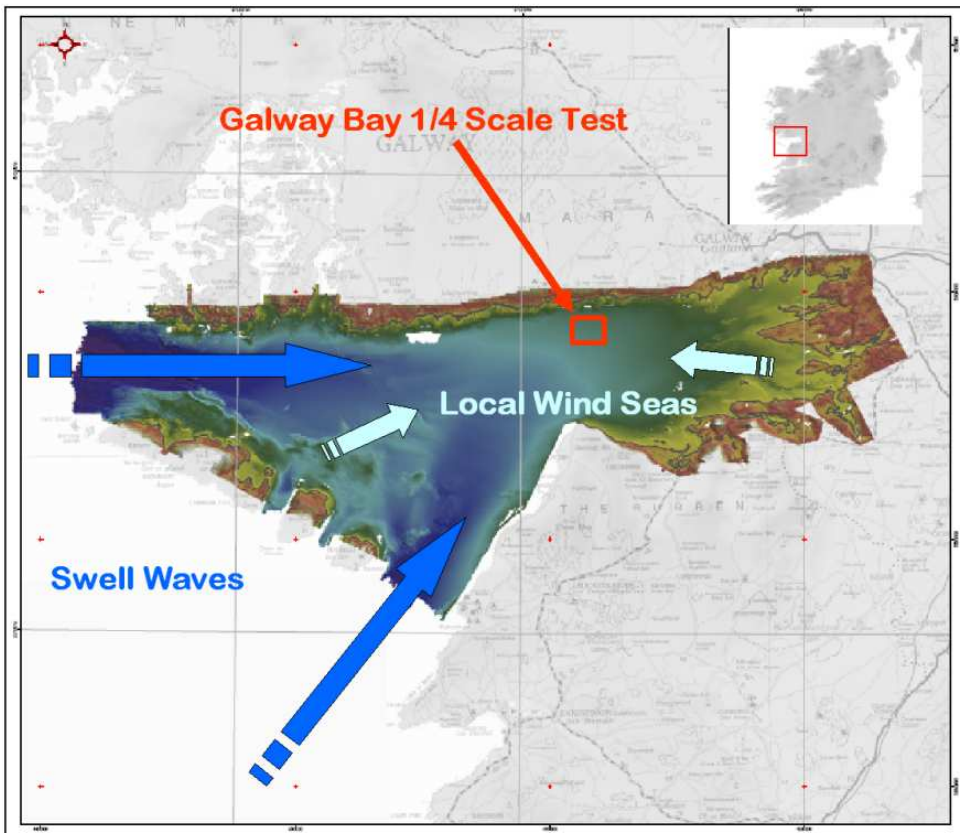

Figure 3.3: Location, bathymetry and prevalent wave conditions experienced at the Quarter Scale Wave Energy Test Site in Galway Bay.

To date three separate sets of WEC sea trials have been undertaken at the Galway Bay site. Ocean Energy Ltd's OE Buoy underwent extensive testing between 2006-2009,

which has allowed the company to progress along the development pathway and begin to plan for the installation of a full scale device at Wave Hub in Cornwall (Ocean Energy Ltd. 2012). Wavebob also deployed their ADM1 model at the site in between 2006-2007. The OE Buoy was redeployed for approximately four months in 2011 as part of Components for Ocean Renewable Energy Systems (CORES), an EU funded FP7 Collaborative Research Project. These trials have undoubtedly been important in terms of technology development, but they have also had the ancillary advantage of engendering a network of practical skills and experience in offshore operations within Ireland which should benefit the wave energy industry as it moves towards commercialisation (Thiebaut et al. 2011; Alcorn et al. 2012; Kelly et al. 2012; O'Callaghan 2012).

3.2.2 Measured Wave Data at the Galway Bay Test Site

Wave measurements have been collected from Galway Bay using individual Datawell Waverider buoys since 2005. A non-directional buoy was located at 53˚ 13.606' N, 9˚ 16.024' W from November 2005 to November 2008. The collection of data from this buoy was phased out through 2008 once a directional buoy, positioned at 53˚ 13.7' N, 9˚ 16.13' W, was installed in April of that year. Concurrent measurements from both buoys exist from this period of overlap and are utilised in an assessment of the spatial variability of the wave energy resource at the site in Chapter 8. The data recorded at the test site is transmitted by high frequency radio to a receiving antenna located on the roof of the Marine Institute building in Rinville, Co. Galway. This data is managed and distributed by the Marine Institute and can be accessed through its Data Request program (Marine Institute Data Requests 2012). The percentage of data retrieved from the site by the Waverider buoys each month for the period 2006-2011 is illustrated in Figs 3.4 - 3.9. An inherent weakness of in-situ wave buoy measurements is that 100% data retrieval is rarely achieved over the course of a monitoring regime. Gaps in the data are evident for each of the years shown. For example, in 2006 (Fig.3.4) the availability of measurements does not exceed 75% for any month between May and October, including months where no data was returned. These gaps can occur for a variety of reasons, such as problems with the radio signal, battery issues and the need to remove the buoy for maintenance purposes. Care must be taken to ensure that they do not introduce bias to analysis results.

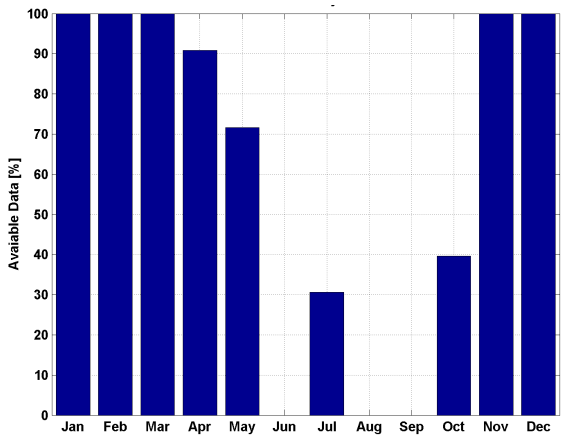

Figure 3.4: Galway Bay wave data availability 2006

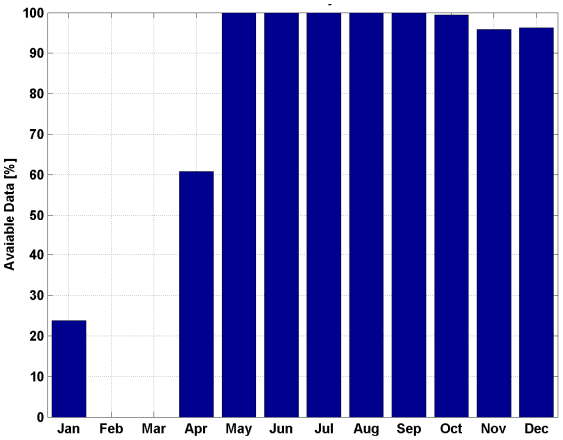

Figure 3.5: Galway Bay wave data availability 2007

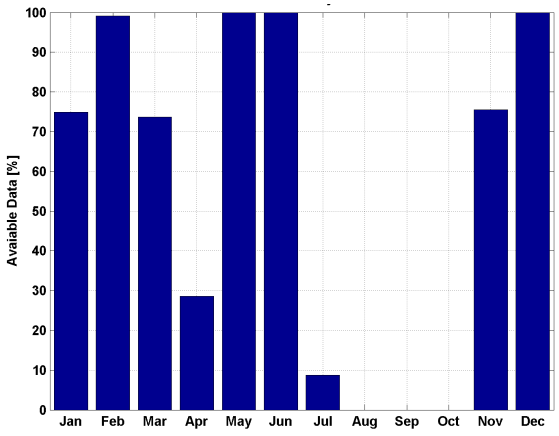

Figure 3.6: Galway Bay wave data availability 2008

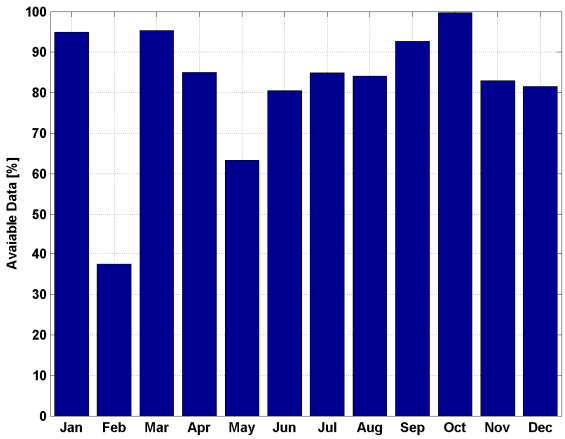

Figure 3.7: Galway Bay wave data availability 2009

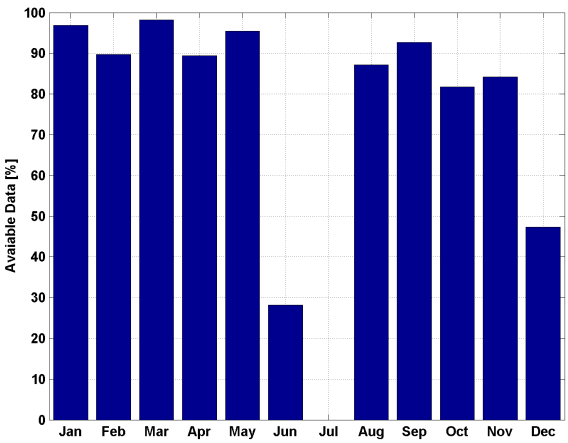

Figure 3.8: Galway Bay wave data availability 2010

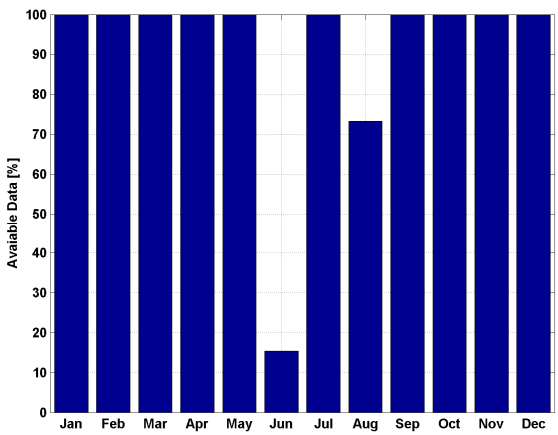

Figure 3.9: Galway Bay wave data availability:2011

3.3 The Atlantic Marine Energy Test Site (AMETS)

3.3.1 Introduction

The Atlantic Marine Energy Test Site (AMETS) is currently being developed by the Sustainable Energy Authority of Ireland (SEAI) near Belmullet, Co. Mayo, on the Irish west coast. Once commissioned, AMETS will offer device developers the opportunity to trial prototype-scale WECs in a harsh, energy rich, wave climate that can be considered typical of exposed, Atlantic facing sites in Ireland and the United Kingdom. As such, it is envisaged that it will be the final proving ground for WEC technologies prior to commercial deployment.

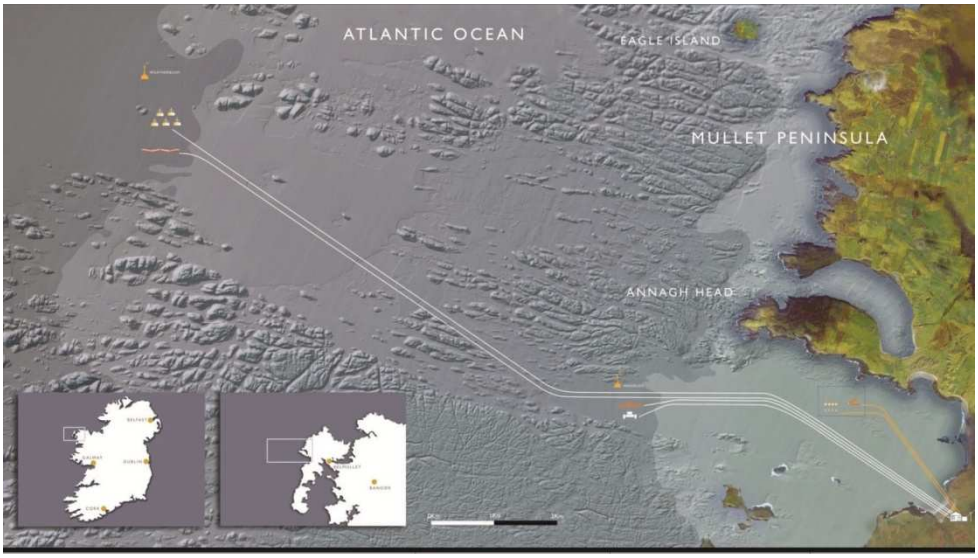

Figure 3.10: Layout of the Atlantic Marine Energy Test Site. (Image courtesy of SEAI).

The site layout of AMETS is illustrated in Fig. 3.10. It will consist of two grid-connected test areas for floating WECs, located at depths of 50 m and 100 m, with a maximum export capacity of 10 MW. This physical infrastructure has yet to be installed, however several important steps have been taken in preparation for the eventual deployment of WECs. An application for a foreshore lease, which must be secured prior to carrying out works or placing structures or material on State-owned foreshore, has been submitted to the Department of the Environment, Heritage and Local Government (Sustainable Energy Authority of Ireland 2011a). Site investigations of the seabed have been undertaken, along with the design of the cable configurations for the test berths (Ascoop and Frielding

2010), while a detailed description of the environmental impact assessment work that has been undertaken at the site is provided by Kavanagh et al. (2011).

3.3.2 Measured Wave Data at AMETS

A Datawell Directional Waverider has been gathering data at AMETS since December 2009. This buoy is located at the test berth at the 50m depth contour. It transmits a set of spectral and time series readings to shore every 30 minutes, similar to the Galway Bay Buoy. The percentages of time for which data exist during each calendar month are plotted in Figs. 3.11 – 3.13. Gaps can be seen during summer months as the calm conditions allow the buoy to be accessed for maintenance. Generally the data availability is excellent for the winter months, which ensure that sufficient measurements are collected to capture the wave conditions during high energy seas states. Care must be taken when assessing the average energy resource to ensure these seasonal variations in data availability do not bias the results. Data after April 2012 to the present were not accessed during this project so no figures for availability were calculated. A possible enhancement to the measurement campaign at AMETS would be to maintain an additional buoy onshore as a redundancy measure. This buoy could then replace those being brought ashore for repair to ensure that any interruptions in data collection are reduced.

In addition, from May - October of 2010 and April – August a Fugro Wavescan buoy, was positioned at the planned Deep Water Test Area, approximately 10km North-East of the Waverider buoy at a water depth of 100 m. This buoy returned a set of processed summary statistics every hour, while the raw time series of surface elevation were stored onboard for recovery whenever the instrument was accessed for maintenance purposes. Unfortunately due to an error in the original setup of the buoy software these data were corrupted and it is impossible to extract useful information, such as wave spectra, from them (Fennell 2012). The availability of summary statistics from the buoy during these deployments are illustrated in Figs. 3.14 – 3.15. The Wavescan was replaced by an additional Waverider during the summer of 2012 which has been successfully returning measurements, though these data were not analysed as part of this research.

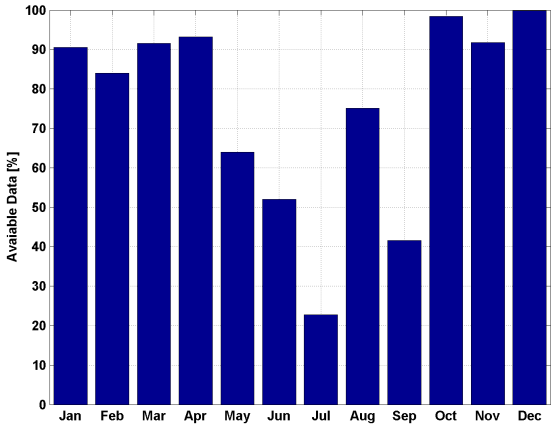

Figure 3.11: AMETS Waverider buoy [50 m] data availability 2010

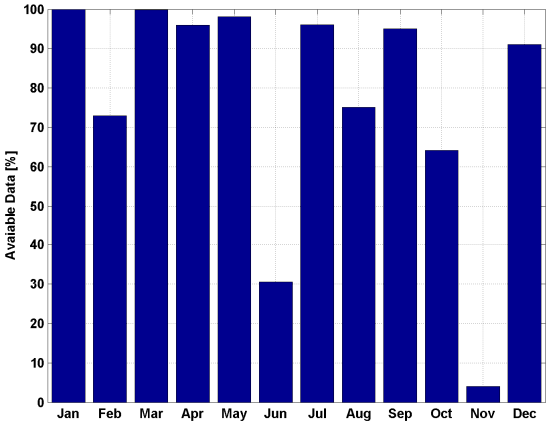

Figure 3.12: AMETS Waverider buoy [50 m] data availability 2011

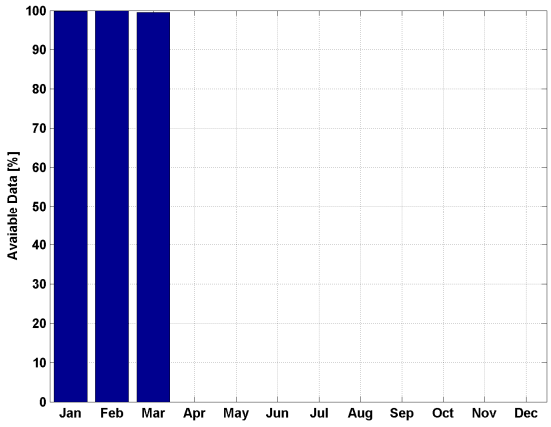

Figure 3.13: AMETS Waverider buoy [50 m] data availability 2012

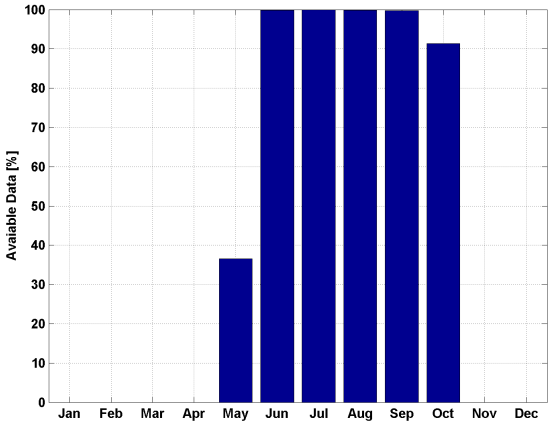

Figure 3.14: AMETS Wavescan buoy [100 m] data availability 2010

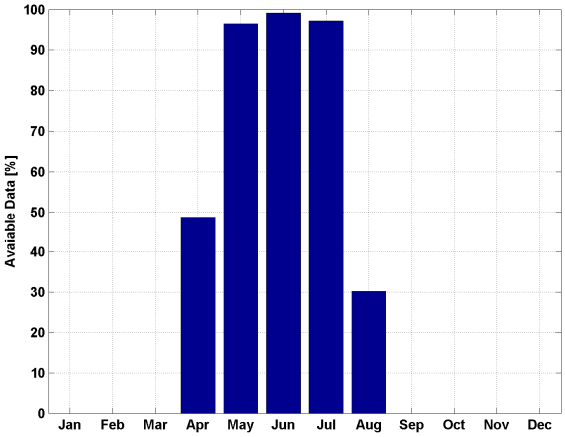

Figure 3.15: AMETS Wavescan buoy [100 m] data availability 2011

3.3.3 AMETS Hindcast Wave Model

The in-situ measurements described in the previous section are complemented by the outputs of a sixteen year numerical climatology of the area surrounding AMETS. This model was commissioned by SEAI and developed by Numerics Warehouse Ltd. A detailed description of bathymetric data used in the model, the downscaling methodology using nested grids of decreasing spatial coverage with increasing resolution to create the model boundary conditions and the setup of the high resolution SWAN model for the test site area is outlined in an accompanying report (Curé 2011a). In summary, a series of nested weather and wave models, of increasingly fine grid sizes, were developed. These ranged from a global scale with a resolution of 270km to the final level SWAN model for the AMETS and its surroundings, which had a resolution of approximately 100m in both the North-South and East-West directions. SWAN is a freely available, open source, software suite and is commonly used in the research community for modelling waves in the near shore environment. The model operates by solving the action balance equation and accounts for both shoaling and the refraction of waves. Further details on the theory behind the SWAN model can be found in the paper by Booij et al. (1999) and the textbook written by Holthuijsen (2007). The bathymetric data used in the model came from a number of sources, primarily SWATH and LIDAR measurements conducted during the INFOMAR project (2007).

The model grid and bathymetry are illustrated in Fig.3.16, along with twenty-one station points which were included to provide more detailed data outputs, including spectra and summary statistics at 30 minute intervals. Fifteen stations were chosen at the intersection of contour lines at every 10m increment of depth (10m-150m). These are illustrated by the red diamonds in Fig. 3.16. Stations were also selected at the positions of the measurement buoys deployed at AMETS (yellow circles). Detailed output points were also included at the coordinates of the Waverider and Wavescan buoys located at depths of 50 m and 100 m respectively. Finally, additional stations (pink triangles) are located to the south and northeast of the main transect, along the 50m and 100m contours.

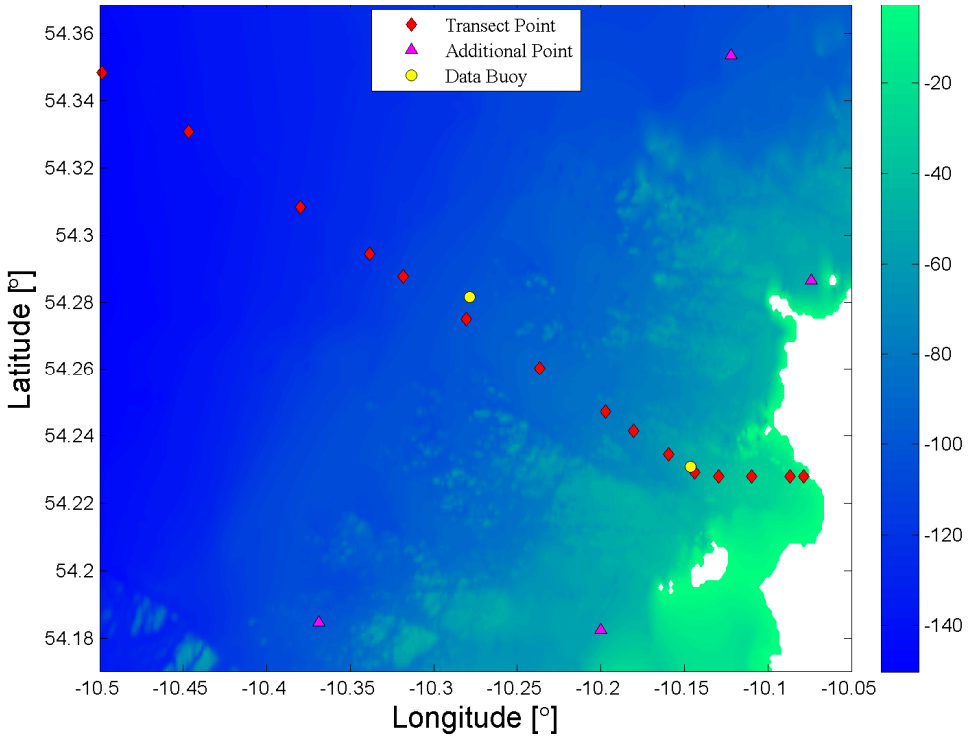

Figure 3.16: SWAN model bathymetry and stations. The colour scale indicates water depth.

3.3.4 Validation of the AMETS Hindcast Model

Validating the outputs of the AMETS model to ensure that they accurately represent the wave climate at the site was an important step prior to using the results in detailed resource characterisation work. This section describes the process that was followed. The model was assessed qualitatively by visually comparing the outputs at the 50 m depth and 100 m depth stations where concurrent, measured data was available from the Waverider and Wavescan buoys respectively. A quantitative validation was also undertaken using a number of common statistical parameters.

Concurrent values of H_{m0} from the model and the measurement buoys are plotted in Fig. 3.17 for the 50 m depth location and in 3.18 for the 100 m depth point. A number of inconsistencies are evident. For example, the model lags, and underestimates, the observed conditions on 27th – 28th November at the 50 m depth, while it also produces excessive values of significant wave height around December 10th. Additionally, the model outputs of H_{m0} do not display the same level of short term variability that exists for

the buoy measurements and tend to follow a much smoother profile. Nevertheless, the model captures the fundamental nature of the wave conditions as they develop and propagate through the site. Scatter plots of concurrent values of H_{m0} and T_{02} are illustrated in Fig 3.19 for the 50 m depth station (A and B) and for the 100 m depth station (C and D). These graphics are similar to the time series plot as they show a reasonable general agreement between the model and measured data but also many instances where there are very large discrepancies.

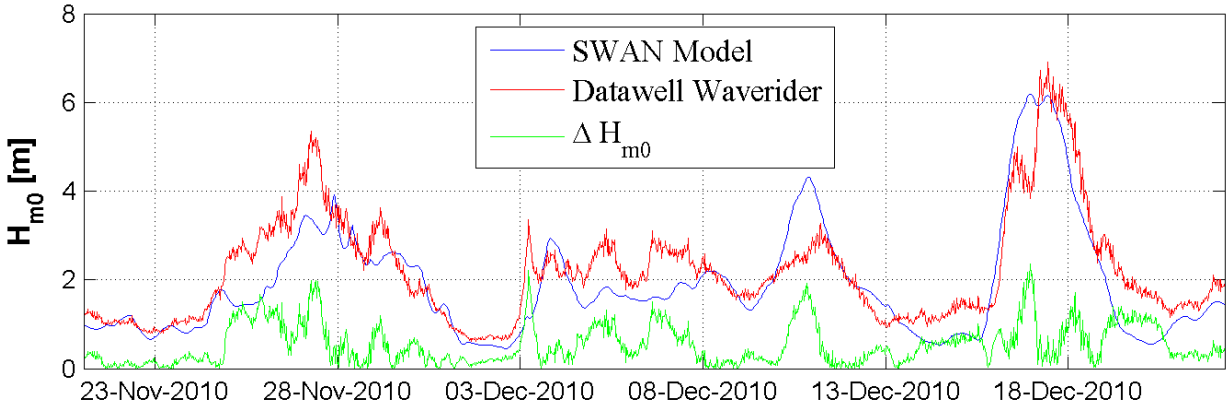

Figure 3.17: Concurrent and co-located H_{m0} values from the SWAN model and the Waverider buoy [50m].

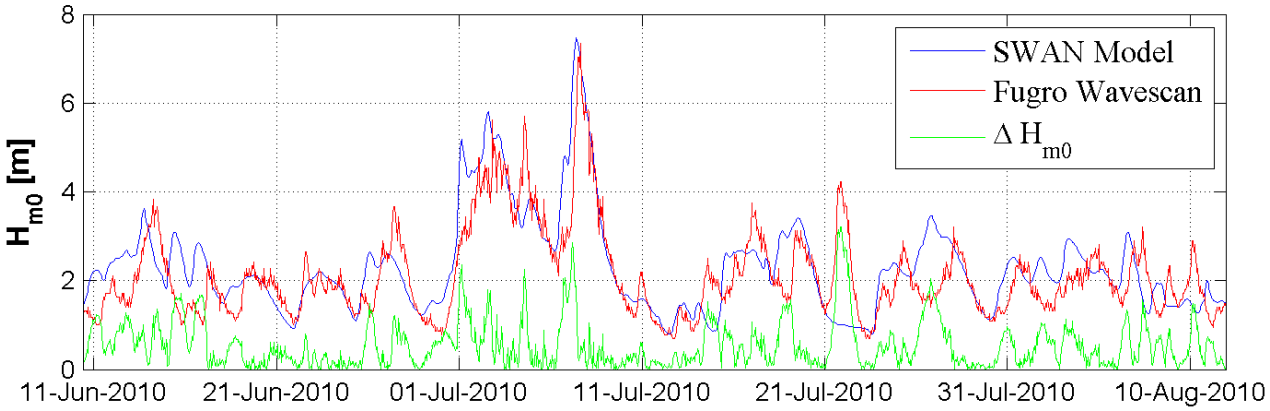

Figure 3.18: Concurrent and co-located H_{m0} values from the SWAN model and the Wavescan buoy [100m].

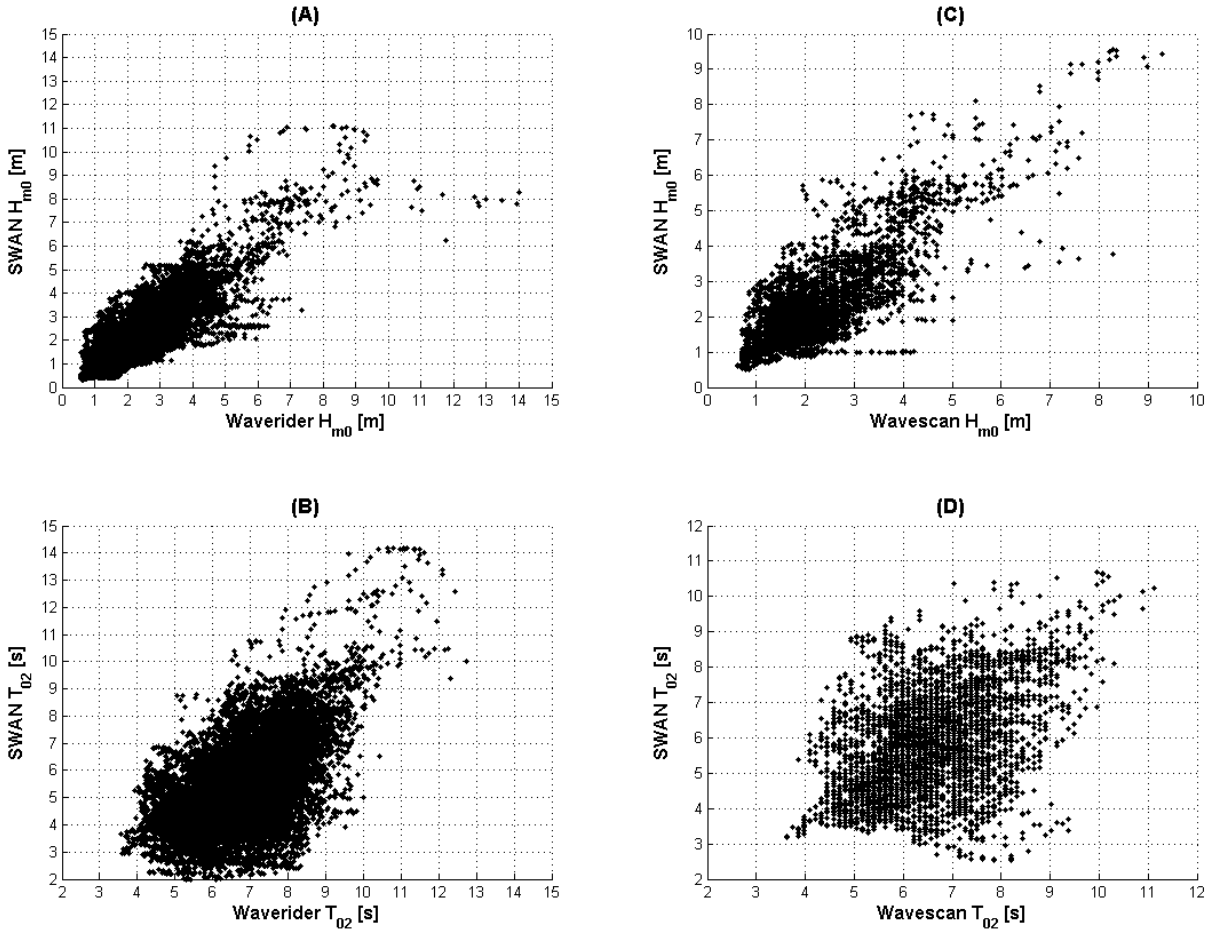

Figure 3.19: Concurrent and co-located H_{m0} values from the SWAN model and the Wavescan buoy [100m].

Quantitative analysis was also utilized to assess the how well the Belmullet SWAN model replicates the real sea conditions experienced at the site and to compare its accuracy to other models from the literature. A number of commonly used statistical parameters were applied to the concurrent data. The bias is representative of a primarily constant in magnitude error between model output, X_{Model}, and the corresponding buoy data with the same timestamp, X_{Buoy}. Another measure of the differences between values predicted by the SWAN Model and the values observed by the measurement buoys is the root mean square error (RMSE. The scatter index (SI**)** is a normalized measure of error with lower values of SI indicating that the datasets are well matched. The final measure used is the correlation coefficient (R). This parameter indicates the strength of the linear relationship between the model outputs with the corresponding buoy data. R is non-

dimensional and ranges from 1 to -1, with R values close to 1 indicative of a perfect correlation. These parameters were calculated using the model output values of H_{m0} and T_{02} with buoy spectrum derived values which shared the same, or closely matched timestamps. The results for concurrent values of H_{m0} and T_{02} are tabulated in Table 3.1. The computed results for the concurrent H_{m0} data are significantly more favourable than for T_{02}, while the values for the 50 m depth location are generally better than those for the 100 m depth position.

	H_{m0}				**T_{02}**			
	RMSE (m)	**SI**	**Bias (m)**	**R**	**RMSE (s)**	**SI**	**Bias (m)**	**R**
SWAN - Waverider	0.733	0.311	-0.11	0.838	1.817	0.207	-1.150	0.52
SWAN – Wavescan	0.805	0.347	0.134	0.803	1.588	0.220	-0.680	0.437

Table. 3.1: Validation parameters calculated for SWAN Model outputs of H_{m0} and T_{02}.

The statistical outputs computed for the SWAN model data are placed in context by comparing them to similar validation results from wave models that were obtained during a search of published literature. Only cases which simulated wave conditions in similar water depths and at locations where the physical geography was not overly site specific were selected. In total, seven models which were validated against measured H_{m0} data were identified. All of the studies noted the R value that was computed, while only two papers returned values for the four parameters included in Table 3.1. It is evident that the AMETS model does not display the high level agreement with concurrent in situ observations that were achieved by the models included in Table 3.2. The R values, 0.838 with the Waverider observations and 0.803 with the Wavescan data, are relatively poor in comparison with the other published results.

Model Details	Validation Data	RMSE (m)	SI	Bias (m)	R
West of Ireland SWAN Model (Rute Bento et al. 2011)	Wavescan Buoy	0.479	0.230	0.174	0.886
Hawaii WaveWatch III Model (Stopa et al.)	Satellite Altimetery	0.42	-	-	0.67
Bimep WAM Model (Ferrer et al. 2010)	Met Station	-	-	-	0.959
Fedje, Norway, WAM Model (Wyatt et al. 2003)	Waverider Buoy	-	-	-	0.94
	WERA Radar	-	-	-	0.93
Irish Coastal point WaveWatch III Model (Arinaga and Cheung 2012)	M4 Databuoy	0.38	-	-	0.95
	M6 Databuoy	0.62	-	-	0.95
Hanstholm, Denmark Mike 21 Model (Fernandez Chozas et al. 2011)	Waverider Buoy	0.31	0.17	0.18	0.93

Table. 3.2: Published validation parameters for model outputs of H_{m0}.

As well as comparing the instantaneous occurrence of H_{m0} and $T_{02,}$ the ability of the model to represent the overall wave climate of the test site was examined. Scatter plots of percentage occurrence of combinations of H_{m0} and T_{02} were drawn for the concurrent datasets, Figs 3.20 – 3.21. While some differences are discernible, especially for the higher sea states, the range and prevalence of the conditions presented are broadly similar. The model was also assessed by comparing the percentage occurrence and cumulative exceedance of these parameters in the buoy and model datasets, as illustrated

for the point at the 50m depth contour in Fig. 3.22. This indicates respectable level agreement between the model outputs of H_{m0} and the measured values, though the corresponding relationship for T_{02} displays a noticeable underestimate in the model outputs. This discrepancy could have implications for the sizing and tuning of devices being deployed at the site, highlighting the need to check the model outputs against physical measurements. The average wave power values calculated from the data are also well matched; 28 kW/m and 31 kW/m for the co-located SWAN and Waverider measurements while both sets of data from the 100 m depth indicate approximately 31 kW/m. This suggests that while the model performs poorly in exactly replicating the time series of wave parameters — as evidenced by Figs. 3.17 – 3.19 and the results of the statistical checks — it provides an adequate approximation of the general wave climate that is experienced at the site and can be applied to further analysis of the AMETS wave energy resource in conjunction with the in-situ observations from the measurement buoys. It should be noted that these values of average wave power are low in comparison to those calculated for other years of model data in Chapter 6 of this thesis, and that the average values for the 50 m and 100 m points are 62 kW/m and 77 kW/m respectively over the 15 years of outputs.

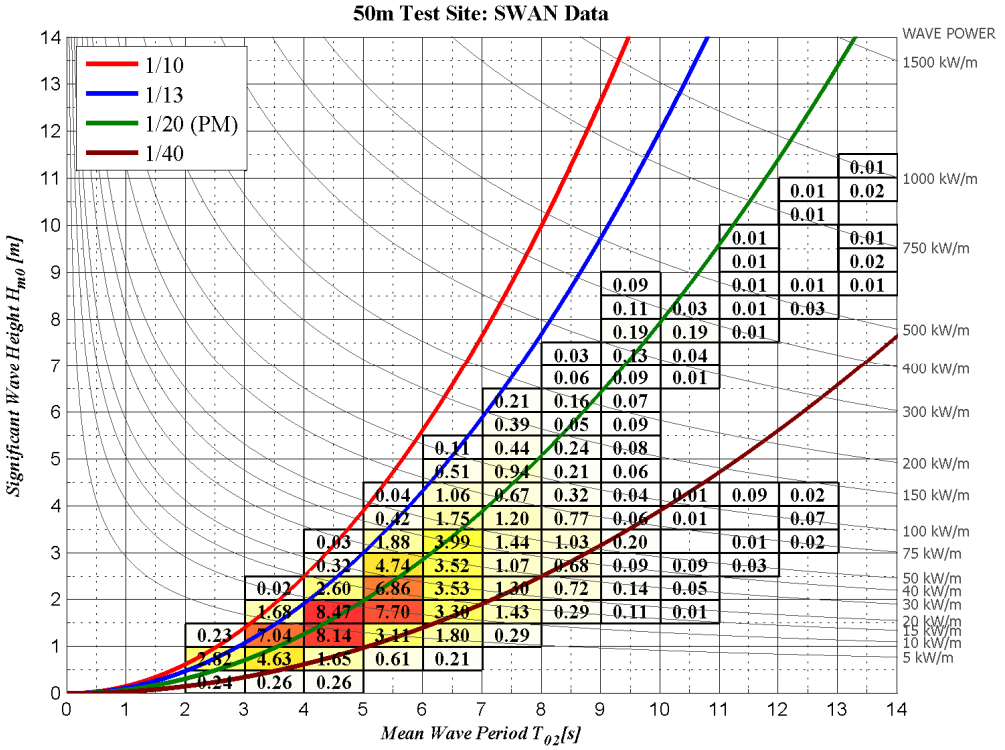

Figure 3.20: H_{m0} and T_{02} percentage occurrence for Modelled SWAN data at the 50 m depth station.

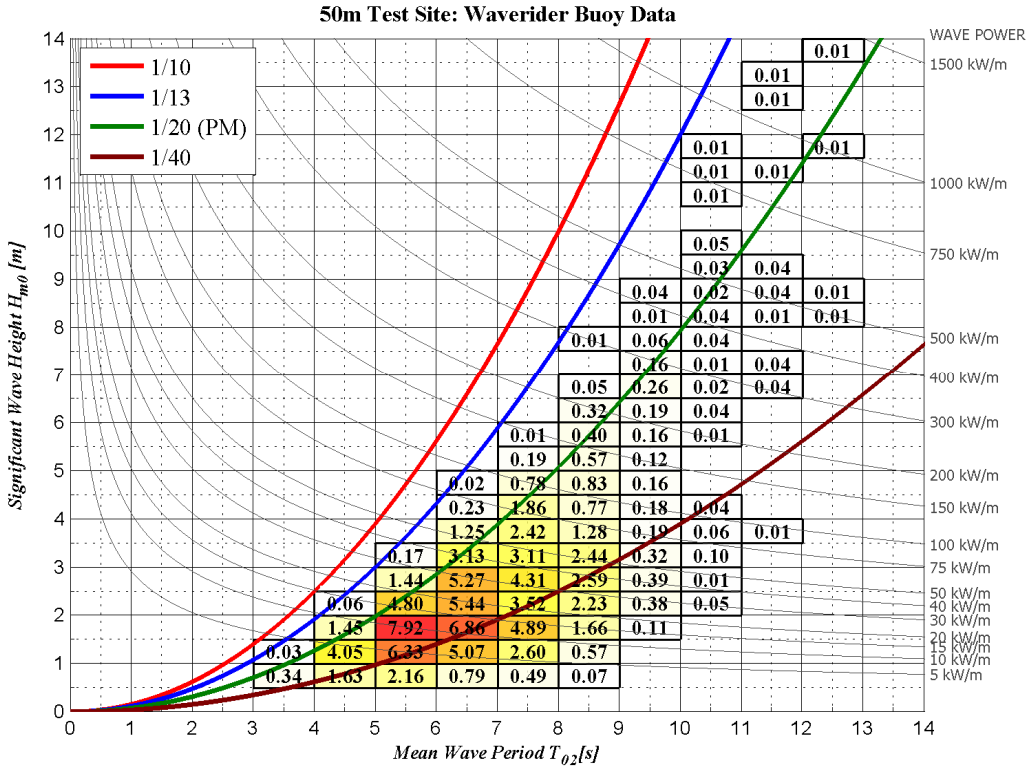

Figure 3.21: H_{m0} and T_{02} percentage occurrence for measured Waverider buoy data at the 50 m depth station.

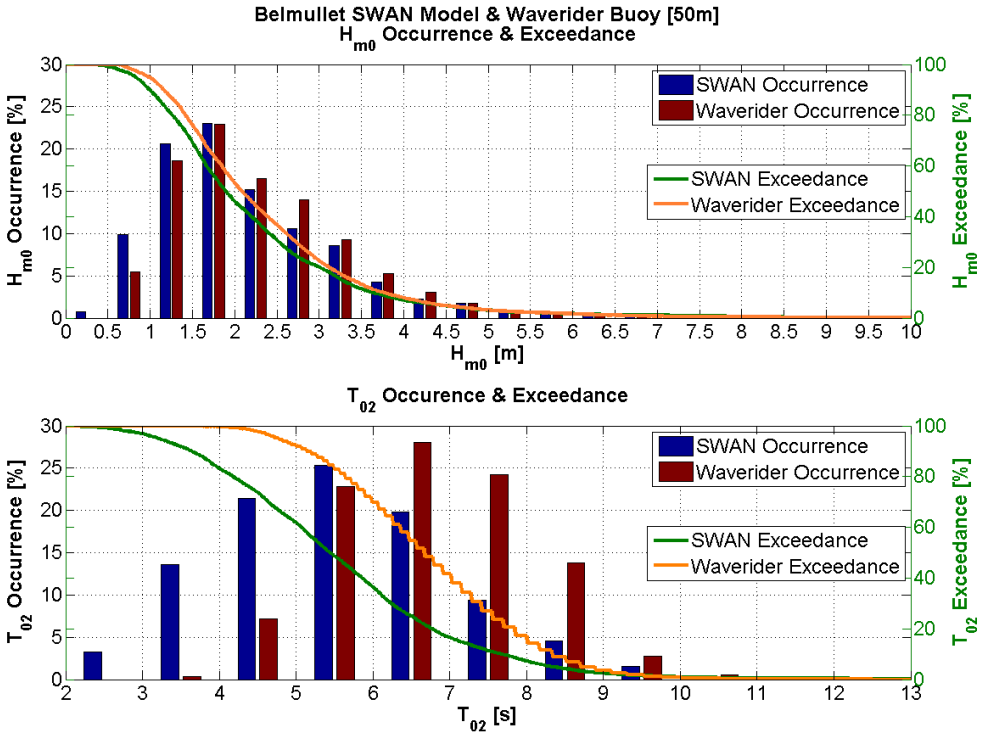

Fig. 3.22: Occurrence and cumulative exceedance of H_{m0} and T_{02} for model and buoy data at the 50m output point.

3.3.5 Issues Encountered with Model Data

A number of secondary issues also had to be confronted and addressed before the model data could be utilised in analysis. It was noticeable that the output parameters at the very start of each time series of data (i.e. first 1-3 days in January of each year) are much lower than would be expected. Correspondence with Marcel Curé, the developer of the model, revealed that this is due to the time required for the boundary conditions to feed through and for the model to reach its steady state as each year was processed separately (Curé 2011b). The user of the data should be able to make a sensible call on the range of values that should be discarded.

The value of the low frequency cut-off in the SWAN model spectra is 0.0464 Hz. This is high when compared to the Datawell Waverider buoy which uses a value of 0.025 Hz. As a result it can be difficult to fully account for the contribution of long period waves, for example when calculating the spectral moments from which sea state parameters are determined. Noticeable variations in the values of parameters calculated from the spectral

moments, such as H_{m0} and T_{02}, were evident depending on how the df term was calculated at the lowest frequency bin when using Equation (2.1). The value of the low frequency cut-off may also account for some of the discrepancies between the overall distribution of sea state occurrence returned from concurrent sets model data and measurements from in-situ buoys at AMETS highlighted in Section 3.3.4.

In the accompanying report it is noted that the wave power (W/m) — an output of the model that was not used in this research — is calculated using the formula

$$P = \frac{\rho g^2}{64\pi} H^2 T \tag{3.1}$$

Here H corresponds to significant wave height and T is the peak wave period. This is an adaption of Equation (2.5), which is similar in form but uses the energy period T_E. For a Bretschneider spectrum $T_p=1.175T_E$, while from analysis of measurements from the Waverider buoy the average ratio between the two parameters is given by $T_p=1.32T_E$, thus the two parameters cannot be considered equivalent. As a result the formula presented in the report overestimates the available wave energy resource.

3.4 Other Sources of Wave Data

Data from sites with different distinguishing features — water depth, fetch length and the incident wave climate — were also accessed and analysed during the course of this research in order to provide comparisons to the Irish data and to further understand certain characteristics of the wave energy resource, for example the variation of the wave period ratio which is studied in Chapter 4. The data were primarily sourced from the National Data Buoy Centre (NDBC) and the Coastal Data Information Program (CDIP), which are described in the following sections. Another benefit to using these measurements is the fact that long term archives, often in excess of 20 years data, exist for many of the sites.

3.4.1 National Data Buoy Centre (NDBC)

The National Data Buoy Centre (NDBC), which operates within the National Oceanic and Atmospheric Administration (NOAA) of the United States Department of Commerce, is responsible for maintaining a network of approximately 90 measurement buoys in the coastal waters — and the Great Lakes — of the USA (Fig. 3.23). The most common type of buoy utilised by the NDBC is the 3-meter Discus Buoy, while the 6-meter NOMAD BUOY and the 12-meter Discus Buoy are more commonly deployed at locations where survivability is important due to rough seas. The measurement buoys are located at a diverse variety of sites, and are moored in water depths of up to 4 km. NDBC makes both summary statistics and spectral data available to users of its website and many stations have archives of measurements which extend beyond 20 years (National Data Buoy Centre 2012).There is no monetary charge, or obligation to sign an access contract, required in order to download the data.

3.4.2 Coastal Data Information Program (CDIP)

The Coastal Data Information program (CDIP) is a wave measurement network operated by the Scripps Institute of Oceanography at the University of California San Diego. CDIP operates a network of more than 50 measurement buoy – primarily Datawell Waveriders – which a predominantly located along the coast of California and the Pacific Northwest. As with the NDBC archives, measured spectral data can be easily accessed, free of charge, from the CDIP website (Coastal Data Information Program 2012).

Figure 3.23: NDBC Measurement buoy network. (Image courtesy of Monterey Bay Aquarium Research Institute).

3.4.3 Rossbeigh Beach, Co. Kerry

Researchers at HMRC have been conducting an ongoing wave measurements campaign at Rossbeigh, a barrier beach in Co. Kerry on the southwest coast of Ireland, as part of a study of a breach in the sand dune system (O'Shea et al. 2011). Physical wave measurements from Rossbeigh were collected using a seabed mounted Valeport pressure gauge at a variety of waters depths, including a point in the surf zone with an average depth of 2 m. These data provide a useful reference for understanding the behaviour of wave properties in very shallow water.

Chapter 4: Ratios between Wave Period Parameters

4.1 Introduction

Characterising the wave energy resource in locations where there is a scarcity of quality wave measurements - particularly spectral data - necessitates the need for assumptions based on theory to be made in order to infer some of the required parameters. For example, the Irish M-Buoy network (Marine Institute 2012) provides values for the average zero-crossing period (T_z or T_{02}) but in the context of wave energy resource assessment parameters such as the peak period (T_p), the energy period (T_E), and increasingly the mean period (T_{01}) are used more frequently. Wave models may suffer from similar shortcomings if their outputs are constrained to a reduced range of parameters in an effort to decrease computation time. In order to determine the necessary T_E values from limited datasets it has been common practice to employ fixed conversion factors based on a theoretical spectral shape, such as Bretschneider or JONSWAP, which is deemed to be representative of the dominant local wave conditions. As a result, assessments of wave energy resource which rely on this practice are sensitive to inaccuracies if the incorrect relationship between parameters is assumed or if the spectral shape considered characteristic for the data is inappropriate.

An illustration of how an unsuitable assumption can result in imprecision in the calculation of the available wave power is contained in the Accessible Wave Energy Resource Atlas (ESB International 2005), the standard reference for Ireland's potential resource. In this study the theoretical wave energy resource was calculated from the summary statistics H_s and T_{02}, generated from a WAM forecast model, as well as from the M-Buoys deployed around the coast, using the formula

$$P = 0.55 H_{m0}^2 T_{02} \tag{4.1}$$

which is based on Equation 2.5 under the assumption that T_E / T_{02}=1.12. This relationship will henceforth be referred to as the wave period ratio (WPR) for the remainder of this chapter. To the best of the author's knowledge the first published reference to this form of the equation is contained in an early review of wave energy research (Glendenning and Count 1976) which assumes that all measured records in a dataset can be represented by

the Bretschneider spectrum. This formula has since been reproduced in other works (Pitt 2005; Barrett 2010; Dalton et al. 2010), as well as in the Irish Wave Atlas. A number of other studies (Crabb 1984; Cornett 2008) - which also assume a Bretschneider spectral shape for the records being analysed – use a slightly different WPR, with T_E/ T_{02}=1.14. The JONSWAP spectrum is considered representative in the assessment of the wave energy resource of the United Kingdom (ABP Marine Environmental Research 2008) and period ratio values ranging from 1.06-1.14 are employed, depending on the magnitude of the model-derived wave period and whether the sea-state is dominated by a swell or wind-sea system.

The prevalence of these disparate values of WPR can be a source of confusion and inaccuracy. This uncertainty can potentially influence both the calculation of the theoretical resource and also the estimation of WEC output from power matrices; many of these require values of T_E as an input, as shown in Section 2.3.1. The growing availability of spectral measurements, and the development of standards to allow for the correct interpretation of these data (European Marine Energy Centre (EMEC) 2009; EquiMar 2011; IEC Technical Committee 114 2012), should remove any ambiguity associated with the calculation of wave power. In cases where the available data are limited, however, the application of a user defined WPR is unavoidable so an improved level of precision is required. It is with this consideration in mind that the research presented in this chapter was undertaken.

In this chapter it is demonstrated that the use of the frequently-employed wave period ratios cited earlier is erroneous and more suitable relationships are presented for the Bretschneider and JONSWAP theoretical spectra. Furthermore, analysis of measured buoy data from real sea-states is used to illustrate that this relationship can in fact vary significantly in practise, depending on geographical location and the prevalent wave conditions. The variability that exists in spectral shape and bandwidth, and the effect this has on the relationship between T_E and T_{02}, is illustrated through the comparison of recorded spectra with the Bretschneider spectrum. Analysis of a fifteen year dataset measured by a buoy off the coast of Southern California is presented to illustrate how the

WPR fluctuates on a seasonal and interannual basis. Ongoing collaborative work to advance this understanding and suggest procedures for selecting suitable conversion factors, undertaken as part of the European Energy Research Alliance (EERA) Joint Programme on Ocean Energy, is also described. It is hoped that this work will allow for more accurate use to be made out of limited datasets such as the measurements produced by the M-Buoy network.

4.2 Wave Period Ratios for Standard Spectral Shapes

As discussed in the previous section, some studies of wave energy resource rely on theoretical spectral formulations to infer more detailed information from the available summary statistics where there is an absence of measured spectral or surface elevation data. Several standard spectral shapes have been derived to describe sea-states by applying fitting techniques to empirically collected data. In this section two commonly used spectra in wave energy research - the Bretschneider Spectrum and the JONSWAP Spectrum - are analysed and the ratios of T_E/T_{02} that can be expected from them are compared to the values used in the references cited in Section 4.1.

4.2.1 Bretschneider Spectrum

In order to derive the WPR for the Bretschneider Spectrum a constant, α_B, is introduced to represent the relationship between the energy period, T_E, and the zero-crossing period, T_{02}:

$$T_E = \alpha_B T_{02} \tag{4.2}$$

This relationship can then be rewritten in terms of spectral moments.

$$\frac{m_{-1}}{m_0} = \alpha_B \sqrt{\frac{m_0}{m_2}} \tag{4.3}$$

By substituting in the values given in Table 2.2, the spectral moments can be rewritten in terms of A and B:

$$\frac{0.2266\frac{A}{\frac{5}{B^{\frac{4}{4}}}}}{\frac{A}{4B}} = \alpha_B \sqrt{\frac{\frac{A}{4B}}{0.443\frac{A}{\sqrt{B}}}} \tag{4.4}$$

Equation (4.4) can be manipulated to show that α_B =1.206. Thus, for a Bretschneider Spectrum the WPR is given by

$$T_E = 1.206T_{02} \tag{4.5}$$

This indicates that the assumptions that the WPR for the Bretschneider spectrum is either 1.12 or 1.14 are inaccurate. By substituting Equation 4.10 into Equation 2.3 it is possible to calculate the average wave power using the summary statistics H_{m0} and T_{02}.

$$P = 0.59H_{m0}^2T_{02} \tag{4.6}$$

If this is compared to Equation 4.1, which assumed a T_E/T_{02} ratio of 1.12 for the Bretschneider Spectrum, it is possible to conclude that studies which assumed the incorrect WPR value, such as the Accessible Wave Energy Resource Atlas (ESB International 2005), underestimated the available wave power by approximately 7% if the Bretschneider spectrum is considered to be representative of the prevalent conditions.

4.2.2 JONSWAP Spectrum

Following the approach used previously for the Bretschneider Spectrum it is possible to derive a wave period ratio (α_J) between the energy period, T_E, and the zero-crossing period, T_{02}, for a JONSWAP Spectrum.

$$T_E = \alpha_J T_{02} \tag{4.7}$$

Equation 4.13 is restated in terms of spectral moments in Equation 4.14.

$$\frac{m_{-1}}{m_0} = \alpha_J \sqrt{\frac{m_0}{m_2}} \tag{4.8}$$

Substituting the values of the spectral moments in terms of H_{m0}, ω_p and γ from Table 2.3 gives

$$\frac{\frac{1}{32\pi}H_s^2 f_p^{-1}\frac{4.2+\gamma}{5+\gamma}}{\frac{1}{16}H_s^2} = \alpha_J \sqrt{\frac{\frac{1}{16}H_s^2}{\frac{\pi^2}{4}H_s^2 f_p^2 \frac{11+\gamma}{5+\gamma}}} \tag{4.9}$$

Equation 4.15 is simplified in stages which allows α_J to be written in terms of γ in Equations 4.10.

$$\alpha_J = \left(\frac{4.2+\gamma}{5+\gamma}\right).\left(\frac{11+\gamma}{5+\gamma}\right)^{\frac{1}{2}} \tag{4.10}$$

By applying Equation 4.10 the WPR value for a JONSWAP Spectrum is given in Table 4.1 for a range of γ values. It is noticeable that as expected the wave period ratio is similar to that of the Bretschneider spectrum when γ=1, though the values are not identical due to slight discrepancies in the generalised values of the spectral moments in Table 2.3 and Table 2.3. The WPR decreases as the peaks of the spectra become more pronounced. Table 4.1 also indicates that it is possible to generate spectra with WPR values of 1.12 and 1.14 which were cited in Section 4.1 using the JONSWAP formula, however to do so requires γ to equal 10 and 7 respectively. It has been shown (Ochi 1998) that γ follows a normal distribution with a mean of 3.3 and a standard deviation of 0.79. This suggests that such high values of γ are unlikely to occur in the ocean. Therefore, the corresponding WPRs are unrepresentative of real sea states and so should be considered inaccurate.

γ	**WPR**
1	1.22
2	1.20
3.3	1.18
5	1.16
7	1.14
10	1.12

Table 4.1: T_E/ T_{02} wave period ratios for JONSWAP Spectra

4.2.3 Effect of Spectral Shift on the Wave Period Ratio

As well as quantifying the correct values of the wave period ratios for the Bretschneider and JONSWAP spectra it was also decided that the position of a fixed spectral shape along the frequency axis should be investigated. The relevance of this analysis will be illustrated in Section 4.4, where it is demonstrated that the average spectral shapes for certain groups of similar sea-states resemble the Bretschneider approximation, but are shifted towards the lower end of the frequency scale. A wave spectrum is generated by inputting the commonly occurring values of H_{m0} = 3m and T_{02} = 7s into Equation 2.8. The resulting spectrum is then translated in discrete steps along the frequency axis, with a maximum shift of 0.05Hz towards the higher and lower frequencies, as illustrated in Fig. 4.1. As the spectrum is shifted the magnitudes of the spectral ordinates and the area beneath the curve remains the same, indicating that the variance and the energy of the wave system being described are constant. The resulting power of the sea-state does vary, however; it is increased as the spectrum moves towards the lower frequencies and reduced as it approaches the higher frequencies.

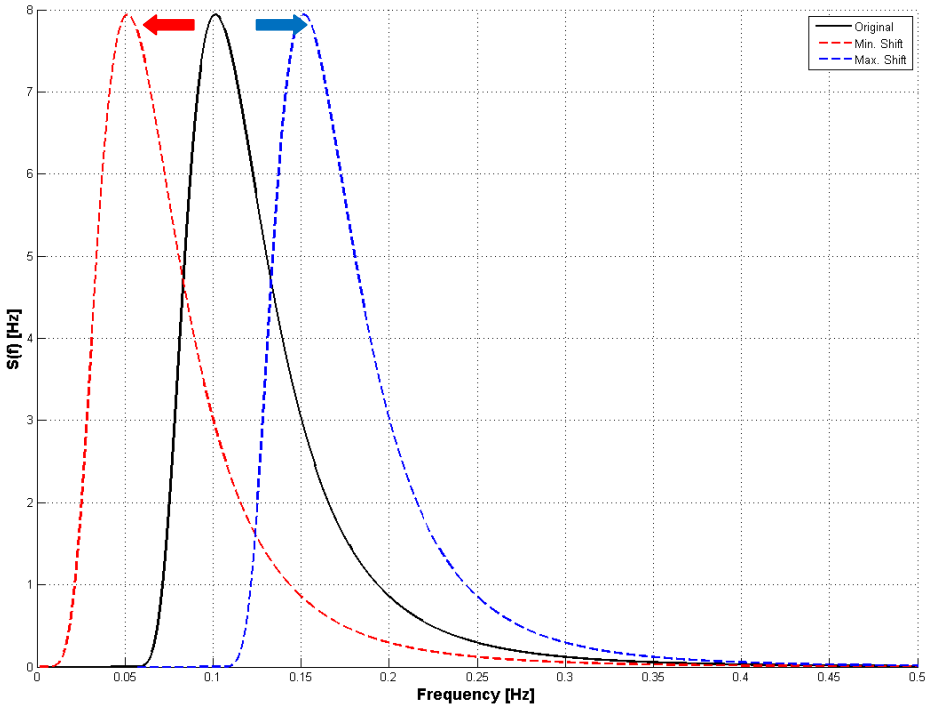

Figure.4.1: Shifted Bretschneider Spectra

From inspection of Equation 2.1 it is evident that this translation of the spectrum along the frequency axis will not affect the various spectral moments to the same extent. The magnitudes of the three spectral moments which influence the T_E and T_{02} parameters, m_{-1}, m_0 and m_2, are graphed against the degree of spectral shift in Fig. 4.2 for a Bretschneider spectrum with inputs of H_{m0}=3 m and T_{02}=7 s. m_{-1} is seen to decrease as the spectrum shifts from low to high frequencies while the value of m_2 increases. m_0 remains constant as the spectrum is translated due to the fact that n = 0 in Equation 2.1.

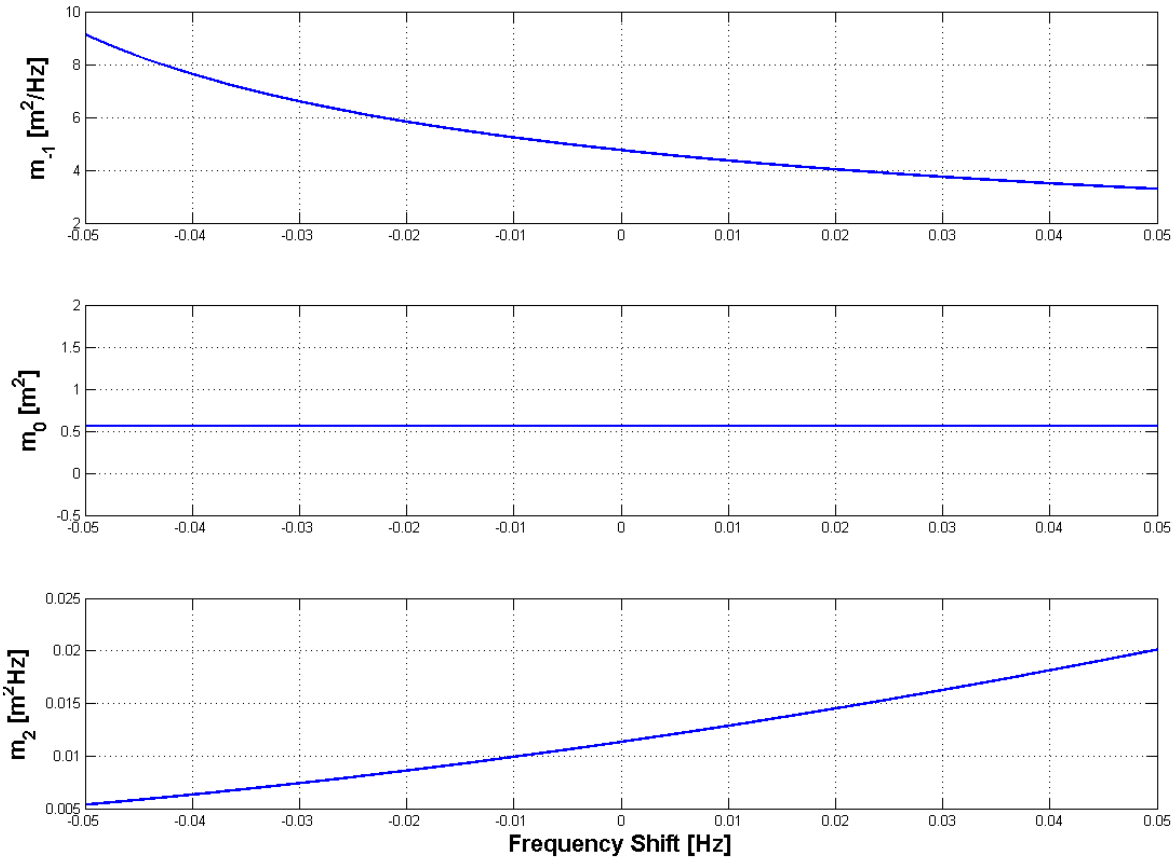

Figure.4.2: Moments of the Bretschneider Spectrum – m_{-1}, m_0 and m_2 – graphed against spectral frequency shift for H_{m0}=3m and T_{02}=7s

Table. 4.1 states that if m_0 is constant then T_E is proportional to m_{-1} whereas T_{02} is proportional to $m_2^{-1/2}$. The resulting effect of translating the position of the Bretschneider spectrum on the parameters T_E and T_{02} is illustrated in Fig. 4.3(a). As expected the magnitudes of both parameters increase as the spectrum is shifted towards lower

frequencies, with the T_E curve displaying a steeper slope. As a result the T_E/T_{02} WPR varies, and can be seen to increase as the spectrum is shifted to lower frequencies (Fig. 4.3(b)). This result is also relevant to real sea-states. In Section 4.3.4 it will be shown that for certain wave climates more of the spectral energy is distributed among the long period components than what would be expected from the Bretschneider spectrum.

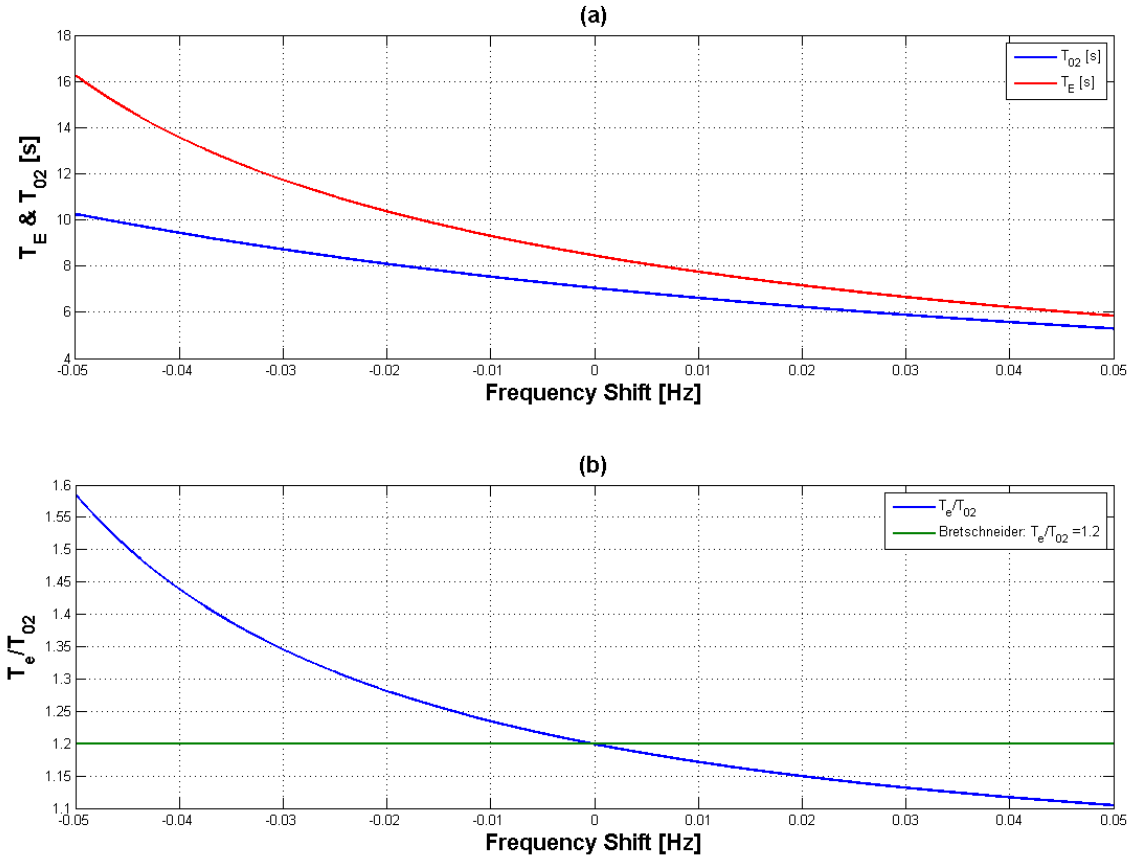

Figure.4.3: T_e and T_{02} (a) and T_E/T_{02} ratio (b) graphed against Spectral Frequency shift

4.3 Wave Period Ratio in Real Saes

As the results detailed in Section 4.2 relate only to the case of theoretical spectra, analysis of measured wave data, collected at a number of different water depths and geographical locations, was carried out in order to assess how applicable the theoretical WPR of 1.2 derived previously is to real sea-states. Measured spectral data were obtained and analysed, rather than relying on archived values of the summary statistics of interest. The

average T_E/T_{02} wave period ratios at each site are presented in Section 4.3.1. More in depth analysis of this relationship is presented for four selected locations in Section 4.3.2, while the correlation between the ratio and spectral shape is examined in Sections 4.3.3-4.3.6

4.3.1 Wave Period Ratio from Measured Data

The nature of the WPR in real seas was analysed using measurements obtained from four geographical regions: Ireland and the United Kingdom; the eastern seaboard of the United States; and the states of Oregon and California on the US Pacific coast. Data from Irish waters were obtained from the wave buoys in Galway Bay and at AMETS, and from a previous measurement campaign near Loop Head, Co. Clare (Holmes and Barret 2007). WPR values were also obtained for EMEC in Orkney, Scotland (Cradden 2012) and the Wave Hub Test site off the coast of Cornwall (Smith 2012) through the European Energy Research Alliance (EERA) Marine Joint Programme. As mentioned in Section 3.4, data from the United States were obtained through the websites of the National Data Buoy Centre (National Data Buoy Centre 2012) and the Scripps Institute of Oceanography (Coastal Data Information Program 2012).

Measured spectral data was processed and analysed for each location, rather than relying on archived values of the summary statistics of interest. Spectral moments and important wave parameters were derived from the observed spectra following the methods described in Chapter 2. The characteristic WPR for each location is defined in Equation 4.19 as the average value of T_E/T_{02}.

$$T_E/T_{02} = \frac{1}{N}\sum_{i=1}^{N}\frac{(T_E)_i}{(T_{02})_i} \tag{4.19}$$

The details of the datasets and the computed WPRs for the various regions that were studied are compiled in Tables 4.5-4.8. A selection of sites with unique characteristics which produced distinctive WPRs is also included in Table 4.9. Data analysed in this section were obtained from a number of different types of measurement buoy, primarily surface following Datawell Waverider buoys and the 3m diameter PRH buoys operated by the NDBC. Where possible, a full year's worth of data was analysed at each location

to prevent seasonal bias affecting the results. Unfortunately there is poor data availability during the summer months for the Belmullet and Loop Head buoys and the operation of the buoy in Lake Michigan was limited in winter due to ice coverage.

It is evident that distinct ranges of the T_E/T_{02} ratio are associated with each of the geographical regions that were studied. The average values of T_E/T_{02} calculated from buoy data measured off the Atlantic coast of the United States (Table 4.3) can be seen to agree quite well with the Bretschneider approximation. Most of the datasets from this region which were analysed were found to have values close to 1.2, though a value of 1.24 was calculated for the Virginia Beach buoy. It is noticeable that the range of values from the Pacific coast conforms poorly to what is expected from the theoretical spectra. The WPRs for the Oregon buoys (Table 4.4) lie in the range 1.26-1.30, while to their south the locations off the Californian coast (Table 4.5) exhibit higher ratios (1.27-1.38) with a greater degree of variation between sites.

WPRs derived from measurements at the exposed Atlantic sites in Ireland and the UK are even higher, ranging from 1.32-1.44 (Table 4.2). This is significant in the context of wave energy resource assessment and economic modelling when one considers that, as mentioned previously, a value of 1.12 has often been assumed. If the WPR derived from the AMETS and Loop Head observations were considered to be characteristic for the entire Irish western seaboard the magnitude of the theoretical wave energy resource presented in the Accessible Wave Energy Atlas (ESB International 2005) could be revised upwards by 18%.

Location	**Data Period**	**Buoy type**	**Water depth**	**T_E/T_{02}**
AMETS	2010	Datawell Waverider	50m	1.32
Loop Head	2004	Datawell Waverider	50m	1.33
EMEC	2010	Datawell Waverider	50m	1.38
Wave Hub	2009-2010	Seawatch Mini	40m	1.44

Table 4.2: Wave period ratios for Irish and UK exposed sites

Location	NDBC Station	Data Period	Buoy type	Water depth	T_E/T_{02}
Nantucket, Massachusetts	41001	2010	NDBC Discus Buoy	65m	1.205
Cape Hatteras, North Carolina	44008	2010	NDBC Discus Buoy	4462m	1.207
Virginia Beach, Virginia	44014	2010	NDBC Discus Buoy	95m	1.244
West of Bermuda	41048	2010	NDBC Discus Buoy (12m)	5261m	1.208

Table 4.3: Wave period ratios for US East Coast Sites

Location	NDBC Station	Data Period	Buoy type	Water depth	T_E/T_{02}
Colorado River Bar, Oregon	46029	2010	NDBC Discus Buoy	135m	1.274
Tillamook, Oregon	46089	2010	NDBC Discus Buoy	2230m	1.260
Stonewall Bank, Oregon	46050	2010	NDBC Discus Buoy	123m	1.263
Umpqua, Oregon	46266	2010	Datawell Waverider	186m	1.299

Table 4.4: Wave period ratios for Oregon sites

Location	NDBC Station	Data Period	Buoy type	Water depth	T_E/T_{02}
San Francisco, California	46028	2010	NDBC Discus Buoy	55m	1.295
Point Sur, California	463298	2010	Datawell Waverider	366m	1.346
Cape San Martin, California	46028	2010	NDBC Discus Buoy	1158m	1.273
Diablo Canyon, California	46215	2010	Datawell Waverider	23m	1.378

Table 4.5: Wave period ratios for California sites

Location	NDBC Station	Data Period	Buoy type	Water depth	T_E/T_{02}
Galway Bay	N/A	2010	Datawell Waverider	25m	1.447
Duck, North Carolina	44100	2010	Datawell Waverider	26m	1.389
Pensacola, Florida	46039	2010	NDBC Discus Buoy	307m	1.133
South Lake Michigan	45007	2010	NDBC Discus Buoy	160m	1.048

Table 4.6: Wave period ratios for miscellaneous sites

Analysis was also carried out on a number of datasets that were recorded at locations that experience site specific wave conditions (Table 4.6) and are presented as examples of WPR values which diverge greatly from those at the open ocean sites discussed previously. Very low ratios were calculated from the measurements taken in the Gulf of Mexico near Pensacola, Florida, and from the buoy in South Lake Michigan. Both of these sites are relatively fetch-limited and rarely experience sea-states with $H_{m0} > 2$ m (though there have been instances in the past where the Pensacola buoy has recorded H_{m0}

> 12 m during hurricane conditions). In contrast, data from Galway Bay – a semi-enclosed site – display much higher WPR that the nearby offshore buoys at AMETS and Loop Head. As illustrated in Chapter 3 Galway Bay experiences a unique mix of local wind seas and longer period swell which can enter the bay through the channels which separate the Aran Islands from the mainland. This results in the frequent occurrence of bi-modal spectra, particularly in low sea-states (H_{m0} < 1 m) where they have been observed to account for 40% of spectra (Barrett et al. 2009). The WPR at Duck is higher than the other location along the US East coast, however this buoy is moored in shallower water close to the shore and experiences intermediate water depth conditions more than 67% of the time, whereas data from the other buoys in this region can be considered to be from predominantly deep water. Thus the spectra measured at this point are likely to have undergone a degree of transformation as they propagated from the oceanic waters towards the coast.

4.3.2 Variability of the Wave Period Ratio

Annual average values were used in the previous section to characterise the expected WPR at the locations being analysed. In reality this relationship is transient and its values can fluctuate significantly at a site depending on the incident wave conditions and the composition of the wave spectra. This variability is illustrated in Fig. 4.4 which plots the evolution of the WPR and the significant wave height measured by the Datawell Waverider at the 50 m depth at AMETS in January 2011.

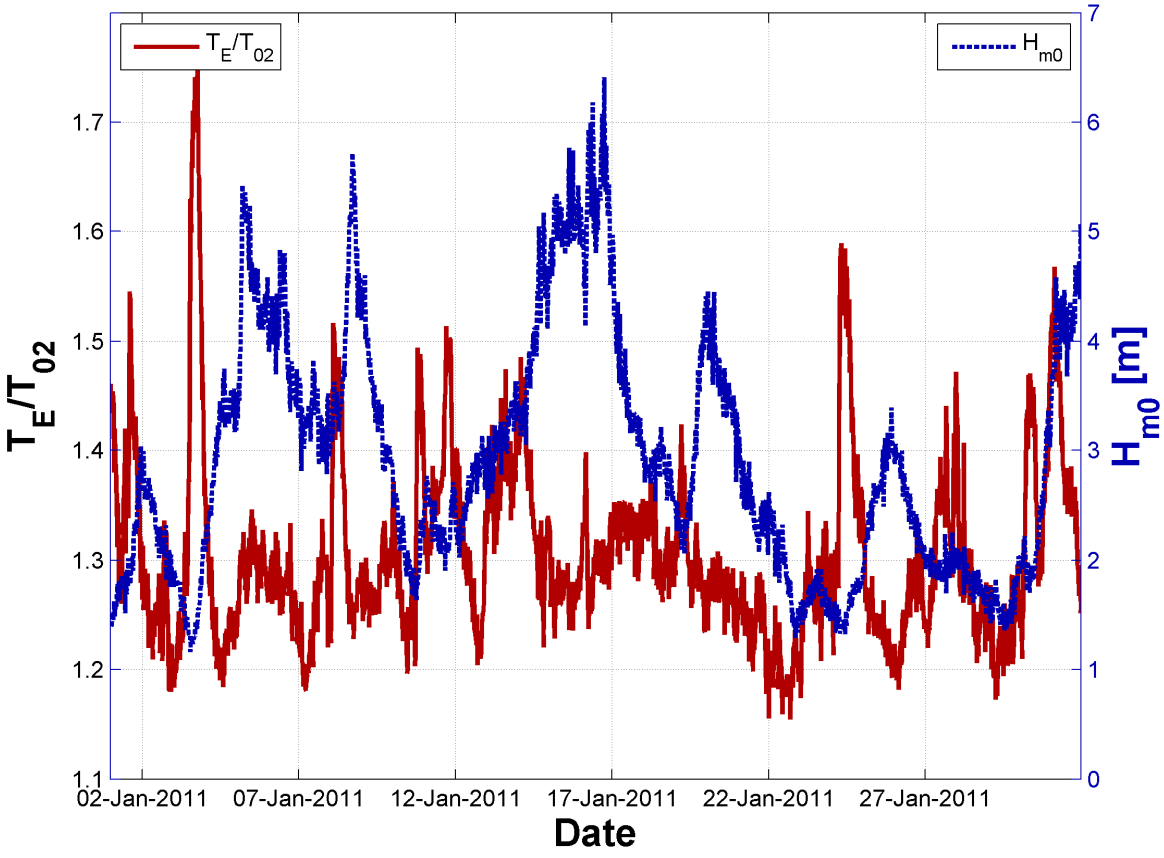

Figure 4.4 Time series of wave period ratio and H_{m0} from AMETS 50 m depth (January 2011)

Fig. 4.4 highlights that the WPR is not a static quantity and that it is loosely correlated to H_{m0}; in general T_E/T_{02} is higher in low sea-states, and vice versa. This relationship is also evident in Figs. 4.5-4.8 where the WPR is plotted against the corresponding H_{m0} values for datasets of one full year. Four sets of measurements from locations deemed to be representative of the general geographic locations introduced previously in Tables 4.5-4.8; AMETS (50 m depth), for the West Coast of Ireland; Nantucket, for the US East Coast, Umqua, Oregon; and the buoy off San Francisco, California, were selected for further analysis.

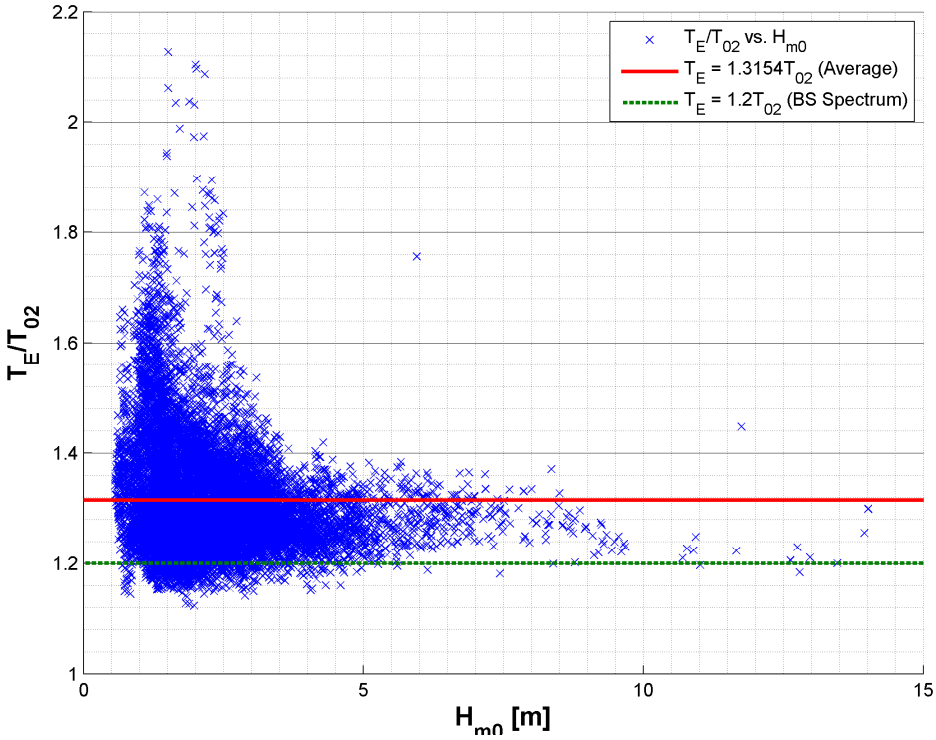

Figure.4.5: Wave period ratio plotted against H_{m0} for AMETS (2010)

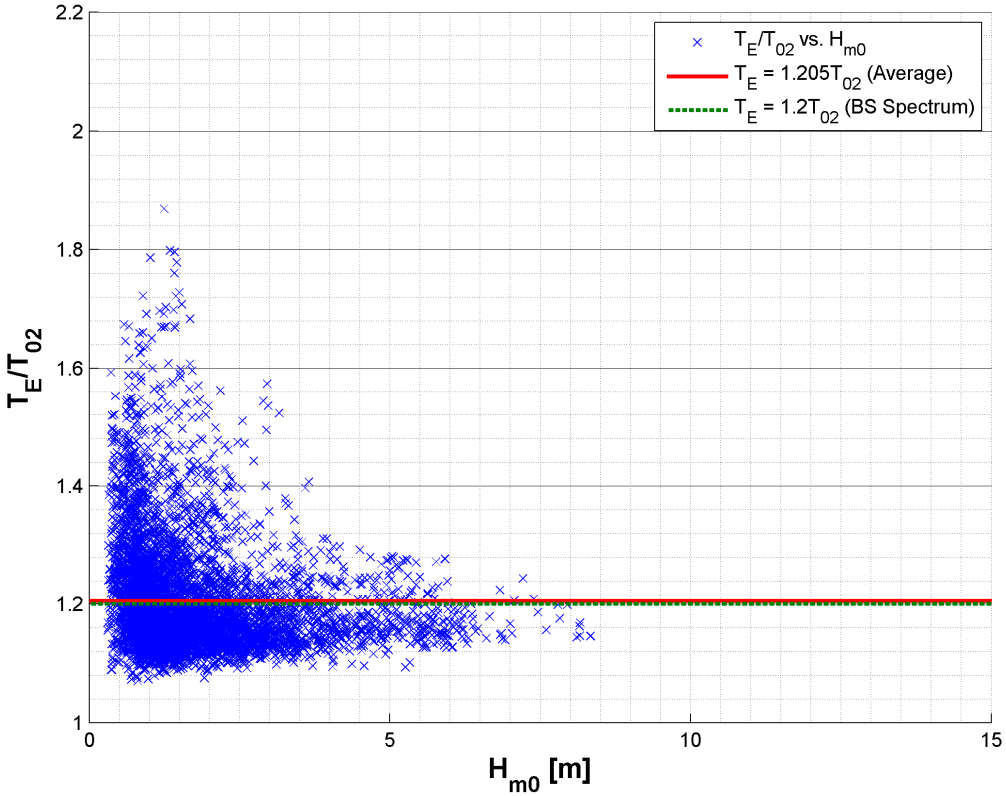

Figure.4.6: Wave period ratio plotted against H_{m0} for Nantucket (2010)

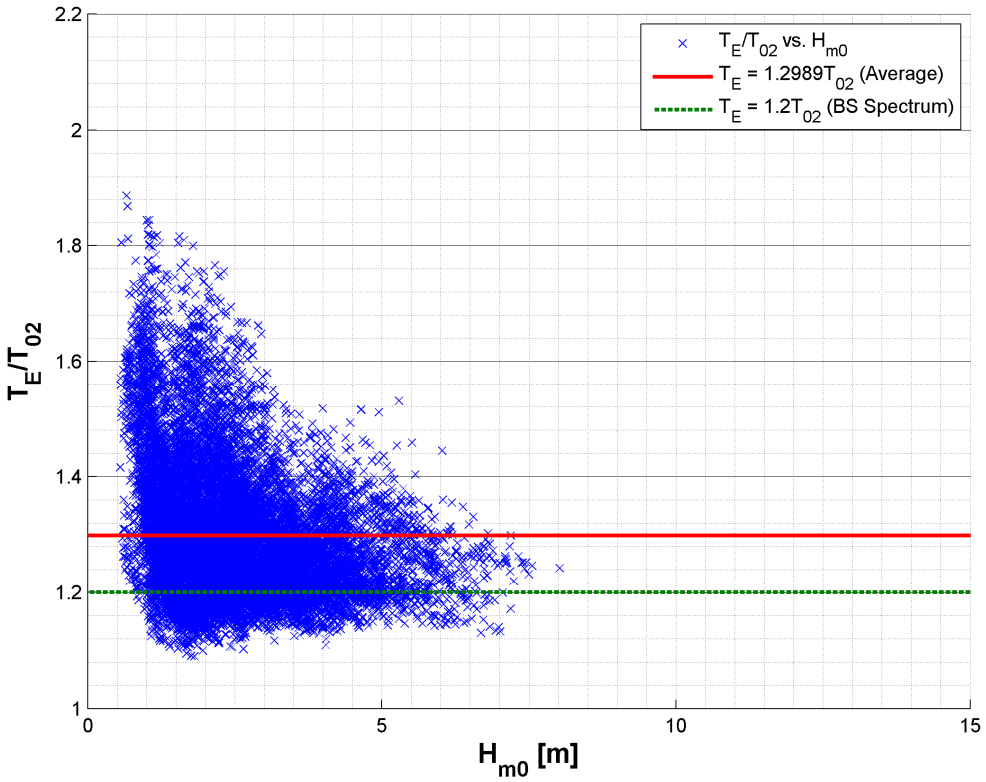

Figure.4.7: Wave period ratio plotted against H_{m0} for Umqua (2010)

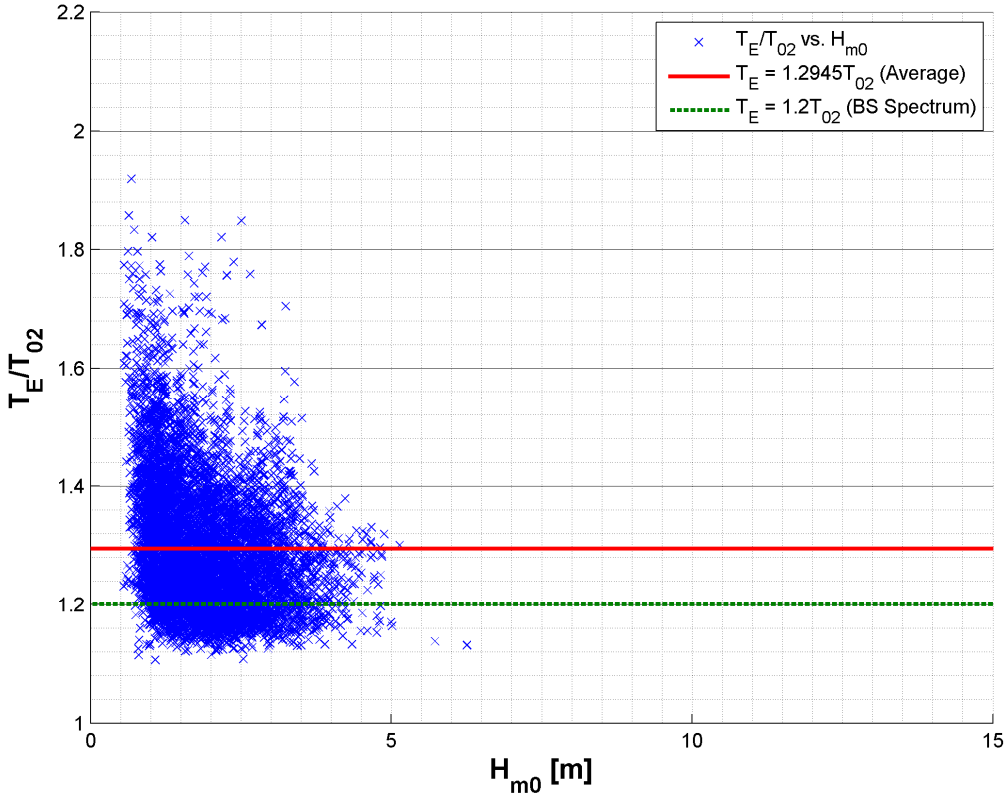

Figure.4.8: Wave period ratio plotted against H_{m0} for San Francisco (2010)

Despite large amount of scatter and many individual outliers similar trends are apparent in all four cases presented in Figs. 4.5-4.8. It is evident that large discrepancies exist in the relationship between T_E and T_{02} when the significant wave height is low and that the highest WPR values tend to occur during these frequently occurring conditions. Conversely, WPRs are constantly closer to the value of 1.2 derived from the Bretschneider spectrum during the greater sea-states. Prominent outliers which occur in Fig. 4.5 for the AMETS measurements are discussed in the next section.

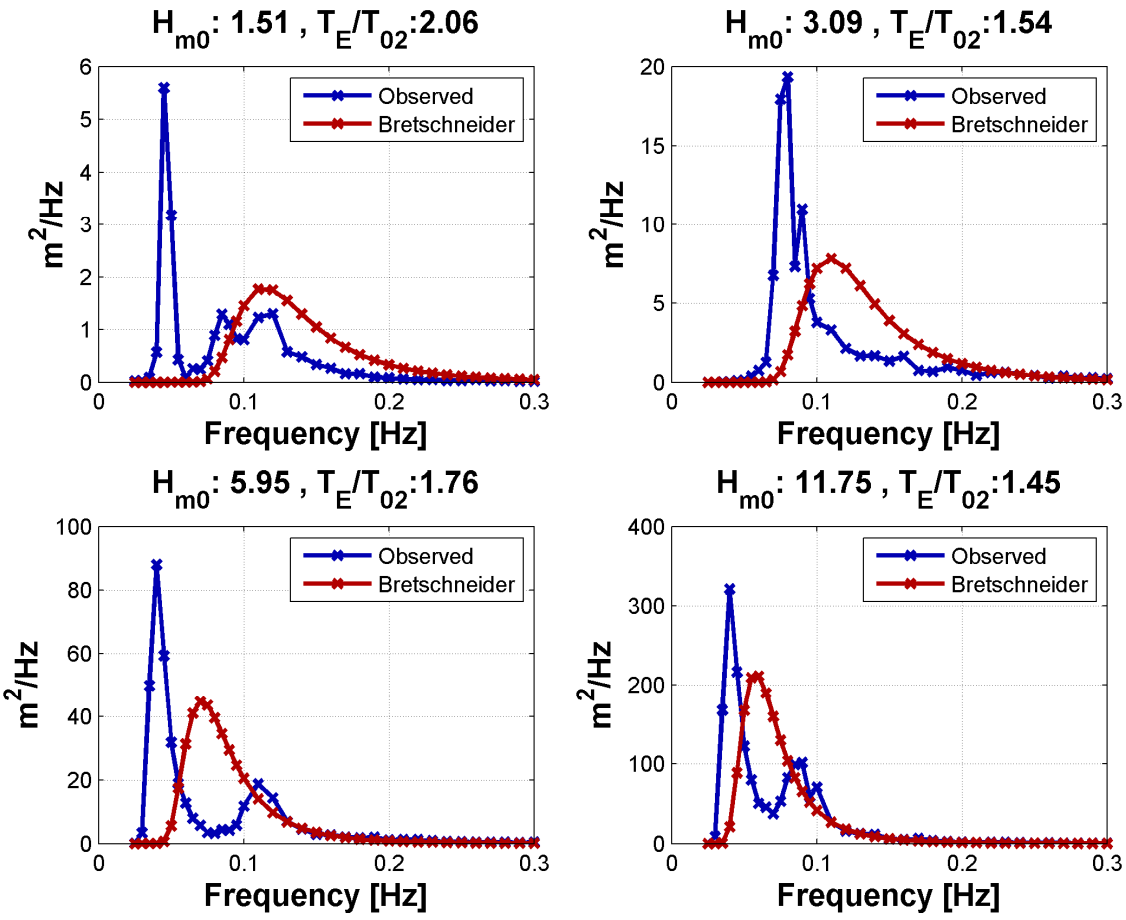

Figure 4.9: Outlier spectra from Fig. 4.6 plotted against their Bretschneider equivalents

4.3.3 Multimodal Spectra

The spectra from four of the outlier points in Fig. 4.5 for the AMETS data are plotted against their equivalent Bretschneider spectrum in Fig. 4.9. Two of the most noticeable

outliers – the points with H_{m0} of 5.95 m and 11.75 m, and T_E/T_{02} equal to 1.76 and 1.45 respectively – are included as they present particularly interesting cases. An obvious similarity is apparent in Fig. 4.9, with multiple peaks evident in the measured spectra and the primary peaks occurring at lower frequencies than the peaks of the corresponding Bretschneider spectra. For these cases much the variance of the spectra is shifted towards the low frequency components; as Fig. 4.3 demonstrated this will result in an increase in the WPR.

In order to investigate any correlation between bimodality and the WPR in a quantitative manner it is first necessary to identify instances of double peaked spectra. Criteria for designing algorithms to detect these events using the confidence intervals of the wave spectrum have been outlined by a number of authors (Guedes Soares 1984; Guedes Soares 1991; Rodríguez and Guedes Soares 1999) while a simple and robust procedure - which has been used previously in the analysis of waves from Galway Bay - was developed by Barrett (2010). Following this methodology a spectral ordinate can be considered to be a valid secondary peak if:

- The peak is a local maximum
- If it has a magnitude of at least 15% of $S(f_{peak})$
- Separated from the primary peak by a period of at least 2 seconds

This method was adapted in the analysis presented here so that various levels of 'multi-peakedness' could be discerned. A further criterion that the magnitude of the secondary peak must be a defined percentage (e.g. 115%) greater than the shallowest point of the trough separating it from the primary peak was introduced and the separating distance between the peaks was varied between 1 s to 5 s. The most stringent case - a secondary peak significantly larger than the trough and separated from the spectral peak by 5 s – selected a small number of instances which could be classed as 'extremely bimodal'.

By applying this methodology to the data measured at AMETS in 2010 (13189 spectra) a series of groups of increasing multimodality were compiled. The method applied by Barrett identified 3723 cases at AMETS for the 2010 dataset, approximately 28% of measurements; this corresponds reasonably well with the work of Guedes Soares who

showed that bimodal spectra composed 22% of observations at a North Atlantic location (Guedes Soares 1984). Separating the multimodal spectra from the general population allows Fig. 4.5 to be redrawn in Fig. 4.10. These spectra are shown to occur primarily during low sea-states (H_{m0} < 3 m) and display a higher WPR (1.352) than the remainder of the measurements (1.300). Single-peaked seas can be seen to account for many of the highest values of the WPR but also contribute most of the instances where the WPR approaches the value of 1.2 derived from the Bretschneider spectrum.

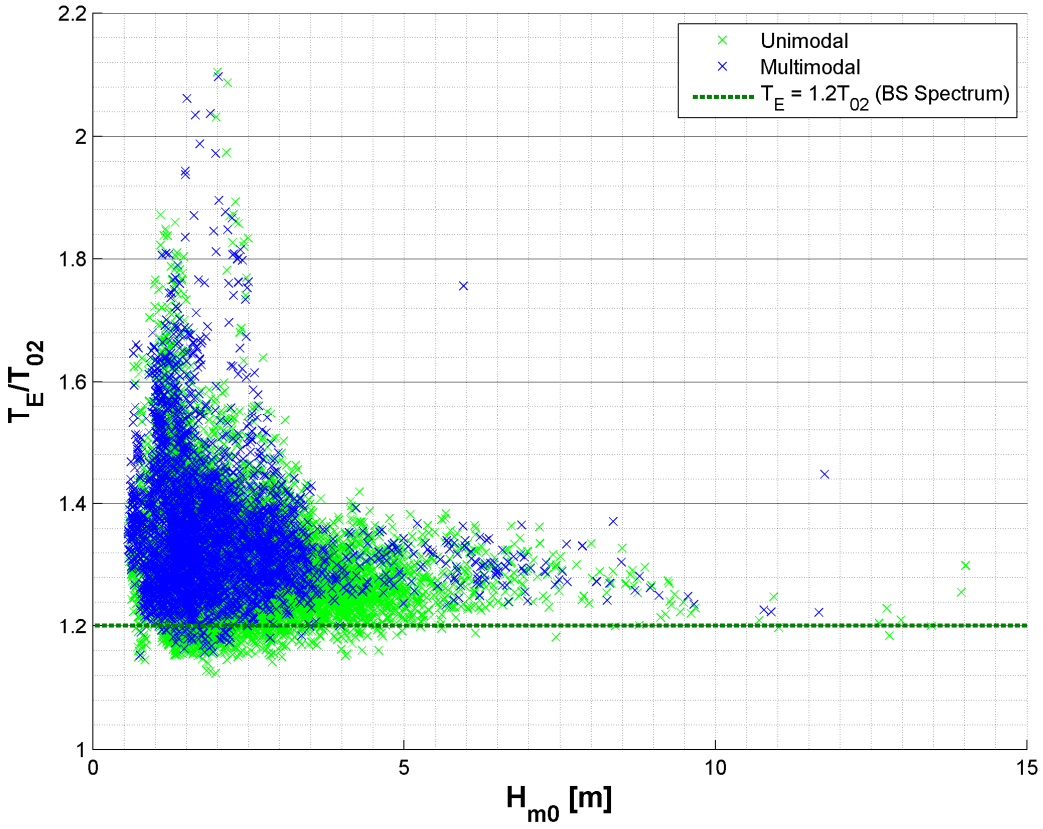

Figure.4.10: Wave period ratio plotted against H_{m0} for unimodal and multimodal seas for AMETS (2010)

Peak Separation [s]	Secondary Peak – Trough Difference				
	105%	**110%**	**115%**	**120%**	**125%**
1	1.350 *(4001)*	1.360 *(3048)*	1.368 *(2475)*	1.375 *(2075)*	1.381 *(1802)*
2	1.352 *(3723)*	1.363 *(2890)*	1.370 *(2389)*	1.376 *(2022)*	1.382 *(1769)*
3	1.365 *(2928)*	1.373 *(2413)*	1.378 *(2086)*	1.383 *(1829)*	1.387 *(1643)*
4	1.383 *(2083)*	1.391 *(1765)*	1.396 *(1556)*	1.400 *(1412)*	1.402 *(1305)*
5	1.409 *(1226)*	1.417 *(1059)*	1.422 *(959)*	1.426 *(887)*	1.428 *(838)*

Table 4.10: Average wave period ratios for selected groups of multimodal spectra. Number of spectra in each group included in brackets.

The average WPR for each of the groups of multi-peaked spectra are collated in Table 4.10. These results show that populations of spectra that have multiple peaks separated by longer and deeper troughs are shown to consistently display the highest average WPR values. The occurrence of a significant proportion of these spectral conditions within the AMETS dataset can be deemed at least partly responsible for the high average WPR, particularly among the low energy sea-states.

4.3.4 Average Spectral Shape

Multimodal spectra represent explicit examples of deviation from the Bretschneider shape. Further analysis was carried out to assess the level of variation exhibited by the general population of data. Spectra from the 2010 AMETS dataset with similar, and frequently occurring, summary statistics — highlighted in the scatter diagram of H_{m0}-T_{02} occurrence presented in Fig. 4.11 — are grouped and plotted in Fig. 4.12. These spectra were obtained from the .spt files produced by the Waverider buoy, described in Section 2.2. The chosen scatter diagram elements are as follows:

- 1.5 m < H_{m0} < 2 m, 4 s < T_{02} < 5 s (very few instances of this sea-state occurred at the San Francisco buoy so the range 5 s < T_{02} < 6 s used instead)
- 2 m < H_{m0} < 2.5 m, 5 s < T_{02} < 6 s
- 3 m < H_{m0} < 3.5 m, 6 s < T_{02} < 7 s
- 4 m < H_{m0} < 4.5 m, 7 s < T_{02} < 8 s

The same sea-states were also analyzed for the Nantucket (Fig. 4.13), Umqua (Fig. 4.14) and San Francisco (Fig. 4.15) datasets. Sea-states were grouped using T_{02} rather than other alternative measures – T_E, T_p, T_{01} etc. - as this is the most commonly featured wave period parameter in the limited datasets that exist for the west coast of Ireland.

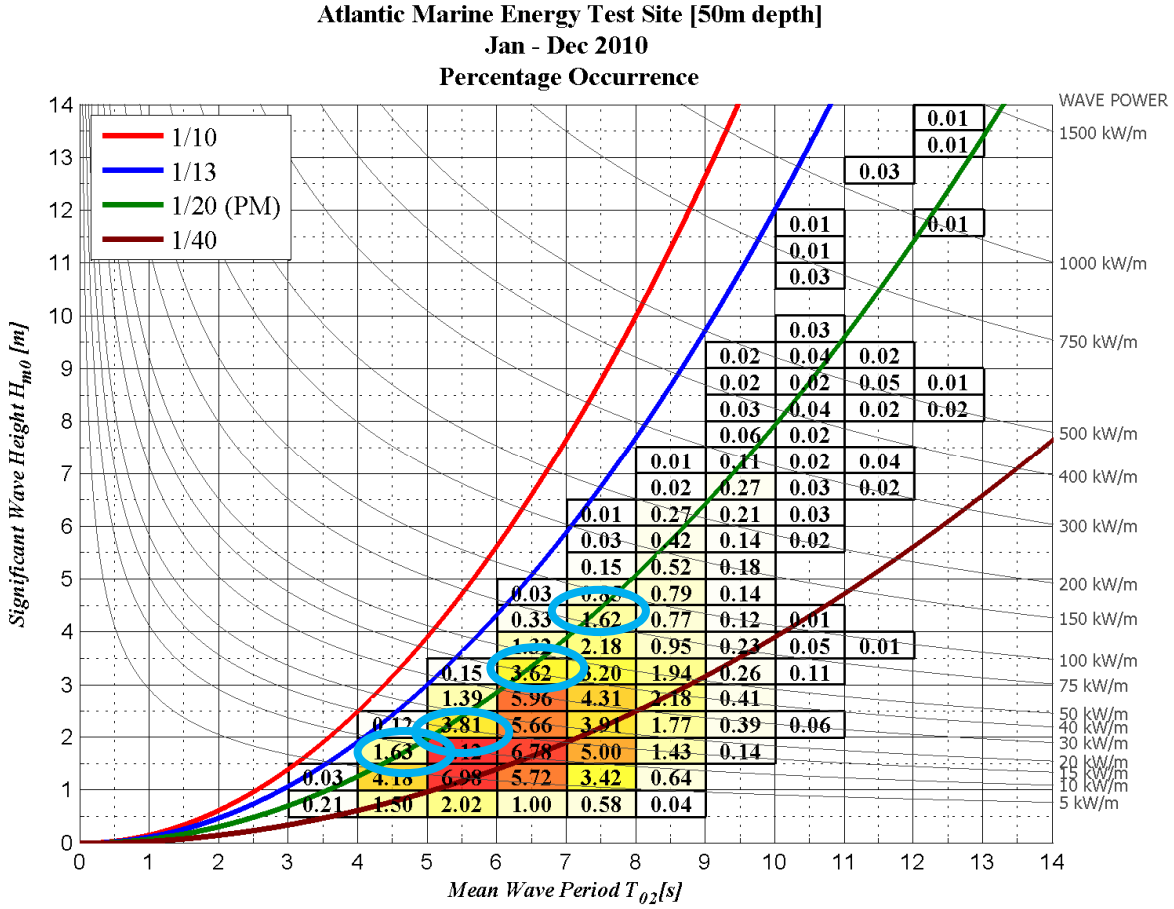

Figure.4.11: Occurrence Scatter plot for the Belmullet site with cells selected for analysis highlighted.

In Figs. 4.12-4.15 all of the measured spectra that occurred within these ranges at each site are plotted, with the maximum and minimum spectral ordinate at each frequency component indicated by the solid black line. The average of the spectral ordinates is shown as the blue line and gives a general indication of the spectral shape that can be

expected at each site. The equivalent Bretschneider spectrum that is also plotted is derived from calculating the spectral moments of the average spectrum and fitting the spectrum using Equation 2.8. Comparison between these two spectra indicates qualitatively how well the theoretical spectrum describes the real conditions at the various locations.

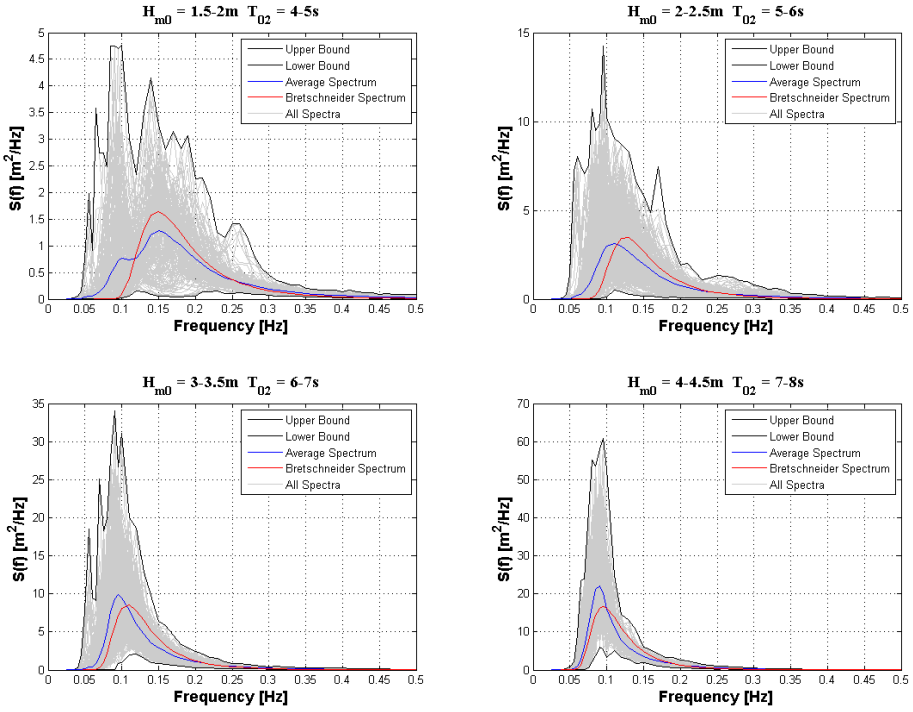

Figure.4.12: Individual, average and equivalent Bretschneider spectra for selected sea-states from AMETS.

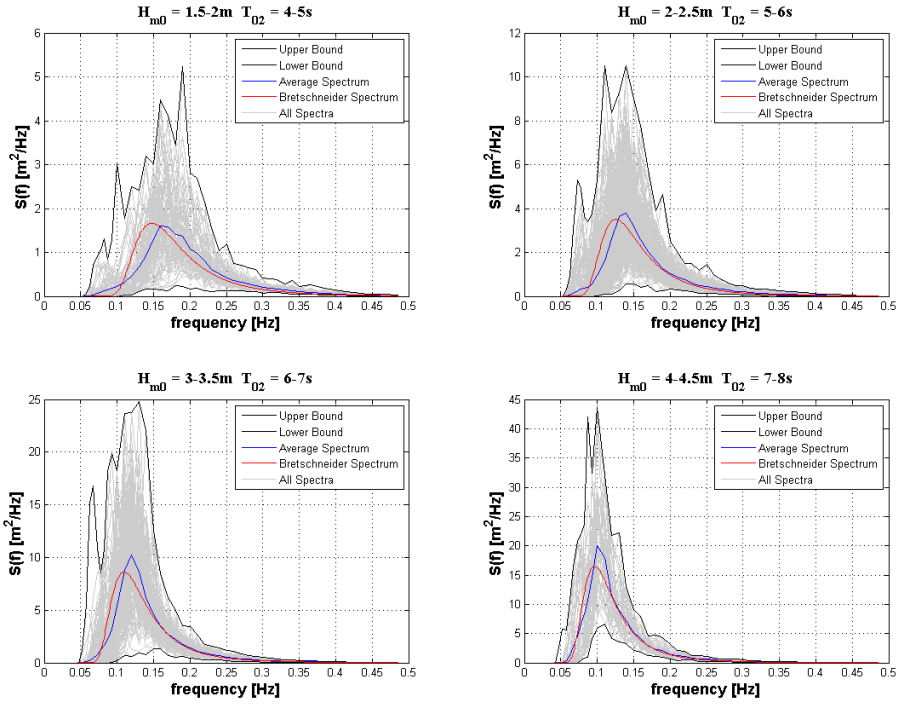

Figure.4.13: Individual, average and equivalent Bretschneider spectra for selected sea-states from Nantucket.

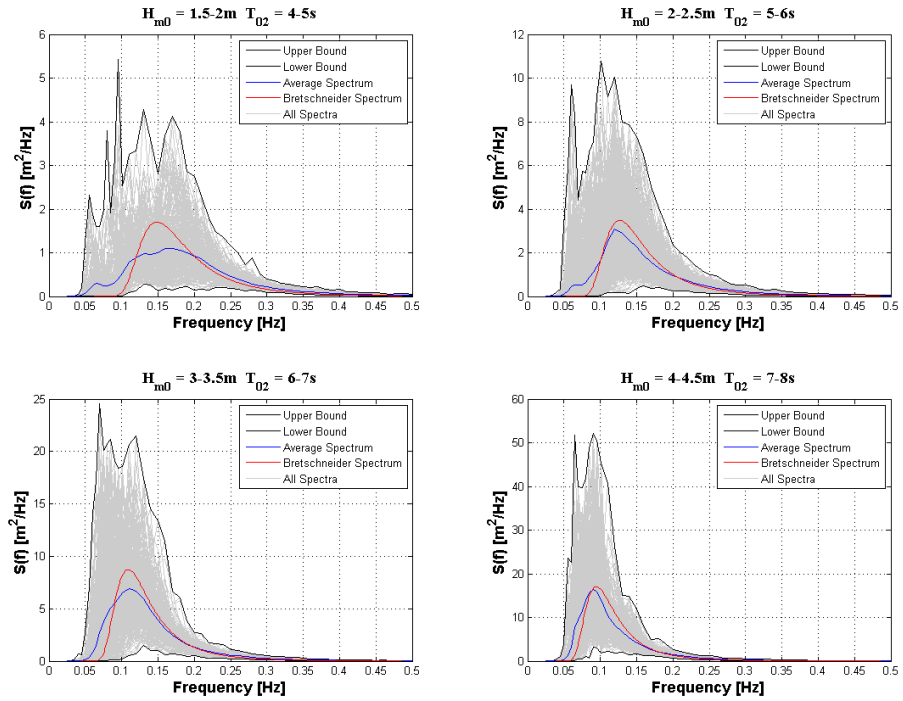

Figure.4.14: Individual, average and equivalent Bretschneider spectra for selected sea-states from Umqua.

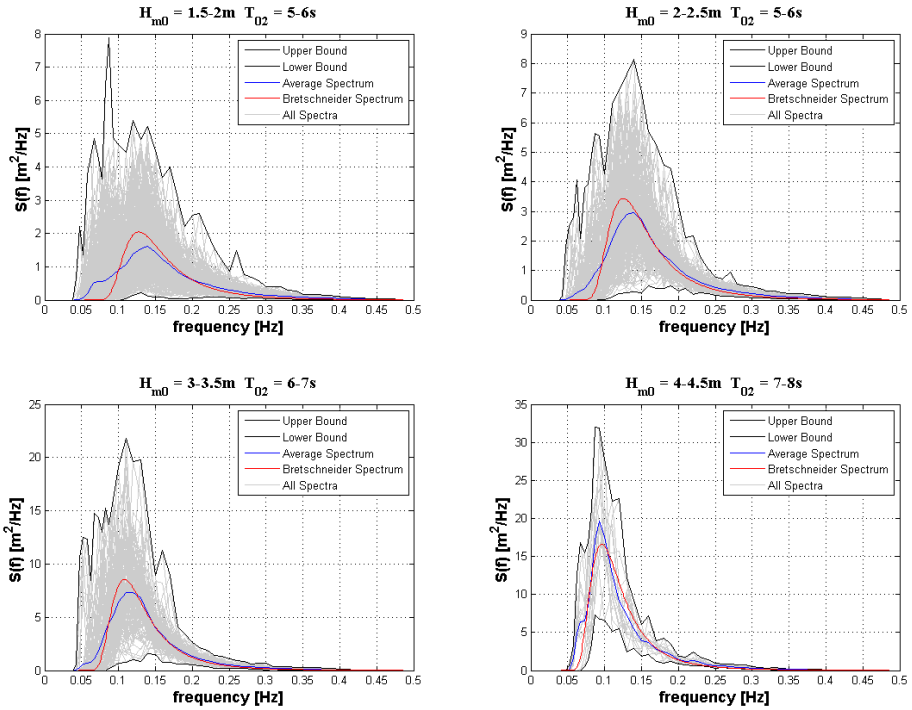

Figure.4.15: Individual, average and equivalent Bretschneider spectra for selected sea-states from San Francisco.

From visual inspection of Figs. 4.12-4.15 it appears that the average spectra from Nantucket closely match the theoretical spectral shapes, though their peaks become more pronounced as H_{m0} increases. Measurements from this site had an average WPR of 1.205, similar to that derived for the Bretschneider Spectrum It is notable that while the average spectra from the AMETS, Umqua and San Francisco datasets also display reasonable agreement with their equivalent Bretschneider spectrum, they are shifted towards the lower frequency components. As with the cases of the multimodal spectra in the previous section this influences the derived spectral moments and results in a higher WPR. These plots also show that the resemblance of the average spectra to the equivalent Bretschneider shape is poor for the low sea-states at each site, while the greater sea-states exhibit good agreement. This corresponds well with the plots of WPR against H_{m0} (Figs. 4.5 – 4.8) where T_E/T_{02} approaches 1.2 more consistently as H_{m0} increased.

4.3.5 Level of Fit

The level of fit between wave spectra has been computed in previous studies using a range of statistical tools. In this section the agreement that exists between the shapes of the measured spectra and their Bretschneider equivalents is investigated quantitatively using the error measures proposed by Sakhare and Deo (2009), namely the correlation coefficient R, the root mean square error, RMSE, and the mean absolute error, MAE. These parameters are derived using the following equations:

$$R = \frac{\sum[S_{meas}(f_i) - \overline{S_{meas}(f_i)}][S_{theory}(f_i) - \overline{S_{theory}(f_i)}]}{\sqrt{\sum[S_{meas}(f_i) - \overline{S_{meas}(f_i)}]^2 \sum[[S_{theory}(f_i) - \overline{[S_{theory}(f_i)}]^2}} \quad (4.19)$$

$$RMSE = \sqrt{\frac{1}{N}\sum_{i=1}^{N}(S_{meas}(f_i) - S_{theory}(f_i))^2} \quad (4.20)$$

$$MAE = \frac{1}{N}\sum_{i=1}^{N}\left|S_{meas}(f_i) - S_{theory}(f_i)\right| \quad (4.21)$$

The calculation of R was limited to the frequency range $0.05Hz<f_p<0.2hz$, where f_p is the frequency of the maximum spectral ordinate, as components outside this range will tend to have little influence on the derived spectral moments while RMSE and MAE, both of which have units of m^2/Hz, were normalised by dividing by the maximum spectral ordinate, i.e. the value of $S_{meas}(f_p)$. Negative values of R are rare, but where they are detected they are seen to correspond to cases where a slight inverse relationship exists between the spectra, such as for bimodal spectra where the peak of the Bretschneider spectrum lies between the wind sea and swell components. Selected measured spectra from the AMETS dataset that display both high and low values of agreement with their equivalent Bretschneider spectra - defined by their R value - are presented in Fig. 4.16.

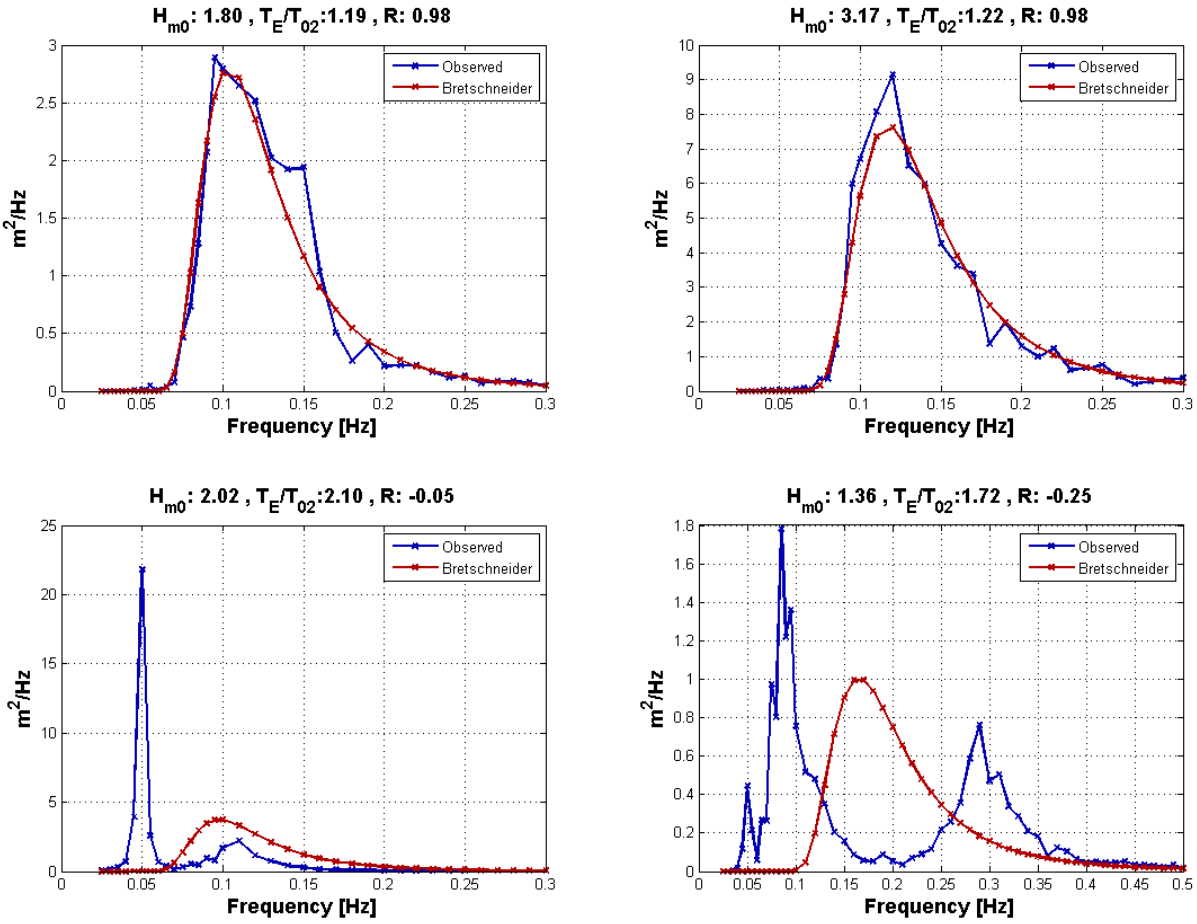

Figure.4.16: Outlier spectra from Fig. 4.6 plotted against their Bretschneider equivalents

The average values of R, RMSE and MAE computed from the datasets from each of the four locations — AMETS, Nantucket, Umqua and San Francisco — are compiled in Table 4.11. These values do not yield an obvious relationship between spectra which display good agreement with the Bretschneider spectrum and a low WPR; in fact these results indicate that the AMETS observations — which produced the highest average WPR — exhibit the highest level of conformity. More obvious trends are noticeable when individual values of the fit parameter R are plotted against the corresponding WPR in Figs 4.17-20. A colour scale is also included in these figures as a means to highlight the density of occurrence of individual points within the centre of the overall scatter. For all four datasets it can be seen that while many outliers exist, in general the spectra that have the best levels of fit with the Bretschneider spectrum tend to have the lowest ratios. Equivalent figures are included in Appendix I for RMSE and in Appendix II for MAE.

Station	R	RMSE	MAE	T_e/T_{02}
AMETS	0.745	0.124	0.051	1.32
Nantucket	0.735	0.142	0.072	1.205
Umqua	0.736	0.123	0.053	1.299
San Francisco	0.711	0.154	0.077	1.295

Table 4.11: Average values for fit parameters for Belmullet, Nantucket, Umqua and San Francisco locations

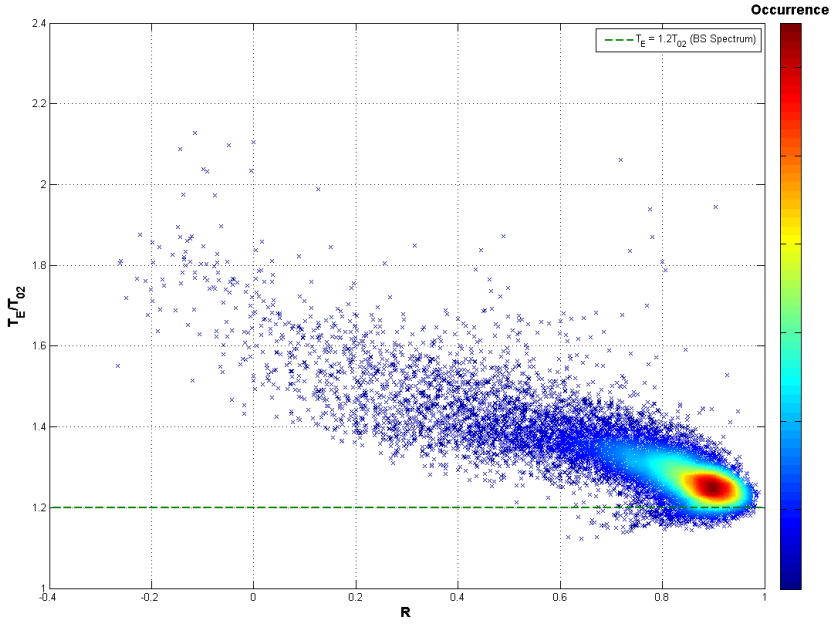

Figure.4.17: Wave period ratio plotted against Correlation Coefficient, R, for AMETS (2010)

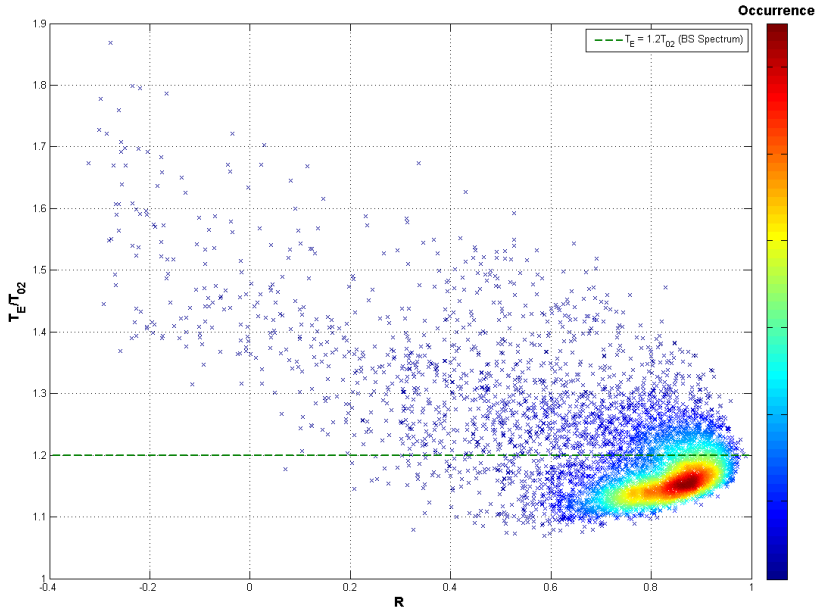

Figure.4.18: Wave period ratio plotted against Correlation Coefficient, R, for Nantucket (2010)

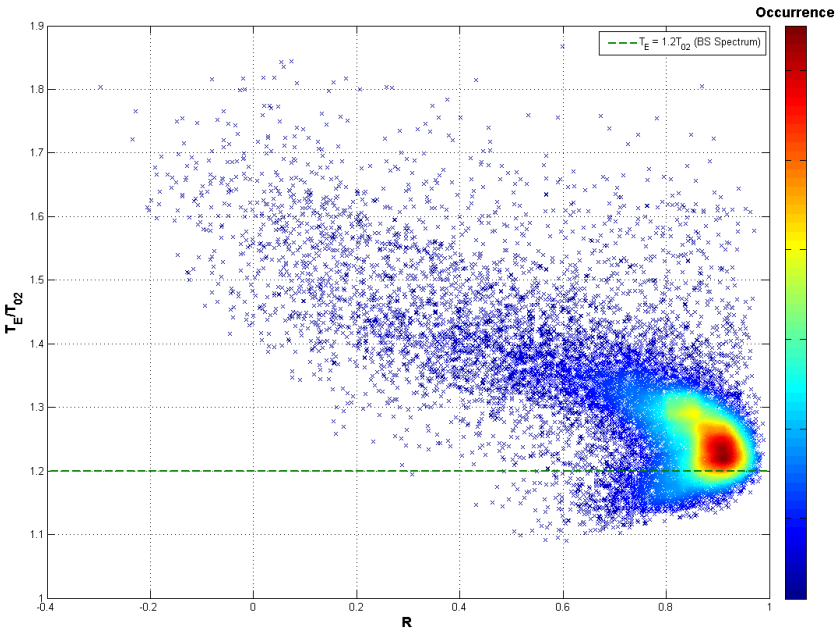

Figure.4.19: Wave period ratio plotted against Correlation Coefficient, R, for Umqua (2010)

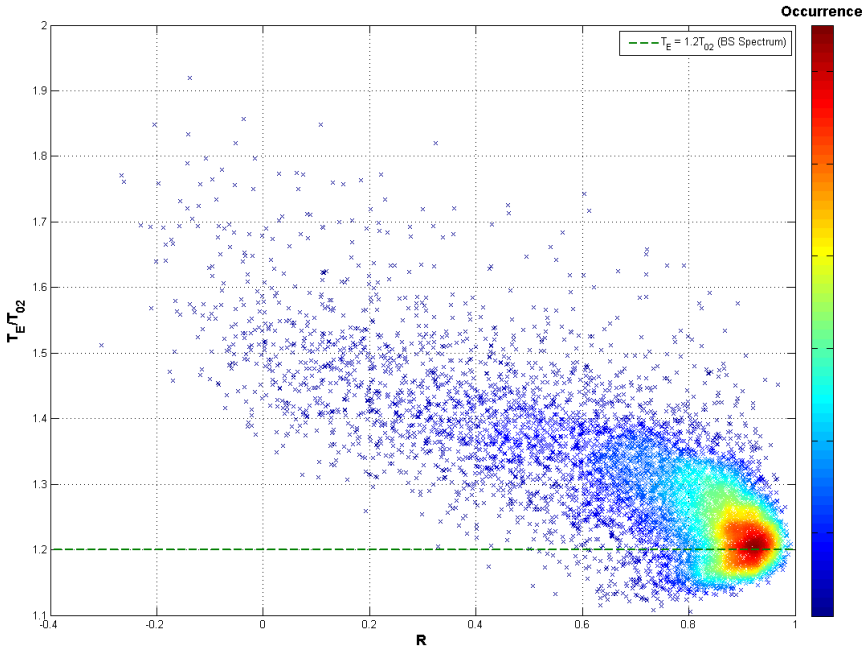

Figure.4. 20: Wave period ratio plotted against Correlation Coefficient, R, for San Francisco (2010)

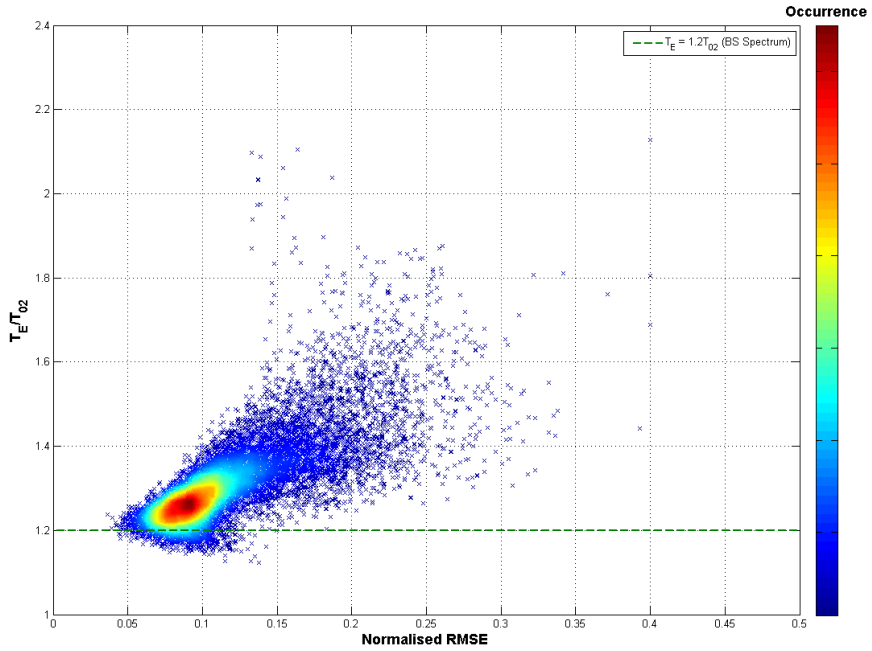

Figure.4.21: Wave Period ratio plotted against Root Mean Square Error, RMSE, for AMETS (2010)

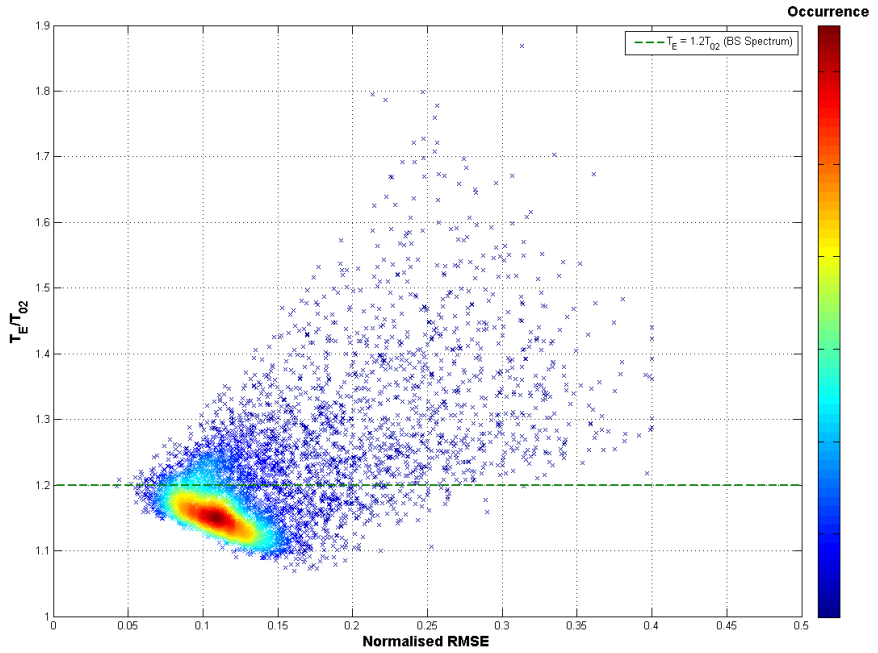

Figure.4.22: Wave period ratio plotted against Root Mean Square Error, RMSE, for Nantucket (2010)

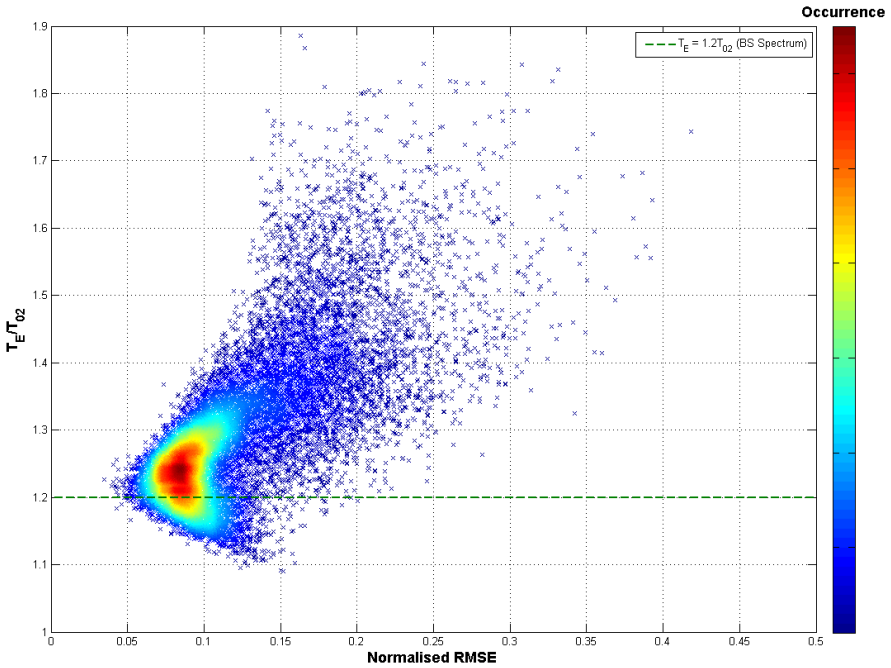

Figure.4.23: Wave period ratio plotted against Root Mean Square Error, RMSE, for Umqua (2010)

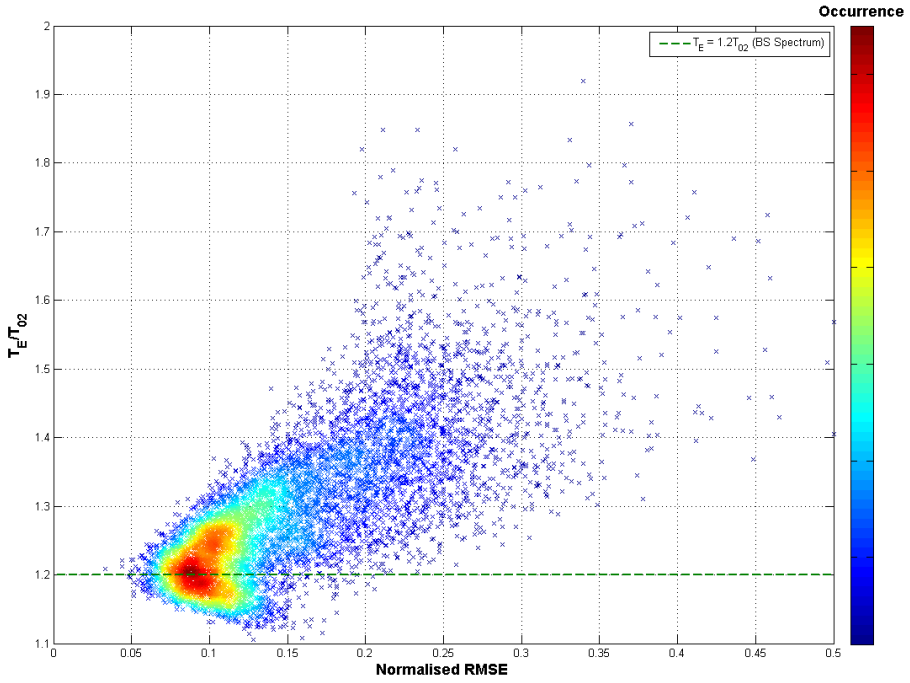

Figure.4.24: Wave period ratio plotted against Root Mean Square Error, RMSE, for San Francisco (2010)

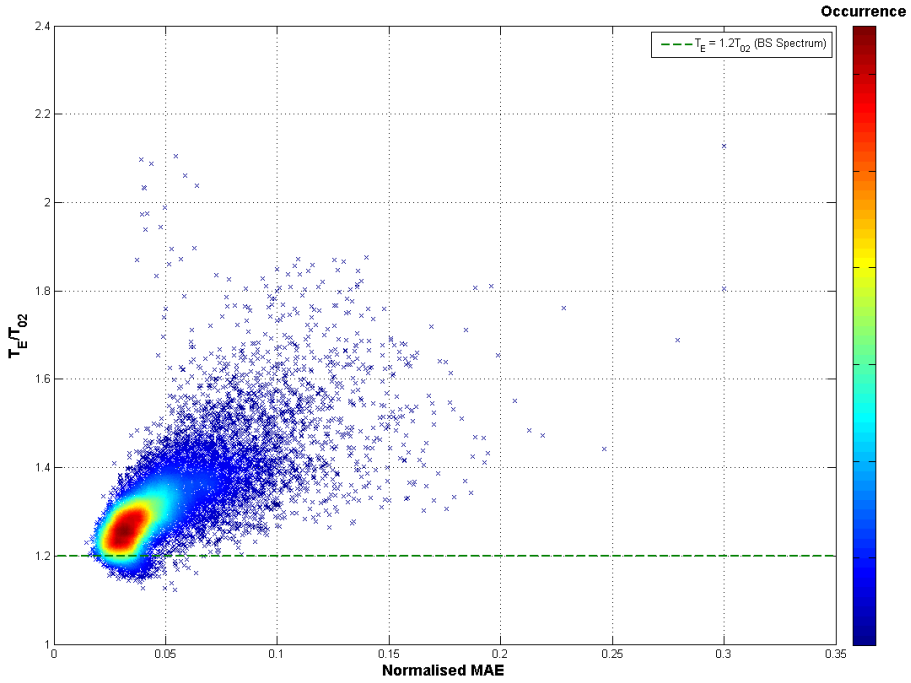

Figure.4.25: Wave period ratio plotted against Mean Absolute Error, MAE, for Belmullet (2010)

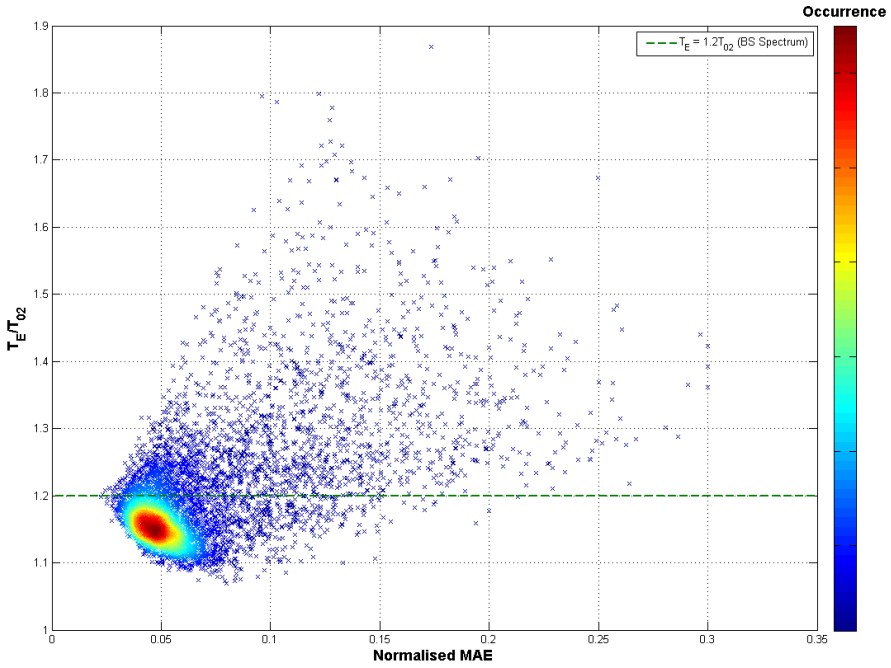

Figure.4.26: Wave period ratio plotted against Mean Absolute Error, MAE, for Nantucket (2010)

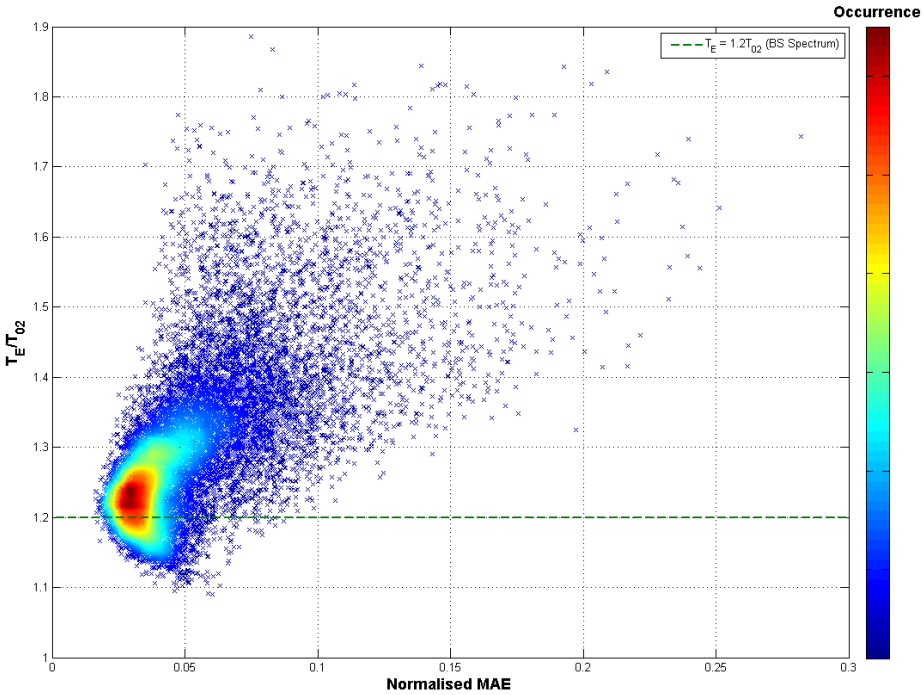

Figure.4.27: Wave period ratio plotted against Mean Absolute Error, MAE, for Umqua (2010)

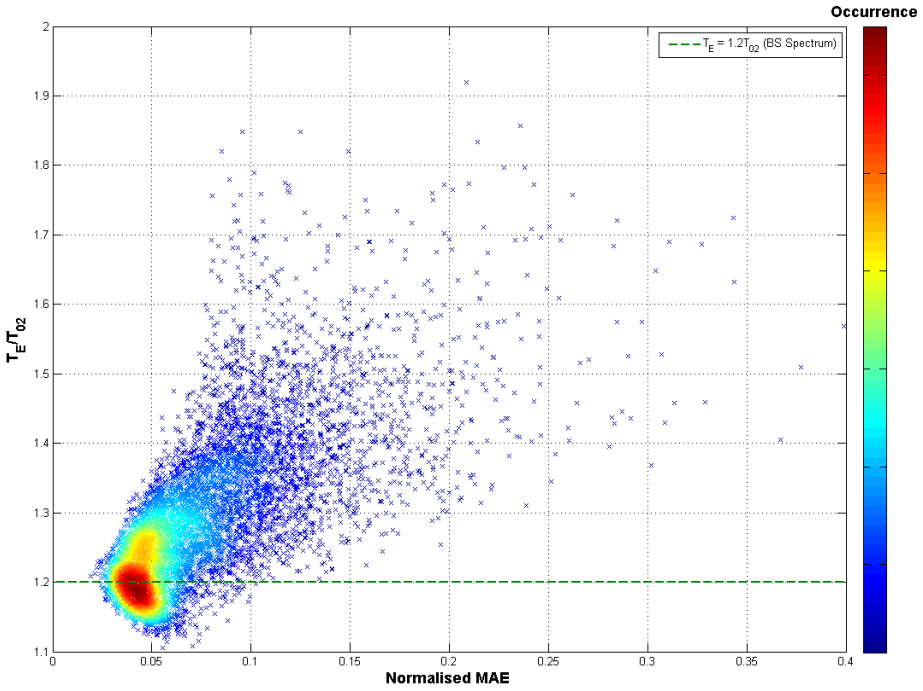

Figure.4.28: Wave period ratio plotted against Mean Absolute Error, MAE, for Umqua (2010)

4.3.6 Spectral Bandwidth

Spectral bandwidth is an important parameter for the representation of sea-states and is particularly useful in the study of spectral shape. In Figs. 4.21-4.24 values of the WPR derived from observed spectra from the Belmullet, Nantucket, Umqua and San Francisco buoys are plotted against the corresponding bandwidth parameters ε_1 and ε_2 given by Equation (2.6) and Equation (2.7). These figures display a strong relationship between T_E/T_{02} and spectral bandwidth at each of the locations. It is noticeable that the narrowest spectra, i.e. those with values of ε_1 and ε_2 approaching 0, also tend to display the lowest T_E/T_{02} ratios. Conversely, the wide banded spectra account for the higher values of T_E/T_{02} and mainly occur when H_{m0} is low, which agrees with the conclusions presented earlier in this chapter. This relationship would be a useful tool for selecting an appropriate WPR for different sea states — a linear best-fit line could be easily added to Figs. 4.21-4.24 — however in the majority of cases values of the bandwidth tend not to be supplied in the absence of spectral data.

These results also help confirm the suppositions drawn from the visual analysis of observed spectra in the previous sections. The averages of the measured spectra taken from the AMETS, Umqua and San Francisco buoys tend to contain additional low frequency components, leading to an increased spectral bandwidth and consequently a higher T_E/T_{02} than their Bretschneider equivalents, while the spectra observed at the Nantucket buoy were seen to be slightly narrower, with more pronounced peaks, though they still produced an average T_e/T_{02} of 1.21 which is close to what is expected from a Bretschneider spectrum. The combination of these studies provides a valuable insight into the importance of the dominant spectral shape in determining the relationship between T_E and T_{02} at a particular location.

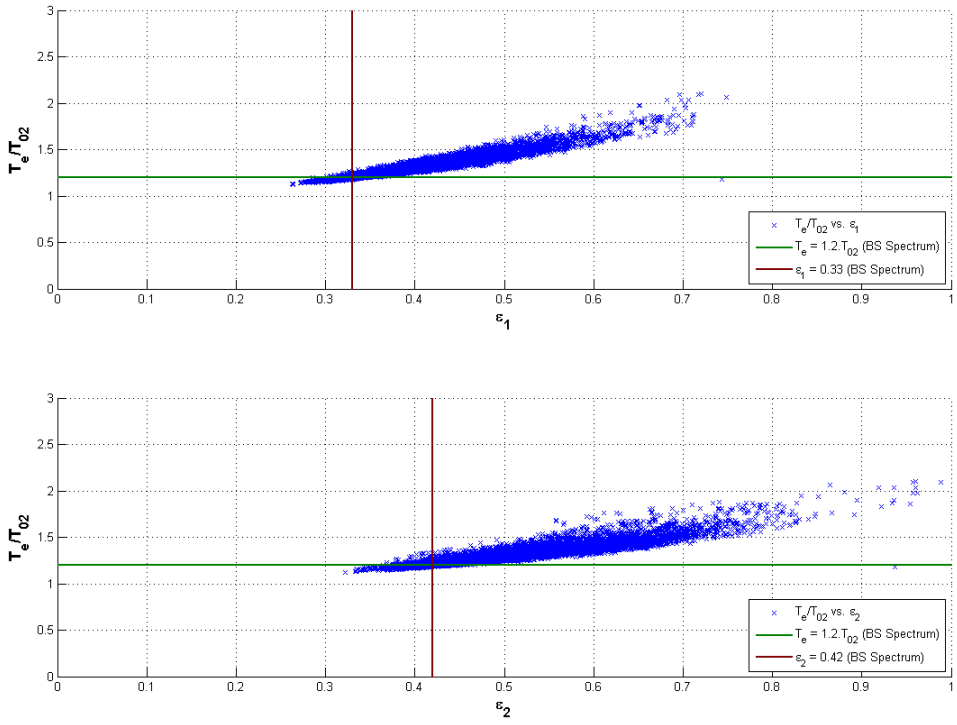

Figure.4.29: Wave period ratio plotted against bandwidth parameters ε_1 (top) and ε_2 (bottom) for AMETS (2010)

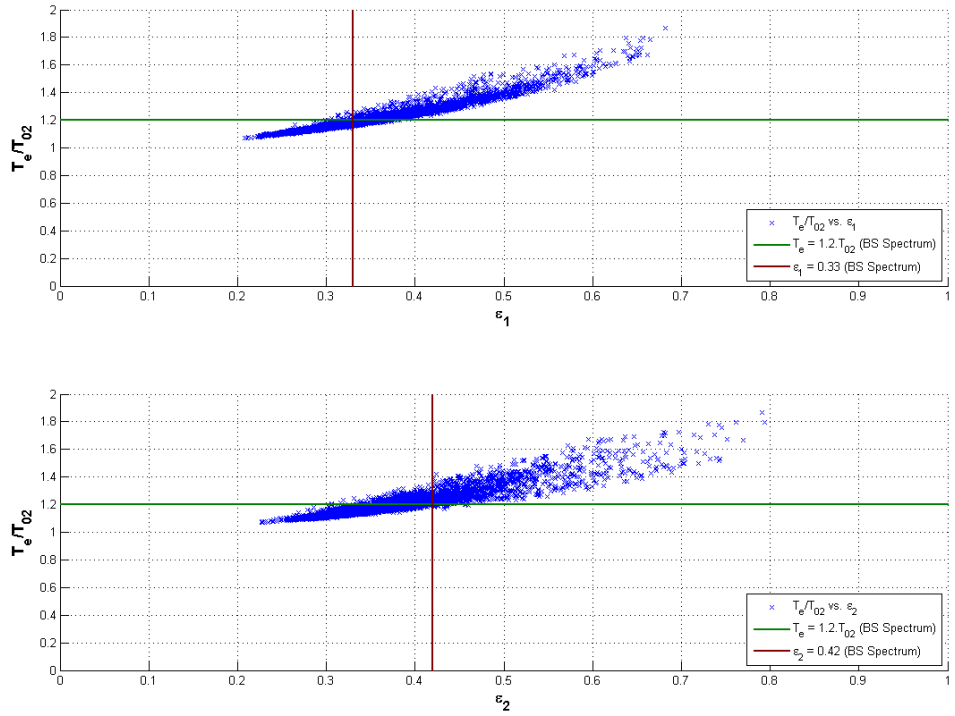

Figure.4.30: Wave period ratio plotted against bandwidth parameters ε_1 (top) and ε_2 (bottom) for Nantucket (2010)

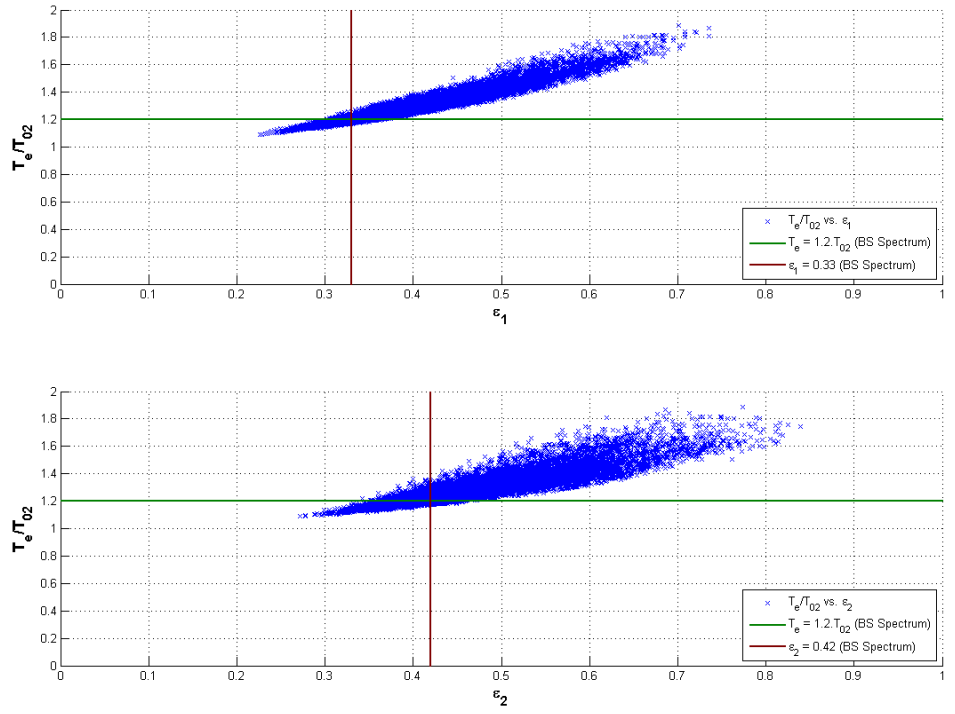

Figure.4.31: Wave period ratio plotted against bandwidth parameters ε_1 (top) and ε_2 (bottom) for Umqua (2010)

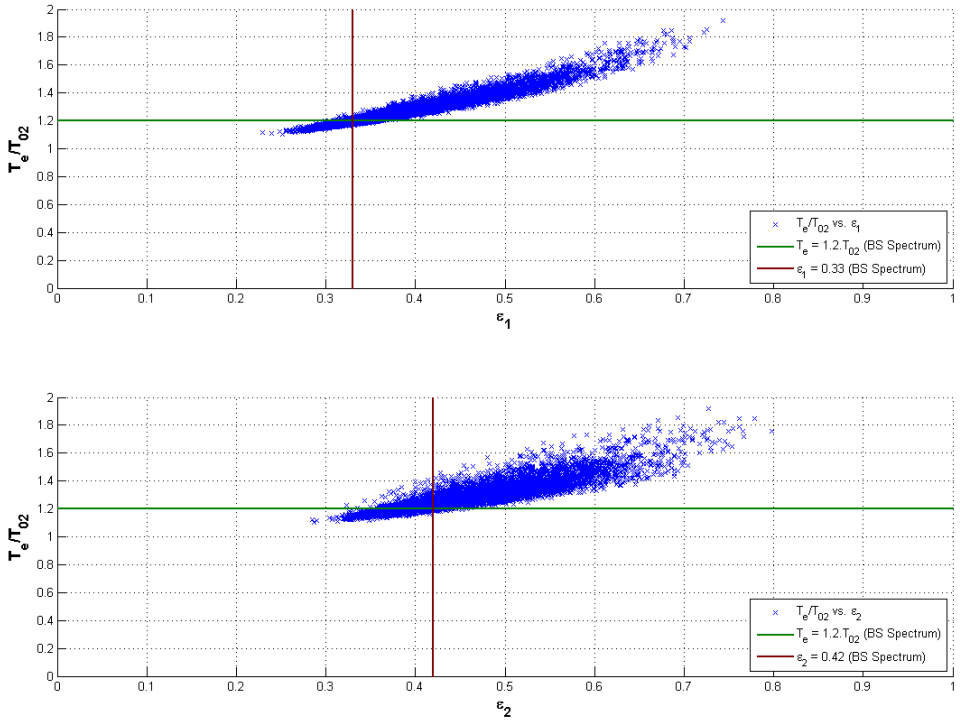

Figure.4.32: Wave period ratio plotted against bandwidth parameters ε_1 (top) and ε_2 (bottom) for San Francisco (2010)

4.4 Long Term Variability in the Wave Period Ratio

Wave conditions are known to exhibit variability over seasonal, interannual and decadal time scales. The possibility of the WPR displaying long term trends was investigated in order to assess whether any variations should be considered significant over the lifetime of a WEC development. Due to the lack of records of sufficient duration from the buoys off the Irish coasts a 15 year dataset of measurements (1997-2011) taken from NDBC Buoy 46215 located near Diablo Canyon in Southern California was analysed. In Table 4.8 it was noted that the average WPR calculated for this location for the year 2010 was 1.378. The prevailing wave climate measured by this buoy over the 15 year period is summarised in the scatter plot of H_{m0}-T_E occurrence (Fig. 4.26). Metocean conditions at this location are noticeably more benign than those at the Atlantic facing sites off the coasts of Ireland and the United Kingdom. The average incident wave power is 14.9 kW/m and few sea states with H_{m0} greater than 4m are encountered.

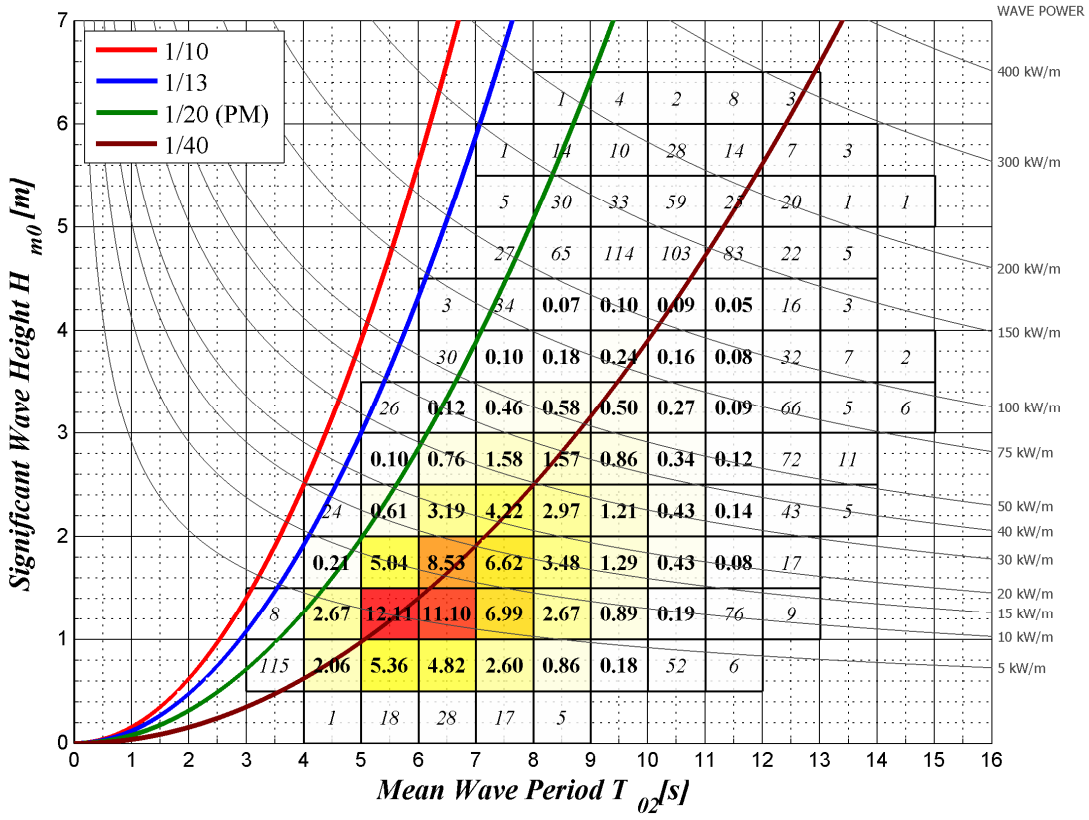

Figure 4.33: H_{m0}-T_E percentage occurrence for Diablo Canyon buoy (1997-2010)

4.4.1 Interannual Variability

The average annual values of wave period for each of the 15 years of available data were computed from the measured wave spectra. The results are illustrated in Fig. 4.27. These values of the WPR range from 1.37 to 1.41, a percentage difference of approximately 3%. The overall average figure for the 15 year period was 1.4. The average values of the WPR are also plotted against the annual average annual wave power for each year in Fig. 4.28 While the previous analyses indicated that individual sea-states with low values of T_E/T_{02} are associated with increasing wave power there is no discernable trend apparent when annual averages are assessed, with the most energetic years displaying a wide spread of values.

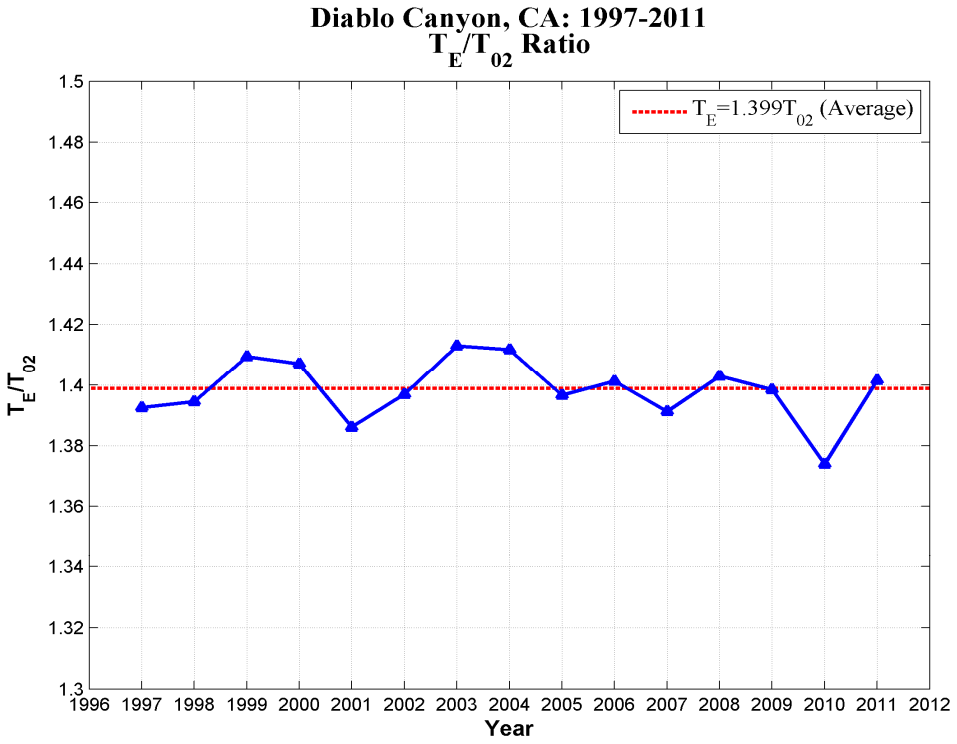

Figure 4.34 Annual average wave period ratio for Diablo Canyon buoy (1997-2011)

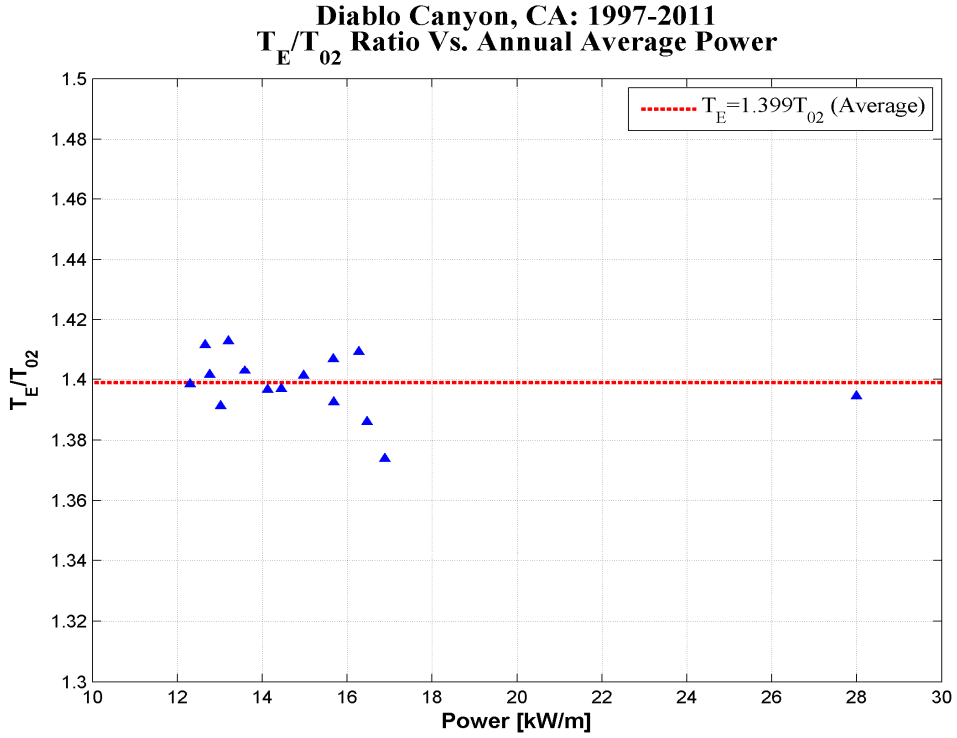

Figure 4.35 Annual average wave period ratio vs. annual average wave power for Diablo Canyon (1997-2011)

4.4.2 Seasonal Variability

Rolling averages of T_E/T_{02} and wave power were computed with window length of one week, one month and three months and the results illustrated in Figs. 4.29 - 4.31. The strong seasonal trends in wave power are evident, with well defined peaks for each winter period and corresponding troughs in the summer months, though the plots of the period ratio tend not to follow as smooth a profile. These seasonal trends are most easily identifiable in Fig. 4.31 where the 3 month window was applied. Visual inspection of Fig. 4.31 suggests that in general peaks of wave power coincide with lower value of T_E/T_{02}, though instances where the opposite is true are also evident. This is confirmed by statistical checks which indicate that there is a small degree of negative correlation (-0.24) between the two series.

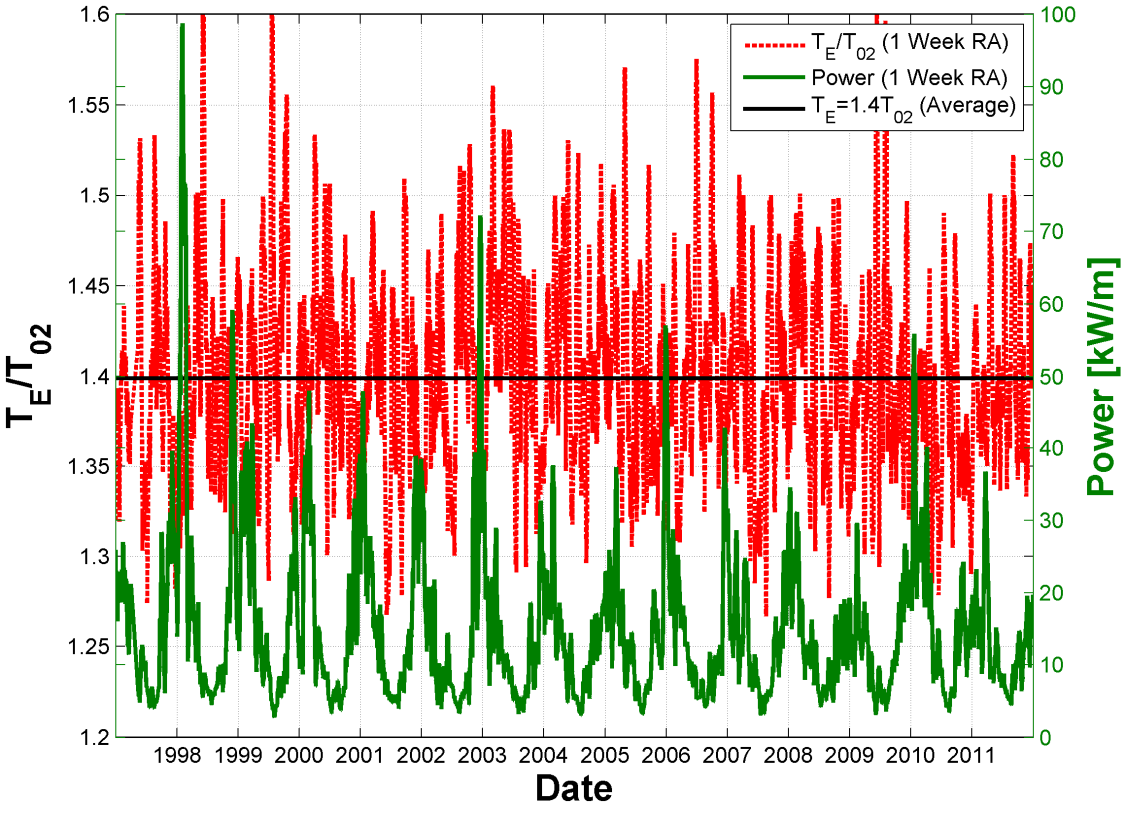

Figure 4.36: One week rolling average of T_E/T_{02} and wave power (1997-2011)

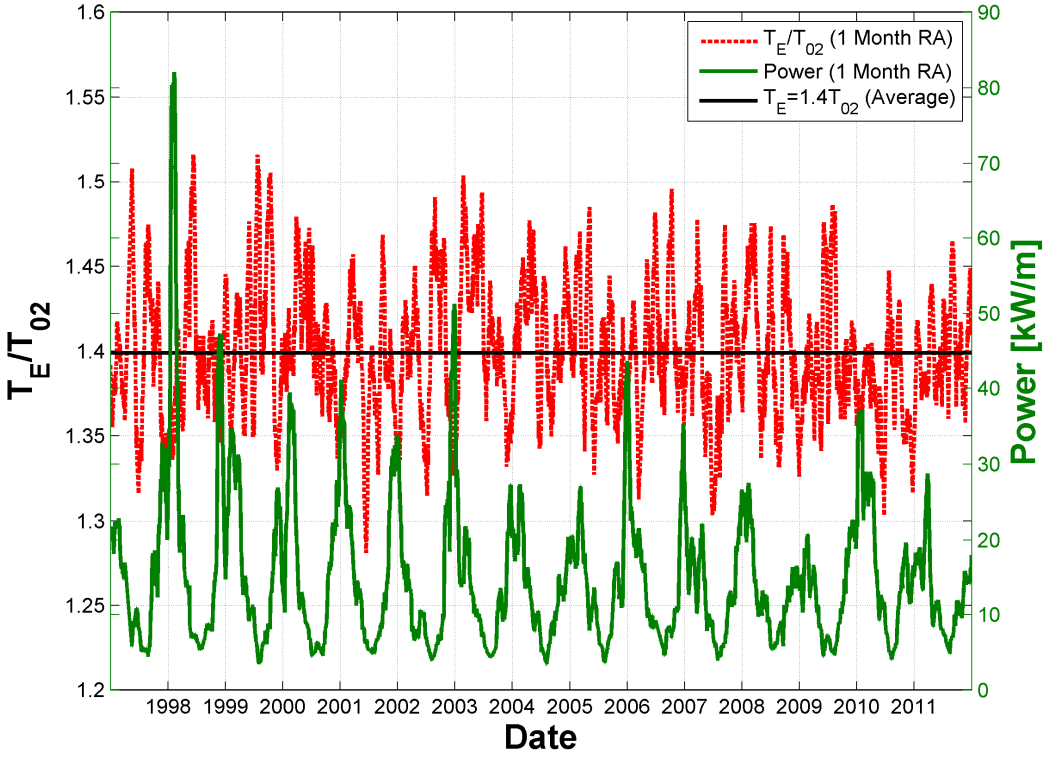

Figure 4.37: One month rolling average of T_E/T_{02} and wave power (1997-2011)

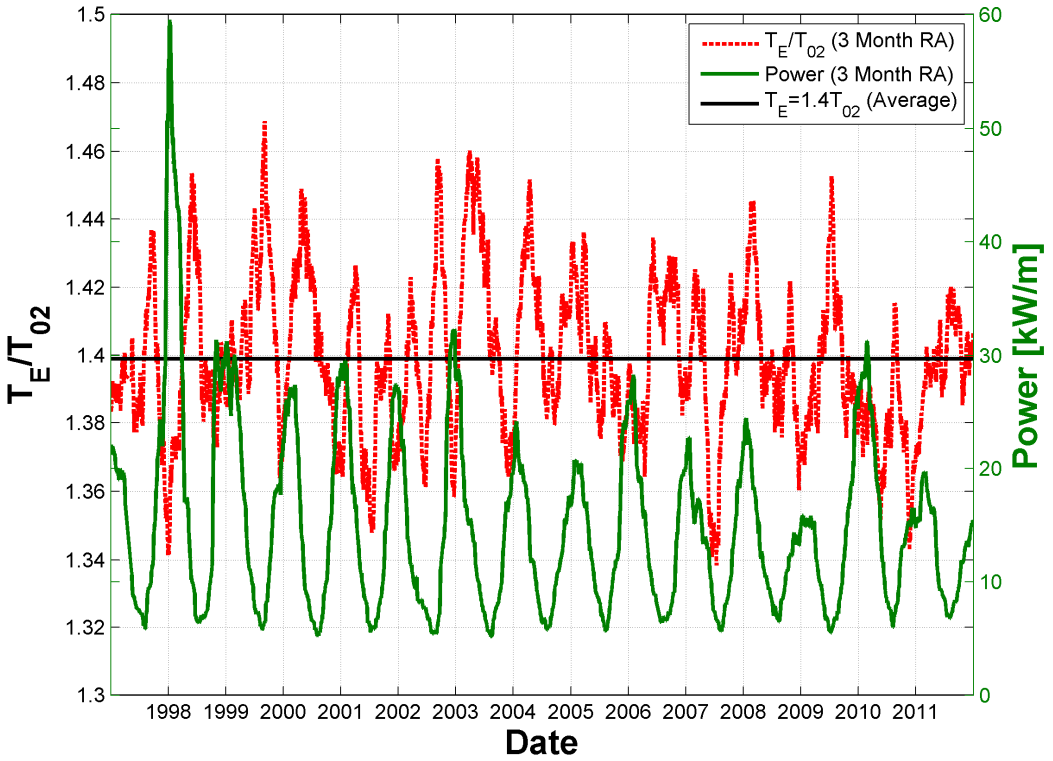

Figure 4.38: Three month rolling average of wave period ratio and wave power for Diablo Canyon (1997-2011)

4.5 Discussions and Guidelines for Selecting Appropriate Wave Period Ratios

This chapter has defined a new parameter, the wave period ratio (WPR), and demonstrated that WPR values of 1.12 and 1.14 which have previously been employed in some studies are unrepresentative of either the Bretschneider or JONSWAP spectra. It has been shown that $T_E=1.2T_{02}$ is the correct relationship if the Bretschneider shape is assumed to represent the sea-states, while for the most common JONSWAP form ($\gamma=3.3$) $T_E=1.18T_{02}$ should be used to convert the zero-crossing period to the energy period for the calculation of wave power. Furthermore, the analysis of observed spectra in Section 4.3 indicates that the WPR is generally higher than these theoretical relationships for real sea conditions, depending on the geographical location and the prevailing wave climate. It has been shown that T_E is approximately equal to $1.32T_{02}$ off the West Coast of Ireland. If this ratio is assumed to be uniform off the Irish seaboard the value of the theoretical wave energy resource presented in the Irish Accessible Wave Energy Atlas (ESB International 2005) should be revised upwards by 18%.

It has been also been shown that the relationship between T_E and T_{02} is heavily influenced by spectral shape. As Section 4.3.6 illustrates, there is a close correlation between spectral bandwidth and the WPR, while it was observed in Section 4.3.5 that degree to which sea-states' spectra conform to the Bretschneider formulation is generally indicative of the value of T_E/T_{02}. While the average spectral shapes at the Irish and US Pacific coasts show reasonable agreement with the equivalent Bretschneider spectra they can be seen to contain greater contributions from long period components, particularly for low sea-states. This deviation from the theoretical shape is compounded by the occurrence of multimodal spectra which contain both sea and swell inputs and which display high WPR values. As Section 4.2.3 demonstrated, WPR will increase if the variance of the wave spectrum is shifted towards the lower frequencies; this may explain why the WPRs at these locations were greater that the theoretical assumption.

In practice, to avoid errors associated with the variation in the WPR for real conditions, sea-state parameters should be derived directly from observed spectral data if available, rather than relying on archived summary statistics in isolation. Similar analysis could be carried out for other wave period parameters. For example Tp is often included in limited datasets. The T_E/T_P ratio for a Bretschneider spectrum is 0.85 while an average value of 0.83 is derived from the measured data from Belmullet. It is recommended that an appropriate WPR should be calculated from measurements from a nearby buoy or wave model grid point if spectral data are unavailable at a location of interest, rather than assuming a value from a theoretical spectrum. The buoys near AMETS and Loop Head returned similar WPR values (1.32 and 1.33 respectively) despite their physical separation; a comparable value could be used to enhance the summary statistics provided by limited datasets off the Irish west coast such at the M-buoy network. Similarly, WPRs derived from the closest measurement buoy could be applied for the other regions analysed in this chapter; the US Atlantic coast, Oregon and California. Section 4.4. highlighted the seasonal trends in the WPR, thus a full calendar year's worth of data should be analysed to ensure an unbiased result. Further collaborative research is being carried out as part of the EERA Marine Energy Joint Program with the aim of collating data from exposed Atlantic locations in Europe, identifying regional trends in the WPR and defining standardised guidelines for estimating the wave energy resource from limited datasets.

Chapter 5 Wave Energy Resource Characterisation

Chapter 2 showed that the gross, theoretical, wave power has been the primary output of many previous research studies, however it should not be considered as the sole criterion when assessing the energy resource during a site selection process. As illustrated in Section 2.3, various other characteristics will influence WEC performance and should also be investigated. Identifying the importance of these characteristics constitutes the focus of this project. The previous chapter challenged the use of unsuitable wave period ratios in the analysis of ocean wave data. Here, the validity of the deep water assumption — required to justify the use of Equation 2.5 to calculate wave power — is contested using examples drawn from the analysis of the measured and modelled wave data that have recently been made available from AMETS. This issue impacts on the accuracy of estimates of the available energy at a potential wave farm location, and outputs from the fifteen year SWAN model of the test site, which include data from depths ranging from 10 m-150 m, are used to demonstrate this influence quantitatively. The general nature of the wave energy resource is also characterized, including the identification of the most energy rich sea-states and an assessment of the sensitivity of devices to the probability distribution of combinations of wave height and period. Spectral variability, and its potential implications on WEC performance, is also demonstrated and discussed.

5.1 Influence of Water Depth on the Calculation of Wave Power

The relative depth — the metric used to define the appropriate depth conditions — will not be constant at typical deployment sites for floating WECs. Relative depth is dependent on the length of the incident waves, thus it will vary in relation to the prevailing climate, as well as the water depth. As described in the previous section, wave power is commonly calculated with the assumption of deep water conditions. The influence that the variation of relative depth has on this assumption is investigated in the following sections.

5.2.1 Variation of C_g and P in Finite Depths

The properties of the frequency components of the wave spectrum are influenced by the water depth, d. According to convention three different depth regimes are proposed; deep, intermediate and shallow. These conditions are defined by their relative depth, which is the ratio between d and the deepwater wavelength, λ_0, of the prevailing waves. For deep water the relative depth is sufficiently large so that $\tanh(2\pi d/\lambda_0) \approx 1$. This is generally accepted as occurring when $d > \lambda_0/2$ (Kinsman 1965; USACE 2002), though Tucker and Pitt (2001) note that waves properties begin to be affected by depth when $d > \lambda_0/4$. The corresponding threshold between intermediate and shallow water is in practise considered to be $d < \lambda_0/20$ (USACE 2002).

The different relative depths for each of the frequency components that form a wave spectrum have implications for the calculation of power. The group velocity term, C_g, is present in Equation (2.3), and is a depth-dependant parameter. The values of C_g for deep, intermediate and shallow conditions can be determined from the equations contained in Table 5.1, along with the respective formulae for λ and the wave celerity, C. It can be seen that C_g is constant in deep water, which allows for the simplification of Equation (2.3) to Equation (2.5). For Shallow water $C_g = C$.

	Shallow Water	**Intermediate Water**	**Deep Water**
Relative Depth	$d < \lambda_0/20$	$\lambda_0/20 < d < \lambda_0/2$	$d > \lambda_0/2$
λ	$\lambda = T\sqrt{gd}$	$\lambda = \frac{gT^2}{2\pi}\tanh\frac{2\pi d}{\lambda}$	$\lambda = \frac{gT^2}{2\pi} = \lambda_0$
C	$C = \sqrt{gd}$	$C = \frac{gT}{2\pi}\tanh\frac{2\pi d}{\lambda}$	$C = \frac{gT}{2\pi}$
C_g	$C_g = \sqrt{gd}$	$C_g = \frac{1}{2}\left[1 + \frac{4\pi d/\lambda}{\sinh(4\pi d/\lambda)}\right]C$	$C_g = \frac{gT}{4\pi} = C_{g0}$

Table 5.1 Depth-Dependant Wave Characteristics

The behaviour of λ and C_g due to the hyperbolic tanh and sinh functions as they transition through intermediate water depths are illustrated in Fig. 5.1 for the case of a regular wave

— H = 2 m, T = 5 s — using the approach followed by Kinsman (1965). The parameters are normalised as a ratios of their deep water values, and plotted against the relative depth. The boundary between the deep and intermediate water depth regime is represented by the red, vertical line. λ becomes shorter as water depth decreases, whereas the group velocity initially increases in relation to its deep water value before its magnitude begins to reduce towards the lower relative depths. It is also noteworthy that C_g begins to change slightly before the relative depth passes below the deep water threshold, as suggested by Tucker and Pitt (2001).

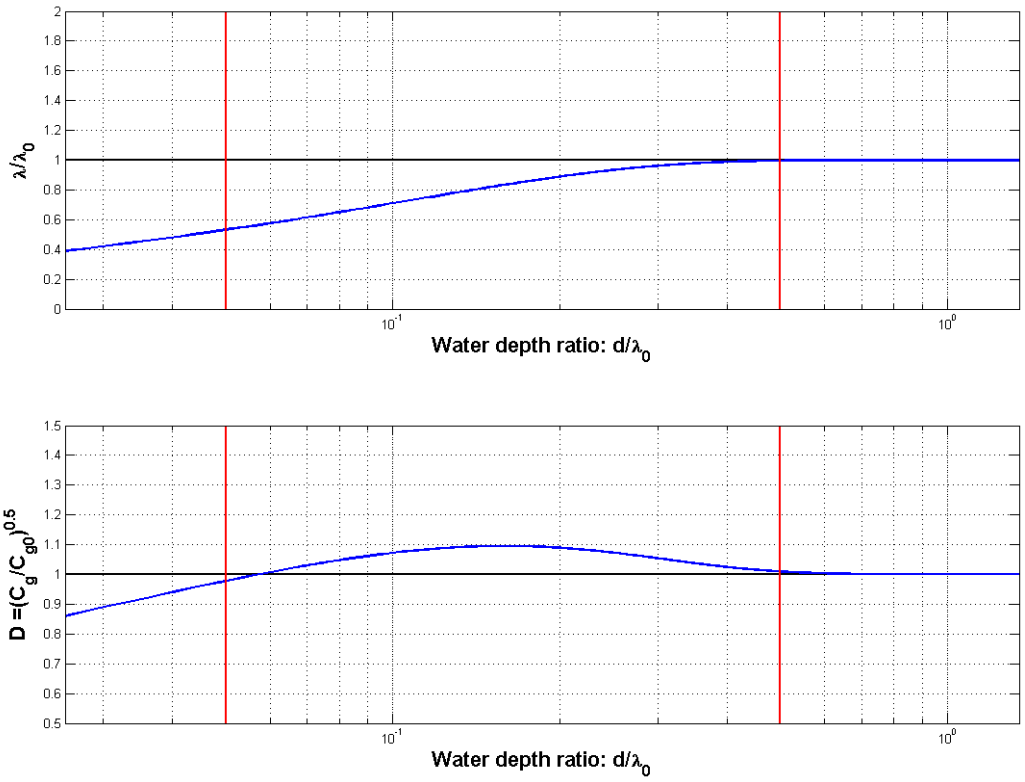

Figure 5.1: Wave length, λ, and group velocity, C_g, ratios as a function of water depth. Red lines indicate the boundaries of intermediate depth

Similar illustrations of the behaviour of the height and power of a regular wave in intermediate depth are provided in Fig. 5.2. The values of depth-adjusted H were computed from Equation (5.1), where K is a constant refraction factor. For this idealised case K = 1. Power is calculated using the depth adjusted values of H and C_g from Equation (5.2), an adapted version of Equation (2.2).

$$H = K\sqrt{\frac{C_{g0}}{C_g}}H_0 \tag{5.1}$$

$$P = \frac{1}{8}\rho g C_g H^2 \quad [W/m] \tag{5.2}$$

The variation of H as the depth decreases opposes that of C_g, as suggested by their relationship in Equation (5.1). There is an initial reduction in wave height, but as the group velocity begins to decreases the height is amplified; a process known as shoaling. Similarly, it can be seen that the wave power calculated from Equation (5.2) remains constant regardless of water depth; changes in the wave height are balanced by complementary variations in the group velocity term in the power calculation. This highlights the conservation of energy for these idealised conditions, an important concept once the calculation of wave power from spectra featuring a range of frequency components is being considered.

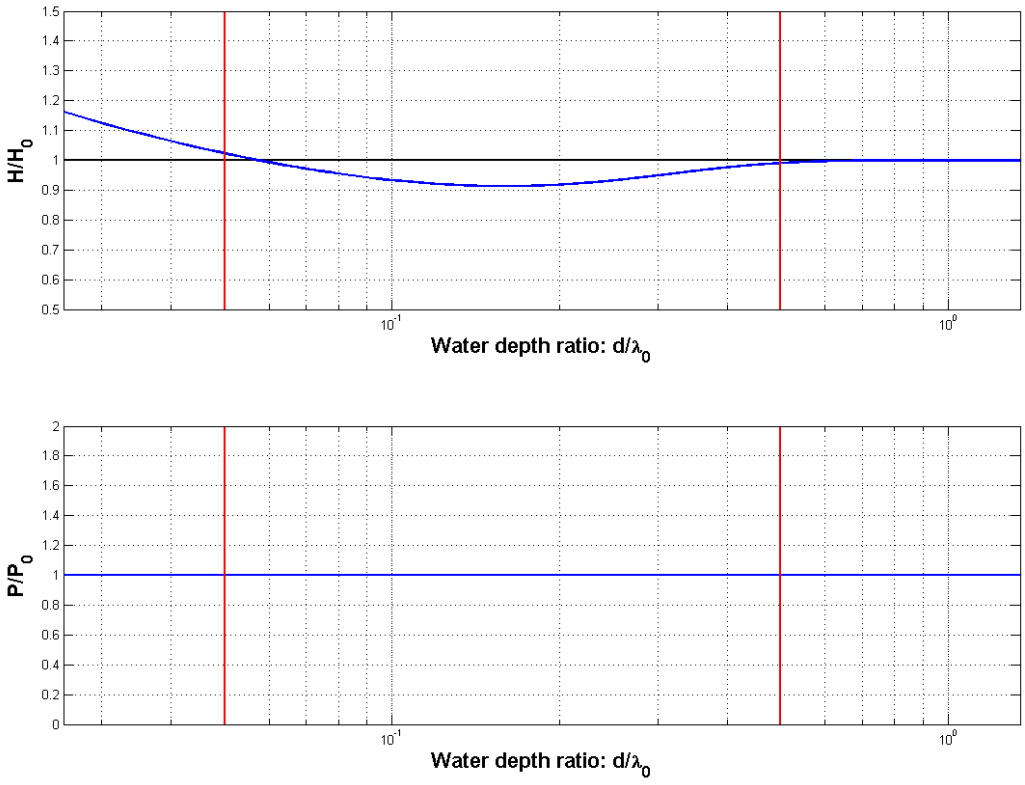

Figure 5.2: Wave height, H, and power, P, ratios as a function of water depth. Red lines indicate the boundaries of intermediate depth

The variation of C_g for the frequency components in a wave spectrum is illustrated in Fig. 5.3 for several different water depths. The low frequency cut-off used is 0.0464 Hz, the value used in the spectra produced by the AMETS SWAN model. For infinite depth, C_g increases with 1/f towards the low values of the frequency scale. For the larger values of d — 50 m and 150 m — C_g is always equal to, or greater than, its deep water equivalent. As a result, values of power computed using Equation (2.3) will always be greater than if the deep water assumption is applied. C_g falls below the magnitude of the deep water value for frequency components with long wavelengths at the shallower depths of 10 m and 20 m. Thus the difference between the deep water and depth-adjusted wave power will depend on the magnitude, and distribution of the frequency components. Practical examples are presented in Figure 5.4 and Figure 5.5. These figures are composed of three parts: the deep water and depth-adjusted values of C_g for the frequency components at the site depth (top); the measured wave spectra (middle); and the contribution of each frequency components to total energy calculated using both the deep water and finite depth values of C_g. Figure 5.4 uses a three month dataset from a Waverider buoy located near Diablo Canyon in Southern California. The water depth at this site is approximately 23 m. Utilising the intermediate depth group velocity results in a slight, but perceptible, increase in energy contribution from components in the range 0.075 – 0.125 Hz, for which C_g is greater than the deepwater approximation. The corollary of this is the increased contribution to total energy by the lowest frequency components. The spectra in Figure 5.5 were derived from the Valeport pressure gauge deployed in the nearshore zone at Rossbeigh beach in Co. Kerry, Ireland, introduced in Section 3.4.3. The average water depth was 2.1 m, though this varied due to the tidal range. This was a short term deployment and only 12 spectra were returned, however it is still instructive. The spectra's low frequency cut-off, 0.002 Hz, is equivalent to a regular wavelength of 375 km. This results in the enormous deep water values of C_g towards the low end of the frequency scale. These frequency components are seen to contribute disproportionately to the total energy, even though the variance contributed by these components is minute, and the result of signal noise rather than genuine waves.

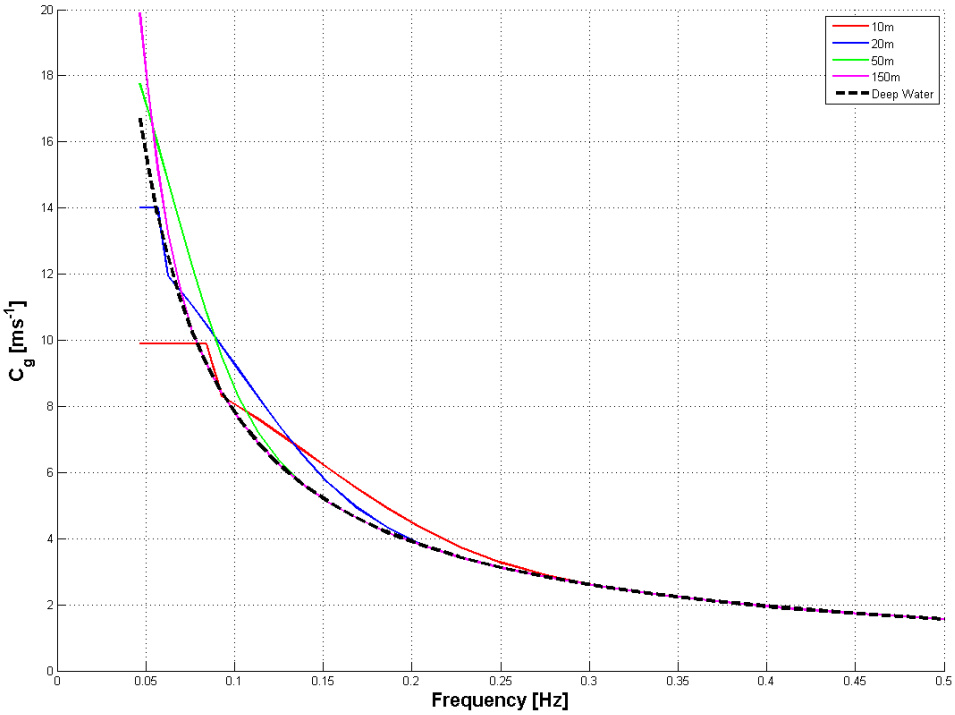

Figure 5.3: C_g values for spectral frequency components in finite depths and deep water.

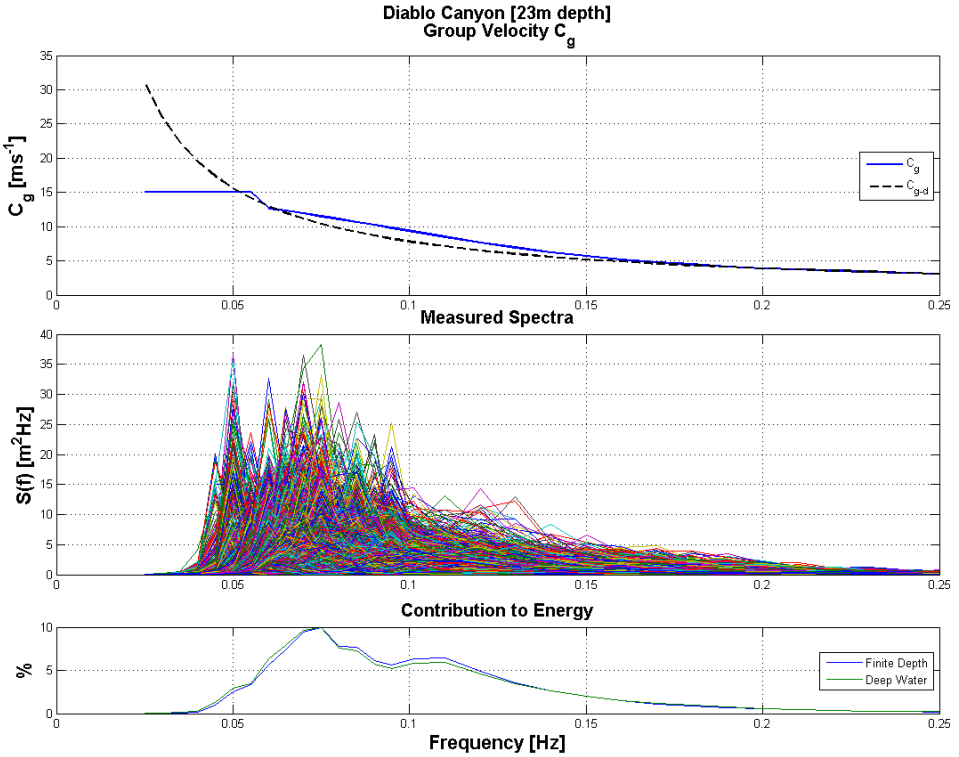

Figure 5.4: Frequency components' C_g, spectral ordinates and contribution to energy, Diablo Canyon data.

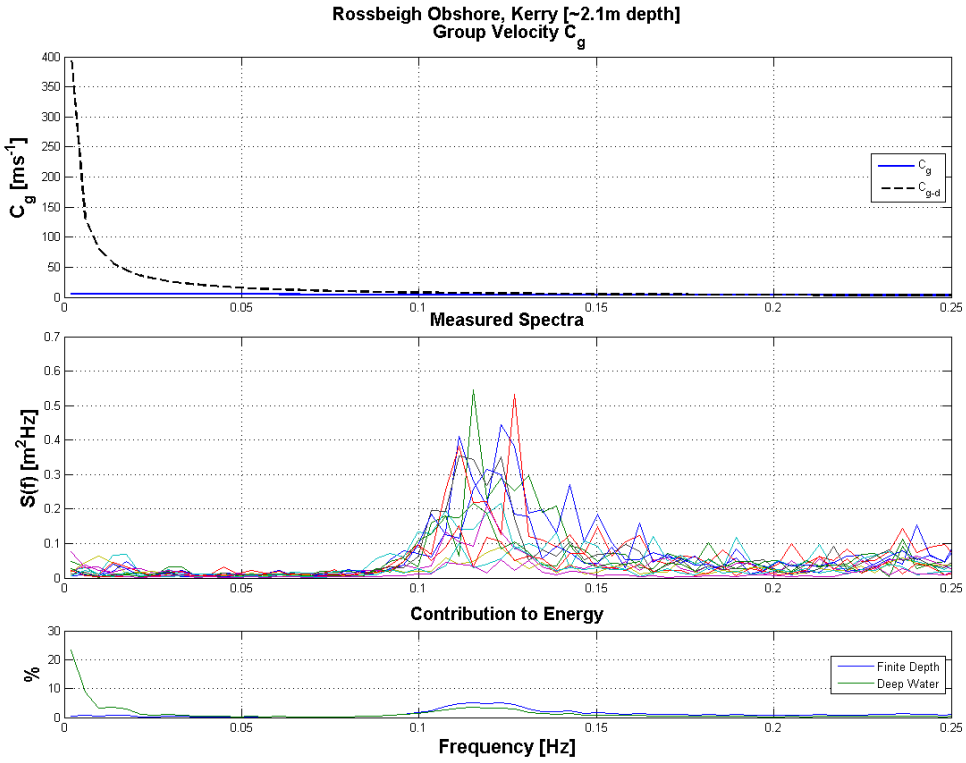

Figure 5.5: Frequency components' C_g, spectral ordinates and contribution to energy, Rossbeigh data.

5.2.2 Influence of Water Depth on Average Annual Power Values from the AMETS SWAN Model

The significance of accounting for water depth in the calculation of wave power was assessed using the outputs of the AMETS SWAN model introduced in Chapter 3. Fifteen points highlighted by red diamonds in Fig. 3.16, each with fifteen years of spectral data and water depths ranging from 10 m to 150 m in increments of 10 m, were selected and analysed. Wave power was calculated using the deep water assumption from Equation (2.5), and denoted P_0, and from the full spectral form presented in Equation (2.3)

For each 30 minute record at each station an initial estimate was made as to which water depth condition was valid. The T_E value calculated from the wave spectrum was taken as the representative wave period for the calculation of λ_0 and the relative depth. This is the most appropriate method for assessing the depth conditions at a site if summary statistics are the only data available, though it is somewhat sensitive to the choice of wave period

parameter. Using T_p instead of T_E would suggest of more cases of intermediate depth, whereas T_{02} would gives deep water conditions more frequently. The variation of the percentage occurrence of the three water depth conditions at each water depth over the fifteen years of data outputs is illustrated in Fig. 5.6. Deep water conditions exist almost all of the time for depths of 100 m and above and are still valid for greater than 80% of records until water depth is less than 50 m. The intermediate condition is the most common for depths below 30 m. Even at the 10 m station the shallow water condition is not met for any of the modelled sea states.

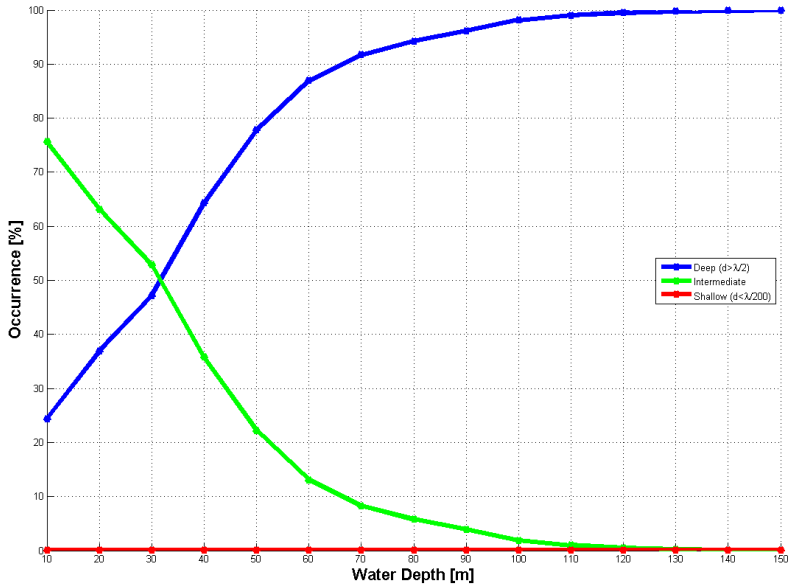

Figure 5.6: Percentage occurrence of water depth conditions at AMETS SWAN model stations.

The fifteen year averages of P_0 and P are illustrated in the top portion of Fig. 5.7 for the fifteen stations, with the percentage difference between the values indicated underneath. From both of these figures it is evident that including the influence of water depth has a significant effect on the calculated energy resource. P is consistently greater than P_0 for water depths in the range 30 m-100 m. For these cases more of the C_g components are in the region where they exceed the deep water equivalent, as shown in Fig. 5.3 for a number of the water depths studied here. In contrast, for the station at the 10 m water depth more of the long period frequency components, which contribute significantly to spectral energy, have low values of relative depth and C_g is reduced. This is further

illustrated in Fig. 5.8, which indicates the depth condition of each frequency component, at each water depth, and in Fig. 5.9, where the contribution of each frequency component to the total energy at each station is shown.

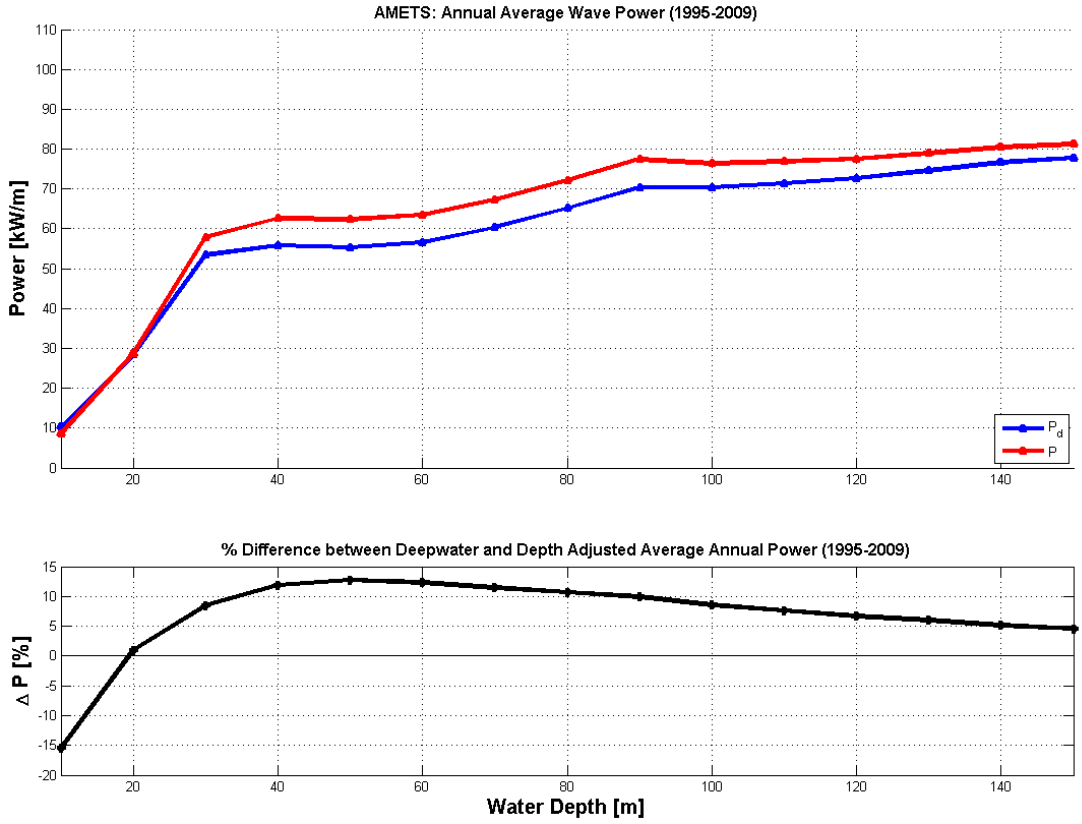

Figure 5.7: Deepwater, P_0, and depth adjusted, P, annual average values of wave power at AMETS (top) and percentage differences (bottom).

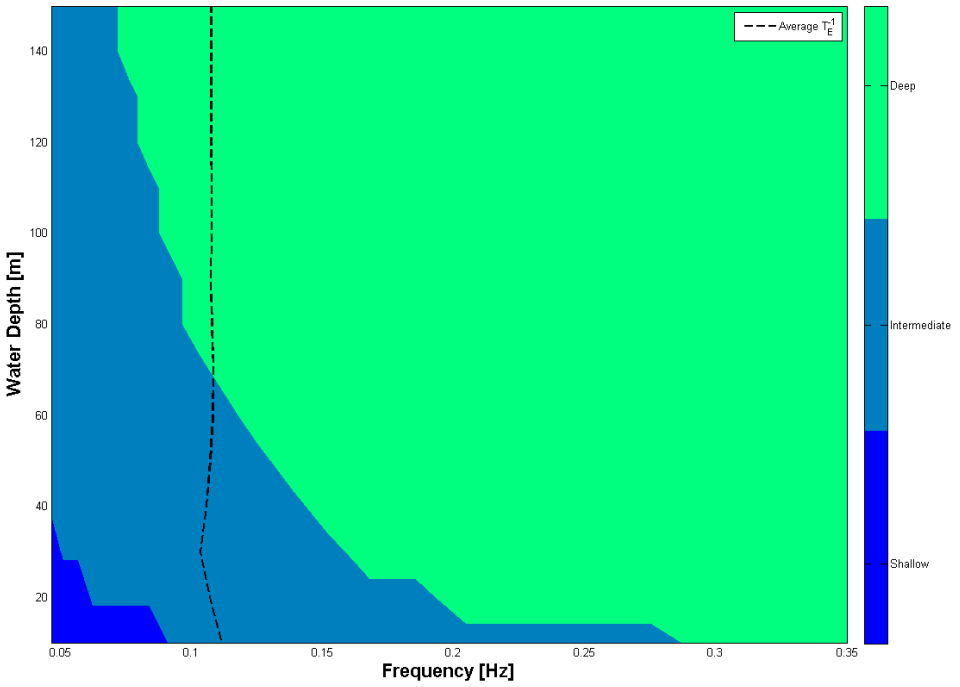

Figure 5.8: Depth condition for each frequency component in the SWAN model spectra.

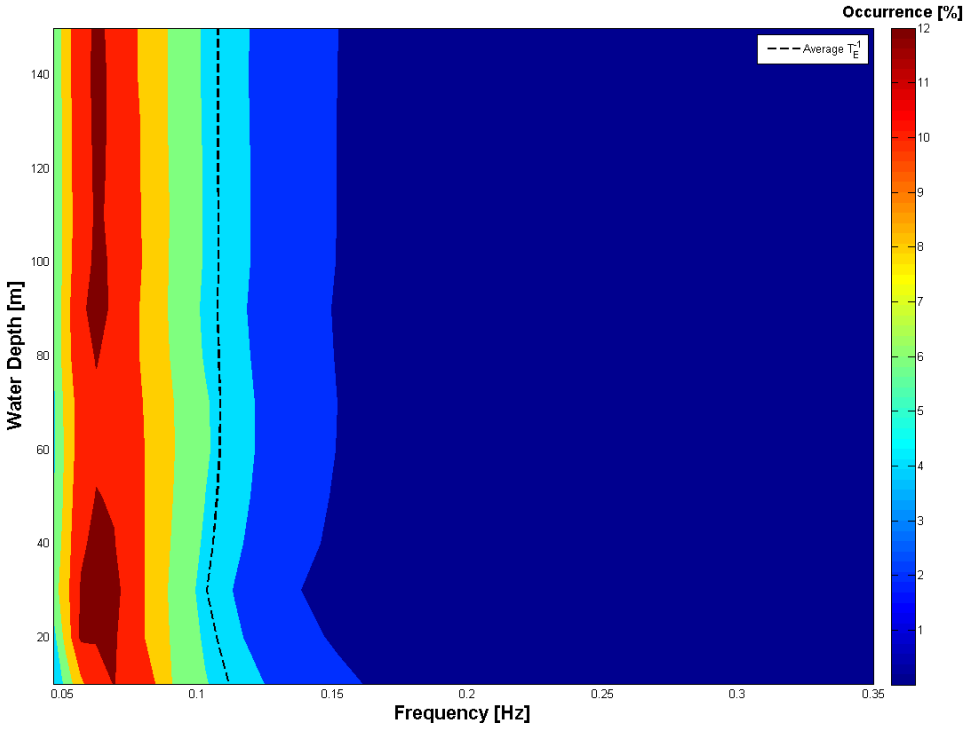

Figure 5.9: Energy contribution of each frequency component in the SWAN model spectra over 15 years of data.

5.3 Sea State Occurrence and Energy Contribution

The sea states experienced at AMETS in 2010, defined by H_{m0} and T_E, are presented in Fig. 5.10 using the scatter plot format introduced in Section 2.3.1. This figure allows the wide range of conditions that were experienced at the site to be observed. The colour scale indicates which sea states occur most frequently and allow the most typical sea states at the site to be identified. Fig. 3.11 illustrated that data gaps exist for 2010, particularly during the summer months, so it should be noted there is some inherent bias in this graphic. Nevertheless, it is a reasonable initial depiction of the nature of the conditions at AMETS.

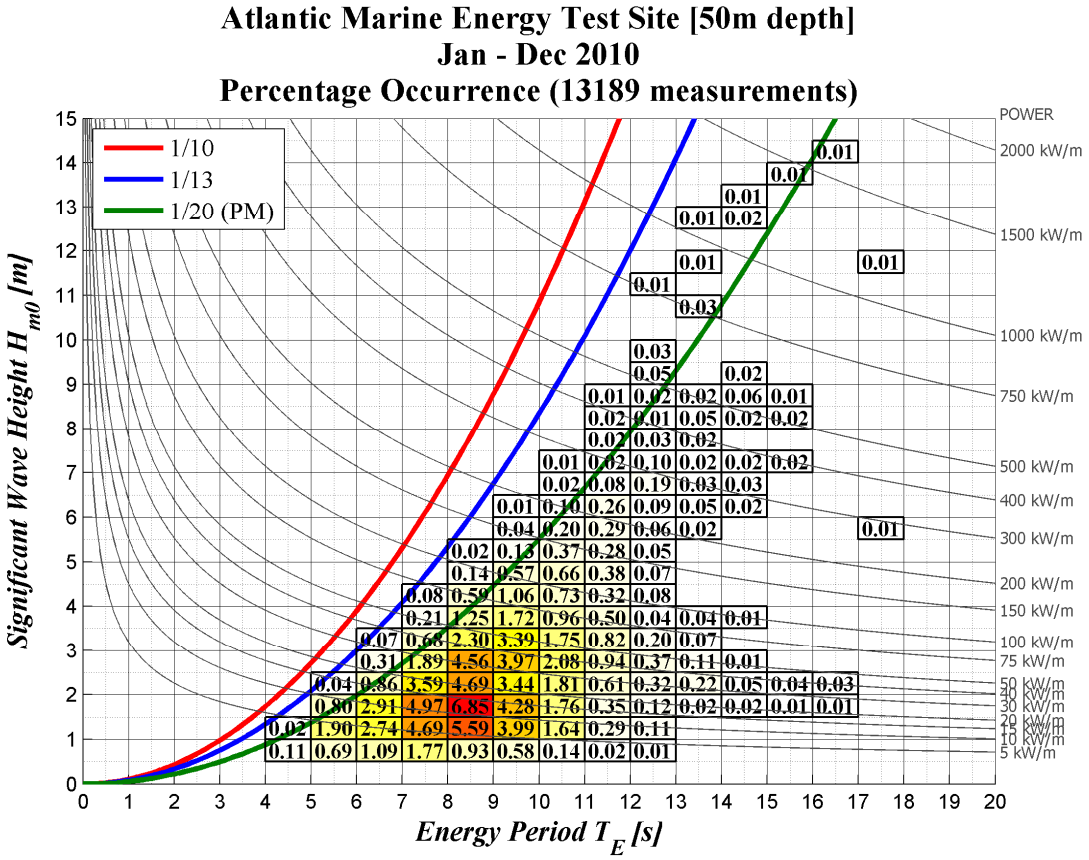

Figure 5.10: H_{m0} – T_E scatter plot of percentage occurrence from AMETS 50 m depth (2010).

The AMETS scatter diagram is redrawn in Fig. 5.11 with the percentage occurrence replaced by the percentage contribution of each sea state to total incident wave energy at the site for 2010. This allows the most energy rich sea states to be identified. When this

diagram is compared with Fig. 5.10 it can be seen that the cells with the highest contribution are not necessarily those with the highest occurrence. There is an obvious upward shift in the positions of the most significant sea states. WEC developers can take advantage of this by designing their devices to capture as much of the available power as possible at the sea states that prove to be the most energetic (when considered over the course of a year) at a potential wave farm site, rather than targeting the conditions which occur most frequently. It is also notable that a number of very rare sea states that are the product of extreme storm events have a disproportionate contribution to total energy. For example, the five sea states (0.03% of total occurrences) that were measured within the range 12.5 m < H_{m0} < 13 m and 13 s < T_E < 17 s, were found to be responsible for over 2% of the total energy for the year. In reality the performance of a WEC would be reduced in these conditions due to losses in efficiency, or even reduced to zero as the device enters survival mode.

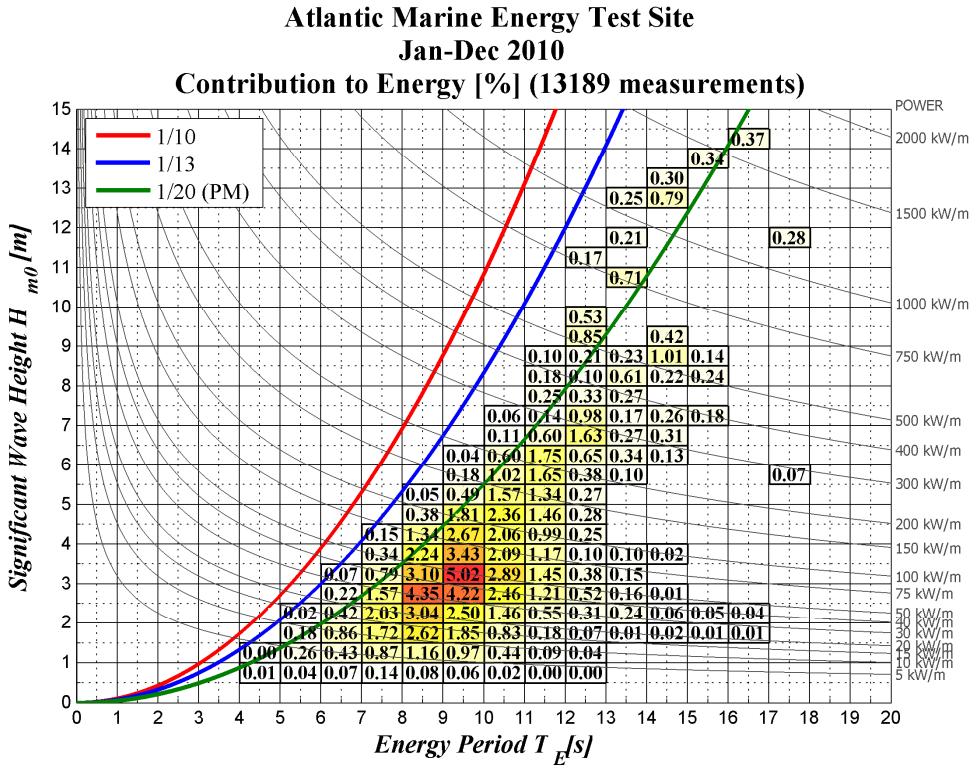

Figure 5.11: H_{m0} – T_E scatter plot of contribution to total energy from AMETS 50 m depth (2010).

5.4 Spatial Variability of the Wave Energy Resource

The spatial variability in the measured wave energy resource at AMETS is investigated through the comparison of data collected by the Wavescan buoy positioned at a depth of 100 m and the Waverider deployed at 50 m depth. The distance between the buoys is approximately 10 km. While there will be a time lag in the propagation of energy and changes in sea state between the two points — over 20 minutes for T_E = 10 s — this will not manifest itself in comparisons of the overall climates at the 100 m and 50 m depths. To remove the bias that seasonality and individual storm events may have on the results only datasets that were measured concurrently at the two buoys were selected for analysis. Occurrence and cumulative exceedance of summary statistics returned from the buoys are compared in Fig. 5.12 for concurrent measurements taken at the 100 m and 50 m depths. The T_E parameter was not included in the outputs of the Wavescan buoy so the two locations are compared using bins of T_{02} instead. Both of these figures indicate that in general the Wavescan buoy experiences sea states of greater significant wave height and of longer periods. This may be in part due to the shelter from waves approaching from the south that the 50 m location receives from the nearby Inishglora and Inishkea islands. This sheltering effect at the 50 m point is also illustrated in Fig. 5.13 where the directional wave roses from the two datasets are compared. The directional parameter used is θ_p, the wave direction associated with the spectral peak. Sea states recorded by the Wavescan buoy are seen to arrive from a wide spread of directions whereas there is more pronounced dominant wave bearing (WNW) at the 50 m site. This direction is perpendicular to the orientation of the depth contours at the 50 m point, suggesting there is some refraction of the waves between the 100 m and 50 m depths.

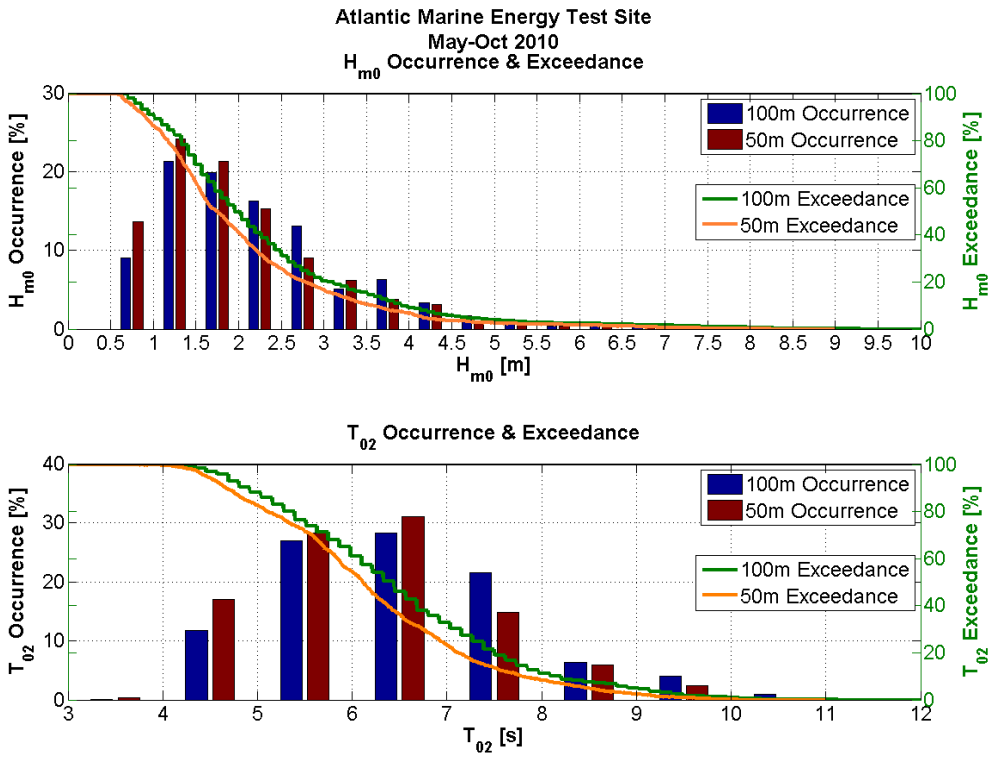

Fig. 5.12: Occurrence (bars, left hand axis) and cumulative exceedance (solid lines, right hand axis) of H_{m0} (top) and T_{02} (bottom) for 100m and 50m depths at AMETS.

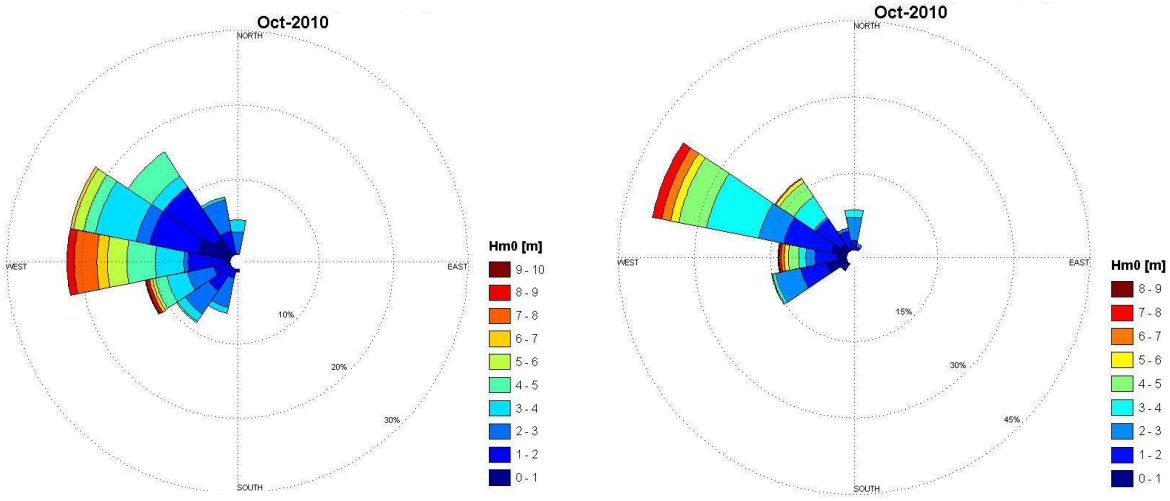

Fig. 5.13: Directional wave roses (θ_p) from the 100m and 50m depths at AMETS (October 2010).

The variability of incident wave power between the 100 m and 50 m depths at AMETS is observed in Fig. 5.14. It was necessary to employ the formula for deep water wave power as spectral information was unavailable from the Wavescan buoy, thus precluding the use of Equation (2.3). The characteristic WPR for AMETS, $T_E=1.32T_{02}$, was applied to

calculate P_0 for the Wavescan data using the measured H_{m0} and T_{02}. It has already been shown that, in general, the 100 m site experiences wave conditions that are both slightly higher and longer than those at the 50 m location. Therefore, it is unsurprising that the average power experienced at the 100 m depth is greater than that at the 50 m location. The slope of the trend line indicates that the power at the 50m location is less than 80% of what can be expected at the 100 m point.

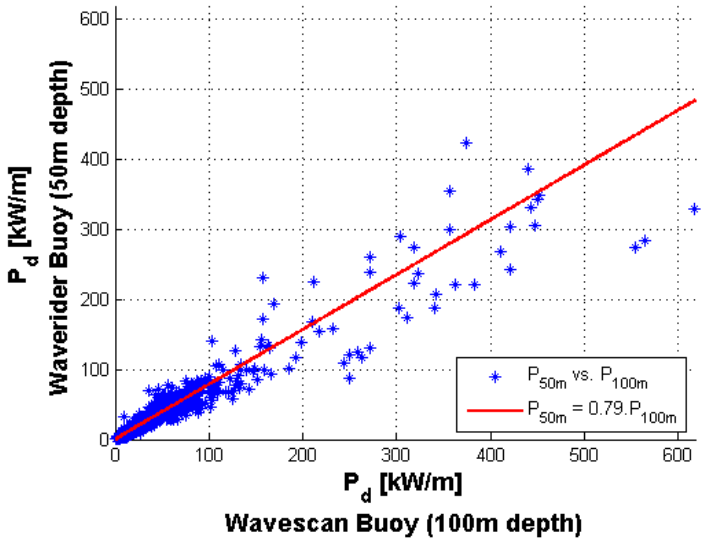

Fig. 5.14: Concurrent values of wave power measured at the AMETS 50 m and 100 m sites.

5.5 Technical Resource

Fig. 5.11 highlights how relatively rare storms can distort the distribution of energy contribution towards very high sea states. It will be difficult for WECs to capture energy efficiently and safely in these conditions. As a result it is also appropriate to estimate the amount of wave energy it may be feasible to extract from a potential wave farm site. An approximation of the technically extractable wave energy resource was computed using metrics described in Section 2.3.1. This allows a more meaningful scatter plot of sea state contribution to the total exploitable energy to be constructed, as shown in Fig. 2.15. Even though extreme sea states still account for some of the total incident energy — Folley and Whittaker's P_{exp} does not reduce to zero the threshold (approximately 140 kW/m in this instance) is exceeded (Folley and Whittaker 2009) — their contribution is greatly

reduced. This accounts for the difficulty associated with operating WECs in such severe storms. Meanwhile, the concentration of energy among the sea states that sit in the centre of the diagram remains relatively unchanged.

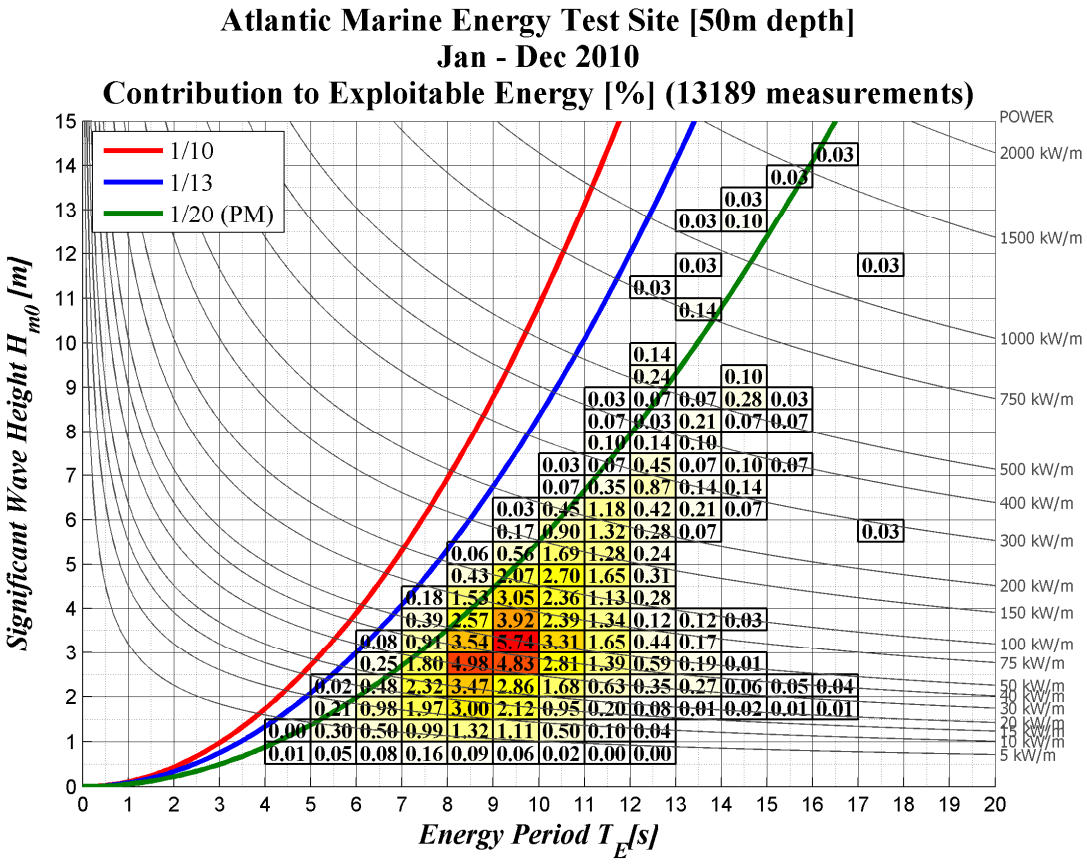

Figure 5.15: H_{m0} – T_E scatter plot of contribution to total exploitable energy from AMETS (2010).

These results refer to the theoretical wave energy resource, rather than the performance of real devices. It is therefore instructive to study the variation in the output of typical WECs over the range of sea states experienced at a site. The annual energy production (AEP) over the course of a year was calculated for the three WEC types; point absorber (AWS), attenuator (Pelamis) and overtopping device (Wave Dragon), whose power matrices were introduced in Section 2.3.1. The power matrices from these devices are shown in Figs. 2.15 -17. These power matrices are relatively old, and have likely been made redundant by recent advances in the development of these devices. They are applied here, however, as representatives of general WEC behaviour. The measured

AMETS data were again utilised, along with the observations from the threes US locations — Nantucket, Umqua (Oregon) and San Francisco — studied in Chapter 4. AEP was computed by multiplying the average device output by the number of hours in a year (8760), and the results are compiled in Table 5.2. Comparing the results from the four sites, which experience different wave climates, allows the sensitivity of the WECs to variations in resource to be observed. A similar approach to the work described previously was followed; the incident wave conditions were separated into bins of H_{m0} (bin width = 0.5 m) and the frequency of occurrence and contribution to AEP of each bin was computed. This analysis was undertaken for each WEC type at the four locations being studied. The results are presented in Figs. 5. 16 – 19, which compare curves of sea state occurrence (solid lines) to contribution to AEP (dashed lines) for the H_{m0} bins. The disparity between sea states' occurrence and AEP contribution is again evident, particularly at the AMETS and Oregon, the locations which produce the highest values of AEP for each of the devices. Sea state occurrence is closely matched to contribution to AEP at the San Francisco site, however device performs poorly. If a device could be designed and tuned with the specific wave climate in mind it would be possible to improve upon this AEP output.

Device	**Device Type**	**AEP [GWh]**			
		AMETS	***Oregon***	***San Francisco***	***Nantucket***
AWS [2.5 MW]	Point Absorber	2.93	3.79	1.94	1.28
Pelamis [0.75 MW]	Attenuator	1.55	1.77	1.05	1.15
Wave Dragon [7 MW]	Overtopping	6.84	8.64	4.53	3.99

Table 5.2: AEPs of AWS, Pelamis and Wave Dragon WECs at four locations.

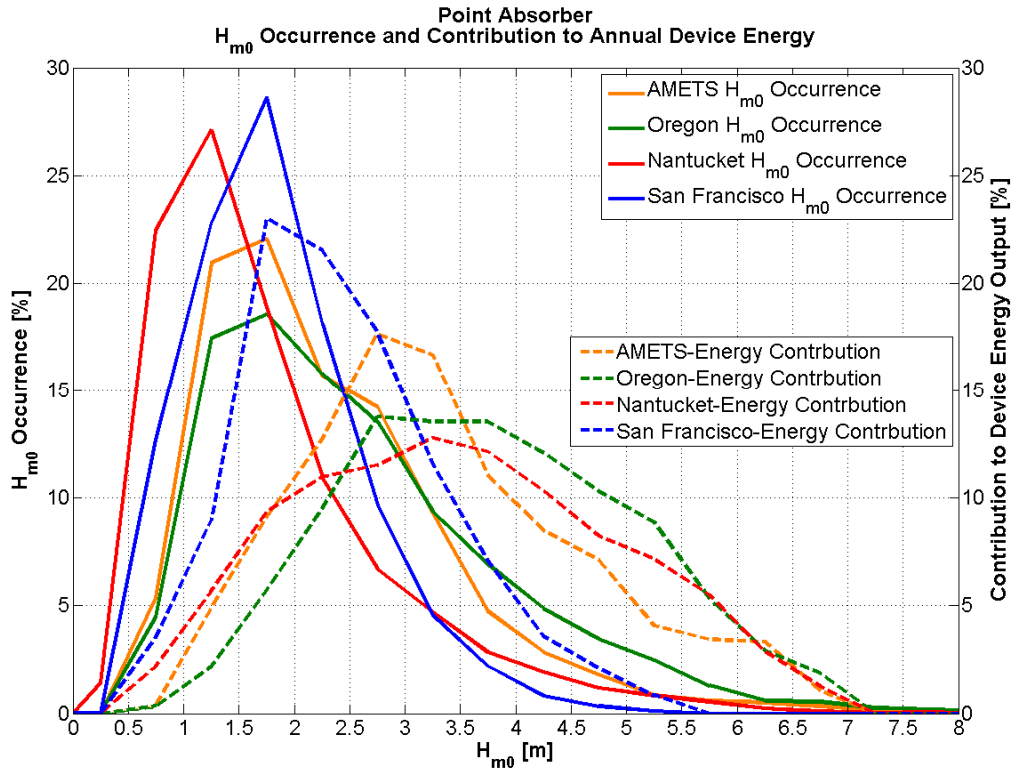

Figure 5.16: H_{m0} occurrence and contribution to total annual point absorber (AWS) energy production

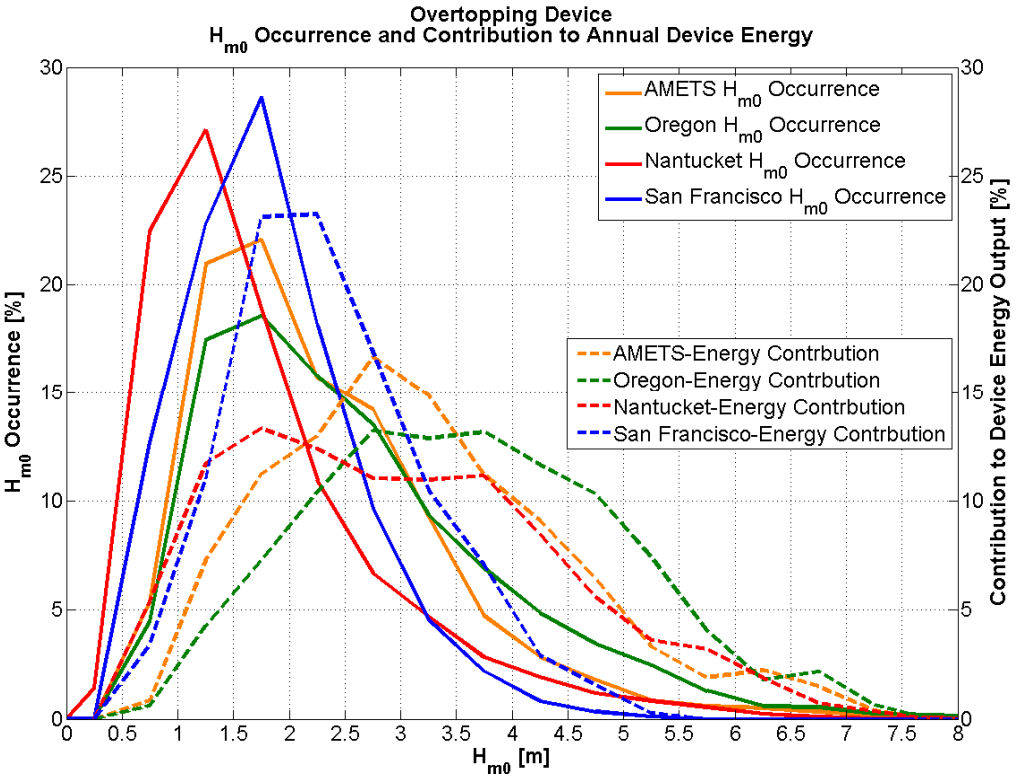

Figure 5.17: H_{m0} occurrence and contribution to total annual overtopping device (Wave Dragon) energy production

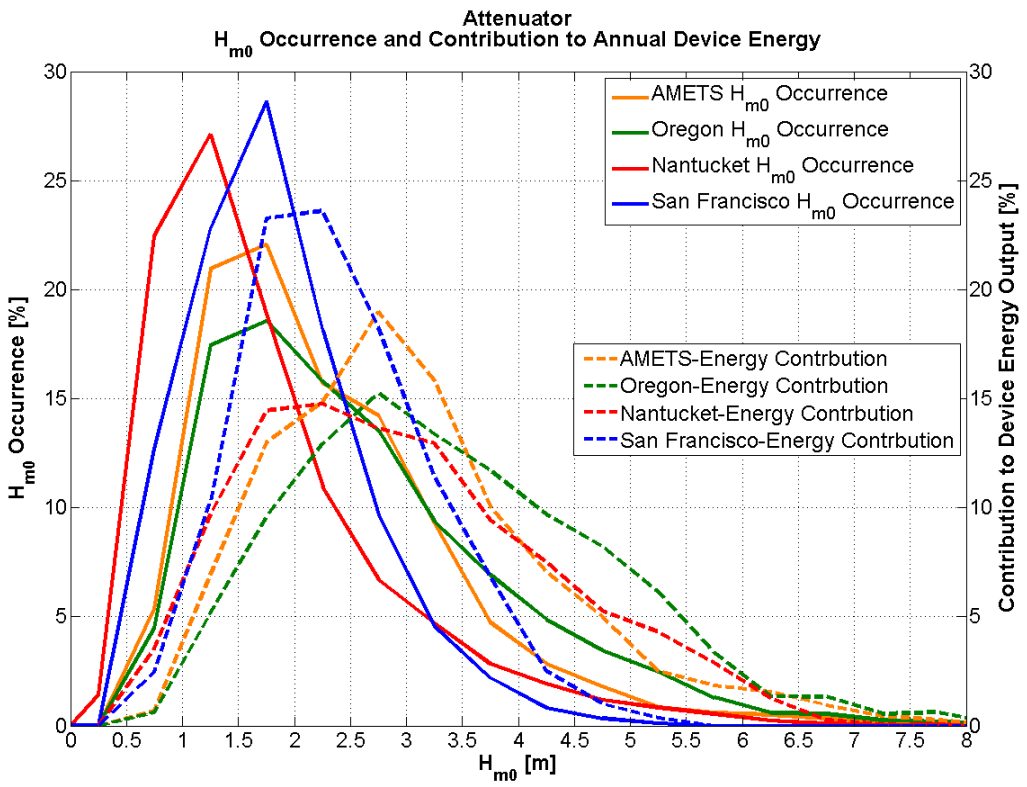

Figure 5.18. H_{m0}: occurrence and contribution to total annual attenuator device (Pelamis) energy production

Device performance at each location was also assessed by calculating how frequently the devices achieve particular capacity factor levels (Fig. 5.19). Capacity factor is defined as the average power the device produces over the course of a year divided by the rated power of the device, i.e. it is the ratio of mean power production to peak power production. As expected, the sites which experienced the least energetic sea states, Nantucket and San Francisco, displayed the lowest average capacity factors. All three devices performed best, according to this measure, at the site off the coast of Oregon and at AMETS on the Irish western seaboard, with average capacity factors in the range 20-30% being achieved. The capacity factors for Pelamis and Wave Dragon are similar to those calculated by Dunnett and Wallace (2009) for several Canadian sites, but are lower at the AMETS site than those reported previously by Dalton and Lewis (2011). This can be explained by the fact that their study used data from the M4 buoy that is 90 km to the north of AMETS, at a water depth of approximately 150 m. It is likely that the wave climate at this point is more energetic than at 50 m depth at AMETS. Additionally, the

records used by Dalton and Lewis were collected in 2007, whereas this study analysed measurements from 2010. Analysis of the AMETS SWAN model has indicated that wave conditions at the site were relatively benign over this period compared to the generally observed climate.

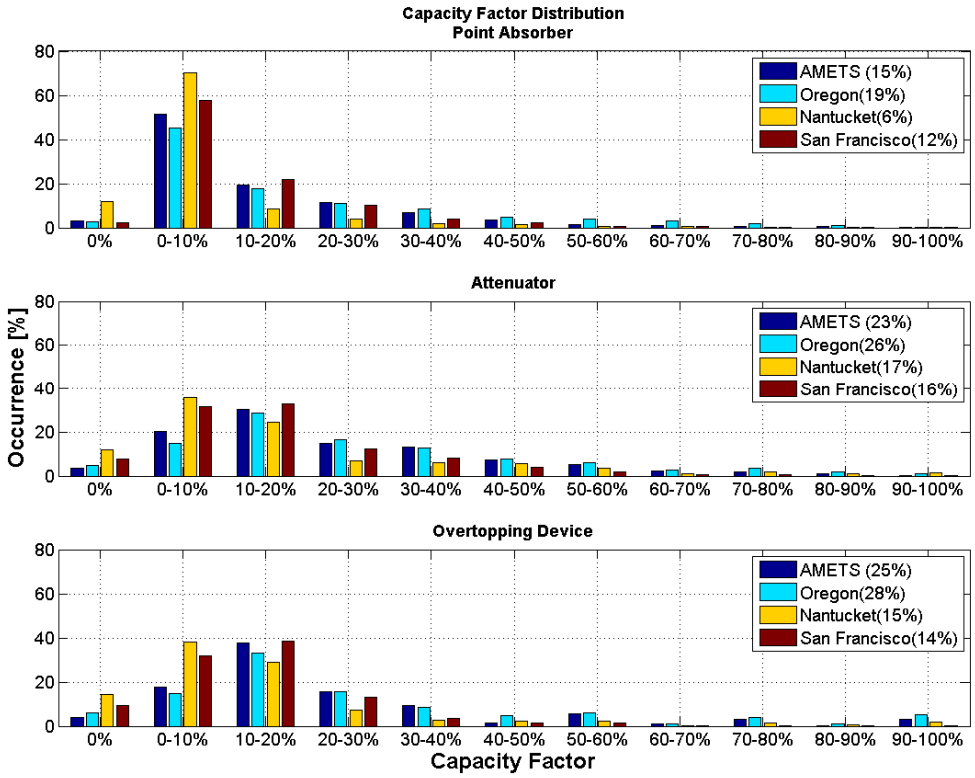

Figure 5.19: Histogram of device capacity factor. Average capacity factor in brackets.

5.6 Variability of Spectral Shape

The implications of these results should be considered when the wave energy resource at a site is being studied, or if several different locations are being compared. Individual spectra with the same summary statistics (H_{m0} and T_E) were previously plotted in Figs 4.12 – 15, along with the average spectrum and the representative Bretschneider shape for each sea state. From inspection of the average spectral shapes it is noticeable that the most energetic conditions, at each of the four locations, produce spectra whose variance is spread across a reasonably narrow range of frequency components. Their average

spectral shapes also show good agreement with the shape predicted by the Bretschneider formula. Conversely, for low sea states — for example 1.5 m < H_{m0} < 2.0 m and 4 s < T_E < 5 s — the spectra are spread across a wider range of frequencies and there is considerable divergence from the representative spectrum. There is also likely to be an increased proportion of occurrences of multi-modal spectra at these low seas states, as has been demonstrated in Fig. 4.11 for the case of AMETS and by Guedes Soares (1984; 1991)and Barrett (2010) for other locations.

These observations are important when comparing the suitability of different locations for WEC installations. Sites such as Nantucket and San Francisco rely on low energy sea states, which occur frequently, for a large proportion of a device's annual power output (Figs. 5.16-18). Power matrices do not account for the increased spectral variability that is associated with these sea states, however. The occurrence of spectra with wide bandwidths, whose energy is spread across a many frequency components or multiple peaks, is likely to diminish the performance of devices, resulting in reduced energy output from what would have been considered these sites' most significant H_{m0} bands. Conversely, WECS deployed at the higher energy sites that were studied, AMETS and Umqua, Oregon, were seen to generate most of their annual energy yields when H_{m0} is relatively high (2.0 m < H_{m0} < 5.0 m). These sea states are shown to display a greater uniformity in spectral shape, which should in turn result in fewer uncertainties in WEC output.

5.7 Discussion

The research presented in this chapter has demonstrated the uncertainties associated with assessing wave energy resource when using summary statistics in place of spectra. It has been demonstrated through analysis of the outputs from the fifteen year wave model of the AMETS area that the deepwater assumption, often made in the calculation of annual average wave power, produces a significant underestimate at the water depths where WECs are most likely to be deployed. Differences in the deep water and depth-adjusted annual average wave power persist in the offshore area, at depth of up to 150 m. These

results highlight the importance of applying the full spectral formula, Equation (2.3), when calculating the theoretical wave power. Even where spectral data is unavailable it would be preferable to generate spectra from summary statistics, and to use these to calculate power while accounting for variations in the depth dependent C_g of the low frequency components.

AMETS has been shown to experience a wide range of sea states, with significant wave heights in excess of 14 m measured by the Waverider buoy at the 50 m depth. It was also demonstrated that these storm conditions account for a disproportionately high contribution to the gross energy resource at the site. The exploitable power parameter, P_{exp}, has been applied to provide a practical adjustment to interpretations of the contribution particular sea states make to the annual incident energy. The difference between the occurrence of bins of H_{m0} values and their contribution to the annual energy output of representative devices has also been illustrated. The results indicate that WEC developers will need to make a design decision on whether to optimize or tune their devices for operating in the most commonly experienced wave conditions or the sea sates which provide the majority of energy at their deployment site. This distinction is important; while extracting as much of the incident wave power as possible is a valuable attribute, issues such as intermittency of production and device capacity factor must also be considered

Defining the wave energy resource and the power output of WECs using a minimal number of summary statistics was shown to conceal important site characteristics, such as the variability that exists in spectral shape. Low sea states were shown to exhibit greater spectral variability, suggesting an increased difficulty in energy capture during these conditions. As a result, sites such as AMETS, whose incident energy resource is concentrated towards higher sea states, will generally provide WECs with a more favourable operating environment for energy capture. These results validate the recommendations of authors who have proposed that the group of summary statistics used to describe wave energy resource be expanded to include parameters such as spectral bandwidth (Kerbiriou M.A et al. 2007; Saulnier et al. 2011).

The conclusions presented in this chapter should be considered preliminary, as they were derived from datasets of short duration — less than one year — measured at a single point, with less than 80% data return. Standards that have been developed in this area suggest that numerical wave models are appropriate tools for characterising the spatial and temporal of the wave energy resource (EquiMar Group 2010a; Folley et al. 2012; IEC TC114 2012). The processes outlined here are expanded in Chapter 6, where the outputs of the 15 year SWAN model of AMETS are analysed to determine how the characteristics of the test site vary with changes in water depth and over long time frames.

Chapter 6 Resource Characterisation: AMETS Case Study

The characterisation of the AMETS wave energy resource presented previously in Chapter 5 is inherently limited; it is derived from observations from a small number of data buoys, located at fixed water depths, from which relatively short durations of measurements are available. The research described in this chapter utilises the output from a fifteen year SWAN wave model of the AMETS wave field — validated against buoy measurements at the site in Chapter 3 — to develop more detailed conclusions regarding the nature of the wave climate at the site. Analysis of the model outputs allows the spatial inhomogeneity in the incident wave power, due to changes in bathymetry, to be quantified, while the interannual variability of the theoretical and technically exploitable resources is also investigated.

This chapter also addresses the degree of scalability between the wave climates experienced at Ireland's wave energy test centres, and assesses whether performance results derived from sub-prototype scale sea trials in Galway Bay can be easily extrapolated to predict device operation and output at AMETS.

6.1 Magnitude and Variability of the Wave Energy Resource at AMETS

The degree to which the incident resource varies from year to year is an important consideration in the planning of WEC farm, as it will influence the energy output and potentially the economic viability of the installation. This has been demonstrated by Mackay et al. (2010), who quantified the variability displayed by power outputs from the Pelamis power matrix using a 51 year hindcast model. It was shown that the mean power levels for two consecutive periods of 20 years — 1960-1980 and 1980-2000 —differed by 9%, and that this variability is closely correlated to the North Atlantic Oscillation (NAO) climatic process (Hurrell et al. 2003). Climate change may also be influential. In a study of the Wave Hub site in the United Kingdom predicted that while the impacts of

climate change would be relatively small when compared to the natural variability they may well be important when considered over the lifetime of a wave farm (Reeve et al. 2011). This study also indicated that climate change may cause more instances of both calm and extreme sea states, resulting in reduced operating periods for WECs. Long term datasets of wave conditions from hindcast models, such as the AMETS SWAN model utilised here, are thus an important resource for quantifying this variation and reducing uncertainty, in contrast to measured buoy data which is generally of short duration.

6.1.1 Theoretically Available Resource

Fifteen stations from the AMETS SWAN model, with water depths ranging from 10 m to 150 m, were selected for the analysis of the variability in the incident wave energy. These points follow the likely route of the cable that will be deployed at AMETS to connect WECs undergoing sea trials to the local electrical grid, as shown in Fig. 3.13. The average power values at each station, computed for 15 years of the available data, are plotted as the solid line in Fig. 6.1. This figure illustrates the enormous energy potential at AMETS and other exposed site on the Irish west coast. The average power exceed 60 kW/m for depths in excess of 30 m and reaches a maximum value of approximately 81 kW/m at the station that is located furthest offshore. This agrees with the results shown by Mollison, who estimated an average power value of 77 kW/m near Belmullet (Mollison 1982). The Irish Accessible Wave Atlas (ESB International 2005) reports much lower values of theoretical power — 50-60 kW/m within 25 km of the west coast — but these results underestimate the resource due to errors in the calculation of power, as demonstrated in Chapter 4 of this thesis. The average power values that fall within one standard deviation of the average are bounded by the dotted line and the outliers, the most and least energetic years, are marked by the triangle symbols. These provide an indication of the fluctuations that exist in the average power values at each water depth over the 15 year period. The percentage difference between the years with the highest and lowest energy resources at each location are also included beneath the main figure. Fig. 6.1 illustrates that a great deal of variability — with average annual power for some years over 85% greater than others — of the incident wave energy exists at the site, and that these anomalies are relatively similar across the range of water depths that were analysed.

A fall off in average power levels is observed for the less exposed, nearshore, locations, though the average power at the 20 m depth is approximately 30 kW/m which should be substantial enough for many nearshore device concepts to operate in efficiently.

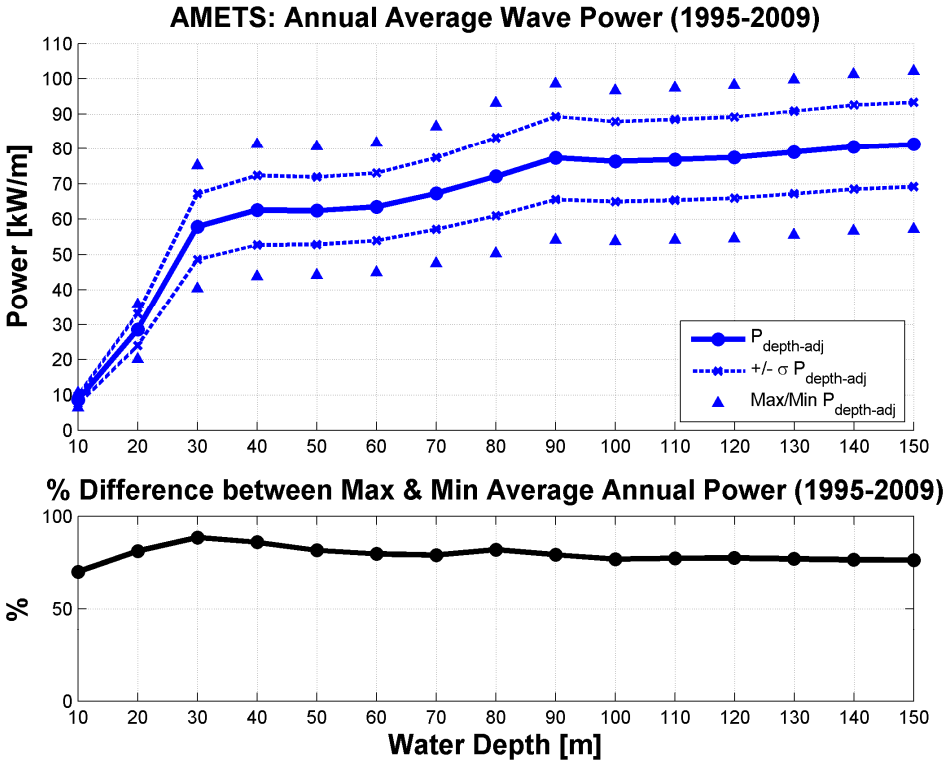

Figure 6.1: AMETS annual average wave power (P)

6.1.2 Technical Resource

Knowledge of the climatic variability of the theoretical wave resource is important, however fluctuations in the technically available energy will be of greater influence on the economic viability of a project. The exploitable power parameter, P_{exp}, that was introduced in Section 2.3.1 is utilised once more once more as a measure of the amount of energy that could be potentially extracted from the site. Limiting the influence of severe storms that exceed the P_{exp} threshold is observed to diminish the available resource — from 81 kW/m to just under 70 kW/m at the 150 m depth station — but it also reduces the variability in the annual average power values; both the standard deviations and

outliers are closer to the mean values. The percentage difference between the most and least energetic years is also revised downward when the P_{exp} metric is applied. There are still significant disparities, however, most notably at the depths in the range 30 m to 60 m — likely deployment sites for floating WECs — where 60% more extractable energy reached the site during the years with the greatest resource than during the most benign years.

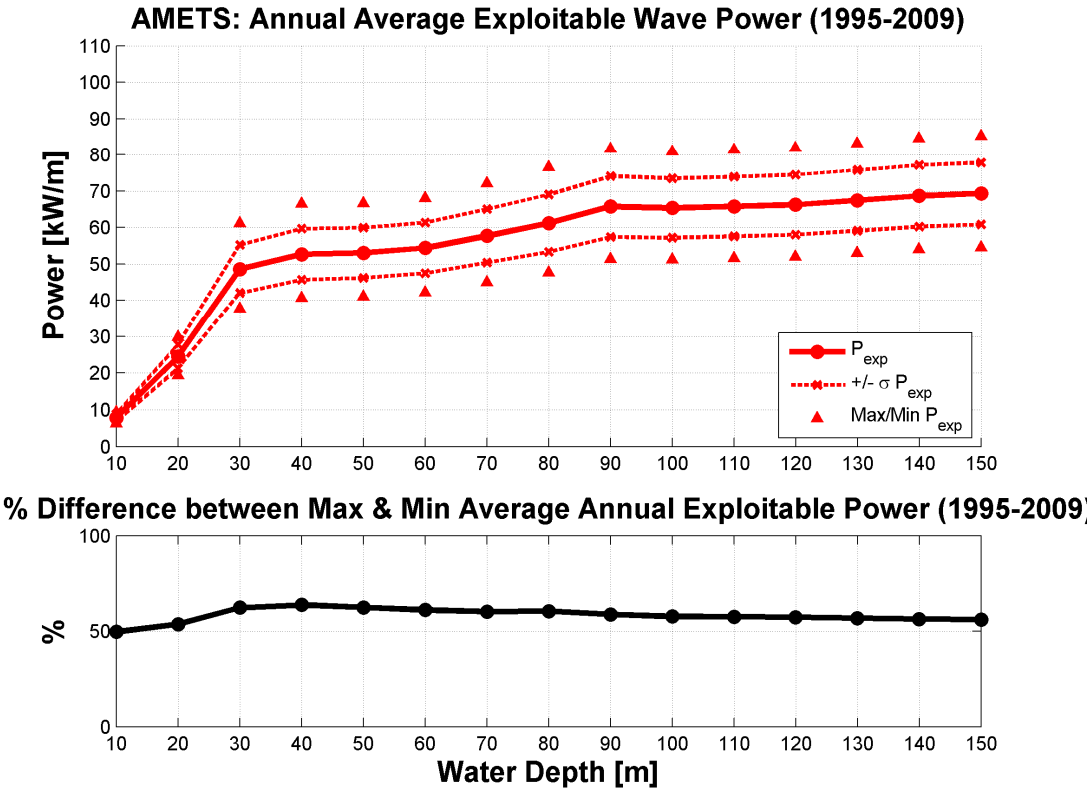

Figure 6.2: AMETS annual average wave power and variability (P_{exp})

The power outputs of the three representative WECs analysed in Chapter 5 — AWS, Pelamis and Wave Dragon — were also computed at each depth station, for each year of available data. The resulting AEP values are shown in the upper portion of Fig. 6.3. These approximate well with the variations seen in Fig. 6.1 and Fig. 6.2, and the output of all three devices is shown to be poor in the nearshore zone, at depths less than 30 m. It should be noted that the values for the 50 m site differ slightly from those presented in Fig. 5.19 which were drawn from one year's worth of measured buoy data.

It is not equitable to compare the devices solely on their individual AEP; Wave Dragon is rated at 7 MW, while AWS (2.5 MW) and Pelamis (0.75 MW) both display much lower maximum power output according to their respective power matrices. The average capacity factor is used as a normalised metric, and its variability across the range of water depths is illustrated in the bottom half of Fig. 6.3. All three devices are observed to perform poorly at the two stations closest to the shore. This is unsurprising; these devices were designed to operate further offshore and the resource at these points is greatly diminished due to sheltering, as the previous sections have demonstrated. Pelamis displays the highest average capacity factors at all of the model stations. The device's production continues to rise in line with the amplification in theoretical and exploitable wave power as water depth increases. Conversely, the average capacity factors for the AWS device plateau at around 20% from depths of 30 m and above. This indicates that the device produces a minimal amount of additional energy, even as it is exposed in increasing wave energy — both theoretical and exploitable — further offshore. This suggests that there would be little benefit to deploying these devices at the deeper water sites, where the costs associated with cables and moorings rise significantly (Dalton and Lewis 2011).

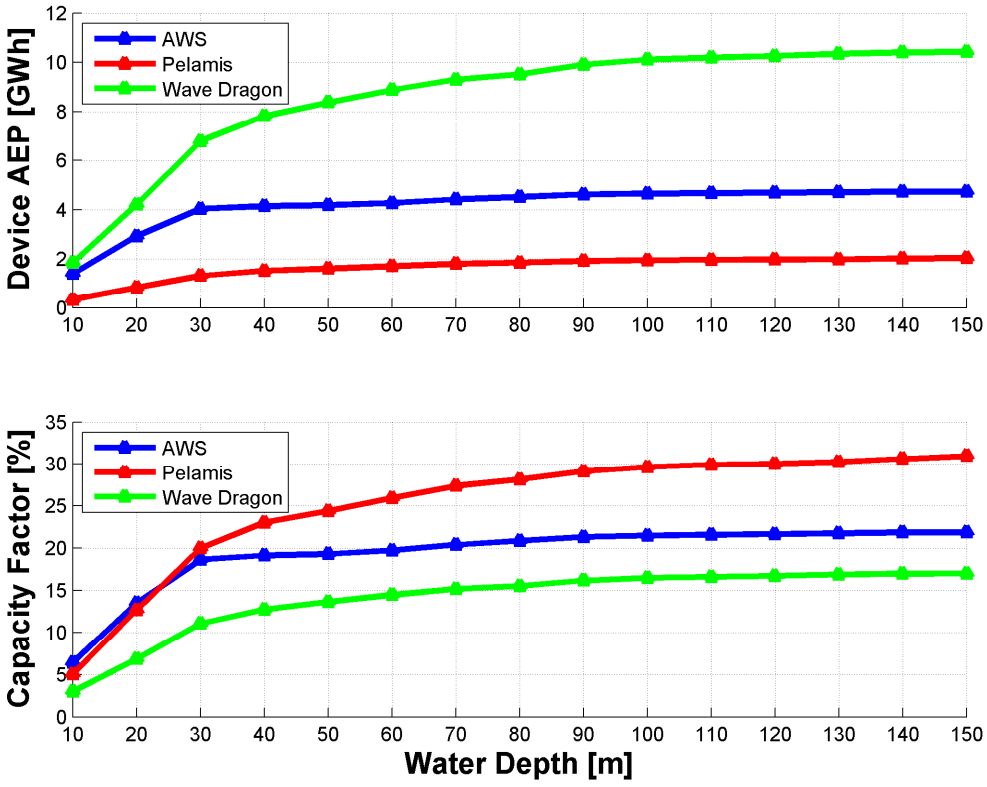

Figure 6.3: AEP (top) and average capacity factor (bottom) for three WECs at AMETS

6.2 AMETS Resource Characterisation

6.2.1 Occurrence versus Contribution

Chapter 5 of this thesis identified the disconnect that exists between the frequency of occurrence of particular sea states and the extent to which they contribute the total energy that is experienced at a point. Analysis of the AMETS model outputs allows this relationship to be observed over a range of water depths. Distributions of occurrence and energy contribution, with H_{m0} bins of 0.5 m, are presented in Fig. 6.4 and Fig. 6.5. Similar illustrations of the occurrence and contribution to energy of T_E values are provided in Fig. 6.6 and Fig. 6.7.

Data from the stations with water depths of 30 m and greater produce very similar distribution curves. The most energy rich sea states at these points are shown to be

higher, and of longer period, that those that are observed most frequently. This corresponds well with the results presented previously for the case of the measured buoy data. The resource at the near shore sites, with depths of 10 m and 20 m, is shown to behave differently, however, when the sea states are arranged by H_{m0}. These points are an interesting case as they are less exposed than the deeper sites due to the shelter they receive to the north and southwest. Here, the most energy rich H_{m0} bins also account for a large proportion of sea sates that were observed at the site, while the available energy is concentrated within a much narrower distribution. The differences these sites exhibit in comparison to the sites further offshore is less evident for bins of T_E. The presence of short period seas — 3 to 6 s — can be detected in Fig. 6.6, but these sea states contribute very little energy so the associated distributions in Fig. 6.7 follow those of the deeper sites. The challenge that this disconnect between sea state occurrence and energy contribution presents when attempting to match a device to a site was discussed in the previous chapter. In contrast, it is feasible that a nearshore WEC like Aquamarine's Oyster would be able to operate within a reduced design envelope, as most of the incident energy is available for capture from a contracted range of sea states, to which the device could be tuned to achieve optimal performance.

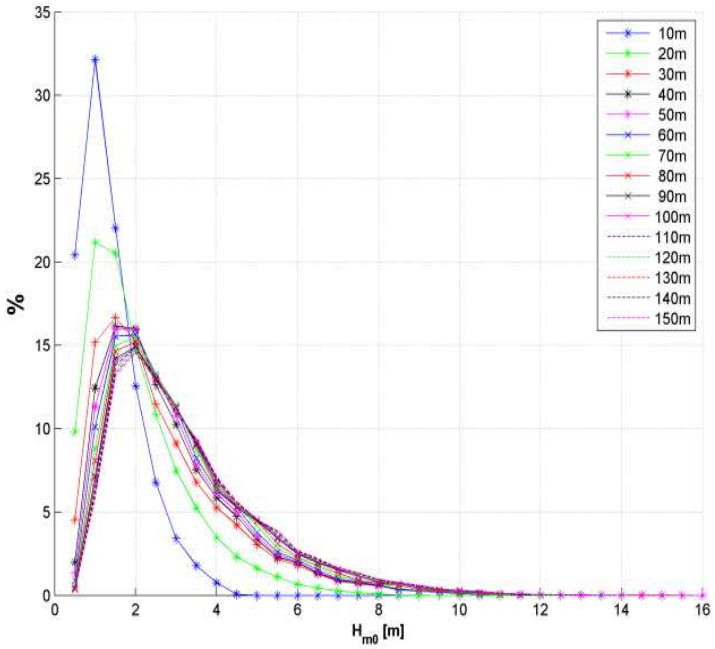

Figure 6.4: % occurrence of sea states within H_{m0} bins

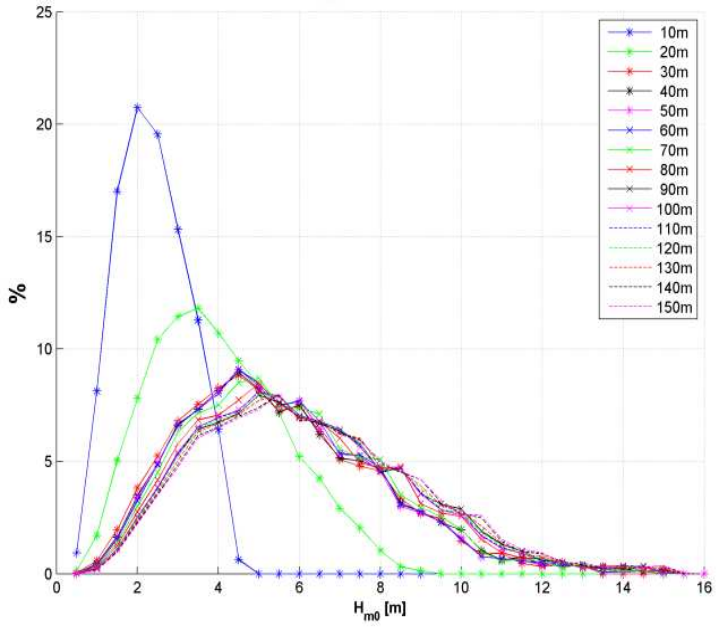

Figure 6.5: Contribution of H_{m0} bins to total energy

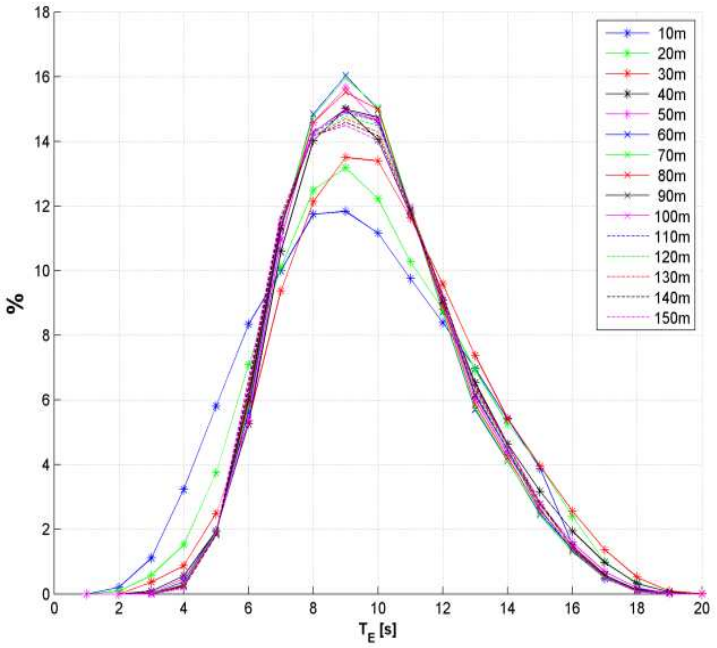

Figure 6.6: % occurrence of sea states within T_E bins

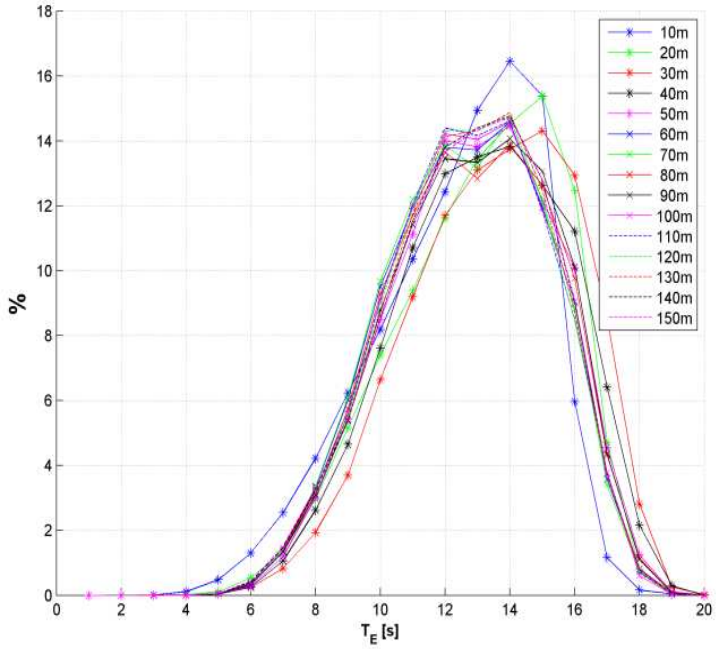

Figure 6.7: Contribution of T_E bins to total energy

6.1.2 Wave Directionality and Spectral Bandwidth

The performance of many types of WECs is highly dependent on wave directionality, especially if they sit on a fixed foundation or if their moorings do not allow them to 'weather vane' to face the prevailing waves. Following the approach outline in the previous section the occurrence of sea states within 10° bins of the mean wave direction of approach, θ_{mean}, was compared to their contribution to the total energy passing each station. A Cartesian convention, with East corresponding to 0°, was used in the model (Curé 2011a). The results of this analysis are illustrated in Fig. 6.8 and Fig. 6.9. It is noticeable that the amount of energy arriving at the various station points from particular directions is closely related to the frequency of occurrence, unlike the previous results for H_{m0} and T_E. It is also evident that the spread of incoming wave directions is more concentrated within a narrow band at the shallower water depths, due to a combination of refraction and shelter. This characteristic should be advantageous for the capture of energy, though as results of Section 6.1 demonstrate it is offset by the reduction in incident wave power.

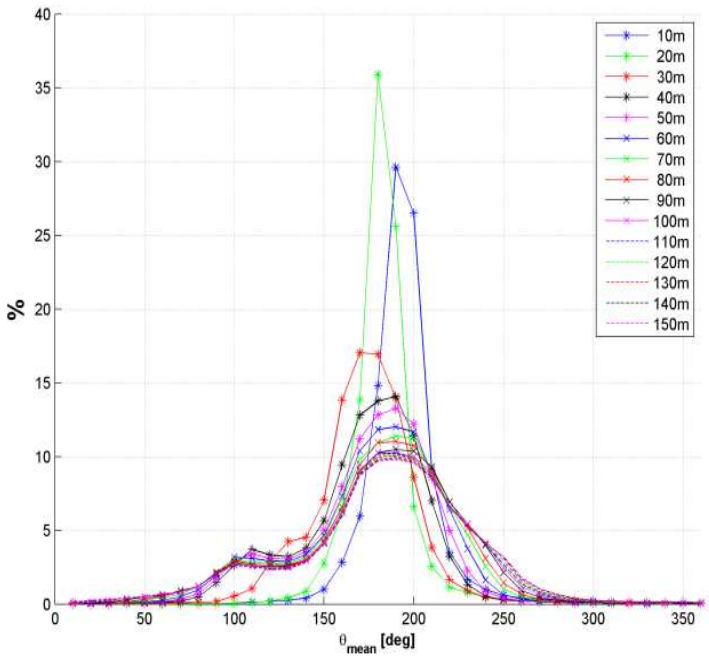

Figure 6.8: % occurrence of sea states within directional bins. Cartesian coordinates, East=0°

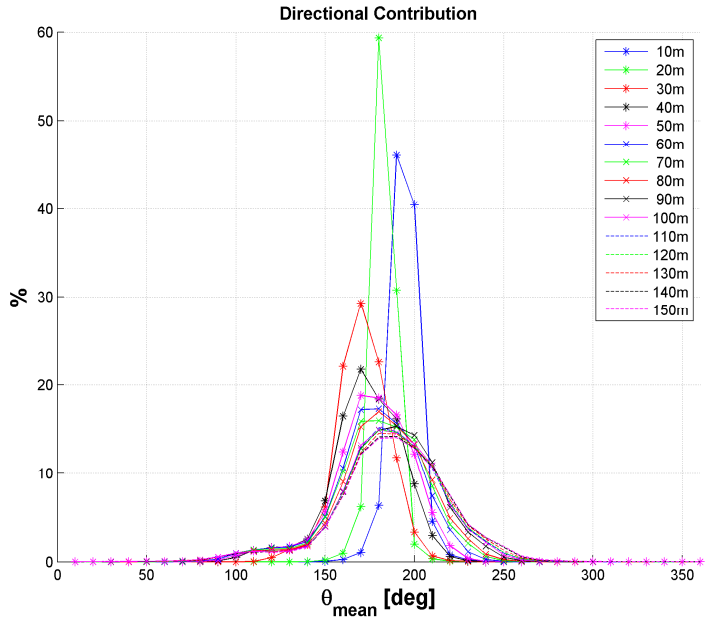

Figure 6.9: Contribution of directional bins to total energy. Cartesian coordinates, East=0°

The concept of spectral bandwidth, and its influence of on the performance of certain types of WECs (Saulnier et al. 2011), has been discussed in previous sections of this thesis. Occurrence and energy contribution of the range of bandwidth values observed in

the model outputs are shown in Fig. 6.10 and Fig. 6.11. Occurrence and energy contribution appear to be well matched for the cases presented here. The offshore sites are dominated by ε_1 values between 0.4-0.5, whereas the nearshore locations are seen to experience more wide banded spectra.

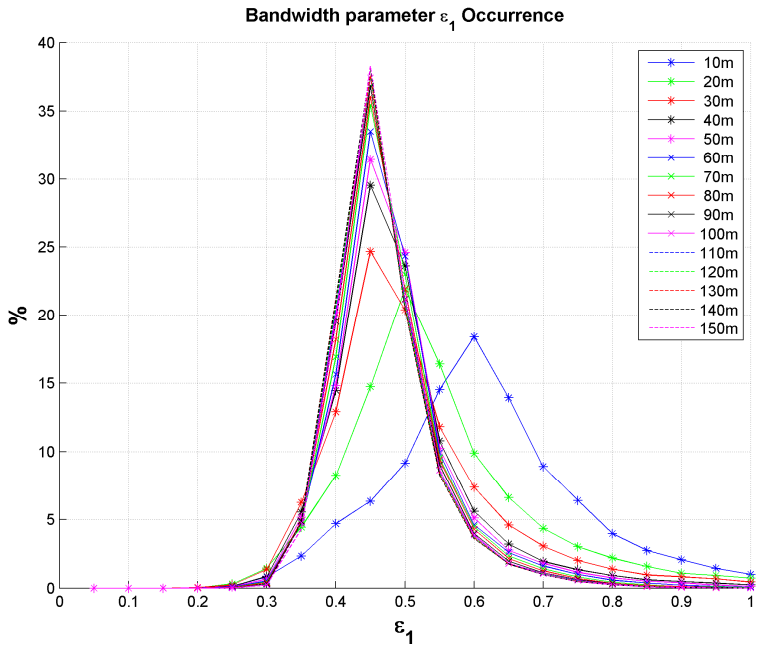

Figure 6.10: % occurrence of sea states within bandwidth (ε_1) bins.

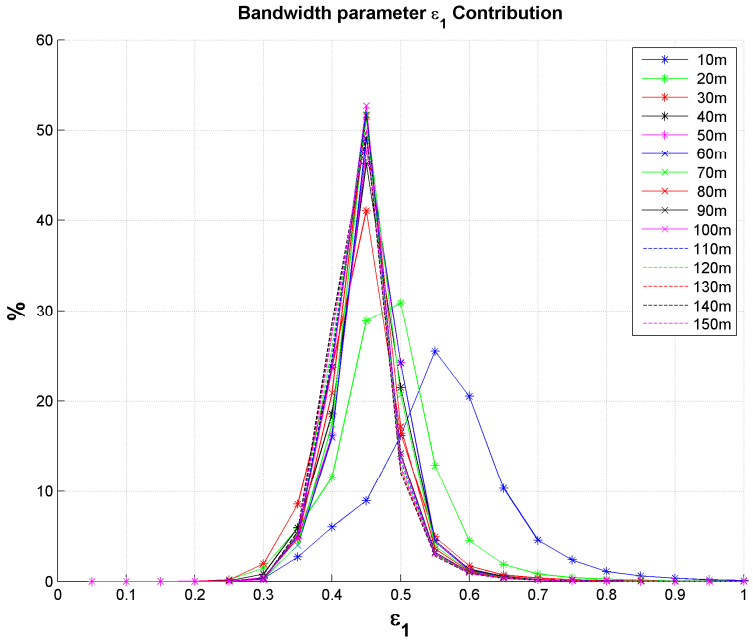

Figure 6.11: Contribution of bandwidth (ε_1) bins to total energy.

6.3 Resource Scalability between Galway Bay and AMETS

Developers who will deploy WECs at the Galway Bay quarter scale site as part of a staged test programme will need to analyse performance results to gain an understanding of how their technology will operate at full scale. These results would be of little use if the incident wave conditions during sea trials were not representative of the metocean environment expected for full scale, commercial projects. In this section comparisons are made between the measured wave resource from Galway Bay and the wave climate that has been recorded and modelled at a depth of 50m at AMETS in order to assess the suitability of Galway Bay for testing devices of approximately quarter scale.

6.3.1 Sea State Occurrence

AMETS can be considered to be typical of the exposed, energy rich, sites that can be found along the west coast of Ireland and is therefore a suitable point of reference for Galway Bay. Values for the summary statistics H_{m0} and T_E were calculated from a full years worth of measurements (2010) from the Waverider buoy located in Galway Bay. Froude scaling (Hughes 1993) was then applied to convert the scatter diagram from Galway Bay for 2010 to full-scale (Fig 6.12). Visual comparisons can be made with the equivalent scatter plot derived that was illustrated in Fig. 5.10 from the measured data collected at AMETS over the same period. Consulting these figures indicates that while the percentage occurrence of individual sea states may vary between the two sites, the overall range of conditions that occur at AMETS is fully replicated, at approximately quarter scale, in Galway Bay. This distinct correlation ensures that WECs deployed at the test site will encounter a sufficiently large spread of wave conditions, and consequently gather ample amounts of operational data, to allow for accurate predictions of device performance at full scale to be established. There is a strong similarity in the occurrences of extreme conditions measured at the test sites, particularly in terms of sea state slopes which follow the constant 1/13 line. This association will provide developers who deploy in Galway Bay during winter months with the opportunity to prove the survivability of their devices in scaled conditions equivalent to the storms experienced at exposed locations off the west coast of Ireland. This figure illustration differs slightly from the

version developed by Barrett (2007), who defined sea states in terms of H_{m0} and T_{02}. Applying this approach results in a reduced range of period bins, and consequently a greater concentration of sea state occurrence towards the 1/20 steepness line.

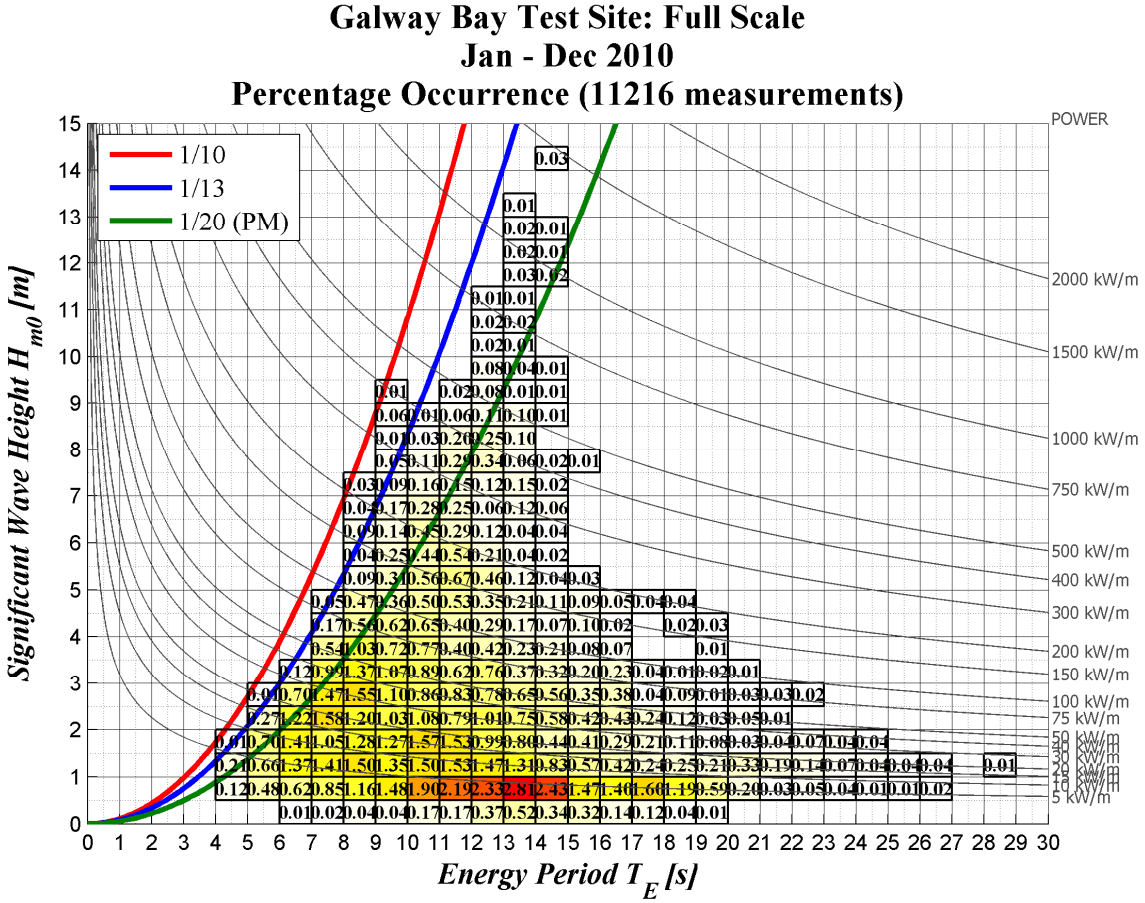

Figure 6.12: Bi-variate scatter plot of H_{m0} – T_E occurrence for Galway Bay converted to 'full-scale'.

It is notable, however, that the Galway Bay scatter diagram displays a greater contribution from long period sea states with a relatively low significant wave height. These sea states do not have any equivalent in the AMETS figure. The influence of these swell dominated sea states can be seen in the plots of occurrence and cumulative exceedance for H_{m0} and T_E displayed in Fig. 6.13. While the scaled values of H_{m0} from Galway Bay are generally well matched with those from AMETS, they exhibit a much greater occurrence of sea states with $H_{m0} < 1$ m. Agreement is worse for the T_E values, as had been suggested by Fig. 6.13. Results gained from testing during these long period sea states — $T_E > 12$ s at full scale — would provide little relevant knowledge about the performance of a WEC concept in realistic, full scale, conditions. Device developers

should be careful to ensure that these sea states are excluded from performance analysis, though in general their impact can be considered negligible, however, as they generally occur when wave energy is low and below the operating threshold of devices; for example, during the CORES deployment in 2011 the OWC turbine did not generate power until H_{m0} exceeded 0.8 m (Thiebaut et al. 2011).

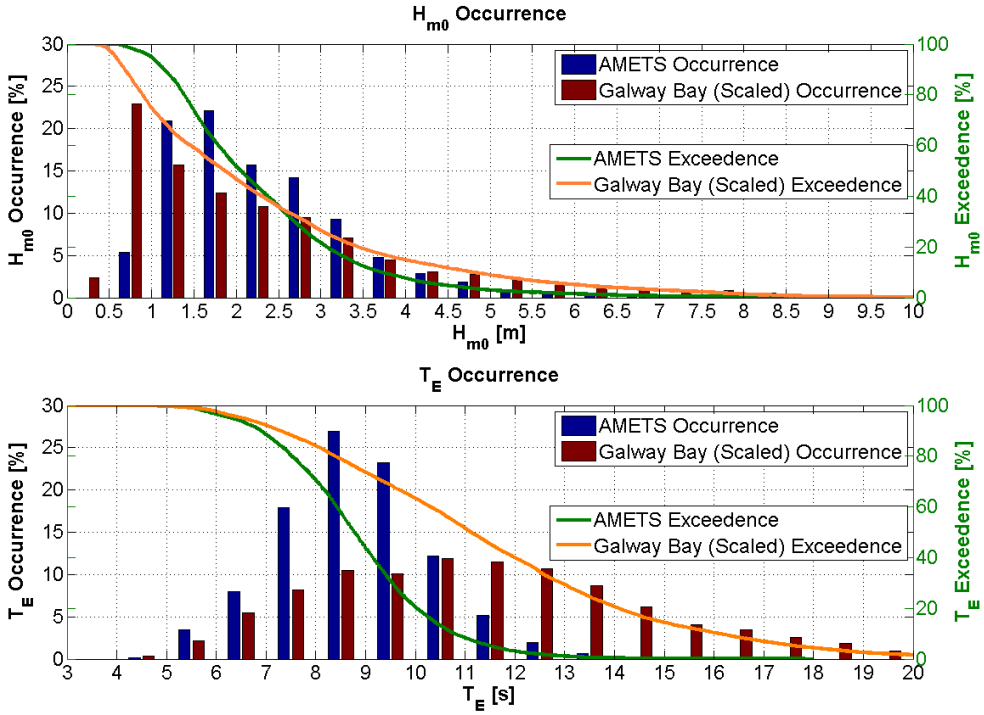

Figure 6.13: Occurrence and cumulative exceedance of H_{m0} (top) and T_E (bottom) for AMETS and Galway Bay measurements at full-scale

6.3.2 Average Wave Power in Galway Bay

The annual average wave power for AMETS from the available 2010 measurements was found to be 33kW/m by applying Equation (2.3). The annual average wave power for Galway Bay for the same period was approximately 1.4kW/m. Though the sets of data from Galway Bay and AMETS contain gaps (see Fig. 3.8 and Fig. 3.11) these tended to occur during the summer months at both sites so seasonal bias should not be significant. Assuming that Galway Bay is at quarter scale to open ocean conditions and applying Froude scaling (Hughes 1993) gives a full scale value of approximately 45 kW/m. While this is of the same order of magnitude as the AMETS value it is still noticeably higher,

possibly due to the fact that the sea states observed in Galway Bay tend to be of a longer period than the open ocean site, as illustrated in the previous section.

The results presented in Section 6.1 give an annual average wave power of approximately 62 kW/m at the 50m depth and 76 kW/m at 100m, indicating that 2010 was a particularly benign year. Correspondingly, the values of annual average wave power in Galway Bay were found to be higher for other years from which data were available (Figs. 3.5 – 10), ranging from 2.0 kW/m to 2.6 kW/m, equivalent to 64 kW/m to 83 kW/m full scale.

6.3.3 Spectral Shape

The presence of long period swell waves can also be detected in the analysis of spectral shapes. In Fig. 6.14 the measured spectra that fall within the range 0.625 m < H_{m0} < 0.75 m and 3.0 s < T_{02} < 3.5 s are plotted together, along with the average of the spectral ordinates and the classical Bretschneider spectrum for similar summary statistics. Two distinct components are noticeable; swell cantered on frequencies below 0.1Hz mixed with a wind sea component cantered around 0.3Hz which is appropriate for a one quarter scale seaway. In contrast, spectra measured by the AMETS Waverider which fall within the equivalent full scale range (2.5 m < H_{m0} < 3.0 m and 6 s < T_{02} < 7s) and are plotted in Fig. 6.15 are found to conform relatively well with what would be expected from an open ocean site, as evidenced by the likeness of the average spectral shape to the Bretschneider spectrum. This highlights once again the importance of exercising caution when selecting performance data from sea trials to ensure that the results are derived from sea states whose spectra are equivalent to those that are expected at full scale conditions.

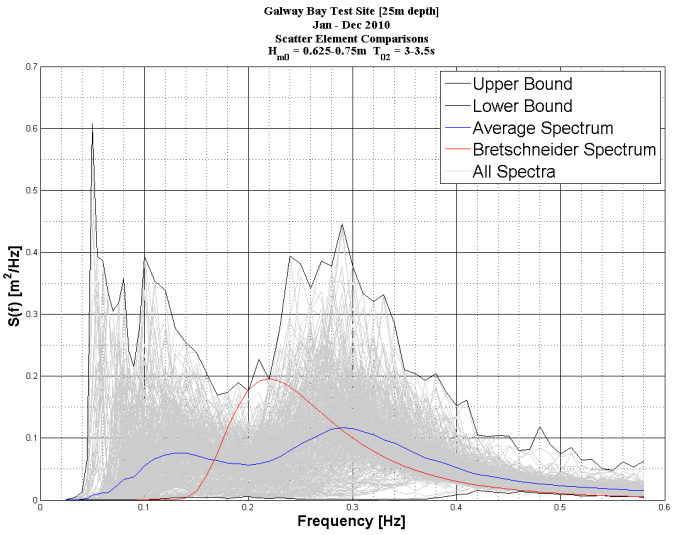

Figure 6.14: Individual, averaged and theoretical spectra within the range 0.625m < H_{m0} < 0.75m and 3.0s < T_{02} < 3.5s for the Galway Bay test site (equivalent to Fig. 6.15)

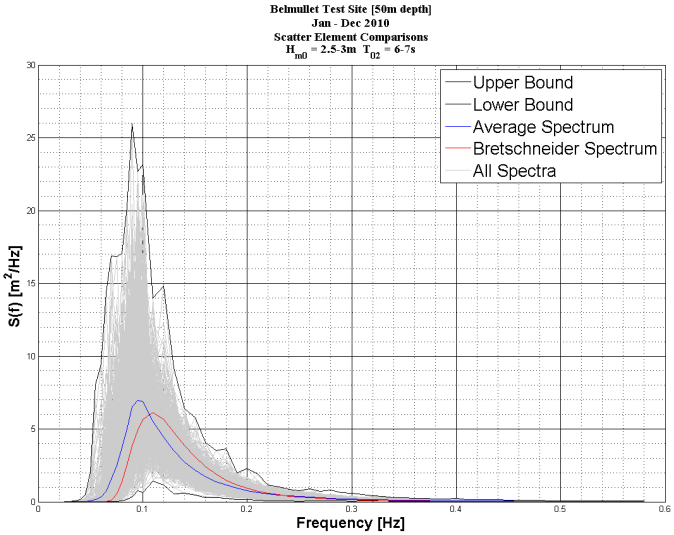

Figure 6.15: Individual, averaged and theoretical spectra within the range 2.5m < H_m0 < 3.0m and 6s < T_{02} < 7s for the AMETS location (50m depth). (equivalent to Fig. 6.14)

6.4 Discussion

This research has demonstrated the interannual variability in the wave energy resource at AMETS is significant for all water depths that were analysed. The difference between the most and least energy rich years is reduced from an average of 81% for the offshore model stations to 59% when a technical measure of power, such as P_{exp}, is used in place of the theoretical wave power as the influence of the most severe storms is filtered out. These results also highlight the value of long term datasets that wave models can provide,

and that can rarely be retrieved from buoy measurement campaigns. If a project developer attempted to calculate the available resource on the basis of only a few years worth of records they could easily be left with an unrealistic estimate, particularly if the measurements had happened to be taken during one of the outlier years. This would in turn have a significant impact on the economic returns from the project. There are uncertainties associated with model outputs however — illustrated in Section 3.3.4 of this work for the AMETS SWAN model — so any results should also be interpreted in conjunction with physical measurements.

The difference between the occurrence and energy contribution of particular values of important sea state descriptors — H_{m0}, T_E, θ_{mean} and ε_1 — was illustrated for the various water depths. There is a particularly strong disconnect visible in the distributions for H_{m0} for water depths greater than 30 m, and for T_E at all depths. This confirms the preliminary results presented in the previous chapter results and indicates that WEC developers will need to make a design decision on whether to optimize their devices for operating in the most commonly experienced wave conditions or the sea sates which provide the majority of energy at their deployment site. The occurrence of significant wave height and direction were shown to be well matched with their respective energy contributions at the nearshore locations. The variability of the incident power — both theoretical and exploitable — was also seen to be slightly reduced at these points. This indicates that nearshore WECs can be designed to target a narrower range of sea states for energy capture, especially when allied to the fact that extreme conditions at these water depths are greatly reduced.

The overall wave climate at the benign test site in Galway Bay was shown to be well matched, at quarter scale, to that at AMETS for locally generated wind seas. It was also demonstrated, however, that there is a significant occurrence of longer period seas which do not scale to any conditions experienced at the Belmullet site, so it is imperative that device developers are careful when interpreting device performance results collected during these conditions.

Chapter 7 Extreme Wave Conditions at AMETS

7.1 Introduction

Knowledge of potential extreme metocean events is fundamental to the design of WECs, particularly if they are to operate in areas with highly energetic resources such as the west coast of Ireland. Determining the most onerous wave conditions that a device is likely to encounter while deployed and operating at sea is one of the key challenges facing WEC developers. Without this information it is difficult to estimate realistic design loads is difficult without this information, leading to the system being over- or under-designed. This, in turn, has the potential to result in either excessively high costs, which reduce the economic viability of the project, or possible component failures and irreparable structural damage.

The susceptibility of WECs to extreme waves is dependent on the geometry and operating principles of individual devices; a floating point-absorber that operates in heave is likely to react differently to large waves than would a submerged, pressure-based, system. Many studies of design conditions have focused on particular WEC concepts. For example, a study of the design sea-states that should be assumed at the Biscay Marine Energy Platform (bimep) test site in Northern Spain, for return periods of up to 100 years, was carried out by Duperray et al. (2011). Once the extreme metocean parameters — covering waves, winds and tides — were extrapolated from archived buoy data, the authors could calculate the most severe loads and motions for the mooring system of a numerically modelled WEC. Similar work detailed by Doherty et al. (2011) predicted the extreme foundation loads for the Oyster WEC being developed by Aquamarine Power Ltd. Analyses such as these are vital in ensuring reliability and reduced risk in wave energy projects. Many floating structures are also susceptible to wave groups — successions of high waves that are especially prevalent in narrow banded swell seas — while slamming loads caused by wave breaking should also be considered for the purpose of WEC design (Hovland 2010).

In this chapter the Atlantic Marine Energy Test Site (AMETS) is used as a case study for the study of extreme wave events. Given its open ocean location it is arguably representative of the most energetic locations for the potential development of WEC projects. Two categories of dataset that have previously been unavailable for Irish coastal sites — time series of water surface elevation from an exposed site and a long term model outputs of summary statistics — exist for AMETS and are utilised in an attempt to develop a better understanding of the extreme conditions that should be expected in exposed Atlantic seaways. This work considers both large and unexpected individual waves as well as extrapolated predictions of the most severe sea-states that a WEC should be expected to encounter over its operational lifetime. Results derived from the analysis of the AMETS datasets are presented. Also, conclusions, with implications for the development of wave energy farms, are outlined.

7.2 Extreme Individual Waves

7.2.1 Observations of Extreme Wave Heights

The likelihood that the heights of the largest waves that exist in nature are being recorded quantitatively is low, given the sparse distribution of wave measurement instruments in the open ocean. The largest waves that have been observed by wave buoys have occurred off the coast of Canada, particularly in the western North Atlantic. Cardone (1996) reported that maximum individual wave heights (H_{Max}) greater than 30 m have been recorded at Buoy 44137, moored 150 NM southeast of Halifax, Nova Scotia, during the "Halloween Storm" of 1991 and the "Storm of the Century" in 1993. Waves in excess of 30 m were also measured in Canadian waters during Hurricane Luis (1995) by a moored NOMAD buoy and were also observed by the crew of the cruise liner *Queen Elizabeth II* (Bowyer 2000). A 30.8 m wave, recorded in 1993 by a NOMAD buoy moored in a water depth of 2125 m off of British Columbia on Canada's Pacific coast, was reported by Thomas (1995), though doubts were expressed about the reliability of this measurement as it was significantly larger than the surrounding sea (H_{m0}=12.8 m) and other values of H_{Max} recorded nearby (19-23 m). Furthermore, Skey et al. (1998) noted that the buoys in the Canadian network at this time calculated H_{Max} by doubling the maximum positive

surface elevation in each record rather than by using an upcrossing method to measure the true crest-trough or trough-crest height. In reality it is unlikely that the wave profile will be symmetrical so the buoy will overestimate H_{Max} in the case of large crests and underestimate it when the troughs are deep. For these reasons, caution should accompany the interpretation of these results.

The highest H_{Max} values recorded in the eastern North Atlantic were obtained from a Shipborne Wave Recorder MkIV (SBWR) mounted in the hull of the RSS *Discovery*, which was caught in severe storm conditions near the Rockall Bank to the northwest of Ireland on 8th-9th February 2000. These measurements are detailed in a research paper prepared by a number of scientists aboard the vessel (Holliday et al. 2006), while a dramatised account of the event is recounted by Casey (2010). As conditions worsened – the measured significant wave height peaked at 18.5 m with a maximum wind speed of 24 ms^{-1} – the ship was required to maintain a hove-to course as a safety measure. During this period the highest individual zero-upcross wave measured by the SBWR was 29.05 m, while waves of 29.01 m and 28.27 m were also observed.

Until recently the outputs from the measurement buoy network in Irish coastal waters were confined to summary statistics, resulting in a scarcity of recordings of water surface elevations and information pertaining to large individual waves. As a result, researchers have been forced to supplement their knowledge of individual waves by other means. O'Brien and Dias (2012) compiled a catalogue of extreme waves in Irish waters using a combination of qualitative sources such as boulder deposits, newspaper articles and eyewitness accounts. It was noted that damage sustained during storms to the lighthouse close to AMETS on Eagle Island — located 67 m above sea level — is attributed to extreme wave events, though one can only speculate as to the true heights of the waves in question. The Commissioners for Irish Lights vessel *Daunt* did record a wave height of 42 ft (12.8 m) using a SBWR off Cork on January 12th 1969 (Draper 1971). While not particularly large in the context of the waves already described in this section it was over 2.5 times greater than the surrounding sea-state which had a significant wave height of 16.5 ft (5.0 m).

The growth of interest in wave energy and the development of test areas such as AMETS and the Galway Bay quarter scale site have precipitated the installation of more sophisticated instrumentation in the seas around Ireland. The Datawell Waverider buoys that have been deployed record and store measurements of water surface elevation at a sampling frequency of 1.28 Hz. This allows for crest to trough heights to be identified from the incident wave conditions. For example, the Galway Bay buoy has recorded values of H_{Max} in excess of 8 m in December 2006 during the original sea trials of the OE Buoy WEC. This is the equivalent of a full-scale device encountering a 32 m wave in the open ocean (Barrett et al. 2007). A buoy was originally deployed at a depth of 50 m at AMETS in late 2009. Since then the largest observed wave height at the site occurred on November 11th 2010 measuring a trough to crest height of 23.87 m with a period of about 15 s (Fig. 7.1). This is believed to be the largest wave ever recorded in Irish waters, surpassing a 20.4 m wave identified by Met Éireann at the M4 buoy in November 2011. A wave of 21.12 m was also measured earlier in the 30 minute time series and the calculated H_{m0} was 14.2 m, indicating the severity of the conditions at the time. The AMETS wave was initially identified by the Waverider buoy — which calculates H_{Max} using a zero-upcross algorithm — as having a height of 21.9 m. The evolution of the conditions, from which this wave was generated, over the course of November 11th-12th is illustrated in Fig. 7.2, including H_{Max} calculated using both the upcross and downcross methods. Differences can be observed between these two values for H_{Max}, which should be considered when the time series data are being processed, though in general they are not overly significant. The highest wave recorded by the Wavescan buoy, located at AMETS at a depth of 100m during the periods May-October 2010 and April-August 2011, was calculated from upcrossing analysis to be 18.9 m and occurred during a storm in May 2011 (maximum H_{m0} = 11.9 m). Unfortunately no time series of surface elevation exist to allow for further investigation and the buoy was never deployed during the winter when the highest sea-states would be expected.

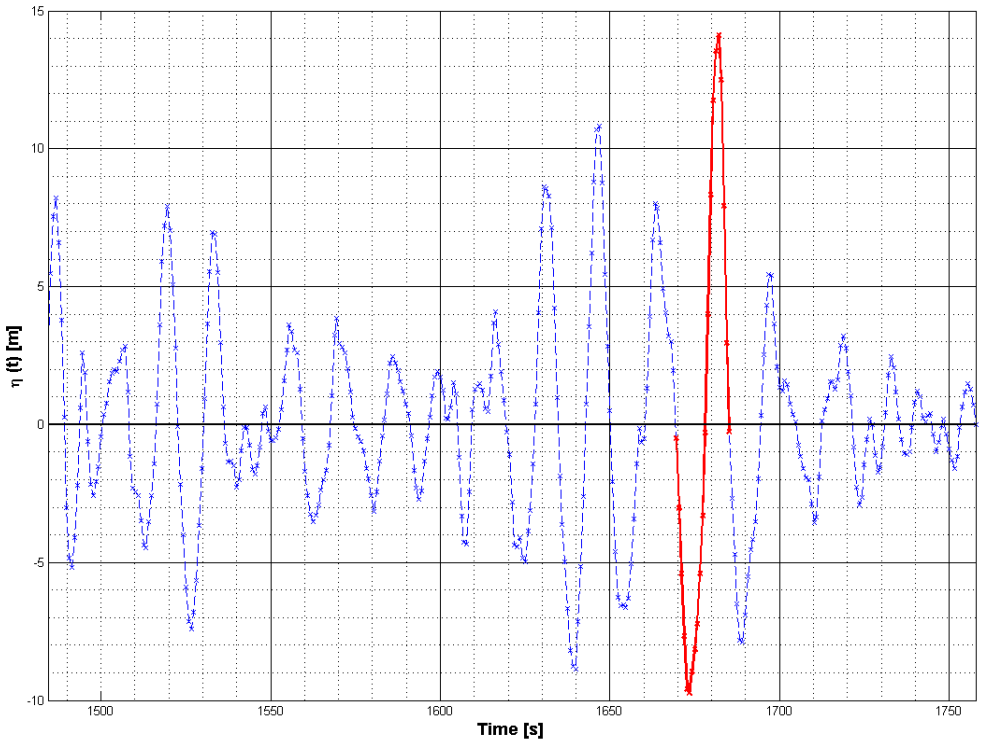

Figure 7.1 23.87m wave recorded at AMETS on November 11th 2010

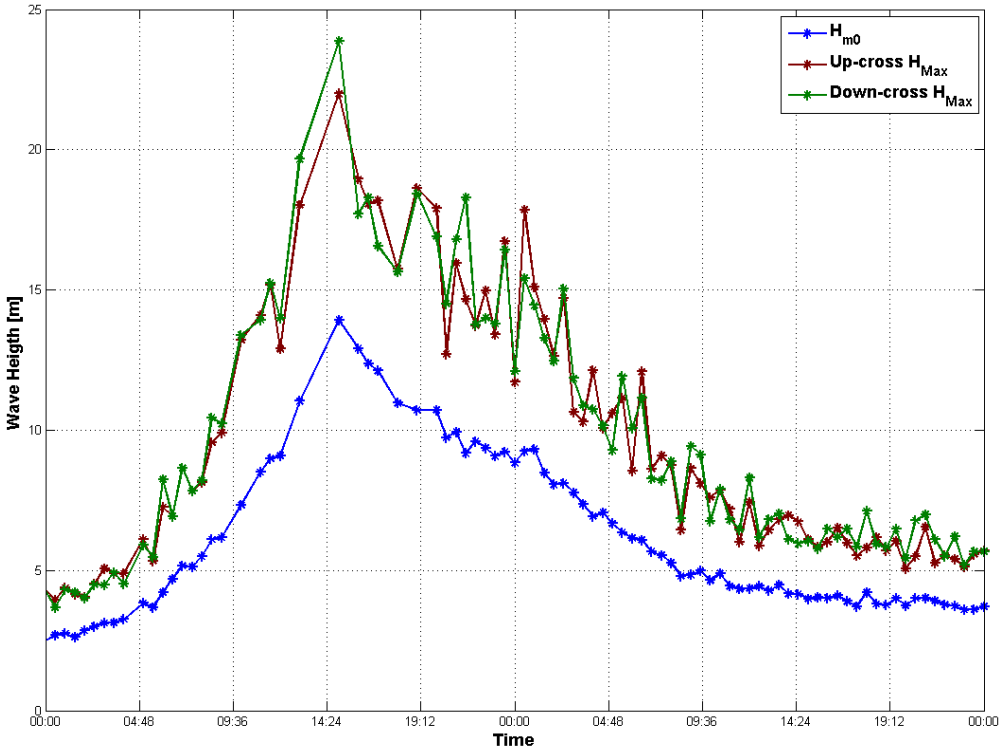

Fig. 7.2 Evolution of H_{m0} and H_{Max} thought the November 11th -12th storm at AMETS

While even greater wave heights approaching 40 m have been identified in the summary statistics returned by the Waverider buoy at the 50 m depth, further inspection of the time series has shown them to be erroneous and artefacts of unusual sensor behaviour. Two such examples are presented in Figs. 7.3 and 7.4. The first series looks like an obvious error. The profile is smooth and symmetrical, and plateaus at a value of +/- 20.47 m, which is close to the operating limits of the instrument (Datawell BV 2010). The second example appears to be more reasonable but is preceded by a sharp spike earlier in the record. Correspondence with Datawell technicians and other users of Waverider buoy data indicated that these extreme oscillations are likely due to a digital filter applied during the conversion of the measured acceleration to displacement through double integration (Stoker 2012; Volger 2012). The filter coefficients are plotted as a function of time in Fig. 7.6. Non-wave accelerations induce spikes in the filter, which manifest themselves as long period oscillations with a delay of 170 samples, or 133 s at a sampling rate of 1.28 Hz (Datawell BV 2012b). This lag between the initial disturbance and the erroneous surface elevation signal is evident in Fig. 7.4. It is possible to implement automatic identification of filter-contaminated time series in the quality control of the data, however visual inspection of the time series is invaluable as the long period, symmetrical shape of the disturbance can be easily recognised.

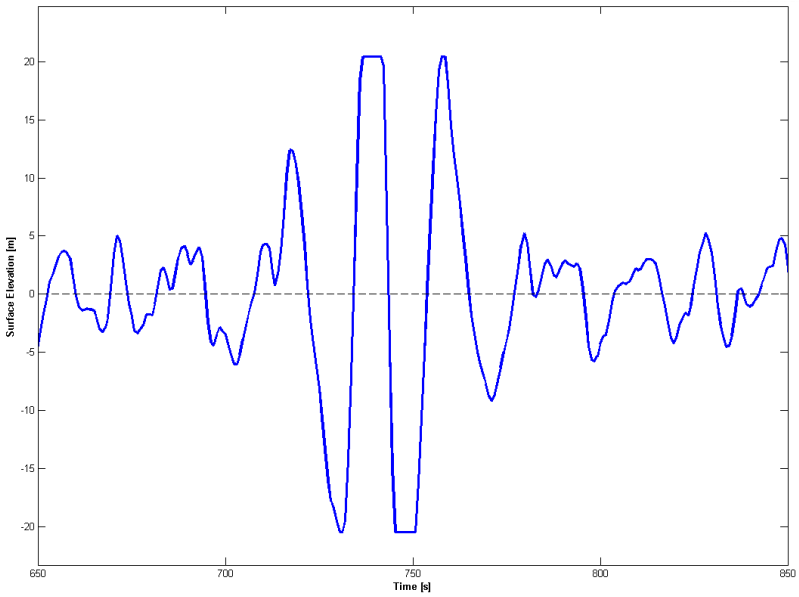

Fig. 7.3 Erroneous surface elevation signal, H_{Max} = 40.94 m.

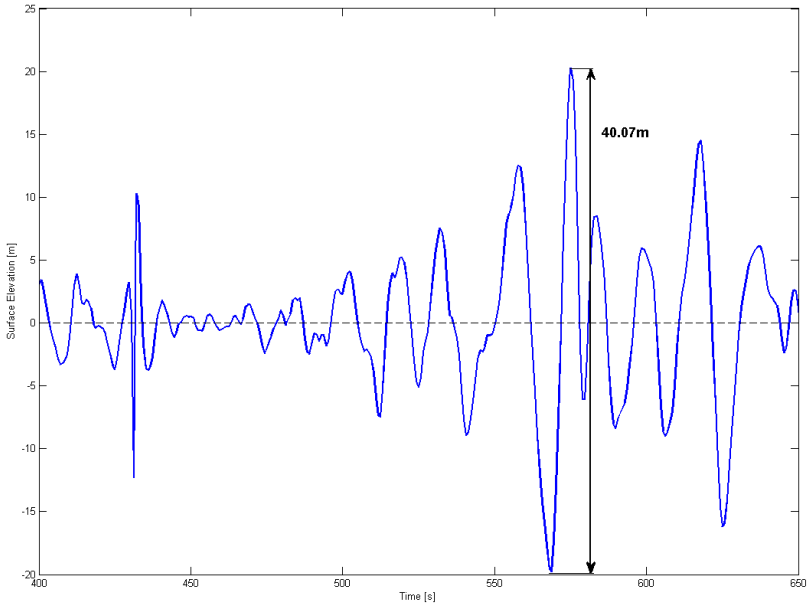

Fig. 7.4 Erroneous surface elevation signal, H_{Max} = 40.07 m.

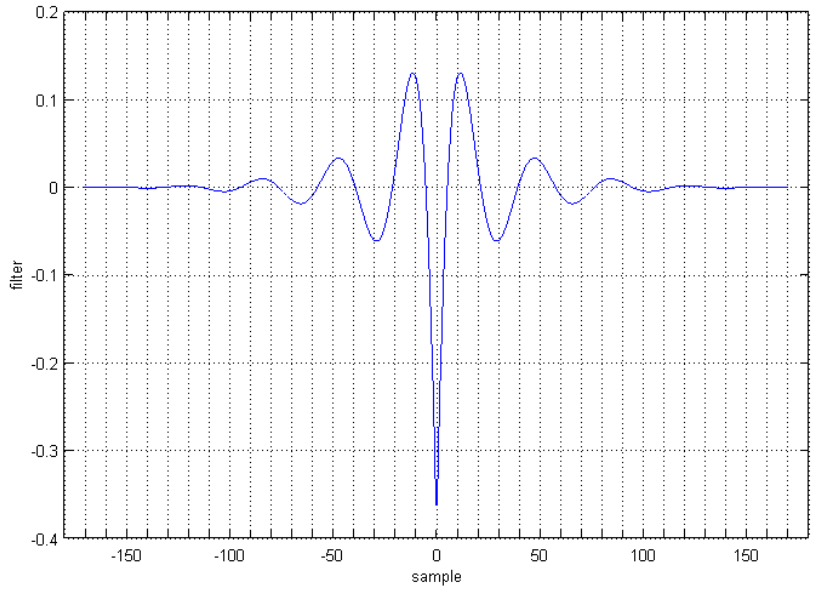

Fig. 7.4 Datawell waverider filter coefficients (Stoker 2012).

7.2.2 H_{Max}/H_{m0} Ratios

A straightforward method to estimate the highest individual wave from a sea-state (H_{Max}) when only summary statistics or spectral data are available is to assume a constant relationship between H_{Max} and H_{m0} of the surrounding waves. This ratio is often referred

to as the Abnormality Index (AI), particularly in the study of freak or rogue waves which are commonly defined as events with AI values greater than 2 (Guedes Soares et al. 2003; Haver 2004a; Dysthe et al. 2008). Accounts which describe 'walls of water' and 'holes in the sea' have long been part of maritime lore, however these events were brought to the attention of the scientific community when a downward looked laser-based wave sensor on Statoil's Draupner E platform in the North Sea recorded a wave measuring 25.6 m, with a crest height of 18.5 m, in a sea with a 12 m significant wave height on January 1st, 1995 (Haver 2004b). This became known as The New Year wave and is illustrated in Fig. 7.5

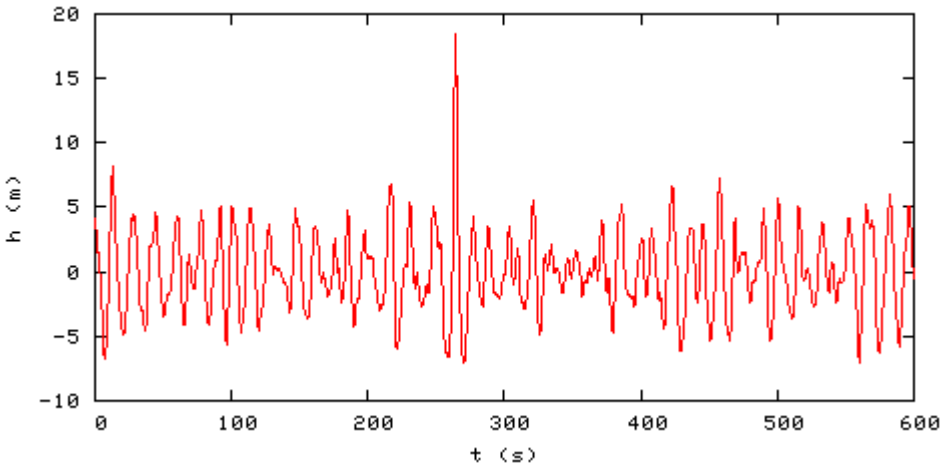

Fig. 7.5 The Draupner New Year's wave (Haver 2004b)

The operational definition of freak waves - $H_{Max}/H_{m0} > 2$ - is derived from the application of the Rayleigh distribution for wave heights in a record. Manipulating the Rayleigh distribution allows for the most probable H_{Max} from a record with N_z waves to be given by equation (7.1).

$$H_{Max} \approx K H_{m0} \sqrt{\frac{\ln N_z}{2}} \tag{7.1}$$

K is an empirical constant and has a value of 1 for a narrow spectrum. This relationship predicts that $H_{Max}/H_{m0} > 2$ could be expected approximately once every 3000 waves. Thus freak waves should not be considered to be unrealistic events. Rather, according to Haver and Andersen (2000), they should be thought of as "rare realizations of a typical population" or "typical realizations of a rare population". Some authors have proposed

that study of freak waves should be extended beyond linear theory and that a Tayfun distribution should be considered to account for waves having sharper crests than troughs (Müller et al. 2005).

In order to characterise the possible occurrence of freak waves at AMETS measurements from the Waverider buoy taken in 2011 — 77% data recovery — were analysed and the AI values plotted against H_{m0}. Exactly 300 measured sea-states, corresponding to approximately 2% of the records retrieved from the buoy, display AI values greater than 2. This approximates to one rogue event among every 11,000 waves, a noticeably infrequent rate of occurrence when compared to the 1 in 3000 waves probability predicted by theory. It is also notable that no sea-states where H_{m0} > 8m display AI values greater than 2, though it is likely that this is due to the relatively small population size and not an indication that a reduced factor could be used to estimate the largest wave heights in these stormy sea-states.

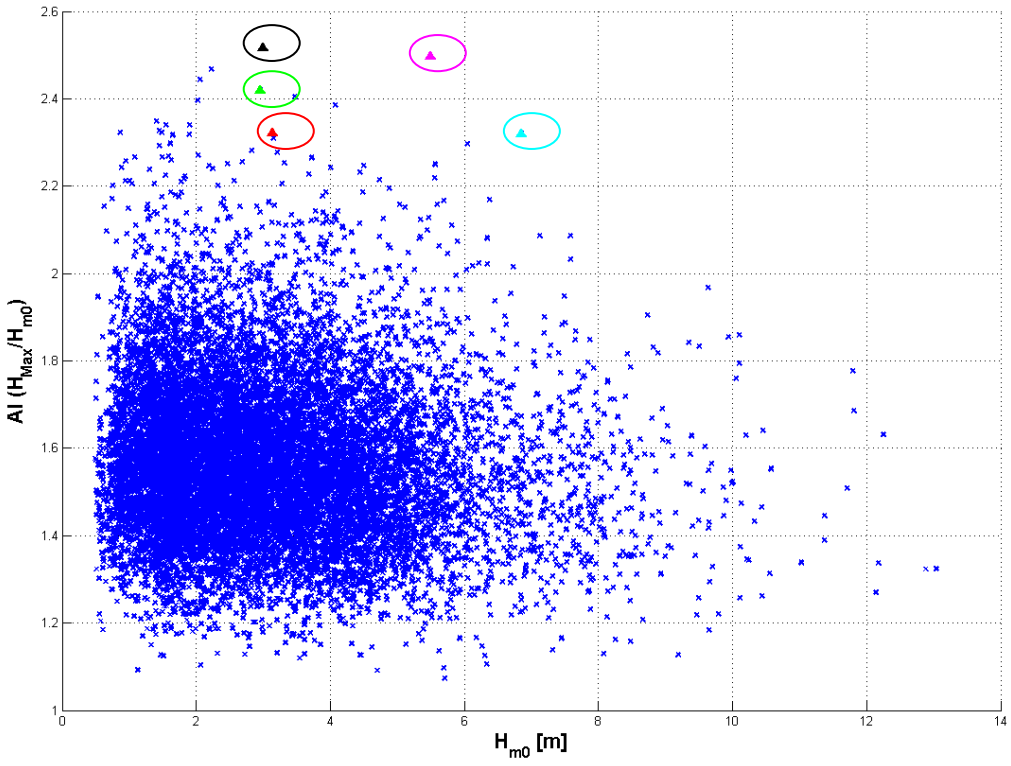

Figure 7.6 AI vs. H_{m0} for 2011 AMETS Waverider measurements. Selected records plotted in Fig. 7.7 marked by coloured triangles

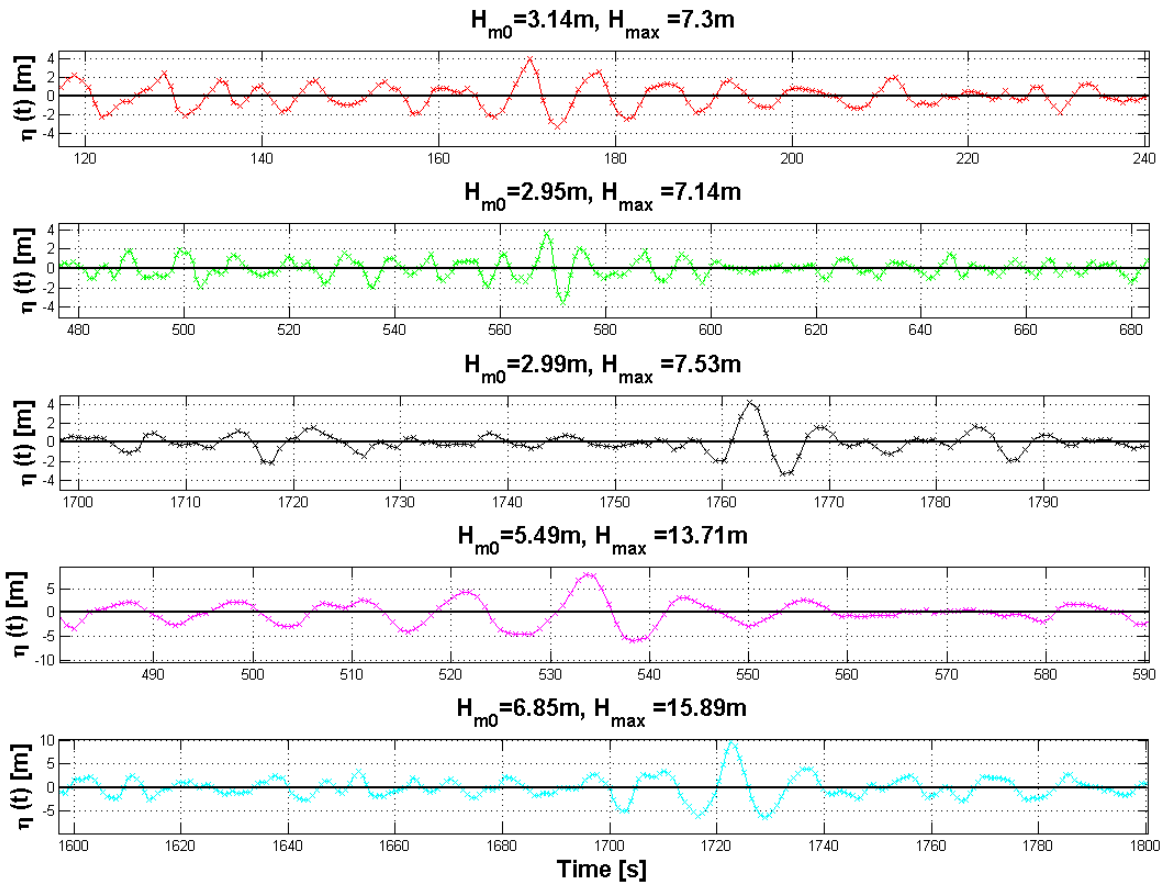

Figure 7.7 Selected surface elevation profiles from Fig.7.6.

A selection of time series which produced very high AI values, identified by the coloured triangles in Fig. 7.6, is illustrated in Fig. 7.7. This figure demonstrates that these measurements are reasonable surface profiles, rather than erroneous readings. The third profile — the record with the highest observed AI value — is particularly interesting, as it shows a 7.53 m wave that was preceded by several waves with heights of less than 2 m. Furthermore, no other wave in this 30 minute record exceeded a height of 5 m. Large waves that follow an extended quiescent period, such as the example illustrated above, have been identified as being extremely dangerous during offshore operations or marine recreation activities, as sailors or bystanders on the shore may be caught unawares having had their attention drawn away from the seemingly calm wave field (Gemmrich et al. 2009).

In the context of energy conversion, unexpected large waves that follow periods of relatively benign wave action may be significant. When faced with extreme sea-states, many WECs are designed to enter 'survival mode' in an attempt to evade the damaging structural impacts of waves of the type illustrated in Fig. 7.1. Conversely, an unexpectedly large wave that a device encounters while it is still operating may potentially prove more detrimental to components such as the power take-off and control system. To ensure device survivability prior to large scale deployment, the impacts of wave trains like this should be considered in the design phase, including physical modelling of the WEC concept in laboratory basins. An appropriate method for producing relatively large individual waves at small scale is to use focused wave groups (Tromans et al. 1991). These wave groups are composed of individual, linear, wave trains that arrive in phase at a location of interest in the wave tank at one point in time. It is possible to generate both crest-focused and trough-focused wave groups by shifting the phases of the various frequency components. Average crest and trough shapes during storm conditions has also been shown to provide a valuable representation of extreme waves (Taylor and Williams 2004).

Similar analysis was also carried out for measurements from the Wavescan buoy deployed at the 100m depth (Fig. 7.7). Unfortunately the time series of surface elevation produced by this buoy was corrupted; therefore zero-crossing analysis could not be carried out to individually indentify the wave heights. Instead, it was necessary to rely on the summary statistics of H_{m0} and H_{Max} that were transferred to shore while the instrument was deployed. The values of these parameters tend to be rounded to a number of repeating figures, hence the noticeable pattern and lack of spread in Fig. 7.7. Less than 1% of records were identified with $H_{Max}/H_{m0} > 2$. This is significantly lower than for the 50m site, possibly indicating that the Waverider buoy follows the profile of the wave crests more accurately than the larger, discus-shaped, Wavescan. A Wavescan buoy has recently been deployed at the M4 station location (Fig. 1.4); analysis of the time series that will be retrieved from this buoy would be useful for ascertaining the appropriateness of this type of instrument for measuring large waves.

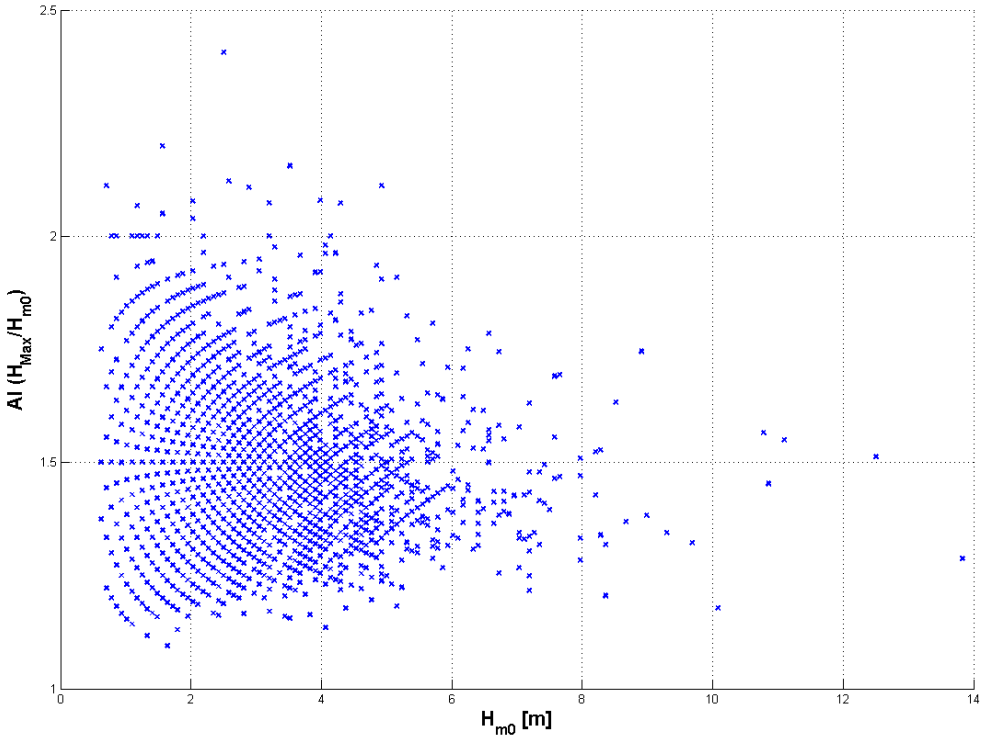

Figure 7.8 AI vs. H_{m0} for 2010 and 2011 AMETS Wavescan measurements.

7.3 Extreme Value Analysis of H_{m0} Design Values

7.3.1 Introduction

Wave Energy installations, like all ocean engineering developments, require trustworthy predictions of the most extreme sea states that are likely to be encountered over the lifespan of the project. Various methods of extreme value analysis (EVA) have been developed in response to this need in order to provide estimates of the conditions that offshore structures must be designed to withstand. These generally consist of fitting a statistical distribution to a set of measured or modelled parameters and extrapolating to long return periods – the average intervals between the occurrences of the design condition – to determine the required extremes. In this study the commonly used Peaks Over Threshold (POT) approach proposed by Goda (1988), and outlined as a step-by-step approach by Ward et al. (2003), is applied to extrapolate H_{m0} values from the available data from AMETS. These results can then be used in conjunction with the observations detailed in Section 7.2 to estimate the largest individual wave height that could

potentially be encountered at the site. Similar studies for the test site have been carried out previously but have been limited to single locations and water depths (Curé 2011a; Murphy 2011). The POT method is described in detail in Section 7.3.2., with the results of the analysis applied to the AMETS wave model data presented in Section 7.3.3. This method could also be used to determine the design conditions for other meteorological processes in the marine environment, such as currents and wind speeds, though for the case of AMETS the necessary data is not available from the hindcast model. It is not advisable to use the EVA approach to determine the wave period associated with the design values of H_{m0}; joint probabilities of height and period should be utilised if a full sea state description is necessary (EquiMar Group 2011).

The appropriateness of alternatives to the POT method were also assessed for use in this study, but ultimately discounted. An extension of the POT approach is the annual maxima method. This involves fitting an empirical distribution to the only highest recorded value of H_{m0} from each year of available data. It is recommended, however, that this approach is only followed when long duration datasets are available. The EquiMar standards suggests several decades worth of records are required (EquiMar Group 2011) while Ward et al. (2003) propose at least 20 years, so it was not suitable for the case of AMETS and the 16 year SWAN model. It is also possible to fit distributions to the entire population of data that is available, known as the Initial Distribution Approach. This method was used frequently prior to the POT method gaining widespread acceptance and is described in many textbooks (Ochi 1998; Tucker and Pitt 2001; Holthuijsen 2007). Anderson et al. and van Os et al. both set out strong arguments against the use of the Initial Distribution Approach, however, as it violates the assumptions of independence and stationarity that are integral to the statistical methods that EVA is predicated on (Anderson et al. 2001; van Os et al. 2011).

Selecting an appropriate dataset from which design conditions with long return period can be derived requires careful consideration. The Equimar Protocols suggest that the wave data being used should have a duration that is at least $1/5^{th}$ of the desired return period. In-situ measurement campaigns, while accurate, tend to be of short duration

(EquiMar Group 2011). They are therefore unsuitable for providing sufficient data to allow for accurate extrapolations of design parameters over the time scales relevant to commercial WEC deployments, which would be expected to operate for up to 25 years and would require even longer return periods for risk assessment and insurance purposes. In contrast, numerical hindcast models can produce long term outputs, though they may be afflicted by bias, particularly if compromises such as reduced grid size and simplifications to the background coastal processes are required to reduce computational time. A particularly useful data resource is the global ERA-40 model, a re-analysis of meteorological observations from September 1957 to August 2002 produced by the European Centre for Medium-Range Weather Forecasts (ECMWF) which includes a 1.5◦-resolution ocean wave model (Uppala et al. 2005). Based on the recommendations in the EquiMar guidelines (2011) the 16 year AMETS model allows for the extrapolation of the 80 year return value of parameters such as H_{m0}. Satellite altimeter or synthetic aperture radar (SAR) measurements provide a possible complement to point recordings and numerical models as they combine the relative accuracy of instruments with long historical archives of data. The primary disadvantage associated with these datasets, however, is the possibility that some significant storm events can be overlooked due to the poor temporal sampling rate – up to several days depending on the satellite – and the sensor can perform poorly close to the coast where many ocean energy developments will be sited (GlobWave Project 2012).

7.3.2 Peaks Over Threshold Method of Extreme Value Analysis

The POT method involves fitting an empirical distribution to selected storm values of H_{m0} which exceed a user defined threshold, H_o, to calculate the return values. This study follows the approach taken by Goda and Ward et al. and applies the Weibull and Fisher-Tippett Type I (FT-I) functions as the extremal distribution (Goda 1988; Ward et al. 2003). The generalised Pareto distribution (GPD) is another formulation that is commonly employed but it was not considered for this work as it is more cumbersome to implement than the Weibull and FT-I. Van Os et al. (2011) advise that at least 10 peaks should be returned when choosing an appropriate threshold, with an upper bound limit of at most 10 values per year of data. The average number of storms identified per year is

referred to as the mean rate, and denoted by λ. It is also necessary to ensure that the selected peaks are statistically independent and are not products of the same storm system.

If x is one of the N_T selected storms that exceeds H_o then F(x), the probability of nonexceedence of x, is given by Equation (7.2) for the FT-I function — also known as the Gumbel distribution — and by Equation (7.3) for the Weibull distribution. The k term in Equation (7.2) is known as the shape parameter and is given values of 0.75, 1.0, 1.4 and 2.0, as suggested by Goda (1988).

FT-I $$F(x) = \exp\{-\exp[\frac{-(x-B)}{A}]\} \tag{7.2}$$

Weibull $$F(x) = 1 - \exp\left[\frac{-(x-B)}{A}\right]^{k} \tag{7.3}$$

The selected storms are rearranged in descending order, so the m^{th} largest storm is x_m. The plotting function for the FT-I and Weibull functions are given by Equation (7.4) and Equation (7.5) respectively

FT-I $$F_m = 1 - \frac{m - 0.44}{N_T + 0.12} \tag{7.4}$$

Weibull $$F_m = 1 - \frac{m - \alpha}{N_T + \beta} \tag{7.5}$$

The terms α and β in Equation (7.5) are determined from

$$\alpha = 0.20 + 0.27/\sqrt{k}$$
$$\beta = 0.20 + 0.23/\sqrt{k} \tag{7.6}$$

Once the nonexceedence probability is calculated for each of the storm data points their respective reduced variates, y_m, are determined using Equation (7.7) for the FT-1 distribution and Equation (7.8) for the Weibull distribution.

FT-I $$y_m = -\ln[-\ln F_m] \quad (7.7)$$

Weibull $$y_m = [-\ln(1 - F_m)]^{1/k} \quad (7.8)$$

The set of storm values for which $H_{m0} > H_o$ are then linearly related to y_m so that

$$x_m = \hat{A}\mathrm{y_m} + \hat{\mathrm{B}} \quad (7.9)$$

$$x_R = \hat{A}y_R + \hat{B} \quad (7.10)$$

where $\hat{A}$ and $\hat{B}$ are solved using the least squares method and are the estimates of the scale and location parameters in Equation (7.10). It is then possible to calculate the expected H_{m0} for the return period R, denoted as x_R, once y_R is determined from either Equation (7.11) for the FT-I distribution or Equation (7.12) for the Weibull.

FT-1 $$y_R = -\ln\{-\ln[1 - 1/(\lambda R)]\} \quad (7.11)$$

Weibull $$y_R = [\ln(\lambda R)]^{1/k} \quad (7.12)$$

7.3.3 POT Analysis of AMETS Model Data

A POT analysis of the AMETS test area was carried out using an automated process which implemented the approach outlined in Section 7.3.2 to the outputs of the SWAN model described in Chapter 3. Fifteen points at depths ranging from 10 m -150 m, illustrated in Fig. 3.16, were included. A variety of thresholds, H_o, were applied to each set of data. These H_o values were selected to ensure that a reasonable number of peaks (N_T) were returned, following the recommendations of van Os et al. (2011). A 36 hour separation of peak events which exceeded H_o was introduced to ensure the values are statistically independent. This is illustrated in Fig. 7.10 for the case of the 50 m station with H_o = 8.5 m. H_{m0} values which exceed the threshold are marked in green, but only points with the sufficient temporal separation of 36 hours, marked in red, were carried forward for analysis. The number of peaks returned for a range of thresholds is shown in Fig. 7.11, with N_T decreasing as H_o is increased.

The selected peaks for each H_o value were ranked by height in descending order (x_m) and fitted to the five plotting functions – FT-I and Weibull with k values of 0.75, 1.0, 1.4 and 2.0 – given by Equation (7.4) and Equation (7.5). Calculating the reduced variates, y_m, from Equation (7.7) and Equation (7.8) and plotting them against x_m allows the scale ($\hat{A}$) and location ($\hat{B}$) parameters to be calculated for Equation (7.10) using a least squares best fit line, as illustrated in Fig. 7.12. The R^2 values computed at this stage were then used as the selection criteria for choosing the most suitable combination of threshold and extremal distribution to represent the outputs of H_{m0} from each of the station points in the SWAN model, though the results were also visually assessed to ensure that the fit was sensible in order to verify their validity.

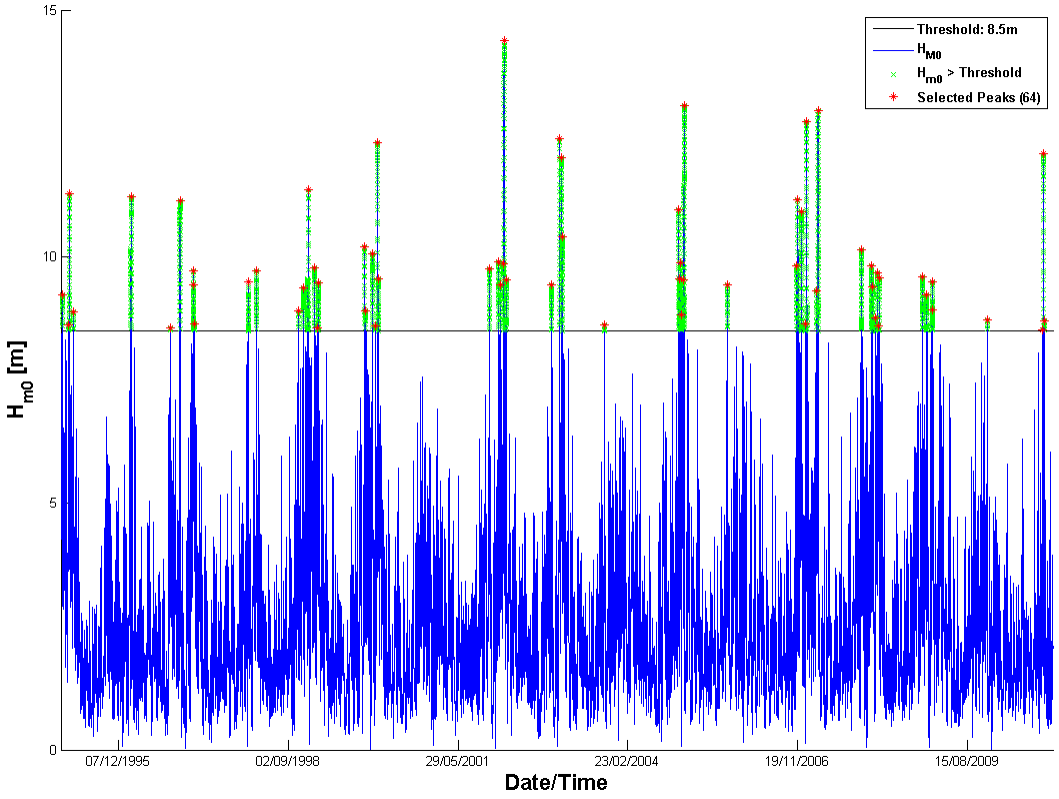

Figure 7.10: Selected peaks greater than the 8.5 m threshold for the 50m station in the AMETS SWAN model.

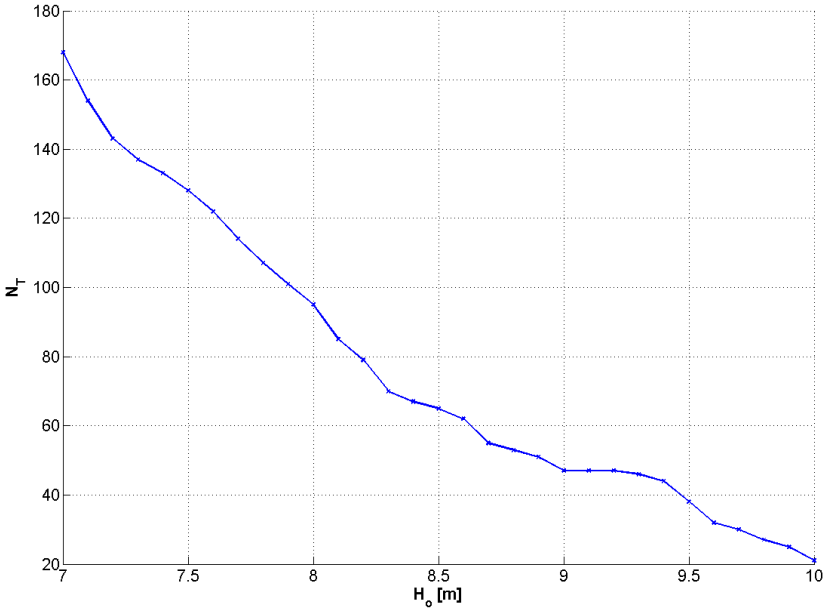

Figure 7.11: Number of peaks (N_T) returned for each threshold value (H_o) for the 50m station in the AMETS SWAN model.

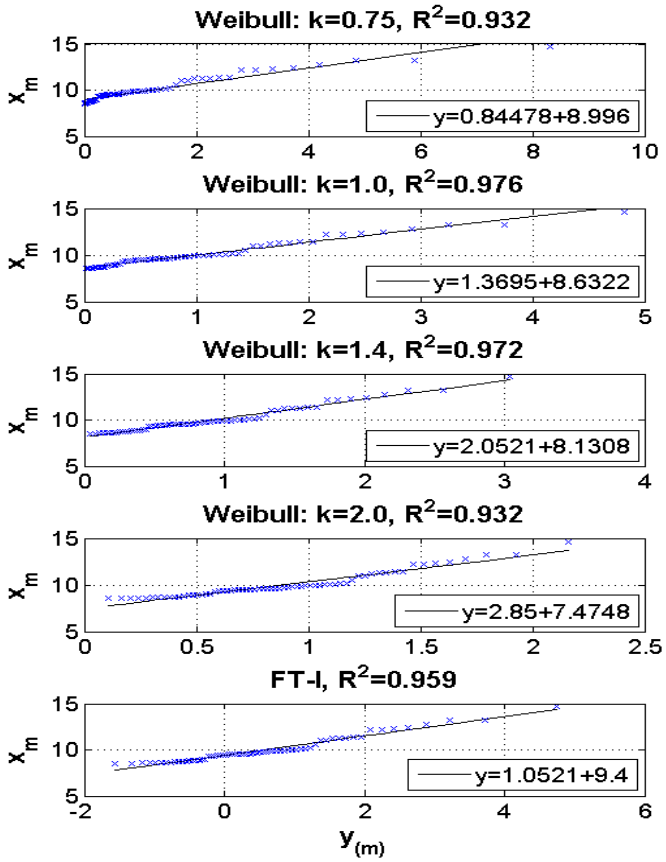

Figure 7.12: x_m plotted against y_m for H_o = 8.5 m for the 50m station in the AMETS SWAN model.

Extrapolated design values of H_{m0}, given by x_R, for return periods of up to 80 years are plotted in Fig. 7.13 for the range of thresholds that were deemed to be reasonable for the data from the 50 m station. The level of uncertainty associated with this method is evident from the spread of curves produced by the different thresholds. Significant differences in the extrapolated values of H_{m0} derived from the fitted Weibull and FT-I distributions can be seen, particularly for the longer return periods. For this case the analysis was carried out to produce a general understanding of the extreme conditions at AMETS, and exposed sites on the Irish west coast in general. More detailed design studies could include confidence intervals in the results to quantify the underlying uncertainties.

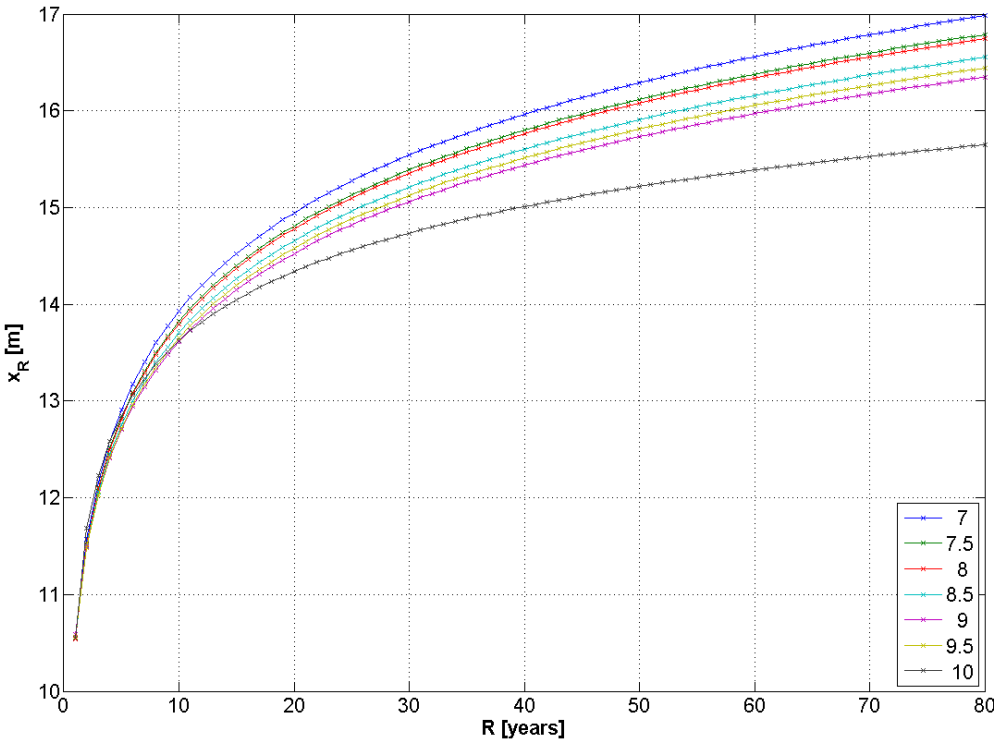

Figure 7.13: Return values of x_R for H_o = 7 m – 10 m for the 50m station in the AMETS SWAN model.

The $\hat{A}$ and $\hat{B}$ pairs which produced the highest R^2 values — see Fig 7.12 — were chosen to represent the extremal distribution for each of the 15 stations which were analysed. A set of x_R values was computed for each water depth from Equation (7.10) and the results presented in Fig. 7.14 for selected return periods of up to 80 years. It is likely that H_{m0} values in excess of 15 m will be experienced at offshore sites in water depths of greater

than 40 m over the potential 25 year lifetime of a WEC deployment. This value was surpassed only once in the 16 years of outputs from the SWAN model, at the station location at the 150 m depth contour. Over longer return periods, sea states approaching 17 m are possible.

A surprising aspect of these results is that the H_{m0} values extrapolated for the longest return period are highest at the station at 40 m rather than the sites at the greatest water depths. This result seems counterintuitive, however when the averages of the highest values of H_{m0} returned by the model at each depth are plotted in Fig. 7.15 it can be seen that extreme wave conditions experienced at this point exceed those further offshore. This result may simply be a manifestation of discrepancies in the model, though the possibility that this location is a hot-spot, where wave heights are amplified due to shallow water processes during the severe storms that are selected during the POT analysis should be investigated further through in-situ measurements at this location.

The design values of H_{m0} for the locations in water depths 10 m – 30 m are significantly lower than those at the points further offshore. A decrease in wave height is to be expected in the near shore environment, however the considerable reduction illustrated in Fig. 7.14 and Fig. 7.15 can probably be explained by the shelter these locations are afforded from Annagh Head to the north and Inishglora Island to the southwest. As a result these return values are not representative of other sites along the Irish west coast that are similarly close to the shore but that are fully exposed to the Atlantic storms.

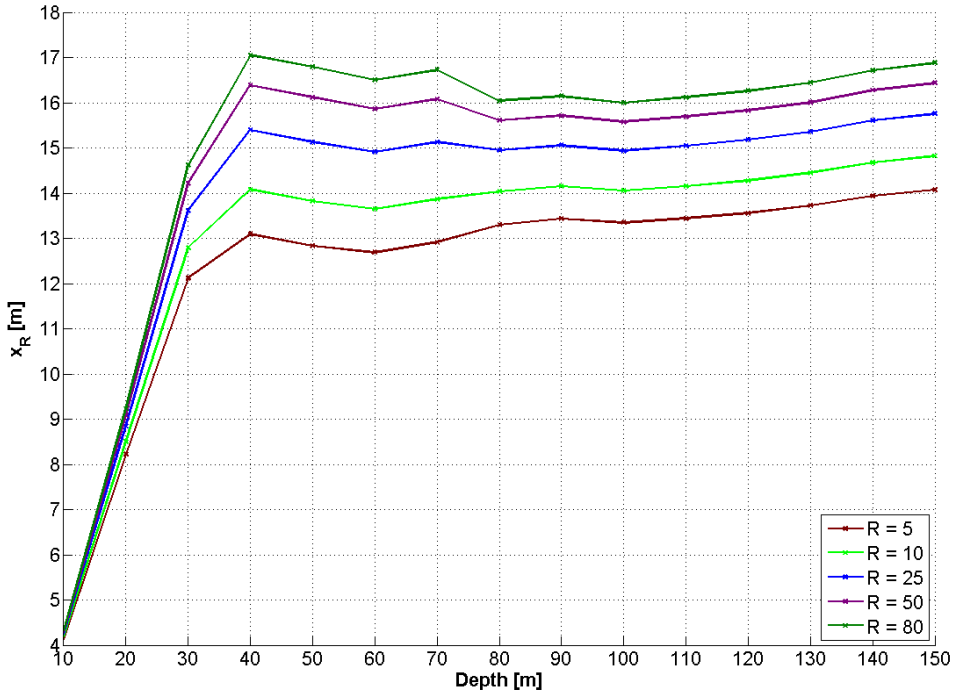

Figure 7.14: Design values of H_{m0} (x_R) at each station in the AMETS SWAN model for a range of Return Periods (R).

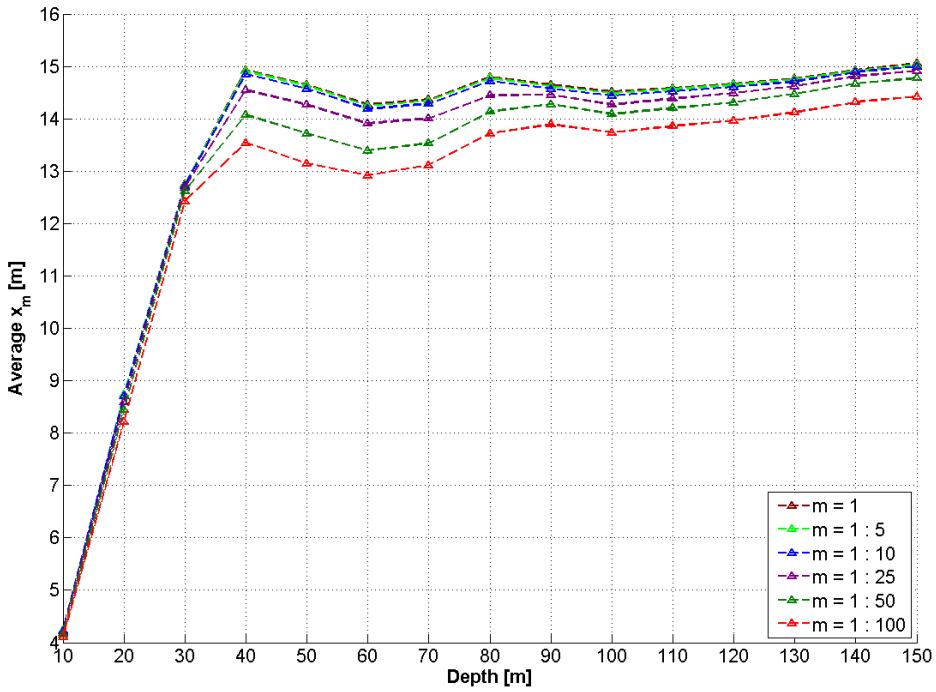

Figure 7.15: Average of the m highest values of H_{m0} returned for each station in the AMETS SWAN model.

7.3 Discussion

The research outlined in this chapter has utilised measured and modelled wave data from AMETS to investigate the extreme wave conditions at the site, which, with the exception of the nearshore points, could be considered typical of those experienced at exposed ocean locations on the Irish west coast. The experience of processing and analysing the measured data from the site has also allowed for the development of both quantitative and qualitative approaches for verifying the validity of buoy records of extreme wave height. Extreme individual waves with heights of up to 24 m have been observed at the test site, though it is likely that even larger waves also occur but go unrecorded. Rogue waves, which a device may encounter during its normal operational conditions, were observed to occur less frequently at AMETS than suggested by theory but are another risk that should be accounted for in the design of a WEC.

The POT analysis applied to the outputs from the 16 year AMETS SWAN model identified that sea states with H_{m0} values of approximately 15 m should be expected over the duration of floating WEC deployments in water depth of 40 m and greater. For the longest return period included in the analysis, 80 years, the return values approach 17 m at a number of locations. These extrapolated conditions could also be typical of many exposed sites on the west coast of Ireland. The results come with a caveat however; there is a level of uncertainty associated with long term extrapolations of design conditions, particularly from hindcast model data which themselves may contain bias. Furthermore, it would be unwise to attempt to extrapolate design conditions for longer return periods, such as 1000 years, due the relatively short time frame covered by the model.

There are insufficient measured data to predict accurately what is the most suitable H_{Max}/H_{m0} ratio for the most extreme sea-states at AMETS. Liu and Burcharth (1998) present a formula based on the Rayleigh distribution — Equation (7.13) which also allows the encounter probability of encountering specified individual wave heights over a period of time to be computed.

$$(H_{Max})_{mean} \approx (\frac{lnN}{2} + \frac{0.577}{\sqrt{8lnN}})H_{m0}^{R\ years} \quad (7.13)$$

Assuming $H_{Max} = 2H_{m0}$ is a reasonably conservative estimate and indicates that individual wave heights in excess of 30 m are probable over the life span of a commercial wave energy installation at the site. Furthermore, according to Prevosto et al. (2012) it should not be necessary to consider individual waves with $H_{Max} > 2H_{m0}$ as second-order wave theories are sufficient for the levels of reliability required for ocean energy installations.

Additional research is required to understand why the extremes computed for the station at the 40 m water depth were significantly larger than most of those returned at the points located in deeper water. It is possible that this is merely an inherent idiosyncrasy in the model, rather than a realistic physical process. This should be assessed further using in-situ measurements, and it may also be worth extending the buoy network at AMETS to determine the level of spatial variability that exists in the wave energy resource. There is also considerable potential for further studies of extreme wave conditions in general and their implications for WEC deployments. Increasingly large archives of observed rogue waves are being compiled (Nikolkina and Didenkulova 2011; O'Brien and Dias 2012), with this work being a further example, which will allow for more detailed studies of these events to be conducted. Doubts still persist, however, about whether floating buoys are suitable for accurately measuring the heights of extremely large and steep waves due to the limitations imposed by their moorings and the corrections that are applied to their quasi-Lagrangian motion (Mettlach and Chung-Chu 2010). Additionally, the most hazardous conditions for WEC operation – whether storm induced sea states, individual wave events or particular combinations of metocean processes – must be determined from numerical models and small scale tank testing so that their likelihood of occurrence can be assessed during resource assessment and site selection studies. An appropriate guideline for carrying out this work is provided in the standards by by Det Norske Veritas (2010) which outline the environmental contour concept of defining extreme sea conditions and procedures for estimating the extreme response of offshore installations.

Chapter 8 Short Term and Spatial Variability of Wave Energy

8.1 Introduction

The operation of many WEC concepts is dependent on the incident wave frequency (Thomas 2008; Flocard and Finnigan 2010; Saulnier et al. 2011). As a result, power output may vary over short time scales depending on the composition of the passing wave trains, even while the overall sea state remains unchanged. Saulnier et al. discussed the sensitivity of certain types of WEC to spectral bandwidth and wave groupiness and demonstrated that capture width is increased for when incident spectra are narrow and the device is closely tuned to the dominant frequency of the surrounding wave field. Additionally, the quality of the power produced by WECs could be compromised if the fluctuations in the incident wave energy, and the resultant device output, are excessive. Blavette et al. (2011) highlighted flicker — which can even manifest itself to energy consumers as unsteadiness in the glow from light bulbs — as a possible consequence of poor power quality. Short term energy storage mechanisms have been proposed as possible measures to improve power quality (Murray et al. 2009), while it has also been demonstrated that aggregating the power from the individual devices in an array results in a smother overall output (Molinas et al. 2007; Tissandier et al. 2008; Nambiar et al. 2010).

This smoothing effect of device aggregation is predicated on the inherent spatial variability in the incident wave energy. WECs will be deployed in arrays at the same site, and share infrastructure such as cables, for practical and economic reasons once commercial installations are developed. It is possible that deterministic differences, for example due to bathymetry or currents, will lead to inhomogeneity in the levels of energy available to WECs across the extent of a farm. An accurate understanding of the spatial variability of the resource across a site of interest will greatly aid developers in choosing the most advantageous deployment locations for the capture of energy and in monitoring the performance of their devices once in operation. Unfortunately wave measurement instruments tend to be deployed in isolation and very few sets of concurrent and co-located observations exist. The dataset of concurrent measurements from the Galway Bay

test site presented in this chapter is a rare, if somewhat limited example, and is the unintended consequence of a protracted changeover from a non-directional buoy to a directional model.

Wave spectra derived from measured time series of sea surface elevation have been utilised throughout this research for calculating parameters and estimating the available energy resource. The wave spectrum is calculated by applying a Fourier transform to a measured time series of surface elevation, as described in Chapter 2. It was also noted that this approach has a limited capacity to monitor the temporal variability of both energy and peak frequency. This variability may impact on the power captured by WECs, most of which will only be able to achieve optimal performance over a narrow frequency bandwidth. Many devices will also incorporate control systems, whose design could be better informed by knowledge of the level of variability that can be expected over short time scales (Fusco 2012).

The wavelet transform was introduced in Section 2.6 as a potential tool for quantifying the temporal variability in wave signals and it was demonstrated that the benefit over using the wavelet transform over the Fourier transform is that it allows for precise localization in both the time and frequency domains. The wavelet transform is utilized in this chapter to investigate the short term resource variation at the wave energy test sites at AMETS and in Galway Bay. Data are provided by Datawell Waverider buoys that have been deployed at the sites, including a period of four months between April and July 2008 when both a directional and a non-directional buoy were both in-situ in Galway Bay in similar water depths at a spacing of 200 m. The following sections describe the wavelet analysis that was conducted to assess the temporal changes in wave energy, along with examples of the spatial variability observed in the concurrent measurements.

8.2 Application of Wavelet Analysis

Wavelet analysis is carried out for the measured time series of surface elevation following the approach outlined in Section 2.5. Each set of data was analysed using

Equation 2.13 to produce three dimensional wavelet spectra, with the computed wavelet coefficients, |WT|, dependent on time, t, and scale, b. It has been shown (Massel 2001) that a linear relationship exists between scale, b, and period of a regular wave, T, in the form:

$$b = \alpha T \tag{8.1}$$

where

$$\alpha = \frac{c + \sqrt{c^2 + 2}}{4\pi} \tag{8.2}$$

The term c is taken as 2π by Massel. Applying Equation (8.1) and evaluating the inverse of the period scale allows the wavelet transfer of a signal to be presented in the more familiar units of frequency and time.

A typical time series of measured buoy data is shown in Fig. 8.1, with the absolute values of the wavelet coefficients that form the resulting wavelet spectrum illustrated in Fig 8.2. The red areas in Fig. 8.2 are representative of a significant correlation between the localized portion of the signal and the mother wavelet and indicate a high energy density at that point in time. Whilst the traditional wave spectrum of such a signal would suggest a constant level of energy over the analyzed time series, examination of this wavelet spectrum makes it possible to discern pulses corresponding to individual, and groups of, high waves.

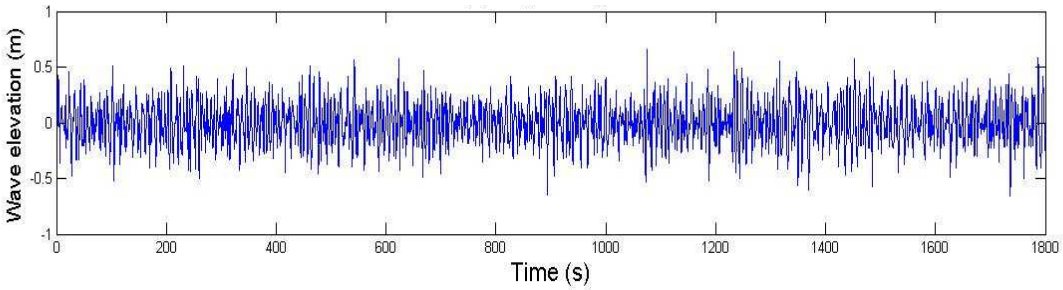

Figure 8.1: Measured surface elevation time series

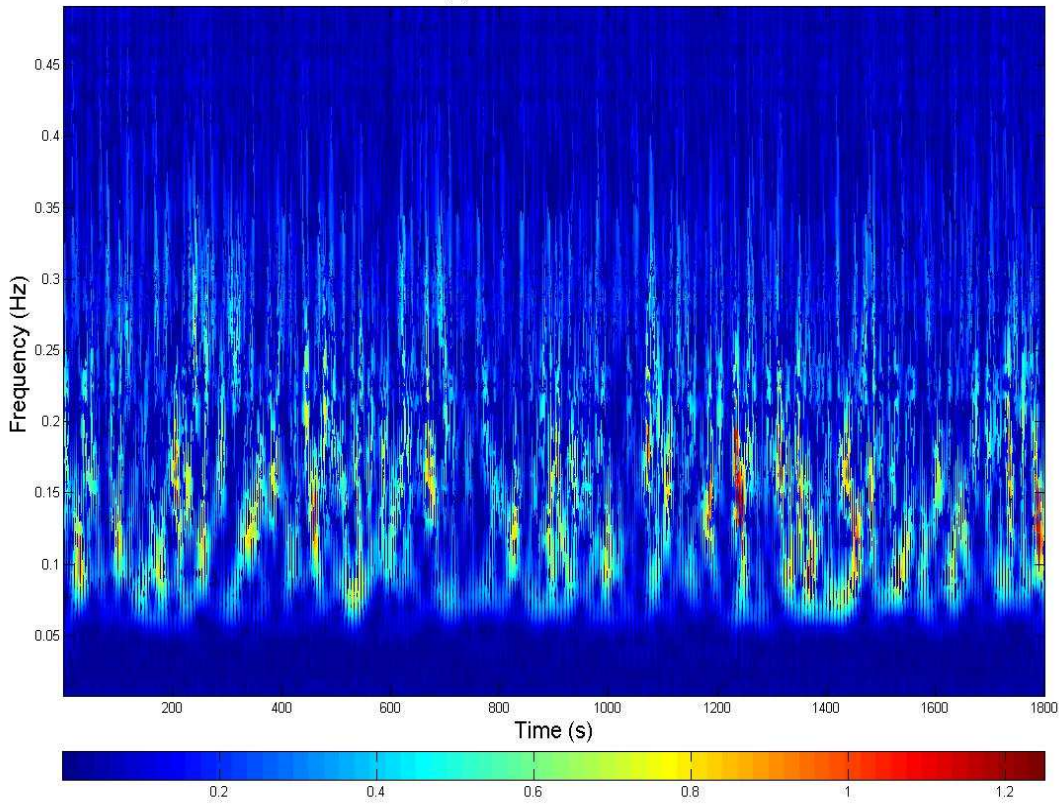

Figure 8.2: Wavelet spectrum computed from the sea surface profile in Fig. 8.1. Colour scale indicates the magnitude of the wavelet coefficients

The instantaneous peak frequency, x_i, at each time point can be easily identified from the wavelet spectrum illustrated in Fig. 3.2, and is plotted in Fig. 8.3. The weighted mean of instantaneous peak frequency is given by Equation (8.3) where w_i is the weight (|WT|) for the i^{th} observation of instantaneous peak frequency. N′ is the number of non-zero

weights while N is the total number of observations. This parameter has previously been proposed as a suitable sea state descriptor that can be derived from wavelet analysis (Nolan et al. 2007), and its inverse is of the same order of magnitude as the more commonly used wave period parameters. The weighting is included to reduce the influence of low energy components at high frequencies that are relatively inconsequential, and which would contribute little to the performance of devices. The computed value of μ_w is also included in Fig. 8.3.

$$\mu_w = \frac{\sum_{i=1}^{N} w_i x_i}{N'} \tag{8.3}$$

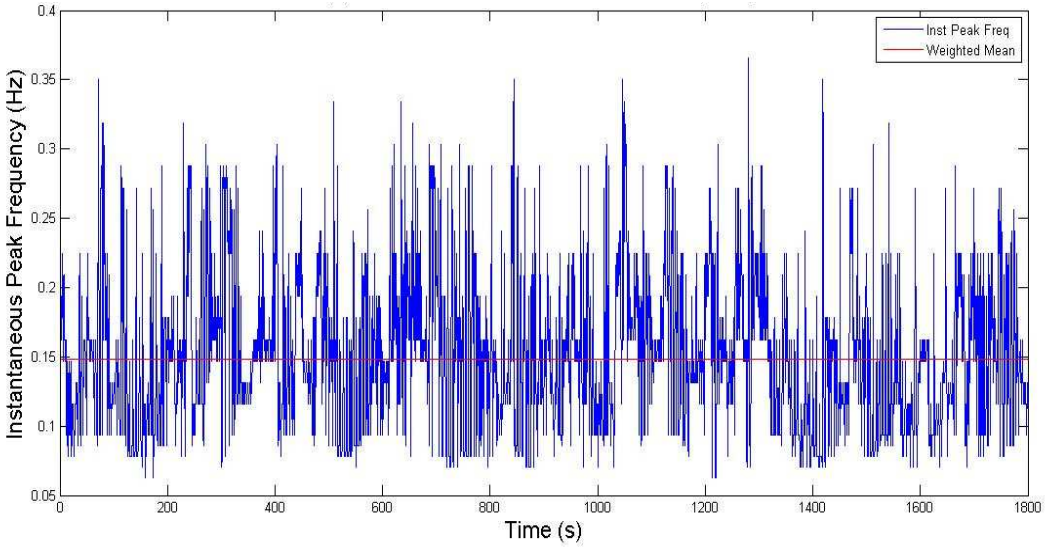

Figure 8.3: Instantaneous peak frequency across the time series from Fig. 8.1.

Nolan et al. also introduced the weighted standard deviation of instantaneous peak frequency, σ_w, as a measure of the temporal variability in the peak frequency within a signal. σ_w is calculated from the processed wavelet transform the using Equation (8.3). High values of σ_w are representative of records exhibiting a significant amount of short term variability while a while a low value is indicative of a more regular wave train which, in theory, should be conducive to efficient WEC performance.

$$\sigma_w = \sqrt{\frac{\sum_{i=1}^{N} w_i (x_i - \mu_i)^2}{\frac{(N' - 1)\sum_{i=1}^{N} w_i}{N'}}} \tag{8.4}$$

8.3 Wavelet Analysis of measured Data and Short Term Variability

Wavelet analysis was applied to one month of measured time series from AMETS (November 2010) and from Galway Bay (November 2008) using the previously outlined methods and the μ_w and σ_w parameters were computed. μ_w is compared to corresponding values of H_{m0} and T_E values for the AMETS data in Fig. 8.4, and for Galway Bay in Fig. 8.5. The fundamental nature of this parameter, and how it varies according to the prevailing sea state, is evident. μ_w is seen to behave similarly to T_E, particularly for the long period seas experienced at AMETS which tend to exhibit a narrow spectral bandwidth. The spread of μ_w is much greater in Galway Bay — between 0.08 – 0.25 Hz — whereas the range of values at AMETS is narrower and tend towards lower frequencies. This is indicative of the fact that sea states at AMETS, an exposed site, will generally feature far more dominant long period swell components in comparison to Galway Bay, which is semi enclosed and where similar contributions of swell and local wind seas are often present simultaneously. This is also reflected in the observation that values of μ_w are less well ordered, with a divergent spread of points, for shorter period sea states at both locations.

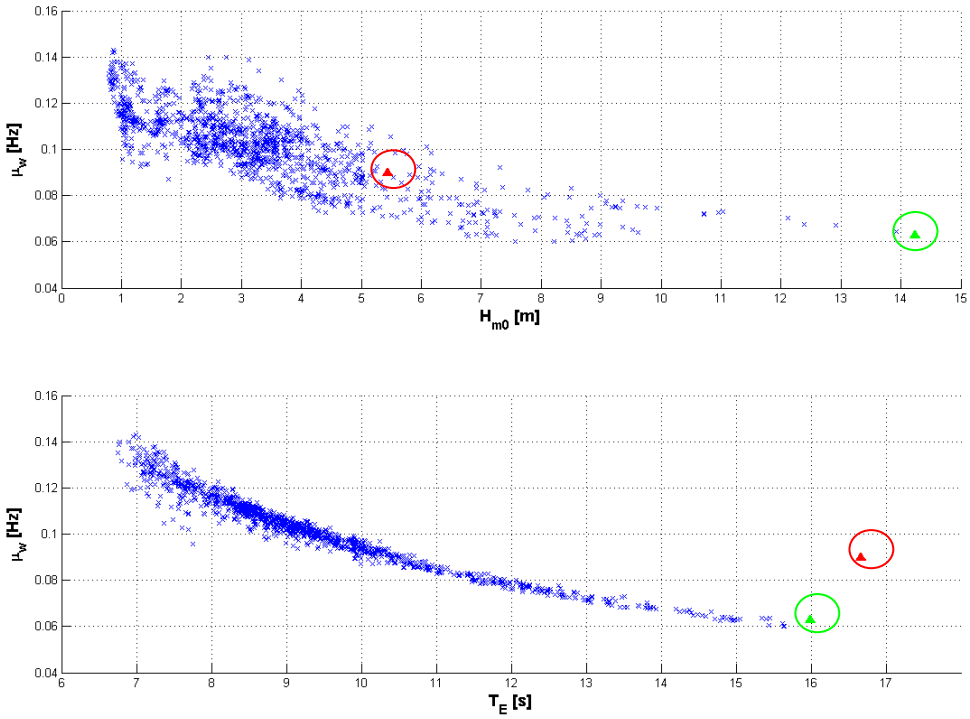

Figure 8.4: μ_w compared to corresponding H_{m0} (top) and T_E (bottom) values for AMETS measurements. Selected outliers indicated by red/green triangles.

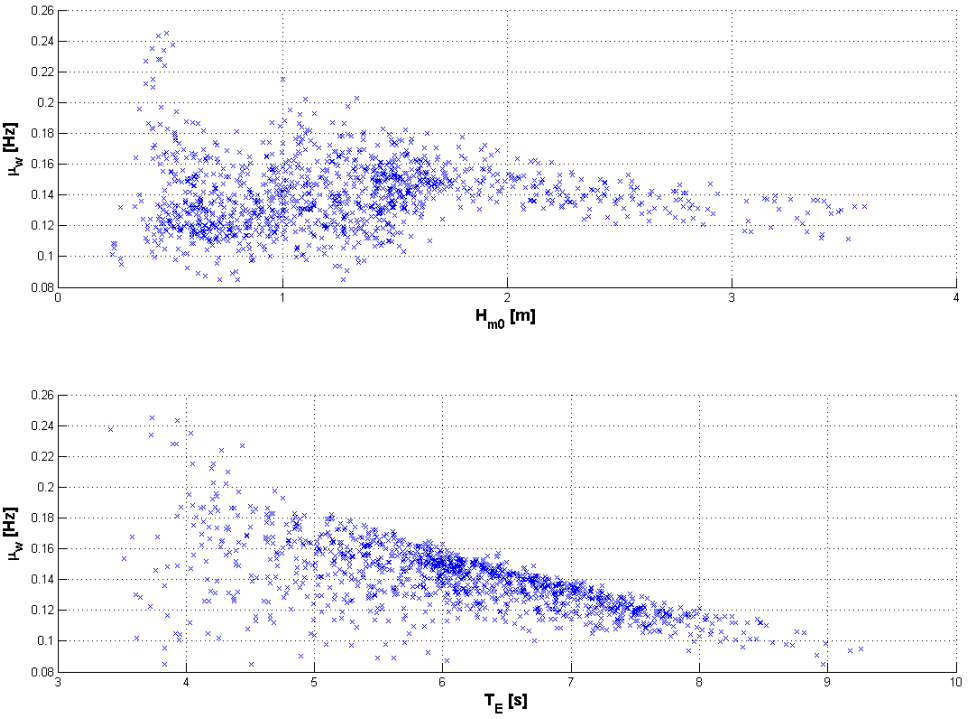

Figure 8.5: μ_w compared to corresponding H_{m0} (top) and T_E (bottom) values for Galway Bay measurements.

$\sigma_{w,}$ the measure of the short-term variability of the peak frequency within a time series of surface elevation, is similarly compared to H_{m0} and T_E in Fig. 8.6 and Fig. 8.7, for AMETS and Galway Bay respectively. Variability is reduced as H_{m0} and T_E increase at both locations. The supposition which explains the results presented in Fig. 8.4 and Fig. 8.5 is equally applicable in this case; higher energy, swell dominated, sea states will produce more regular and well-ordered wave trains and thus display a lower degree of short term variability. These results are encouraging in the context of WEC performance. Chapter 5 identified that sea states with $H_{m0} > 2$ m tend to account for most of the total annual energy at Irish west coast sites. Many developers follow design methodologies which result in theirs devices capturing energy with the greatest efficiency when the wave resource is high, thus in these conditions they should be able to operate without being overly encumbered by the difficulties presented by short term intermittency. The power capture by devices will already be reduced in low sea states, therefore the losses of performance associated with operating in highly variable conditions may be considered to be of less importance.

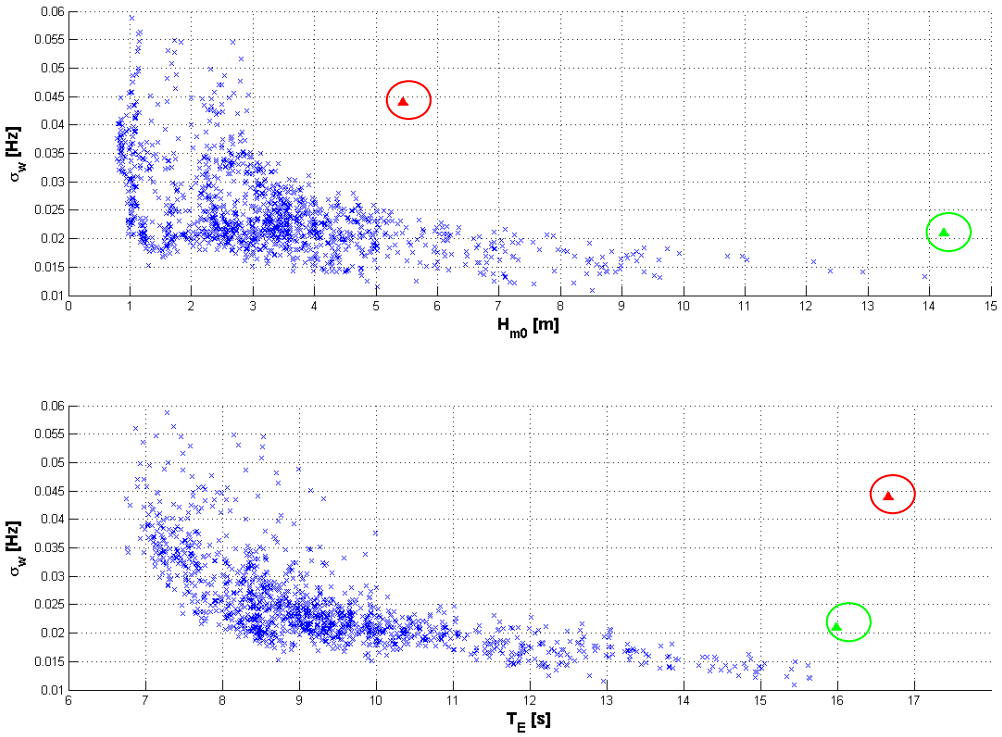

Figure 8.6: σ_w compared to corresponding H_{m0} (top) and T_E (bottom) values for AMETS measurements. Selected outliers indicated by red/green triangles.

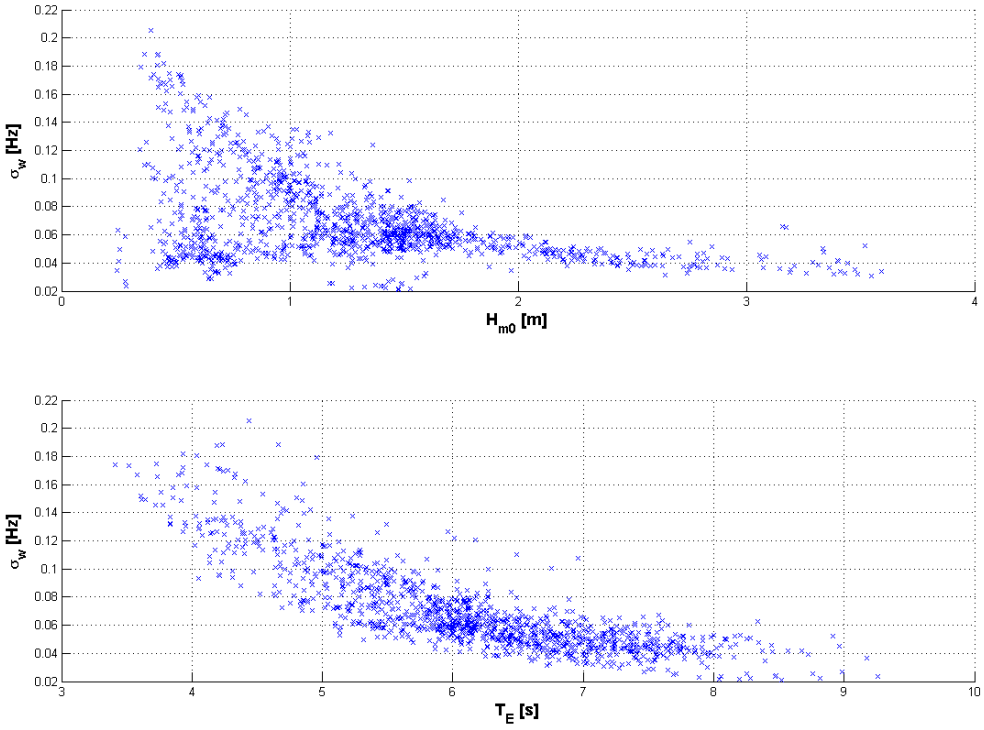

Figure 8.7: σ_w compared to corresponding H_{m0} (top) and T_E (bottom) values for Galway bay measurements.

Two outliers, highlighted as coloured triangles, have been included in Fig 8.4 and Fig 8.6. These are examples of buoy filter-contaminated time series, introduced in Section 7.2.1. These records would normally be removed during the quality control process outlined but have been included here as instructive cases. The time series and their resulting wavelet spectra are reproduced in Fig. 8.8 and Fig. 8.9. The manifest themselves very strongly in the wavelet spectrum in the form of intense pulses that are spread over an wider, and lower, band of frequencies than the surrounding waves. In contrast, when the wavelet analysis procedure is applied to the 23.87 m wave recorded at AMETS — see Section 7.2.1 for further details — it is seen to be reasonably well matched with the frequency of the preceding wave in the record (Fig 8.10). The weighted parameters computed from Equations (8.3-4) are similarly affected, resulting in the outlying discrepancies identified in Fig. 8.4 and Fig. 8.6. The strong signatures left by these erroneous signals suggest that wavelet analysis may potentially be an appropriate tool to augment the QC process if a more quantitative method of identifying these discrepancies could be developed.

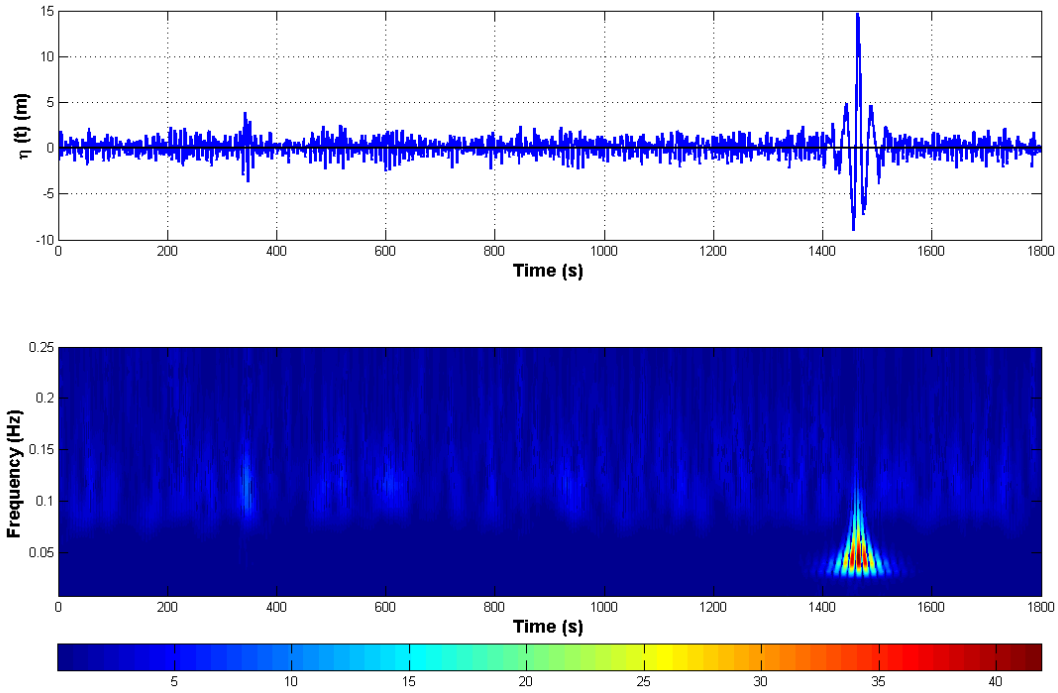

Figure 8.8: Surface elevation (top) and wavelet spectrum (bottom) of corrupted buoy measurement indicated by red triangles in Fig. 8.4 and Fig. 8.6. Colour scale indicates the magnitude of the wavelet coefficients

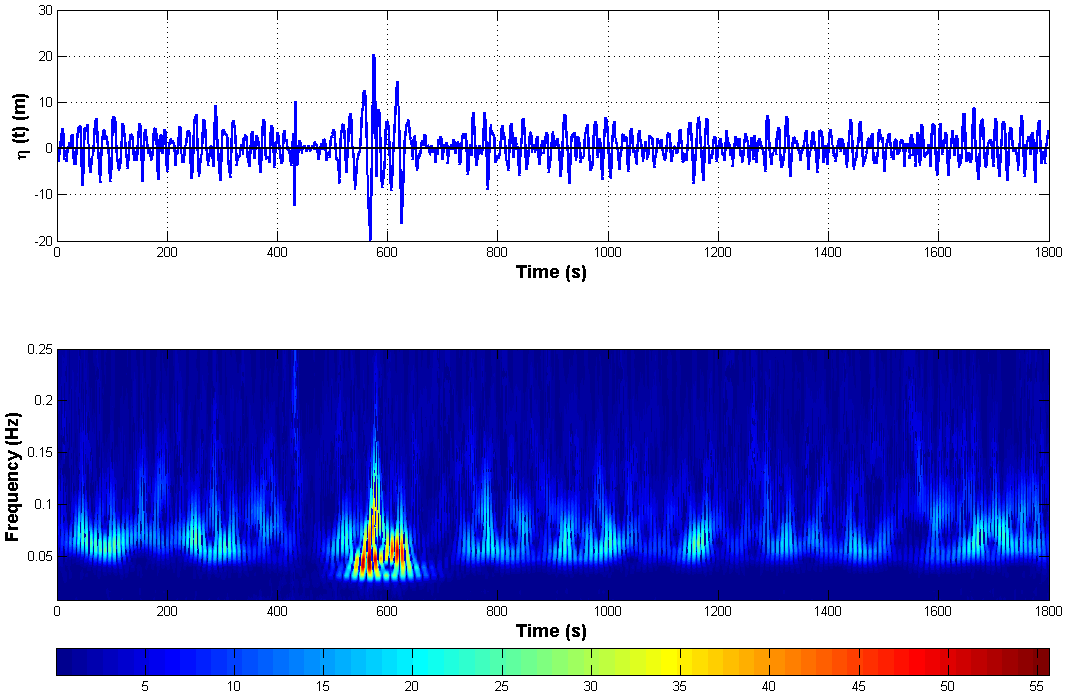

Figure 8.9: Surface elevation (top) and wavelet spectrum (bottom) of corrupted buoy measurement indicated by green triangles in Fig. 8.4 and Fig. 8.6. Colour scale indicates the magnitude of the wavelet coefficients

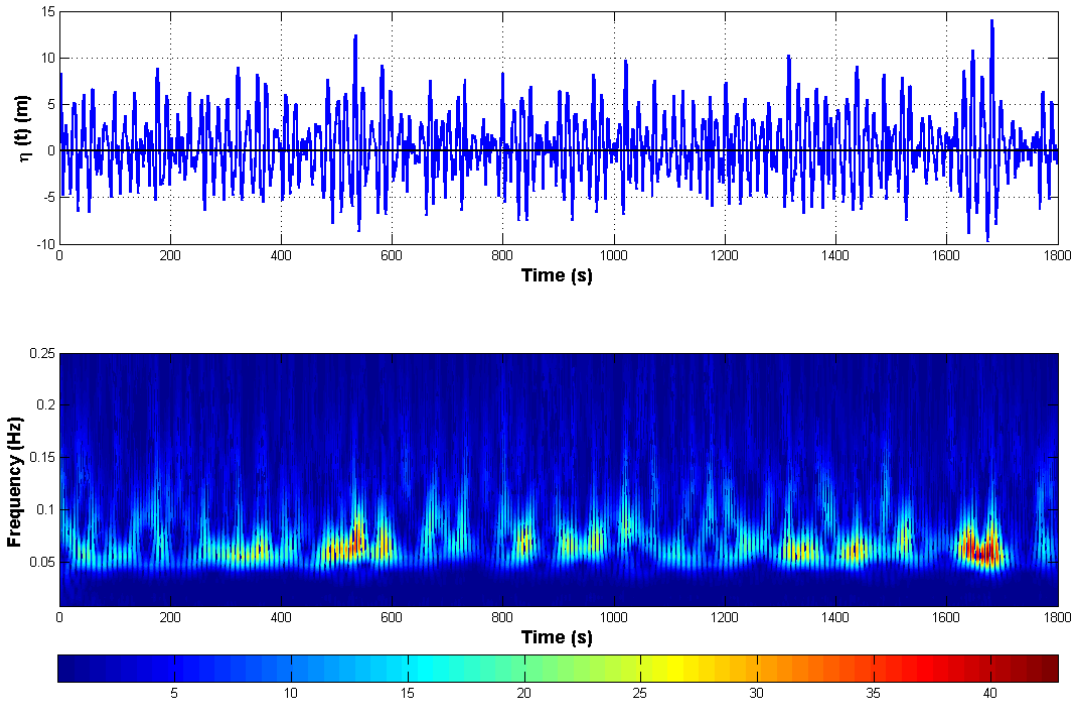

Figure 8.10: Surface elevation (top) and wavelet spectrum (bottom) of the largest wave measured at AMETS (H_{Max} = 23.87 m). Colour scale indicates the magnitude of the wavelet coefficients

8.4 Spatial Differences in Short Term Variability

As mentioned in the introduction to this chapter, the level of variability in the wave resource will impact on the overall performance and operation of array of WECs. As the number of measurement buoys that could be deployed alongside a wave farm will be limited by economic and practical constraints it is necessary to develop an understanding of how important summary statistics can vary due to spatial separation from limited datasets. Applying wavelet analysis to the concurrent wave records from Galway Bay allows the level of inconsistency in the short term variability at the site due to spatial differences to be identified. Unfortunately these data were collected sporadically, and do not cover the entire 4 month period of overlap when both buoys were in situ. In total, close to 1500 simultaneous 30 minute records of surface elevation, have been identified and are summarised in Table 8.1.

Research on this subject has been limited to date. The spatial variation of H_{m0} at the Galway Bay site has previously been studied and compared with concurrent measurements from the EMEC full scale test site in Orkney, Scotland (Barrett et al. 2009). At EMEC the separation distance between the measurement buoys was initially 1500 m but this was later changed to 500 m, providing two sets of unique data. It was found that variability decreased with increasing wave height, though the degree of deviation appeared to be unique to each specific location, indicating the possible presence of local deterministic influences at these sites. The array of four measurement buoys deployed at the Wave Hub test site, separated by 500 m, are a state of the art facility and analysis of their data are yielding further insights into the nature of the spatial variability in wave fields (Ashton 2011). Preliminary results have indicated that inhomogeneity across the extent of the buoy array influences the estimation of spectral and directional parameters (Saulnier et al. 2011) and that the presence of low frequency components within low energy wind seas are associated with increased variability (Ashton 2011). In this section the spatial deviations in the parameters which were computed previously to quantify the short-term resource variability are calculated and compared to the more frequently used sea state descriptors.

Month	Start Date	End Date	Measurements
April	24/4/2008	30/4/2008	306
May	1/5/2008	9/5/2008	300
June	25/6/2008	30/6/2008	225
July	1/7/2008	18/7/2008	643

Table 8.1: Summary of concurrent datasets from the Galway Bay test site

Scatter plots of concurrent recordings a number of sea state parameters are shown in Figs. 8.11 – 8.13. It is clear that the level of agreement between the buoys depends on the parameter being examined. The values of H_{m0} and T_E observed by the directional and non-directional buoys appear to be well matched, while T_P and μ_w appear to be poorly correlated. Some particularly noticeable outliers are present in Fig. 8.12 for the peak period values, such as concurrent measurements of $T_P \sim 10$ s and $T_P \sim 2$ s. Barrett (2010) identified low energy spectra with a wide spread of frequency components, and which display no obvious peak as the source of this divergence.

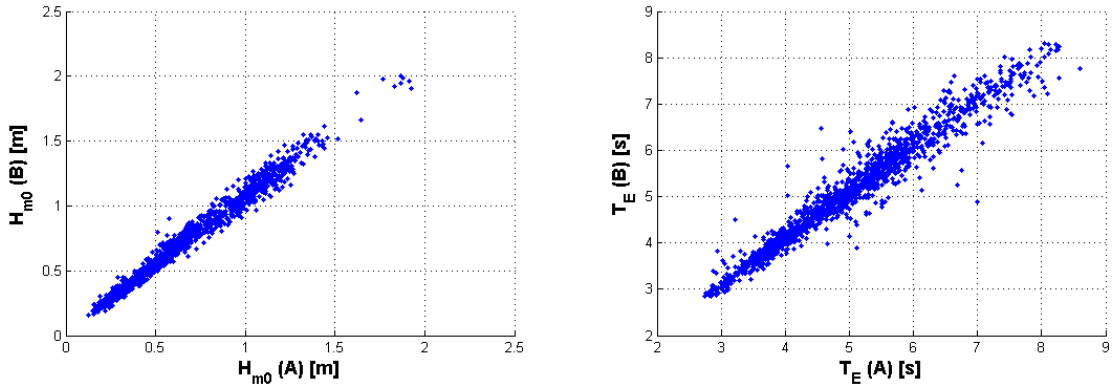

Figure 8.11: Concurrent recordings of H_{m0} and T_E from Galway Bay directional (A) and non-directional (B) buoys.

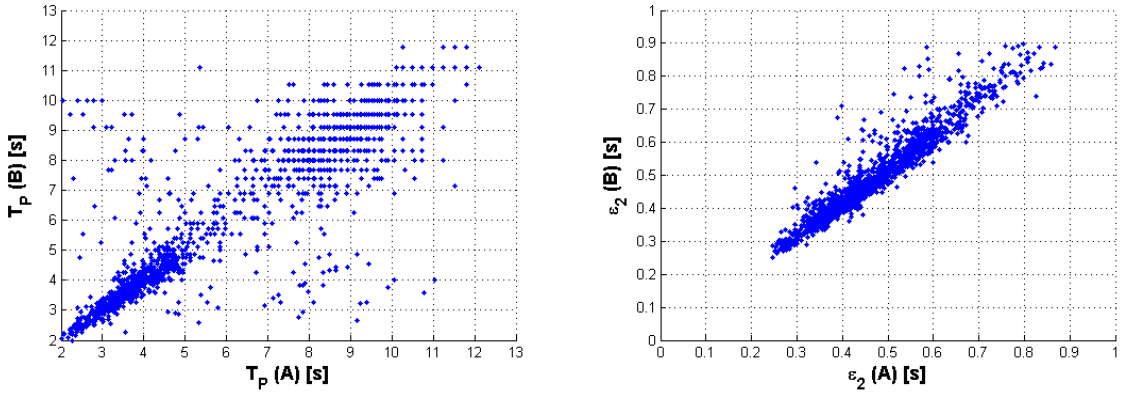

Figure 8.12: Concurrent recordings of T_P and ε_2 from Galway Bay directional (A) and non-directional (B) buoys.

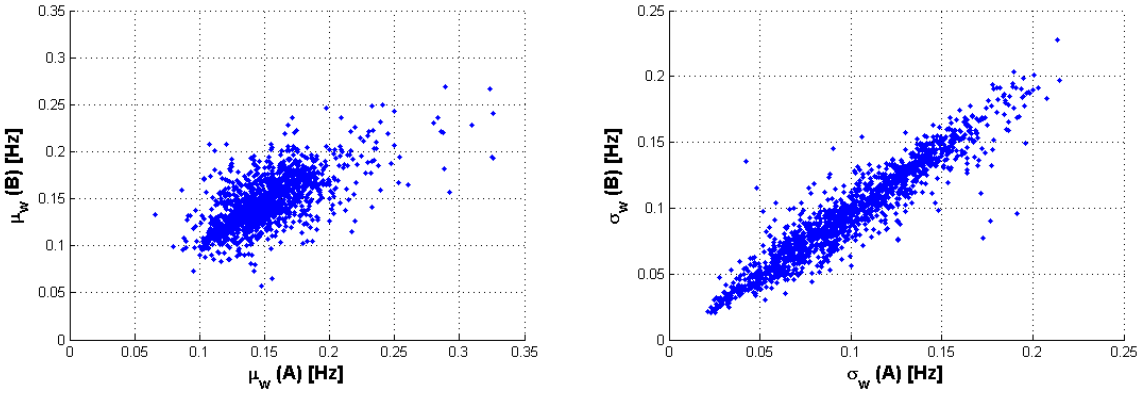

Figure 8.13: Concurrent recordings of μ_w and σ_w from Galway Bay directional (A) and non-directional (B) buoys.

Regression analysis was carried out on the concurrent data sets as a quantitative means to ascertain the variability between the sea state parameters. The correlation coefficients, R, for the concurrent series of parameters were calculated, and the results are compiled in Table 8.2. R is close to 1 for H_{m0} and T_E suggesting a good level of fit between the buoys and confirming a similar analysis carried out by Barrett. The value of R for the bandwidth parameter ε_2 is also high, which indicates similarity in spectral shape. Correlation is relatively poor for T_p. In Section 2.2.3 it was shown that the calculation of this parameter can be sensitive to the estimation method used and this may account for the discrepancies between the two buoys.

There also appears to be a high level of correlation between the values of σ_w determined from the wavelet analysis carried out on the recordings. This implies that the degree of temporal variability across the 200 m separation is relatively consistent, though it would not be sensible to extrapolate this result to more general cases due to the relatively close spacing between the buoys and the specific features of the site. There is poor agreement between the concurrent values of μ_w. This may be due to the predominantly wind generated seas in Galway Bay, resulting in wide-banded spectra and the presence of a wide range of frequency components of equivalent energy which makes the selection of the dominant peak difficult. It would be informative to carry out similar analysis of concurrent measurements at an open ocean site to examine whether this variability is reduced in longer period sea states.

	R
$\mathbf{H_{m0}}$	0.991
$\mathbf{T_E}$	0.974
$\mathbf{T_P}$	0.861
$\mathbf{T_{02}}$	0.929
$\boldsymbol{\varepsilon_2}$	0.952
$\boldsymbol{\mu_w}$	0.753
$\boldsymbol{\sigma_w}$	0.943

Table 8.2: Correlation coefficients (R) between wave parameters from the concurrent datasets at the Galway Bay test site

8.5 Discussion

In this chapter the wavelet transform has been applied to data measured at AMETS and the Galway Bay test site in order to better understand the short term variability of the incident wave resource. It has been presented as a useful tool for temporal analysis of records, and its potential application in quality control of measured wave data has also been identified. There are also limits to the practical use of wavelet analysis for wave energy resource characterisation. In particular it would be instructive if equivalents to commonly employed parameters such as H_{m0} and T_E could be derived from the wavelet transform so that they could be compared quantitatively with the outputs of spectral analysis.

The analysis results indicate that as H_{m0} and T_E increase the resulting time series of surface elevation tend to exhibit lower levels of variation in the dominant wave frequency over short time scales in comparison to more benign conditions. The more energetic sea states are shown to display low values of σ_w, indicating that the wave field is more ordered and regular. This suggests that the output of WECs will be enhanced in these sea states if they are closely tuned to the dominant wave frequencies and that control strategies will be easier to implement.

The correlation between the spatially separated values of the standard deviation of peak frequency, σ_w, was found to be of a similar order to other summary statistics such as H_{m0} and T_E. Further work using datasets from exposed sites, with greater separation distances, such as the Wave Hub buoy array, would be informative and yield additional insights into how this measure of temporal variability changes over greater spatial scales.

These results may be extremely site specific due to the fact that Galway Bay, a semi-enclosed, fetch limited location, presents a quite unique set of sea states. The results may also depend on the particular bathymetry and tidal conditions at the site. It would be therefore unwise to extrapolate more general conclusions from this research without first carrying out similar analysis of a wide range of sites. In addition due to the limited amount of concurrent data available, and the sporadic nature of the measurements that

were obtained, it has not been possible to investigate how this relationship behaves in higher energy, winter conditions. These caveats indicate the knowledge gap that exists in relation to the spatial variability of wave fields, a challenge that can only be addressed through the provision of more measurement buoy arrays similar to the existing arrangement at the Wave Hub site.

Chapter 9 Conclusions

The research has brought together previously unused sources of metocean data from the Irish west coast and applied advanced analysis methods to develop an enhanced understanding of the characteristics of the available wave energy resource. A series of key recommendations were made regarding the most appropriate methods for quantifying this resource, while ancillary issues which will influence device performance, such as extreme conditions and short term energy variability, were also identified and suitable methods for their analysis proposed. The wave energy industry is now reaching a stage of development where consideration is being given to selecting sites for the first commercial installations. An accurate and informed characterisation of the wave energy resource will form a vital part of this process. In this context, this thesis constitutes a valuable and relevant contribution to the field.

Calculation of Wave Power

This thesis challenged a number of assumptions that are frequently made in the calculation of wave energy, and demonstrated the uncertainties and inaccuracies caused by these assumptions. A new parameter, the wave period ratio (WPR), was defined and has been identified as the appropriate conversion factor for calculating wave power from limited datasets where the zero-crossing period, T_Z or T_{02}, is the only wave period parameter available. Additionally, it was shown that assuming deep water conditions results in a significant underestimation of the wave power at the depths many WECs are likely to be deployed in (40 m – 60 m) and that a level of inaccuracy is still present at a depth of 150 m at AMETS.

Existing industry standards have previously suggested that wave power should always be calculated using the full spectral form — including the depth dependent terms — unless spectra and time series data are unavailable (EMEC 2009; EquiMar Group 2010a; Folley et al. 2012). This thesis contributes to these ongoing standardisation efforts by providing

timely case studies that illustrate the importance of this guideline as a means of reducing the uncertainties involved in estimating the wave energy resource.

Characterisation of AMETS Wave Energy Resource

An enhanced understanding about the nature of the wave energy resource at AMETS is an important output of this thesis. While the wave climate at Belmullet was previously shown to be more energetic than other locations along the west coast (Mollison 1982), general conclusions can also be drawn from this work regarding the resource at other potential sites for WEC deployments in Ireland. It has highlighted that a disconnect exists between the most frequently occurring sea states at AMETS and the sea states that have the highest contribution to the annual incident energy. AMETS was also compared to three locations in the United States which experience different prevailing wave climates, and consequently displayed different relationships between occurrence and contribution. These results have obvious implications for the design of WECs and highlights the range of sea states that they will need to be tuned to in order to extract the maximum amount of energy from a particular site. The degree of interannual variability in the incident wave energy was shown to be significant, and relatively uniform, at the range of water depths analysed at AMETS. This variability is reduced, however, if the resource is assessed using metrics such as the exploitable power, P_{exp}, which acts as a filter to reduce the influence of highly energetic storms which are unlikely to contribute to the energy output of WECs.

This work has also highlighted the level of scalability that exists between the wave climates at AMETS and the quarter scale test site in Galway Bay. It was shown that in general there is excellent agreement between the sites and that any particular sea state experienced at AMETS is replicated at scale in Galway Bay. As a result developers who conduct a sufficiently long period of testing at the quarter scale site should gather the necessary performance data to progress to the final stages of testing. Additionally, it was demonstrated that the presence of long period swell produces sea states and spectra that are not suitable for following the same scaling procedures. This indicates that care should be taken when interpreting WEC performance data collected during these conditions.

This aspect of the research is an important contribution to the wider wave energy industry and has been utilised by the Sustainable Energy Authority of Ireland as a work of reference that is provided to device developers considering sea trials at the site (Cahill 2012).

Extreme Wave Conditions

This research applied a new combination of records of measured sea surface elevation and long duration wave model outputs to determine some of the likely extreme conditions that WECS deployed in Irish coastal waters are likely to encounter. This project was responsible for identifying the largest wave that has been recorded off the Irish coast — 23.87 m — and for demonstrating that a number of unexpectedly high records that had been identified by SEAI, the state agency responsible for commissioning AMETS, were in fact artefacts of abnormal buoy behaviour rather than valid observations. Estimates of the most extreme significant wave heights that could be expected for a range of return periods have also been provided. The results provide technology developers with guidelines for informing research into device and component survivability, work that is essential if WEC arrays are to be installed at exposed Atlantic sites.

Wavelet Analysis and Wave Field Variability

A preliminary study of the potential use of wavelet analysis was undertaken as part of this research. The strengths of this method of data processing highlighted the inherent weakness of Fourier analysis in addressing the short term variability of wave energy resource. It was demonstrated that this variability is reduced as the incident wave energy increases; suggesting that improved device performance will be facilitated in the most energy rich sea states due to the more regular wave fields that are present. It proved difficult to derive further quantitative conclusions from the analysis. As a result, wavelet analysis cannot be considered as a potential replacement for Fourier analysis in the context of wave energy resource without developing a more thorough understanding of its functionality. This is discussed further in the following section.

9.1 Further Work

The research described in this thesis has developed an enhanced understanding of the characteristics of the wave energy resource in the seas off the west coast of Ireland. The results of the analysis presented in Chapter 4 demonstrated that many resource assessments erred in the selection of an appropriate WPR for converting T_{02} data to T_E, while in Chapter 5 it was shown that applying the deep water assumption in the calculation of wave power results in inaccuracies, even at depths of 150 m. Both of these errors afflict the Accessible Wave Energy Resource Atlas, the work of reference for the Irish resource (ESB International 2005). This suggests that the theoretically available wave energy has been significantly underestimated, while the technical resource — derived from a Pelamis power matrix with T_E as an input — has likewise been affected. Revising the results documented in the Resource Atlas would not need to entail the onerous task of rerunning the numerical wave models — constant conversion factors could be applied to the existing data — and so should be pursued as a practical means of disseminating the outputs of this thesis.

This research was made possible by the additional measured data that has been made available with the deployment of wave measurement buoys at AMETS. This has alleviated the deficit in high quality spectral data that had existed previously from open ocean locations in Ireland's coastal waters. This thesis has assumed that AMETS is representative of other exposed, Atlantic facing sites. Additional sources of long term, uninterrupted, data from other locations would allow the work presented here to be extended to account for differences in the incident wave climate elsewhere in Ireland. The measurement network will be augmented further in the coming years as the M-buoy network is in the process of being upgraded; with Fugro Wavescan platforms replacing the outdated ODAS model. These buoys will provide time series of surface elevation, allowing wave spectra to be computed and individual wave heights to be determined. The possibility of operating complementary pairings of measurement instruments at Ireland's two wave energy test sites — for example multiple wave buoys and a coastal radar system for measuring spatial variability of the resource — should be explored, along with the deployment of novel systems such as wave gliders and seismic measurement stations

described in Chapter 2. These would add value to the test sites by supplementing the facilities available to help developers increase their understanding about the operation and performance of their devices. The quarter scale site in Galway Bay, which is already being used as a test bed for marine sensors as part of the SmartBay project (Smart Bay 2012), is a particularly suitable candidate for hosting innovative measurement campaigns, and a HF Radar system has recently been installed by NUI Galway to monitor wave conditions (N.U.I. Galway 2011). It would also be instructive to deploy instrumentation to monitor the wave climate at the 40 m depth at AMETS, which returned higher than expected design values of H_{m0}, to assess whether these results were produced by underlying physical processes at the site that may be relevant for WEC deployments or if it is simply an idiosyncrasy in the model outputs.

Chapter 7 demonstrated some of the extreme metocean events that will face WECs deployed at Irish sites, including unexpectedly high waves and severe storms. Whether these conditions constitute the most hazardous conditions for device operations is relatively unknown. Different WEC concepts are likely to have distinct failure modes depending on their operating principle, geometry and arrangement of components such as moorings and the PTO. Additionally, processes such as wave groups, currents and wave directionality are liable to contribute to potential device failures. Information about the specific vulnerabilities of WECs is generally proprietary and commercially sensitive. Generic reference models could be developed, however, and tested at small scales to provide an indication of which combinations of extreme conditions constitute the most critical design state, and if particular sites where these are predicted to occur need to be avoided. The survival flume that is being developed as part of University College Cork's new Beaufort Laboratory will provide an appropriate facility for conducting this experimental work.

Finally, this thesis explored the possibility of applying the wavelet transform as a tool for analysing ocean wave data in the context of WEC performance. This preliminary research highlighted the advantages this form of data processing holds over the commonly utilised Fourier analysis, particularly as a means to qualitatively illustrate the

short term, temporal, variability of the resource. An obvious weakness of wavelet analysis is that methods to compute standard sea state descriptors such as H_{m0} and T_E, or equivalent parameters, have not been identified. Developing this ability could position wavelet analysis as a viable alternative to the traditional wave spectrum, rather than its current status as an interesting, and underutilised, complement to existing analysis methods. The level of temporal variability was quantified by computing the standard deviation of the instantaneous peak frequency, σ_w. The relevance of this parameter to the performance of WECs was not determined, however, so an interesting avenue for future research would be to assess the sensitivity of device performance to changes in σ_w through tests of numerical or physical models.

References

ABP Marine Environmental Research (2008). Atlas of UK Marine Renewable Energy Resources: Technical Report, Report prepared on behalf of the Department of Business, Enterprise and Regulatory Reform.

Aegir Wave Power. (2012). "http://www.aegirwave.com/."

Alcorn, R., M. Healy and A. W. Lewis (2012). Lessons learned from the Galway Bay Seatrials of the EU funded CORES project. International Conference on Ocean Energy, Dublin, Ireland.

Allender, J., T. Audunson, S. F. Barstow, S. Bjerken, H. E. Krogstad, P. Steinbakke, L. Vartdal, L. E. Borgman and C. Graham (1989). "The wadic project: A comprehensive field evaluation of directional wave instrumentation." Ocean Engineering **16**(56): 505-536.

Anderson, C. W., D. J. T. Carter and P. D. Cotton (2001). Wave Climate Variability and Impact on Offshore Design Extremes, Report prepared for Shell International.

Aquamarine Power. (2012). "http://www.aquamarinepower.com/projects/north-west-lewis/."

Arinaga, R. A. and K. F. Cheung (2012). "Atlas of global wave energy from 10 years of reanalysis and hindcast data." Renewable Energy **39**(1): 49-64.

Ascoop, J. and M. Frielding (2010). The Development of a Wave Energy Test Site in Belmullet (Ireland): Experience to Date. 3rd International Conference on Ocean Energy. Bilbao, Spain.

Ashton, I. (2011). Spatial variability of wave fields over the scale of a wave energy test site. Department of Earth Resources, University of Exeter. **Thesis submitted for the degree of Doctor of Philosophy.**

AW-Energy. (2012). "http://www.aw-energy.com."

AXYS Technologies Inc. (2012). "TRIAXYS™ Directional Wave Buoy." from http://www.axystechnologies.com/Portals/0/Brochures/TRIAXYS%20Directional%20Wave%20Buoy.pdf.

Bahaj, A. S. (2011). "Generating electricity from the oceans." Renewable and Sustainable Energy Reviews **15**(7): 3399-3416.

Barrett, S. (2010). Floating Wave Energy Converters: Wave Measurement and Analysis Techniques Department of Civil & Environmental Engineering, University College Cork. **Thesis submitted for the degree of Doctor of Philosophy.**

Barrett, S., I. Ashton, T. Lewis and G. Smith (2009). Spatial & Spectral Variation of Seaways. Proceedings of the 8th European Wave and Tidal Energy Conference, Uppsala, Sweden.

Barrett, S., B. Holmes and A. W. Lewis (2007). Scalability of a Benign Wave Energy Site. 7th European Wave and Tidal Energy Conference (EWTEC). Porto, Portugal.

Barstow, S. F. and T. Kollstad (1991). Field Trials of the Directional Waverider. 1st International Offshore & Polar Engineering Conference. Edinburgh, United Kingdom.

Bassett, C., J. Thomson, B. Polagye and K. Rhinefrank (2011). Underwater noise measurements of a 1/7th scale wave energy converter. MTS/IEEE OCEANS 2011.

Blavette, A., D. L. O'Sullivan, A. W. Lewis and M. G. Egan (2011). Grid Integration of Wave and Tidal Energy. 30th International Conference on Ocean, Offshore and Arctic Engineering (OMAE). Rotterdam, The Netherlands.

Booij, N., R. C. Ris and L. H. Holthuijsen (1999). "A third-generation wave model for coastal regions 1. Model description and validation." J. Geophys. Res. **104**(C4): 7649-7666.

Bowyer, P. J. (2000). Phenomenal waves with a transitioning tropical cyclone (Luis, the Queen, and the Buoys). 24th Conference on Hurricanes and Tropical Meteorology. Fort Lauderdale, Florida, USA.

Cahill, B. G. (2012). Resource Characterisation of the Galway Bay 1/4 Scale Wave Energy Test Site, Prepared on behalf of the Sustainable Energy Authority of Ireland.

Carbon Trust (2005). Variability of UK Marine Resources.

Cardone, V. J., R. E. Jensen, D. T. Resio, V. R. Swail and A. T. Cox (1996). "Evaluation of Contemporary Ocean Wave Models in Rare Extreme Events: The "Halloween Storm" of October 1991 and the "Storm of the Century" of March 1993." Journal of Atmospheric and Oceanic Technology **13**(1): 198-230.

Carnegie Wave Energy. (2012). "http://www.carnegiewave.com/."

Casey, S. (2010). The Wave: In Pursuit of the Rogues, Freaks and Giants of the Ocean, Knopf Doubleday Publishing Group.

Casson, A. (2012). NNMREC Test Facilities (Personal Communication).

Coastal Data Information Program. (2012). "www.cdip.ucsd.edu."

Collard, F., F. Ardhuin and B. Chapron (2009). "Monitoring and analysis of ocean swell fields from space: New methods for routine observations." J. Geophys. Res. **114**(C7): C07023.

Cooley, J. W. and J. W. Tukey (1965). "An algorithm for the machine calculation of complex Fourier series." Math. Comp. **19**.

Cornett, A. M. (2008). A Global Wave Energy Resource Assessment. Proceedings of the Eighteenth International Offshore and Polar Engineering Conference. Vancouver, Canada.

Crabb, J. A. (1984). Assessment of Wave Power Available at Key United Kingdom Sites, Institute of Oceanographic Sciences.

Cradden, L. (2012). Wave Period Ratios at EMEC (Personal Communication).

Cradden, L., H. Mouslim, O. Duperray and D. M. Ingram (2011). Joint Exploitation of Wave and Offshore Wind Power. 9th European wave and Tidal Energy Conference. Southampton, United Kingdom.

Cruz, J., E. Mackay and T. Martins (2007). Advances in Wave Resource Estimation: Measurements and Data Processing. 7th European Wave and Tidal Energy Conference. Porto, Portugal.

Curé, M. (2011a). A Fifteen Year Model Based Wave Climatology of Belmullet, Ireland, Report prepared on behalf of the Sustainable Energy Authority of Ireland (SEAI).

Curé, M. (2011b). Personal Communication.

Dalton, G. J., R. Alcorn and T. Lewis (2010). "Case study feasibility analysis of the Pelamis wave energy convertor in Ireland, Portugal and North America." Renewable Energy **35**(2): 443-455.

Dalton, G. J. and A. W. Lewis (2011). Economic case study of 5 wave energy devices off the west coast of Ireland. The 9th European Wave and Tidal Energy Conference (EWTEC), Southampton, United Kingdom.
Datawell BV (2010). Datawell Waverider Reference Manual.
Datawell BV. (2012a). "Datawell File Formats." from http://www.datawell.nl/faq.php?cid=12.
Datawell BV (2012b). Filter Response in Displacement Data.
Daubechies, I. (1992). Ten lectures on Wavelets, Society for Industrial and Applied Mathematics.
de Vries, J. J., J. Waldron and V. Cunningham (2003). "Field tests of the new Datawell DWR-G GPS wave buoy." Sea Technology(December).
Dean, R. G. and R. A. Dalrymple (1991). Water Wave Mechanics for Engineers and Scientists.
Department of Communications Marine and Natural Resources (2007a). Energy White Paper 2007: Delivering a Sustainable Energy Future for Ireland.
Department of Communications Marine and Natural Resources (2007b). The energy world is going green it is a win-win for Ireland.
Det Norske Veritas (2010). Recommended Practice DNV-RP-C205: Environmental Conditions and Environmental Loads.
Doherty, K., M. Folley, R. Doherty and T. Whittaker (2011). Extreme Value Analysis of Wave Energy Converters. Proceedings of the 21st International Offshore and Polar Engineering Conference (ISOPE), Maui, Hawaii, USA.
Draper, L. (1971). "Severe Wave Conditions at Sea." Journal of the Institute of Navigation **24**(3).
Dunnett, D. and J. S. Wallace (2009). "Electricity generation from wave power in Canada." Renewable Energy **34**(1): 179-195.
Duperray, O., P. Ricci, Y. Torre-Encisco, L. Ferrer and J. L. Villate (2011). Extreme Environmental Parameters for Wave Energy Converters and Moorings at bimep. 9th European Wave and Tidal Energy Conference (EWTEC). Southampton, United Kingdom.
Durrant, T. H. and D. J. M. Greenslade (2007). Validation and application of Jason-1 and Envisat significant wave heights. 10th Int. Workshop on wave hindcasting and forecasting. Oahu, Hawaii, USA.
Dysthe, K., H. E. Krogstad and P. Miller (2008). "Oceanic Rogue Waves." Annual Review of Fluid Mechanics **40**(1): 287-310.
Electric Power Research Institute (2011). Mapping and Assessment of the United States Ocean Wave Energy Resource.
EMEC (2009). Assessment of Wave Energy Resource, European Marine Energy Centre
EMEC. (2012). "Wave Clients." from http://www.emec.org.uk/about-us/wave-clients/.
EquiMar (2011). Wave and Tidal Resource Characterisation
EquiMar Group (2010a). Deliverable D2.7: Protocols for Wave and Tidal Resource Assessment.
Equimar Group (2010b). Deliverable D4.2: Data Analysis & Presentation to Quantify Uncertainty.
EquiMar Group (2011). Deliverable D2.6: Extremes and Long Term Extrapolation.

ESB International (2005). Accessible Wave Energy Resource Atlas: ESBI Report 4D404A-R2 for Marine Institute (MI) and Sustainable Energy Ireland (SEI).

European Marine Energy Centre (EMEC) (2009). Assessment of Wave Energy Resource.

Falcão, A. F. d. O. (2010). "Wave energy utilization: A review of the technologies." Renewable and Sustainable Energy Reviews **14**(3): 899-918.

Falnes, J. (2007). "A review of wave-energy extraction." Marine Structures **20**(4): 185-201.

Fennell, S. (2012). "Marine Institute Data Buoy Operations (Personal Communication)."

Fernandez Chozas, J., N. E. Helstrup Jensen, H. C. Sorensen, J. P. Kofoed and A. Kabuth (2011). Predictability of the Power Output of Three wave Energy Technologies in the Danish North Sea 9th European Wave and Tidal Energy Conference (EWTEC), Southampton, United Kingdom.

Ferrer, L., P. Liria, R. Bolaños, C. Balseiro, P. Carracedo, D. González-Marco, M. González, A. Fontán, J. Mader and C. Hernández (2010). Reliability of coupled meteorological and wave models to estimate wave energy resource in the Bay of Biscay. 3rd International Conference on Ocean Energy (ICOE), Bilbao, Spain.

Fitzgerald, J. and B. Bolund (2012). Technology Readiness for Wave Energy Projects; ESB and Vattenfall classification system. International Conference on Ocean Energy, Dublin, Ireland.

Flocard, F. and T. D. Finnigan (2010). "Laboratory experiments on the power capture of pitching vertical cylinders in waves." Ocean Engineering **37**(11-12): 989-997.

Folley, M., A. M. Cornett, B. Holmes, P. Lenee-Bluhm and P. Liria (2012). Standardising resource assessment for wave energy converters. International Conference on Ocean Energy. Dublin, Ireland.

Folley, M. and T. J. T. Whittaker (2009). "Analysis of the nearshore wave energy resource." Renewable Energy **34**(7): 1709-1715.

Forrest, S. (2010). A methodology for near-Shore Wave Resource Assessment. International Conference on Ocean Energy. Bilbao, Spain.

Fugro OCEANOR (1999). Wavescan Buoy User Manual.

Fusco, F. (2012). Real-time Forecasting and Control for Oscillating Wave Energy Devices. Electronic Engineering Department, NUI Maynooth. **Thesis submitted for the degree of Doctor of Philosophy**.

Fusco, F., G. Nolan and J. V. Ringwood (2010). "Variability reduction through optimal combination of wind/wave resources - An Irish case study." Energy **35**(1): 314-325.

Gemmrich, J., C. Garrett and K. Thompson (2009). Extreme waves in Canadian coastal waters. 11th International Workshop on Wave Hindcasting and Forecasting. Halifax, Nova Scotia, Canada.

Glendenning, I. and B. M. Count (1976). "Wave Power." The Chemical Engineer.

GlobWave Project (2012). Deliverable D.18: Annual Quality Control Report.

Goda, Y. (1988). On the Methodology of Selecting Design Wave Heights. Proceedings of 21st Coastal Engineering Conference (ASCE).

Guedes Soares, C. (1984). "Representation of double-peaked sea wave spectra." Ocean Engineering **11**(2): 185-207.

Guedes Soares, C. (1986). "Assessment of the uncertainty in visual observations of wave height." Ocean Engineering **13**(1): 37-56.

Guedes Soares, C. (1991). "On the occurence of double peaked wave spectra." Ocean Engineering **18**(1-2): 167-171.
Guedes Soares, C. and Z. Cherneva (2005). "Spectrogram analysis of the time-frequency characteristics of ocean wind waves." Ocean Engineering **32**(14-15): 1643-1663.
Guedes Soares, C., Z. Cherneva and E. M. Antão (2003). "Characteristics of abnormal waves in North Sea storm sea states." Applied Ocean Research **25**(6): 337-344.
Gunn, K. and C. Stock-Williams (2012). "Quantifying the global wave power resource." Renewable Energy **44**(0): 296-304.
Hasselmann, K., T. P. Barnett, E. Bouws, H. Carlson, D. E. Cartwright, K. Enke, J. A. Ewing, H. Gienapp, D. E. Hasselmann, P. Kruseman, A. Meerburg, P. Müller, D. J. Olbers, K. Richter, W. Sell and H. Walden (1973). "Measurements of wind-wave growth and swell decay during the Joint North Sea Wave Project (JONSWAP)." Deutschen Hydrographischen Zeitschrift.
Haver, S. (2004a). Freak Waves: A Suggested Definition and Possible Consequences for Marine Structures. Rogue Waves 2004. Brest, France.
Haver, S. (2004b). A possible freak wave event measured at the Draupner Jacket, January 1, 1995. Rogue Waves. Brest, France.
Haver, S. and O. J. Andersen (2000). Freak Waves: Rare Realizations of a Typical Population or Typical Realizations of a Rare Population? Tenth International Offshore and Polar Engineering Conference (ISOPE). Seattle, United States.
Helzel Messtechnik (2009). WERA Operation Manual.
Hine, G., J. Thomas and L. Beatman (2012). Wave Glider – A Coastal Restoration Platform.
Hoitink, A. J. F. and M. Schroevers (2004). Validation of ADCP surface wave measurements in a shelf sea. OCEANS '04. MTTS/IEEE TECHNO-OCEAN '04.
Holliday, N. P., M. J. Yelland, R. Pascal, V. R. Swail, P. K. Taylor, C. R. Griffiths and E. Kent (2006). "Were extreme waves in the Rockall Trough the largest ever recorded?" Geophys. Res. Lett. **33**(5): L05613.
Holmes, B. (2003). Ocean Energy: Development and Evaluation Protocol, Hydraulics and Maritime Research Centre/Marine Institute.
Holmes, B. and S. Barret (2007). Sea and Swell Spectra. 7th European Wave and Tidal Energy Conference. Porto, Portugal.
Holmes, B. and K. Nielsen (2010). Guidelines for the Development & Testing of Wave Energy Systems, International Energy Agency Ocean Energy Systems.
Holthuijsen, L. H. (2007). Waves in Oceanic and Coastal Waters. Cambridge, Cambridge University Press.
Hovland, J. (2010). Predicting Deep Water Breaking Wave Severity, Oregon State University. **Master of Science in Mechanical Engineering**.
Hughes, S. A. (1993). Physical Models and Laboratory Techniques in Coastal Engineering. Singapore, World Scientific Publishing Co.
Hurrell, J. W., Y. Kushnir, G. Ottersen and M. Visbeck (2003). The North Atlantic Oscillation: Climatic Significance and Environmental Impact. Washington, DC, AGU.
IEC TC114 (2012). Wave energy resource assessment and characterization (Draft), International Electrotechnical Commission.

IEC TC114 (2012). Electricity producing wave energy converters – Power performance assessment (Draft). International Electrotechnical Commission.

Iglesias, G. and R. Carballo (2009). "Wave energy potential along the Death Coast (Spain)." Energy **34**(11): 1963-1975.

Iglesias, G. and R. Carballo (2010a). "Wave energy and nearshore hot spots: The case of the SE Bay of Biscay." Renewable Energy **35**(11): 2490-2500.

Iglesias, G. and R. Carballo (2010b). "Wave energy resource in the Estaca de Bares area (Spain)." Renewable Energy **35**(7): 1574-1584.

Implementing Agreement on Ocean Energy Systems (OES-IA) (2010). Annual Report 2010.

INFOMAR (2007). Integrated Mapping for the Sustainable Development of Ireland's Marine Resource: Proposal and Strategy.

James, I. D. (1986). "A note on the theoretical comparison of wave staffs and wave rider buoys in steep gravity waves." Ocean Engineering **13**(2): 209-214.

Jeans, G., C. Primrose, N. Descusse, B. Strong and v. W. P. (2002). A Comparison between directional wave measurements from the RDI Workhorse with Waves and the Datawell directional waverider. IEEE Seventh Working Conference on Current Measurement Technology. San Diego, CA, USA.

Kavanagh, P., M. Fielding, L. Scally, S. Berrow, J. Hunt and B. Kennedy (2011). Environmental Aspects of Developing Ireland's Atlantic Marine Energy Test Site (AMETS). 9th European Wave and Tidal Energy Conference. Southampton, United Kingdom.

Kelly, J., D. O'Sullivan, R. Alcorn and A. W. Lewis (2012). Challenges and Lessons Learned in the Deployment of an Off Shore Oscillating Water Column. Ecological Vehicles and Renewable Energies International Conference and Exhibition, Monaco.

Kennedy, S. (2012). Bridging the Expectation Gap. reNews Global Marine 2012 Report.

Kerbiriou M.A, Prevosto M, Maisondieu C, Babarit A and C. A. (2007). Influence of an improved sea-state description on a wave energy converter production. 26th International Conference on Offshore Mechanics and Arctic Engineering (OMAE), San Diego, California.

Kinsman, B. (1965). Wind Waves: Their Generation and Propagation on the Ocean Surface, Prentice-Hall.

Krogstad, H. E., S. F. Barstow, S. E. Aasen and I. Rodriguez (1999). "Some recent developments in wave buoy measurement technology." Coastal Engineering **37**(3-4): 309-329.

Lee, H. S. and S. H. Kwon (2003). "Wave profile measurement by wavelet transform." Ocean Engineering **30**(18): 2313-2328.

Lenee-Bluhm, P., R. Paasch and H. T. Özkan-Haller (2011). "Characterizing the wave energy resource of the US Pacific Northwest." Renewable Energy **36**(8): 2106-2119.

Lewis, A., S. Estefen, J. Huckerby, W. Musial, T. Pontes and J. Torres-Martinez (2011). Ocean Energy. IPCC Special Report on Renewable Energy Sources and Climate Change Mitigation.

Liquid Robotics. (2012). "PacX Project Blog." from http://pacxdata.liquidr.com.

Liu, Z. and H. F. Burcharth (1998). Encounter Probability of Individual Wave Height. Proceedings of 26th Conference on Coastal Engineering, Copenhagen, Denmark.

Lueck, R. G., F. R. Driscoll and M. Nahon (2000). "A wavelet for predicting the time-domain response of vertically tethered systems." Ocean Engineering **27**(12): 1441-1453.

Mackay, E. B. L., A. S. Bahaj and P. G. Challenor (2010). "Uncertainty in wave energy resource assessment. Part 2: Variability and predictability." Renewable Energy **35**(8): 1809-1819.

Madrigal, A. (2011). Powering the Dream: The History and Promise of Green Technology, Da Capo Press.

Marine Institute. (2012). "www.marine.ie."

Marine Institute Data Requests. (2012). "http://www.marine.ie/home/publicationsdata/RequestForData.htm."

Massel, S. R. (2001). "Wavelet analysis for processing of ocean surface wave records." Ocean Engineering **28**(8): 957-987.

Mayo Today (2012). Ocean energy sector can create 70,000 jobs, Taoiseach tells Ballina conference. Mayo Today.

McCrone, A. (2012). Wave and Tidal Stream - Will it Always be Jam Tomorrow? Bloomberg New Energy Finance.

Mettlach, T. (2010). Ocean Wave Measurement and Analysis. Seattle, USA, Tutorial presentated at MTS/IEEE OCEANS'10 Conference.

Mettlach, T. and T. Chung-Chu (2010). Concepts for an ideal ocean wave-measuring buoy. MTS/IEEE OCEANS 2010, Seattle, U.S.A.

Misiti, M., Y. Misiti, G. Oppenheim and J.-M. Poggi (2010). Wavelet Toolbox 4: User's Guide, The MathWorks.

Molinas, M., O. Skjervheim, B. Sørby, P. Andreasen, S. Lundberg and T. Undeland (2007). Power Smoothing by Aggregation of Wave Energy Converters for Minimizing Electrical Energy Storage Requirements. 7th Europen Wave and Tidal Energy Conference. Porto, Portugal.

Mollison, D. (1982). Ireland's Wave Power Resource, A report to the National Board for Science and Technology and Electricity Supply Board.

Moni, A., S. Donne, C. Bean, D. Craig, M. Mollhoff, F. Hauser, A. Braiden, K. Lambkin, C. Creamer and M. White (2012). Towards ocean wave energy-potential quantification from a terrestrially-based seismic observation system. 4th International Conference on Ocean Energy, Dublin, Ireland.

Mora-Figueroa, V. O., C. Huertas-Olivares, B. Holmes and A. M. O'Hagan (2011). Catalogue of Wave Energy Test Centres, SOWFIA Project.

Mori, N., P. C. Liu and T. Yasuda (2002). "Analysis of freak wave measurements in the Sea of Japan." Ocean Engineering **29**(11): 1399-1414.

Mørk, G., S. F. Barstow, A. Kabuth and T. Pontes (2010). Assessing the Global Wave Energy Potential. 29th International Conference on Ocean, Offshore Mechanics and Artic Engineering Shanghai, China.

Müller, P., C. Garrett and A. R. Osborne (2005). "Meeting Report: Rogue Waves—The Fourteenth 'Aha Huliko'a Hawaiian Winter Workshop " Oceanography **18**(3).

Murphy, J. (2011). Coastal Process Report, Atlantic Marine Energy Test Site Environmental Impact Statement.

Murray, D. B., M. G. Egan, J. G. Hayes and D. L. O'Sullivan (2009). Applications of Supercapacitor Energy Storage for a Wave Energy Converter System. European Wave and Tidal Energy Conference. Uppsala, Sweden.

N.U.I. Galway. (2011). "Coastal Radar Deployed in Galway Bay." from http://www.nuigalway.ie/about-us/news-and-events/news-archive/2011/october2011/coastal-radar-deployed-in-galway-bay.html.

Nambiar, A. J., A. E. Kiprakis, D. I. M. Forehand and A. R. Wallace (2010). Effects of array configuration, network impacts and mitigation of arrays of wave energy converters connected to weak, rural electricity networks. 3rd International Conference on Ocean Energy. Bilbao, Spain.

National Data Buoy Centre. (2012). "www.ndbc.noaa.gov."

Neptune Wave Power (2012). Neptune Wave Power Deploys Second Buoy in the Ocean.

Niclasen, B. A. and K. Simonsen (2007). "Note on wave parameters from moored wave buoys." Applied Ocean Research **29**(4): 231-238.

Nikolkina, I. and I. Didenkulova (2011). "Rogue waves in 2006-2010." Nat. Hazards Earth Syst. Sci. **11**(11): 2913-2924.

Nolan, G., J. V. Ringwood and B. Holmes (2007). Short Term Wave Energy variability off the West Coast of Ireland. 7th European Wave and tidal Energy Conference, Porto, Portugal.

O'Brien, L. and F. Dias (2012). "Extreme wave events in Ireland: 14,680 BP - 2012." Natural Hazards and Earth System Sciences **In Review**.

O'Callaghan, J. (2012). Technical and Practical Guidance for Conducting Sea Trials at Galway Bay Wave Energy Test Site. International Conference on Ocean Energy, Dublin, Ireland.

O'Reilly, W. C., T. H. C. Herbers, R. J. Seymour and R. T. Guza (1996). "A Comparison of Directional Buoy and Fixed Platform Measurements of Pacific Swell." Journal of Atmospheric and Oceanic Technology **13**(1).

O'Shea, M., J. Murphy and P. Sala (2011). Monitoring the morphodynamic behaviour of a breached barrier beach system and its impacts on an estuarine system. OCEANS, 2011 IEEE - Spain.

O'Sullivan, R. (1985). Further Development of an Irregular Wave Generation and Analysis System. Department of Civil Engineering, University College Cork. **Master of Engineering Science**.

Ocean Energy Ltd. (2012). "http://www.oceanenergy.ie."

Ocean Power Technologies. (2012a). "http://www.oceanpowertechnologies.com."

Ocean Power Technologies. (2012b). "Project at Marine Corps Base, Hawaii." from http://www.oceanpowertechnologies.com/hawaii.html.

Ochi, M. K. (1998). Ocean Waves: The Stochastic Approach. Cambridge, UK., Cambridge University Press.

Pecher, A., J. P. Kofoed, T. Larsen and T. Marchalot (2012). Experimental Study of the WEPTOS Wave Energy Converter. 31st International Conference on Ocean, Offshore and Arctic Engineering (OMAE). Rio de Janeiro, Brazil.

Persson, A. and F. Grazzini (2005). User guide to ECMWF forecast products.

Pierson, W. J. and L. Moskowitz (1964). "A Proposed Spectral Form for Fully Developed Wind Seas Based on the Similarity Theory of S. A. Kitaigorodskii." Journal of Geophysical Research **69**: 5181-5190.

Pitt, E. G. (2005). Estimating power from wave measurements at the European Marine Energy Centre (EMEC) test site, Applied Wave Research.

QARTOD (2009). QARTOD V Final Report: Fifth Workshop on the QA/QC of Real-time Oceanographic Data, Quality Assurance of Real-Time Oceanographic Data (QUARTOD) Group.

Reeve, D. E., Y. Chen, S. Pan, V. Magar, D. J. Simmonds and A. Zacharioudaki (2011). "An investigation of the impacts of climate change on wave energy generation: The Wave Hub, Cornwall, UK." Renewable Energy **36**(9): 2404-2413.

Reguero, B. G., C. Vidal, M. Menendez, F. J. Mendez, R. Minguez and I. Losada (2011). Evaluation of global wave energy resource. IEEE/MTS OCEANS 2011, Santander, Spain.

reNews (2012). Global Marine 2012 Report.

Rodríguez, G. and C. Guedes Soares (1999). "A criterion for the automatic identification of multimodal sea wave spectra." Applied Ocean Research **21**(6): 329-333.

Rute Bento, A., P. Martinho, R. Campos and C. Guedes Soares (2011). Modelling Wave Energy Resources in the Irish West Coast. 30th International Conference on Offshore Mechanics and Arctic Engineering (OMAE), Rotterdam, The Netherlands.

Sakhare, S. and M. C. Deo (2009). "Derivation of wave spectrum using data driven methods." Marine Structures **22**(3): 594-609.

Salter, S. (1974). "Wave Power." Nature(249): 720-724.

Salter, S. H. (2008). Chapter 2: Looking Back. Ocean Wave Energy: Current Status and Future Perspectives. J. Cruz, Springer.

Saulnier, J.-B., A. Clément, A. F. d. O. Falcão, T. Pontes, M. Prevosto and P. Ricci (2011). "Wave groupiness and spectral bandwidth as relevant parameters for the performance assessment of wave energy converters." Ocean Engineering **38**(1): 130-147.

Serri, L., A. M. Sempreviva, T. Pontes, J. Murphy, K. Lynch, D. Airoldi, J. Hussey, C. Rudolph and I. Karagali (2012). ORECCA Resource Data and GIS Tool for Offshore Renewable Enegy Projects in Europe.

Sharkey, F. (2012). "ESB's WestWave - Flagship project evaluates wave energy options." Engineers Ireland: The Engineers Journal(March/April 2012).

Sims, R. E. H., R. N. Schock, A. Adegbululgbe, J. Fenhann, I. Konstantinaviciute, W. Moomaw, H. B. Nimir, B. Schlamadinger, J. Torres-Martínez, C. Turner, Y. Uchiyama, S. J. V. Vuori, N. Wamukonya and X. Zhang (2007). Energy supply. In Climate Change 2007: Mitigation. Contribution of Working Group III to the Fourth Assessment Report of the Intergovernmental Panel on Climate Change. Cambridge, United Kingdom and New York,NY, USA

Skey, S. G. P., K. Berger-North and V. R. Swail (1998). Measurement of Winds and Waves from a NOMAD Buoy in High Seastates. 5th International Workshop on Wave Hindcasting and Forecasting. Melbourne, Florida, USA.

Smart Bay. (2012). from http://smartbay.ie/Home.aspx.

Smith, G. H., V. Venugopal and J. Wolfram (2006). "Wave period group statistics for real sea waves and wave energy extraction." Proceedings of the Institution of Mechanical Engineers, Part M: Journal of Engineering for the Maritime Environment **220**(3): 99-115.

Smith, H. (2012). Wave Period Ratios at Wave Hub (Personal Communication).
Smith, H. C. M., C. Pearce and D. L. Millar (2012). "Further analysis of change in nearshore wave climate due to an offshore wave farm: An enhanced case study for the Wave Hub site." Renewable Energy **40**(1).
Stoker, E. (2012). Waverider Operational Limits and Digital Filter (Personal Communication).
Stopa, J. E., K. F. Cheung and Y.-L. Chen "Assessment of wave energy resources in Hawaii." Renewable Energy **36**(2): 554-567.
Stoutenburg, E. D., N. Jenkins and M. Z. Jacobson (2010). "Power output variations of co-located offshore wind turbines and wave energy converters in California." Renewable Energy **35**(12): 2781-2791.
Stratigaki, V., P. Troch, L. Baelus and Y. Keppens (2011). Introducing wave regeneration by wind in a mild-slope wave propagation model MILDwave, to investigate the wake effects in the lee of a farm of wave energy converters. 30th International Conference onOcean, Offshore and Arctic Engineering. Rotterdam, The netherlands.
Strong, B., A. Bouferrouk and S. G. H. (2012). Measurement and Evaluation of the Wave Climate near the Wave Hub using a 5-Beam ADCP. 4th International Conference on Ocean Energy. Dublin, Ireland.
Sustainable Energy Authority of Ireland (2010). Ocean Energy Roadmao to 2050.
Sustainable Energy Authority of Ireland (2011a). Application for Foreshore Lease to Construct an Offshore Electricity Generating Station. , Submitted to the Department of the Environment, Heritage and Local Government.
Sustainable Energy Authority of Ireland (2011b). Energy in Ireland 1990 – 2010.
Taylor, P. H. and B. A. Williams (2004). "Wave Statistics for Intermediate Depth Water—NewWaves and Symmetry." Journal of Offshore Mechanics and Arctic Engineering **126**(1).
Thiebaut, F., D. O'Sullivan, P. Kracht, S. Ceballos, J. López, C. Boake, J. Bard, N. Brinquete, J. Varandas, L. M. C. Gato, R. Alcorn and A. W. lewis (2011). Testing of a floating OWC device with movable guide vane impulse turbine power take-off. 9th European Wave and Tidal Energy Conference. Southampton, United Kingdom.
Thiebaut , F., D. O'Sullivan, P. Kracht, S. Ceballos, J. López, C. Boake, J. Bard, N. Brinquete, J. Varandas, L. M. C. Gato, R. Alcorn and A. W. lewis (2011). Testing of a floating OWC device with movable guide vane impulse turbine power take-off. 9th European Wave and Tidal Energy Conference. Southampton, United Kingdom.
Thomas, B. R. (1995). An Investigation of Apparent Giant Waves off the West Coast of Canada. 4th International Workshop on Wave Hindcasting and Forecasting. Banff, Alberta, Canada.
Thomas, G. (2008). The Theory behind the Conversion of Ocean Wave Energy: A Review. Ocean Wave Energy: Current Status and Future Perspectives. J. Cruz, Springer.
Tissandier, J., A. Babarit and A. H. Clement (2008). Study of the smoothing effect on the power production in an array of SEAREV wave energy converters. Proceedings of the Eighteenth (2008) International Offshore and Polar Engineering

Conference. Vancouver, BC, Canada, The International Society of Offshore and Polar Engineers (ISOPE).
Tolman, H. L. (2002). User Manual and System Documentation for WaveWatch III version 2.22, NOAA/NWS/NCEP/OMB Technical Note.
Torrence, C. and G. P. Compo (1998). "A practical guide to wavelet analysis." Bulletin of the American Meteorological Society(79): 61-78.
Tromans, P. S., A. Anaturk and P. Hagemeijer (1991). A new model for the kinematics of large ocean waves: Application as a design wave. Int. Conf Offshore and Polar Engineering. Edinburgh, UK.
Tucker, M. J. and E. G. Pitt (2001). Waves in Ocean Engineering, Elsevier.
U.S. Department of Energy (2011). U.S. Department of Energy Wind and Water Power Program Funding in the United States: Marine and Hydrokinetic Energy Projects.
University College Cork. (2012). "Plans for €14m Beaufort Laboratory unveiled." from http://www.ucc.ie/en/news/Name-147824-en.html.
Uppala, S. M., P. W. KÅllberg, A. J. Simmons, U. Andrae, V. D. C. Bechtold, M. Fiorino, J. K. Gibson, J. Haseler, A. Hernandez, G. A. Kelly, X. Li, K. Onogi, S. Saarinen, N. Sokka, R. P. Allan, E. Andersson, K. Arpe, M. A. Balmaseda, A. C. M. Beljaars, L. V. D. Berg, J. Bidlot, N. Bormann, S. Caires, F. Chevallier, A. Dethof, M. Dragosavac, M. Fisher, M. Fuentes, S. Hagemann, E. Hólm, B. J. Hoskins, L. Isaksen, P. A. E. M. Janssen, R. Jenne, A. P. McNally, J. F. Mahfouf, J. J. Morcrette, N. A. Rayner, R. W. Saunders, P. Simon, A. Sterl, K. E. Trenberth, A. Untch, D. Vasiljevic, P. Viterbo and J. Woollen (2005). "The ERA-40 re-analysis." Quarterly Journal of the Royal Meteorological Society **131**(612): 2961-3012.
USACE (2002). Coastal Engineering Manual, United States Army Corps of Engineers.
Valeport Ltd. (2004). MIDAS DWR & WTR Wave Recorders Operational Manual.
van Nieuwkoop-McCall, J. C. C., H. C. M. Smith, G. Smith and K. A. Edwards (2012). Effect of water depth on the wave energy resource and extreme wave conditions. International Conference on Ocean Energy. Dublin, Ireland.
van Os, J., S. Caires and M. van Gent (2011). Guidelines for Metocean Data Analysis. Proceedings of the Twenty-first International Offshore and Polar Engineering Conference. Maui, Hawaii, USA.
Venugopal, V. and G. H. Smith (2007). Wave climate investigation for an array of wave power devices. 7th European Wave and Tidal Energy Conference, Porto, Portugal.
Volger, A. (2012). Datawell Waverider Filter Response (Personal Communication).
Ward, D. L., E. F. Thompson and J. Zhang (2003). Selection of Design Wave Height for Coastal Engineering. Advances in Coastal Structure Design. R. K. Mohan, O. Magoon and M. Pirello. Reston, VA, American Society of Civil Engineers Publications.
Waveplam (2009). "State of the Art Analysis: A Cautiously Optimistic Review of the Technical Status of Wave Energy Technology."
WERATLAS (2001). European Wave Energy Atlas.
Wyatt, L. R. (2009). Wave and Tidal Power measurement using HF radar. 8th European Wave and Tidal Energy Conference. Uppsala, Sweden.

Wyatt, L. R., J. J. Green, K. W. Gurgel, J. C. Nieto Borge, K. Reichert, K. Hessner, H. Gunther, W. Rosenthal, O. Saetra and M. Reistad (2003). "Validation and intercomparisons of wave measurements and models during the EuroROSE experiments." Coastal Engineering **48**(1): 1-28.